Multiwavelength behaviour of Cygnus X-3 and related objects

Thesis

Open University Astrophysics

Multiwavelength behaviour of Cygnus X-3 and related objects

Thesis submitted by

Robert P Fender B.Sc.

for the degree of

Doctor of Philosophy

December 1995

Department of Physics
Faculty of Science
Open University
Milton Keynes MK7 6AA
United Kingdom

Abstract

I present a detailed study of the behaviour of the exotic X-ray binary Cygnus X-3 at radio, (sub)mm, infrared, red-optical and X-ray wavelengths. Further unusual properties of the system are unearthed and previously expounded models are refined by new observations. In order to address the broader picture, a multiwavelength comparison of Cygnus X-3 with other 'radio-jet' X-ray binaries is also undertaken.

Infrared observations of Cyg X-3 at high time resolution reveal many rapid flare events superimposed upon the 4.8 hr (presumed) orbital motion. Photometry simultaneously in the H & K-bands allows strong constraints to be placed upon T & N_e for the flaring component. Dereddening of R-I-J-H-K-L-L′ photometry places limits on the likely extinction to Cyg X-3 of $4.5 \leq A_J \leq 7.5$ mag. Further infrared study, simultaneous with radio monitoring and observations with OSSE/GRO and the INT shed greater light on the source, including possible orbital colour changes and a long-term correlation between radio and infrared flux levels. Deep imaging of the field reveals many previously undiscovered infrared sources within a few arcsec of Cyg X-3.

Simultaneous millimetre and radio observations of Cyg X-3 reveal anomalously strong mm fluxes. Interpreting this in terms of significant absorption of the cm fluxes during the passage outwards of the radio-emitting plasmons, strengthens the case for a dense stellar wind in the Cyg X-3 system. Further radio and sub(mm) observations of Cyg X-3 during outburst confirm previously observed phenomena such as quenched radio emission prior to outburst, and establish the importance of radiation loss mechanisms in the decay of radio plasmons ejected from the source. A model describing the qualitative behaviour of the source during outburst is presented.

Acknowledgements

There are lots of people who have helped me, in many ways, through the thirty nine months of my PhD. I hope I don't forget anyone, and that if I do they can ascribe my omission to stress and diminishing numbers of brain cells rather than be offended ...

I would like to thank Jocelyn Bell Burnell for being an excellent supervisor and teacher both of science and those subtle things that aren't quite science but are essential in order to make progress in a competitive and unusual environment. And, of course, for accepting me to do a PhD at the OU in the first place. Early on in my PhD Peredur Williams and Marten van Kerkwijk made themselves available for many useful conversations, for which I thank them. Subsequently I made contact with Ralph Spencer, Guy Pooley and Elizabeth Waltman, all of whom have contributed a great deal to my work, both in the form of collaborations and discussions, and continue to do so. I would also like to thank Josep Martí for his enthusiastic reading and comments upon early drafts of much of my work.

On a more personal level, I would like to thank all the people who have been friends to me during my PhD. Jonathan, Dave H, Peter, Emma et al. all made nights in Milton Keynes more bearable, if a bit *too* alcoholic at times. Sarah, Andy : congratulations on managing to share an office with me ! I would also like to thank my mother and family for being behind me at all times, even though they thought I was stupid to give up the office job ...

Finally, I'd like to thank Josephine for lots of love and support, pasta and tomato sauce, use of her car, house & credit card, and her creative way with the English language ... little did *Pilgrim* know his fate when he first encountered *Alice* ...

Chapter 1

INTRODUCTION

Cygnus X-3 is a highly energetic galactic X-ray binary which displays an exceptionally unusual, possibly unique, combination of observational characteristics. Discovered nearly 30 years ago, the system has persistently evaded easy classification and continues to reveal unexpected properties.

1.1 X-ray binaries

X-ray binaries (XRBs) are binary star systems (ie. two stars orbiting a common centre of mass) in which one of the components is a compact object accreting matter from its companion, emitting X-rays in the process. Common usage restricts the term *X-ray binary* to systems believed to contain neutron stars or black holes, although numerous binary star systems exist in which accretion onto a white dwarf causes the emission of X-rays (primarily *cataclysmic variables* – see e.g. Livio 1992 [1] for a review; also possibly the *supersoft X-ray sources* – e.g. Hasinger 1994 [2]).

X-ray binaries can be broadly divided into two classes, the *high-mass X-ray binaries* (HMXRBs) and the *low-mass X-ray binaries* (LMXRBs) :

In HMXRB systems the companion star to the compact object is typically a young, massive population I OB-type (super)giant. That they are young systems is necessitated by the short lifetimes of such luminous companion stars, and as a result they are concentrated near their birthplaces in the plane of the galaxy, in particular in the spiral arms. OB stars posess

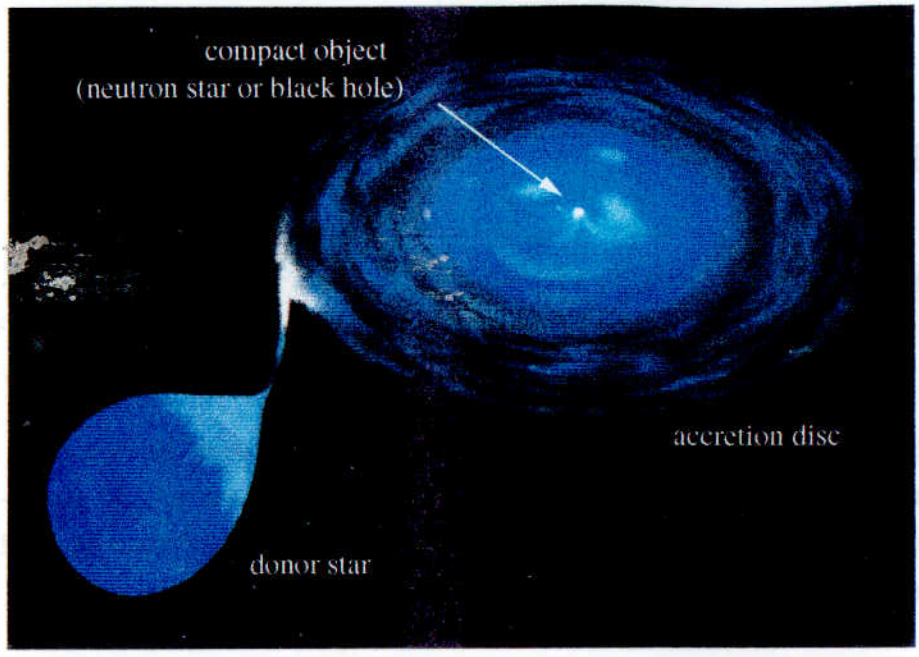

Figure 1.1 A schematic illustration of an X-ray binary in which accretion is taking place via an accretion disc (all LMXRBs and some HMXRBs).

strong fast stellar winds, and it is from the wind matter that accretion takes place, although some systems are also undergoing Roche-lobe overflow (RLOF). RLOF is a process in which matter flows from the gravitational well of the companion to that of the compact object via the inner Lagrangian point - such a process can occur as a result of an expanding companion, a shrinking orbit, or a combination of both. There is evidence that accretion may take place both with or without the presence of an accretion disc. HMXRB systems typically have periods of order a few days to a few weeks, and orbits are often eccentric. These systems often contain X-ray pulsars, indicative of the presence of a highly magnetised neutron star. In HMXRB systems the X-ray luminosity is generally comparable to or less than the optical luminosity of the OB star companion, ie. $L_X/L_{opt} \leq 1$. A large minority of the HMXRB systems ($\sim \frac{1}{3}$) are known to contain a Be star in which there is strong evidence for a circumstellar disc/equatorially concentrated wind through which the compact object may occasionally pass.

LMXRB systems are distinguished from HMXRBs primarily by the nature of the star that is companion to the compact object. In LMXRBs the neutron star or black hole forms a close binary with a lower main sequence dwarf, ie. the compact object is in general the more massive object. These systems typically have circular orbits with periods of ≤ 12 h, and are concentrated toward the galactic bulge and halo (12 in globular clusters). Accretion is via RLOF and an accretion disc, and this disc dominates the optical emission from the system. LMXRBs often display changes in X-ray 'colour' (ie. hardness ratios) attributed to periods of differing accretion rate. These systems also display rapid X-ray bursts, commonly interpreted as being runaway thermonuclear reactions on the surface of the neutron star. The formation of LMXRB systems remains a bit of a mystery as it appears that such systems should have been disrupted by the supernova explosion that formed the compact object. Gentler formation of a neutron star from a white dwarf via accretion-induced collapse (a possible cataclysmic variable $\rightarrow$ LMXRB channel) has been suggested. An important observational difference between the HMXRB and LMXRB systems is that in LMXRBs the X-ray luminosity is typically ~ 100 times the optical luminosity. Thus a determination of L_X/L_{opt} is often one of the first diagnostic tests applied to candidate XRB systems.

Table 1.1 summarises the gross characteristics of the high-mass and low-mass X-ray binaries (numbers from van Paradijs 1993 [3]). A good introduction to the mechanics of interacting binaries exists in chapter 17 of Bowers & Deeming (1984 [4]). More specifically, White (1989 [5]) and Verbunt (1993 [6]), present good introductions and reviews of the subject of X-ray binaries. The most up-to-date volume covering all aspects of the field at the time of writing is *'X-ray binaries'* (Lewin, van Paradijs & van den Heuvel (eds) 1995 [7]).

It should be made clear that not all XRB systems fit neatly into one of the above classes, for example three sources classed as LMXRBs are known to display X-ray pulsations (however no HMXRB systems are known to display X-ray bursts) (van Paradijs 1993 [3]). Note also that for many binary X-ray

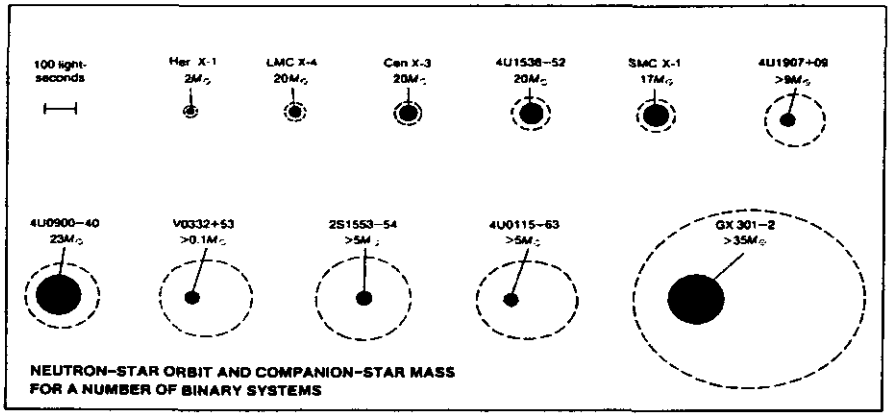

Figure 1.2 Estimated orbital parameters for a number of low and high mass X-ray binaries (Epstein, Lamb & Priedhorsky 1986)

Table 1.1 Typical properties of X-ray binaries in our galaxy

	HMXRB	LMXRB
Number known (1993)	69	124
Age	$\sim 10^6$ yr	$\sim 5 \times 10^9$ yr
Companion star type	OB	lower MS
Companion star mass	10-20 $M_\odot$	$\leq 2M_\odot$
Companion star abs mag	≤ -2	≥ 3
Typical orbital period	1-30 days	2-36 hr
Orbital eccentricity	often large	small
Phenomena	X-ray pulsations	X-ray bursts, *QPOs*
L_X/L_{opt}	≤ 1	~ 100

sources unequivocal identification of an optical counterpart has not yet been made.

The X-rays in XRB systems are produced as gravitational potential energy is converted into kinetic and finally thermal energy when matter plunges into the deep gravitational potential well of a compact object. Despite years of study however the exact method for extracting the gravitational potential energy to produce the extremely high temperatures observed (ie. $> 10^6 K$) remains unclear. See Frank, King & Raine 1992 [8] for a good introduction to the subject. The basic equation governing the amount of energy that

could theoretically be liberated is well known however :

$$L = \frac{MG\dot{M}}{R}$$

where M and R are mass and radius of accreting object, G is gravitational constant and $\dot{M}$ is accretion rate (assuming all gravtitational potential energy extracted).

Thus $L \propto M/R$ and so it can be seen that a neutron star with typical radius 10^6 cm and mass 1 $M_\odot$ is $\sim$ 1000 times more efficient at releasing stored energy via accretion than a white dwarf of similar mass but radius 10^9 cm. An important point to note is that for white dwarf systems hydrogen fusion is more efficient at extracting rest mass energy than accretion, while in neutron star and black hole systems accretion is the more efficient process.

1.2 Cygnus X-3 : A brief history

Cyg X-3 was discovered as the third X-ray source in the constellation of Cygnus in 1966 during a rocket flight (Giacconi et al 1967 [9]). During that time Cyg X-3 was one of many newly-discovered X-ray sources (the first non-solar source, Scorpius X-1, only having been discovered 4 yr earlier - Giacconi et al 1962 [10]) and did not seem to merit any particular attention. In 1972 however, the system leapt into the scientific limelight when a huge radio outburst from its direction was detected (Gregory et al 1972a [11]), prompting a concerted campaign of observations, primarily at radio wavelengths but also at shorter wavelengths (Gregory et al 1972b [12] et seq). During this campaign the X-ray satellites *Uhuru* and *Copernicus* discovered a 4.8 hour modulation of the flux from the source in the 2–6 and 4–12 keV bands respectively (Parsignault et al 1972 [13]; Sanford & Hawkins 1972 [14]) making Cyg X-3 the shortest-period XRB known at that time. This modulation has since been found to be very stable (when averaged over several periods), and is assumed to be the orbital period of the system. The radio observations of Cyg X-3 at this time allowed a precise position for the source to be determined. Equipped with this position Becklin et al (1972 [15]) were able to identify an infrared counterpart of 12th

magnitude in the K-band (2.2 μm). The search for an optical counterpart to the source however proved fruitless, to $\sim$ 24th magnitude (Westphal et al 1972 [16]). Observations at 3.3 mm (Pomphrey & Epstein 1972 [17]) were also made and these seemed to correlate well with the radio activity. 21 cm radio spectra obtained during this period of radio outbursts revealed absorption components which implied that Cyg X-3 lay beyond the local and Perseus spiral arms, placing it at a distance of $\geq$ 8 kpc (Laque, Lequeux & Hguyen-Quang-Rieu [18]) (see Fig 1.12).

Following the 1972 radio outburst it was widely acknowledged that Cyg X-3 was an unusual object and many efforts were made to determine the nature of this enigmatic system. Shortly afterwards Becklin et al (1973 [19]) discovered the 4.8 hour period in the infrared K-band (2.2μm). Since the infrared position had been determined from radio observations this confirmed the association between radio, millimetre, infrared and X-ray sources. The source has continued to erupt sporadically in the radio, with a mean separation between outbursts of $\sim$ 18 months (eg. Johnston et al 1986 [20]; Waltman et al 1994 [21]). VLBI imaging following one such outburst in 1982 revealed the source to be expanding (Geldzahler et al 1983 [22]); subsequent VLBI observations have revealed the presence of relativistic jets in the system following both minor and major flaring activity (eg. Spencer et al 1986 [23]; Molnar, Reid & Grindlay 1988 [24]; Schalinski et al 1995 [25]). This places Cyg X-3 in a select group of galactic X-ray sources with associated relativistic jets with only the celebrated source SS433 being better known (see chapter 6). X-ray satellites have also continued to observe Cyg X-3 and have found the 4.8 hour period to be extremely stable but lengthening on a timescale of tens of thousands of years (e.g. van der Klis & Bonnet-Bidaud 1989 [26]; Kitamoto et al 1992 [27]). A claimed detection of a 12.6 ms periodicity from Cyg X-3 in γ-rays (Chadwick et al 1984 [28]), interpreted as the spin period of an accreting neutron star, remains unconfirmed.

More recently, broad helium and nitrogen emission lines have been detected in infrared spectra of Cyg X-3 (van Kerkwijk et al 1992 [29]), leading to the assertion that Cyg X-3 is the first Wolf – Rayet + compact object

system discovered (van Kerkwijk 1993a [30]; Cherepaschuk & Moffat 1994 [31]). If correct, this moves Cyg X-3 to high-mass classification and makes it the shortest period HMXRB. This discovery has again placed Cyg X-3 back in the astronomical spotlight and reminds us of how little we really know about this bizarre source.

1.3 Observational characteristics across the spectrum

Apart from the energy range 1 eV – 1 keV (corresponding to optical V-band to the EUV), Cygnus X-3 has been detected across more than 20 decades of frequency. In this section I shall review in more detail the observational characteristics in the different observational regimes.

1.3.1 Radio

The behaviour of Cyg X-3 in the radio, both spectral and temporal, is extremely varied. For most of the time Cyg X-3 is in 'quiescent' or low-amplitude flaring states, characterised by flux densities of 50 – 500 mJy at cm wavelengths (where 1 mJy = 10^{-29} W m^{-2} Hz^{-1}). Much of the spectral data relating to these periods has come from long term monitoring by the NRL-Green Bank Interferometer (eg. Waltman et al 1994 [21]) which monitors the source daily at two frequencies in the cm band. The program is described in Waltman et al (1991 [32] – see also chapter 4), and since 1988 has been monitoring > 20 sources daily (including some of the other 'radio-jet' XRBs : SS433, LSI+61° 303 & GRS 1915+105 – see chapter 6) at 3.6 and 13.3 cm (Fig 1.4); some monitoring of the source in fact has been undertaken at NRL-GBI since September 1972. This monitoring has revealed that during periods of low radio activity in Cyg X-3 variations in flux density at the two wavelengths are well correlated with a fairly flat spectrum. Long term monitoring of Cyg X-3 has also been undertaken at 2 cm by Guy Pooley and colleagues using the Ryle Telescope at Cambridge. Chapters 3,4 & 5 utilise to varying degrees data from one or both of these

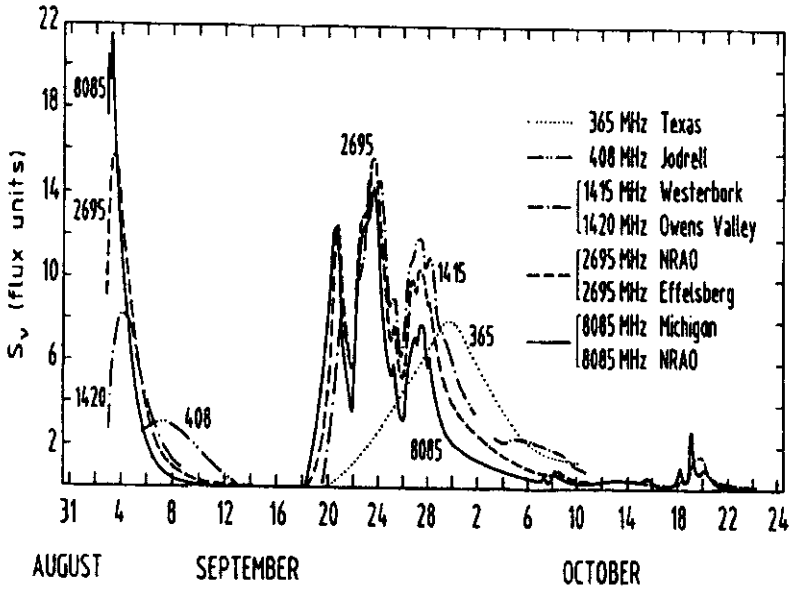

Figure 1.3 Multiwavelength radio monitoring of the 1972 Cyg X-3 radio outburst (from Bonnet-Bidaud & Chardin 1988)

monitoring programs.

During the remaining 5 – 10 % of the time the radio behaviour of Cyg X-3 becomes more dramatic. These periods are characterised by large and rapid increases in radio flux density, by a factor of up to 200 on a timescale of days. These radio flare events were first observed in autumn 1972, shortly after the discovery of a radio source coincident (within positional errors) with the X-ray position of Cyg X-3 (Braes & Miley 1972 [33]). The dramatic nature of the 1972 flare earned Cyg X-3 a dedicated issue of Nature Physical Sciences (vol 239, 1972 Oct 23), which contained no less than 23 papers documenting observations of the source (mostly at radio, but also at shorter wavelengths) (Gregory et al 1972b [12] et seq) (Fig 1.3). It was immediately realised that the flaring radio emission from Cyg X-3 could, at least qualitatively, be reconciled with an expanding volume of synchrotron-emitting electrons as described by van der Laan (1966 [34]), though this model was clearly too simplistic to explain the complex and varied radio

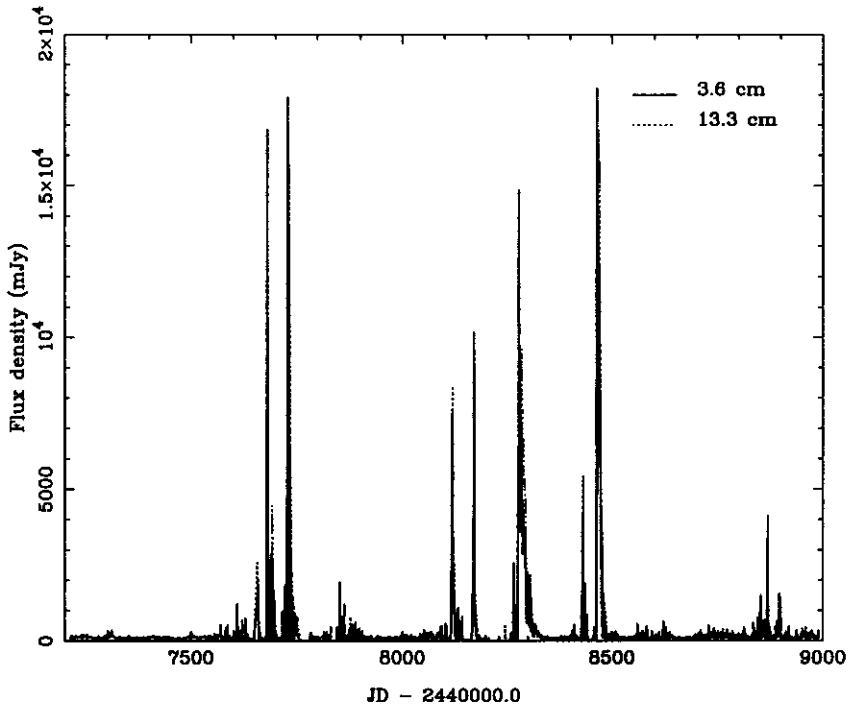

Figure 1.4 A four-year sample (1988–1992) of the Green Bank Cyg X-3 monitoring program, now in operation for over 10 years (Elizabeth Waltman, private communication

light curves in detail (Gregory et al 1972b [35]). The 1972 radio flare remains the most thorougly monitored flare event (see chapter 4 for more recent multi-wavelength observations of radio flares).

Flaring periods typically last between 20 and 40 days, and Waltman et al (1994 [21]) have shown that they appear to be always preceded by a phase of extremely low ($\sim$ 20 mJy) flux densities at cm wavelengths. These periods of extremely low flux densities typically last between 5 and 20 days, though there is no obvious correlation between the amount of time spent in this state and the magnitude of any subsequent flare (Waltman et al 1994 [21]). Watanabe et al (1994 [36]) have shown that periods of radio flaring activity are strongly correlated with X-ray high states (see section 1.3.5), though it should be noted that $\sim$ 7 yr earlier the opposite conclusion was drawn (see discussion in Apparao 1987 [37]).

Following the 1982 and 1983 flares, Cyg X-3 was found to be expanding as a radio source at a rate of about 0.01 arcsec/day (Geldzahler et al 1983 [22]). At a distance of $\sim$ 10 kpc (see section 1.4) this corresponds to an expansion velocity of $\sim$ 0.35c. The appearance of a jet following a radio outburst was confirmed by Spencer et al (1986 [23]) where limits in brightness differences between north and south jet lobes established that the jet axis lay close to the plane of the sky. Molnar, Reid & Grindlay (1988a [24]) also observed relativistic expansion of the source following low-amplitude flaring, with a velocity in the range 0.16 – 0.31 c. More recent work (Schalinksi et al 1995 [25]) is in good agreement with previous results. The jets are aligned roughly north-south, though they appear to be poorly collimated (but see discussion at end of chapter 4). This is the same orientation as an arcsec-scale double-lobed radio structure centred on Cyg X-3, reported by Strom, van Paradijs & van der Klis (1989 [38]), suggesting a connection between jets and lobes similar to that observed in the SS433 system, and also in radio galaxies. See Figs 1.5 and 1.6 for radio images of jet and lobe structure associated with Cyg X-3.

On a larger scale Wendker, Higgs & Landecker (1991 [39]) have observed the Cygnus X region at 6, 21 and 74 cm. They report a region of extended emission surrounding Cyg X-3, of approximately 2 arcmin extent, which they suggest is an HII region associated with the source. At a distance of 10 kpc (see section 1.4) this corresponds to a linear extent of $\sim$ 6 pc. Nebulae of a similar and even greater extent and with a ring or arc morphology have been associated with several galactic Wolf - Rayet stars (see sections 1.3.3 and 1.5 for a discussion of the W-R + c hypothesis for Cyg X-3) (e.g. Smith 1995 [40]; Nichols 1995 [41]).

During the 1972 radio flare Cyg X-3 was bright enough for 21 cm radio spectra to be taken (Laque, Lequeux & Nguyen-Quang-Rieu 1972 [18]) which revealed absorption components coincident with the local and Perseus galactic arms. These observations placed a lower limit on the distance to Cyg X-3 of $\sim$ 8 kpc. Subsequent observations revealed a third absorption component corresponding to a more distant galactic arm (Chu & Beijing

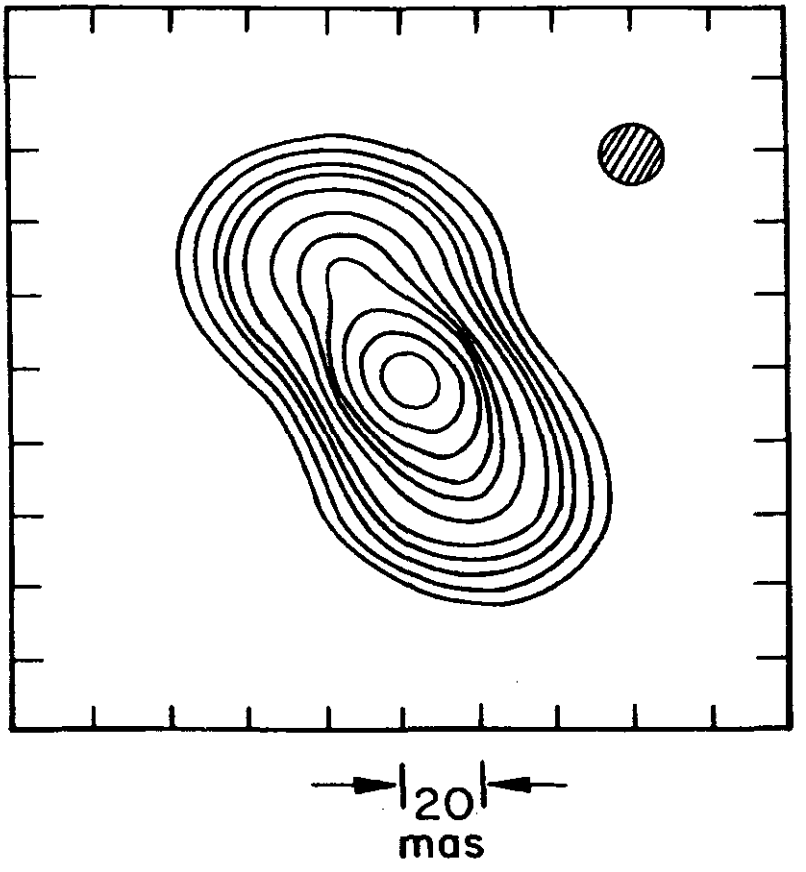

Figure 1.5 Milliarcsecond-scale radio jets revealed in high-resolution radio mapping of Cyg X-3 (Schalinksi et al 1995).

1973 [42]; Laque, Lequeux & Nguyen-Quang-Rieu 1973 [43]; Dickey 1983 [44]). This data was interpreted by Dickey (1983 [44]) as placing a lower limit on the distance to Cyg X-3 of (11.6 - 12.8)($\pi_\odot$/10 kpc), for a flat rotation curve, where $\pi_\odot$ is the galactocentric radius of the sun. The current best estimate for $\pi_\odot$ of $\sim$ 8.5 kpc places Cyg X-3 between 9.9 – 10.9 kpc.

Scattering of radio waves in the direction of Cyg X-3 has been shown to be anisotropic (Wilkinson, Narayan & Spencer 1994 [45]; Molnar et al 1995 [46]; chapter 3), though calculated position angles for the scattering do not entirely agree. This scattering is roughly perpendicular to the position angle

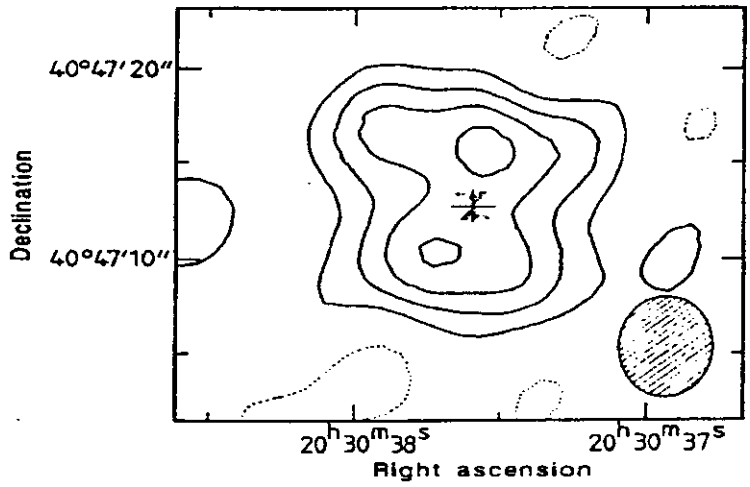

Figure 1.6 Arcsec-scale radio 'lobes' associated with Cyg X-3, roughly aligned with the radio jets (Strom et al 1989)

of infrared polarisation toward Cyg X-3 (Jones et al 1994 [47]), suggesting that scattering of radio waves is occurring perpendicular to the galactic magnetic field.

Models describing the radio emission from Cyg X-3, in particular the flaring behaviour, all concur as to the primarily non-thermal nature of the radiation. Most models of the flaring behaviour have their roots in the expanding synchrotron-emitting cloud formulation of van del Laan (1966 [34]). The idea that there is some significant mass ejection taking place is strongly supported by the VLBI observations of an expanding double-lobed source. However, it is still unclear as to where the magnetic field and shocks necessary to produce the synchrotron emission originate, or even how a binary system goes about ejecting matter via double jets in the first place. There are also problems in that the form of the decay of flares appears to change after a few days, being initially exponential in nature and subsequently power-law with time (eg. Gregory et al 1972b [35]; Hjellming, Brown & Blankenship 1974 [48]; Marti, Paredes & Estalella 1992 [49]; Waltman et al 1995 [50]). This is inconsistent with a simple adiabatically expanding

bubble model but Marti, Paredes & Estalella (1992 [49]) find that it can be explained by considering a double-sided jet which expands exponentially at first and then linearly. Most models also find it necessary to invoke some form of local absorption, whether due to thermal electrons mixed in with the ejecta or due to the dense wind in which the system appears to be embedded (eg. Marsh, Purton & Feldman 1974 [51]; Marti, Paredes & Estalella 1992 [49]; chapter 3).

1.3.2 Millimetre and submillimetre

*Millimetre observations of Cyg X-3 have been few and far between, sub-*millimetre even more so. The first observations of Cyg X-3 in this regime were those of Pomphrey & Epstein (1972 [17]) in which several detections were made of Cyg X-3 at 3.3 mm during the 1972 radio outburst. The flux densities observed were broadly compatible with being the high-frequency tail of synchrotron emission, and were consistent with the twin-jet model developed by Marti, Paredes & Estalella (1992 [49]) to explain the radio emission from Cyg X-3 in outburst. Baars et al (1986 [52]) observed Cyg X-3 simultaneously at 3.3 and 1.3 mm also during a period of flaring activity and found the flares to be much shorter in rise and decay time than those at cm wavelengths.

Previous to the observations reported in Chapter 3, no observations had been made of Cyg X-3 at mm wavelengths during a period of radio quiescence. Chapter 4 describes the first detections of Cyg X-3 at 0.85 & 0.45 mm. Recent (sub)millimetre observations by Tsutsumi, Peracaula & Taylor (*in press* [53]) confirm the anomalously strong mm emission reported in chapter 3.

1.3.3 Infrared

During the 1972 radio outburst Becklin et al (1972 [15]) used the accurately determined radio position of Cyg X-3 to identify an infrared counterpart of 12th magnitude. The relative brightness in the infrared combined with the lack of any optical counterpart immediately suggested a large degree of

interstellar extinction. This was to be expected, given that when looking toward Cyg X-3 one is looking along (at least) the local Cygnus and more distant Perseus spiral arms (see section 1.4). Observations the following year (Becklin et al 1973 [19]) revealed the same 4.8 hr periodicity as observed in X-rays during the 1972 radio outburst. This confirmed the association of radio and X-ray sources. Becklin et al (1973 [19]) also reported a prolonged period of unusually high fluxes in the infrared K-band, during which time the 4.8 h modulation could not be detected.

K-band (2.2 μm) infrared photometry simultaneous with X-ray observations (Mason et al 1976 [54]; Mason, Cordova & White 1986 [55]) has revealed the infrared and X-ray light curves to be in phase and to have very similar (though not identical) shapes (Fig 1.7). However, the degree of modulation in the two wavelength regimes is different, being much less in the infrared (Mason, Cordova & White 1986 [55]). Short timescale large amplitude flaring events are often seen superimposed upon the smooth orbital motion in the infrared (Fig 1.7). Mason, Cordova & White (1986 [55]) found however no X-ray fluctuations correlated with these flare events suggesting that the cause is not a variable accretion rate.

Molnar (1988 [56]) claimed that over several nights of observation in 1988 no infrared flaring events were observed from Cyg X-3, although at least half of the infrared observations of the source appear to display flaring activity (eg. Becklin et al 1973 [19]; Mason et al 1976 [54]; Mason, Cordova & White 1986 [55]; Jones et al 1994 [47]; see also chapters 2, 4 & 5). Mason, Cordova & White [55] suggest that the flares may be related to the injection of a very hot (10^6 K) thermal plasma into the base of the relativistic jets, while Apparao (1987 [37]) suggests that the flares may arise from interactions between clumps of matter in the system and a γ-ray beam. Both schemes predict radio activity correlated with infrared flares, a link which is yet to be established (but see chapters 4 and 5).

The continuum energy distribution of Cyg X-3 in the infrared is also poorly known due to the large degree of extinction towards the source. Molnar (1988 [56]) fit infrared photometric data to a thermal bremsstrahlung

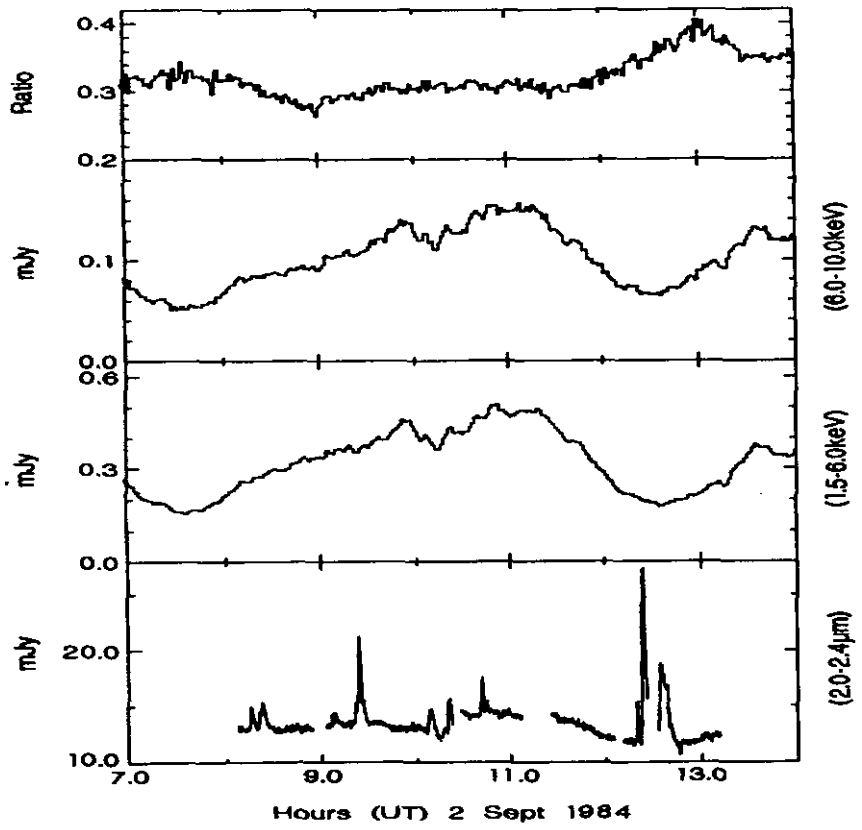

Figure 1.7 Simultaneous infrared and X-ray observations of Cyg X-3 (Mason, Cordova & White 1986). The top panel shows the ratio of the 6.0 – 10.0 keV flux to the 1.5 – 6.0 keV flux, illustrating the spectral hardening in X-rays around minimum light.

spectrum becoming optically thick in the near-infrared, and with an optical extinction of $19 \leq A_V \leq 29$ magnitudes. Van Kerkwijk (1993a [30]) suggests alternatively that the infrared continuum is better fit by a power law of spectral index $\alpha \sim +1.4$ - such power-law continuua appear to be common in galactic Wolf-Rayet stars (see below, and section 1.5) (Morris et al 1993 [57]), though +1.4 is at the steep end of observed spectral indices. The continuum level also appears to vary by $\sim 20\%$ independently of the 4.8 h modulation.

In 1992 van Kerkwijk et al (1992 [29]) discovered strong broad emission

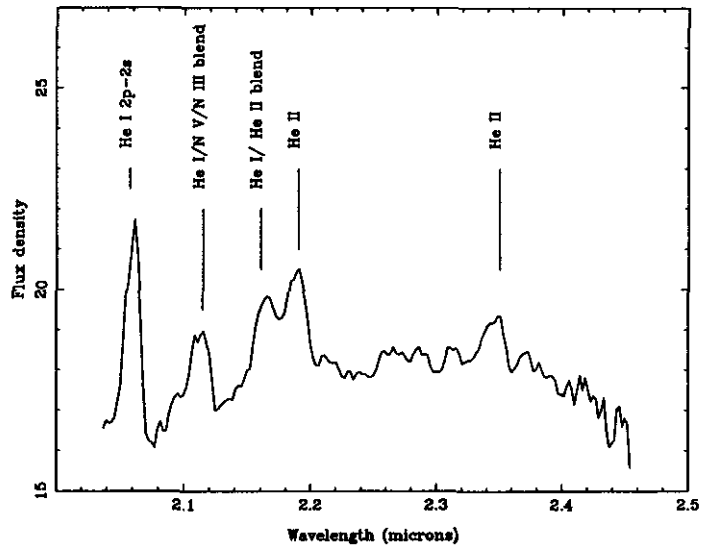

Figure 1.8 K-band infrared spectrum of Cyg X-3, obtained at UKIRT in 1991, displaying strong broad lines of He I, He II and N. Adapted from van Kerkwijk et al 1992.

features of helium and nitrogen in the K and I-band infrared spectra of Cyg X-3 (Fig 1.8), leading to the suggestion that Cyg X-3 is the first observed Wolf - Rayet + compact object (W-R + c) system discovered. If this assertion is correct and Cyg X-3 contains a massive Wolf-Rayet star then Cyg X-3 becomes the shortest-period HMXRB. Further infrared spectroscopy revealed the emission lines to be Doppler shifting with velocity shifts of up to ± 1500 km s^{-1} (see section 1.5 for the model developed by van Kerkwijk to explain this and the smooth modulation of the infrared continuum in phase with the X-rays).

More recently infrared polarimetric observations (Jones et al 1994 [47]) have revealed that the position angle of interstellar polarisation towards Cyg X-3 is perpendicular to the major axis of radio scattering towards the source. These infrared observations also imply a polarisation component inherent to Cyg X-3 which they suggest may be indicative of an accretion disc in the system.

1.3.4 Optical and UV

An optical V-band counterpart to Cyg X-3 has to date escaped detection, due to the extremely heavy interstellar absorption in the direction of the source ($A_V > 20$ mag). The lack of an optical spectum deprives astronomers of one their most tried and tested diagnostic tools and is in part responsible for the large degree of speculation as to the true nature of the source.

During the 1972 radio outburst an attempt was made to identify an optical counterpart to the source - this was unsuccessful but provided an upper limit of 24th magnitude in the V-band (0.55 μm) (Westphal et al 1972 [16]). No successful detection has to date been made in this band, or at shorter optical or UV wavelengths. However, Wagner et al (1990 [58]) have detected a red optical counterpart in the R-band (0.77μm) of magnitude 23.8 $\pm$ (Fig 1.9). This single 16σ observation required 5.6 hours of integration on a medium-sized telescope (the Perkins 1.8 m, Ohio, USA), illustrating the difficulty of such a program. This remains the only good red optical detection (though see chapter 4 for a new marginal detection). The extreme faintness of the source in this band may mean that it won't be until the next generation of 8 m and/or adaptive optics telescopes that a red optical spectrum becomes feasible.

1.3.5 X-ray

Following its discovery in the 1.5 – 12 keV band by rocket flight in 1966 (Giacconi et al 1967 [9]), Cyg X-3 has been observed by nearly all X-ray satellites, including *Uhuru* (Parsignault et al 1972 [13]), *Copernicus* (e.g. Sanford & Hawkins 1972 [14]), *Vela 5B* (e.g. Priedhorsky & Terrel 1986 [59]), EXOSAT (e.g. Rajeev et al 1994 [60]; Berger & van der Klis 1994 [61]), COS-B (e.g. van der Klis 1993 [62]), ROSAT (e.g. Predehl & Schmitt 1995 [63]), *Tenma* (e.g. Kitamoto et al 1987 [64]), *Ginga* (e.g. Kitamoto et al 1992 [27]) and *Asca* (Kitamoto et al 1994 [65]).

The most obvious feature of the X-ray observations is the 4.8 hour modulation (Fig 1.7), assumed to be the orbital period of the system. First reported by Parsignault et al (1972 [13]) and Sanford & Hawkins (1972 [14])

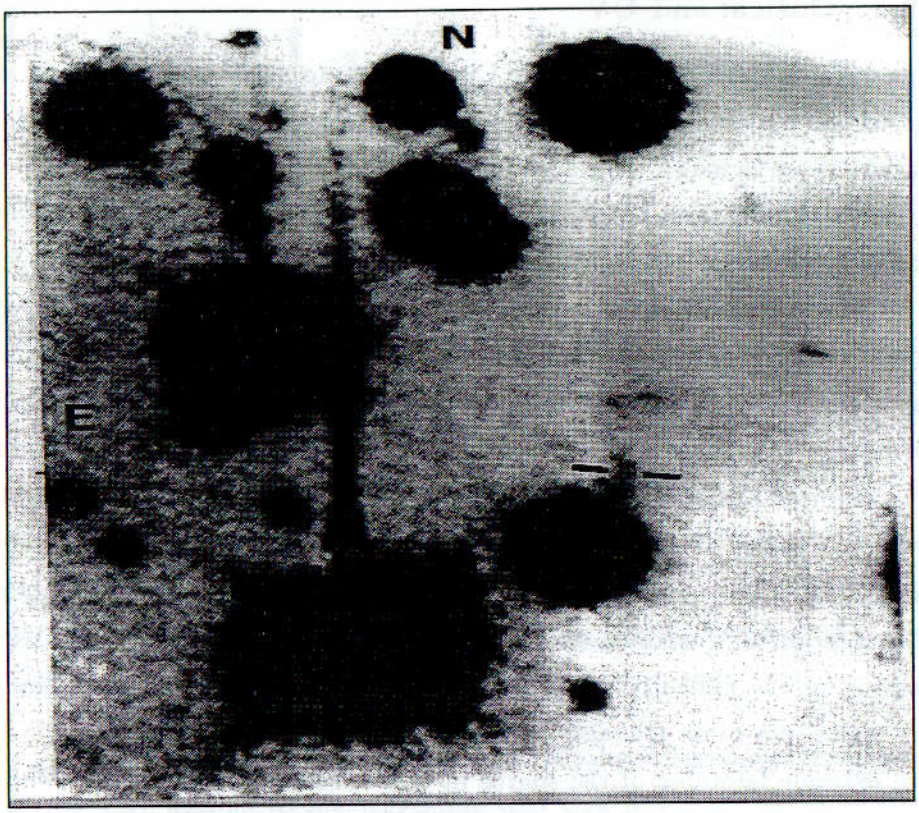

Figure 1.9 24th magnitude red-optical counterpart to Cyg X-3, indicated by tick marks (Wagner 1990)

during the 1972 radio flare, the profile of the modulation may vary from cycle to cycle but is extremely stable when averaged over several orbital periods, generally displaying an aysmmetric sinusoidal-type form (e.g. van der Klis & Bonnet-Bidaud 1989 [26]; van der Klis 1993 [62]). The source is observed to become harder in X-rays at orbital minimum (eg. Mason, Cordova & White 1986 [55]; Fig 1.7). During at least one observation however, when Cyg X-3 was in an extremely bright X-ray state, the light curve was seen to become more symmetric in form (van der Klis 1993 [62]). Using EXOSAT data Willingale, King & Pounds (1985 [66]) have shown that the degree of modulation with the 4.8 h period is approximately constant below $\sim$ 10 keV, but that above this energy it drops sharply. Molnar (1985) [67] has shown that when the phase-scattering effect of the observed dust halo

around Cyg X-3 is taken into account the degree of modulation continues to increase with decreasing energy below 10 keV, reaching an estimated $\sim$ 70 % at 1 keV. However Matz et al (1994 [68]) has shown that there is in fact also strong modulation ($\geq$ 40%) in hard X-rays in the energy range 47–120 keV, suggesting that a different scattering mechanism may be in effect than that which dominates at lower energies. The depth of modulation of the 4.8 h period is also seen to increase with X-ray brightness (e.g. van der Klis et al 1993 [62]). Simultaneous observations in 1984 in X-rays (1.5 - 10 keV) and in the infrared K-band (2.2 μm) showed the X-ray and infrared light curves to be extremely similar (though **not** identical) over one cycle when a scaling factor was introduced (Mason, Cordova & White 1986 [55]) (Fig 1.7).

Fitting of parabolic ephemerides to the X-ray light curve has revealed the period to be increasing on a timescale $P/\dot{P}$ of 7.35(7) $\times 10^5$ yr (e.g. van der Klis & Bonnet-Bidaud 1989 [26]; Kitamoto et al 1992 [27]). Cubic ephemerides have been shown by these authors to produce significantly better fits, but uncertainty as to the nature of any intrinsic scatter in the X-ray arrival times *and* variations in methods of pulse-timing lead to uncertainty as to the reality of any second-order period derivatives (see also chapter 5). Van Kerkwijk (1993b [69]) has proposed that the period increase is due to loss of angular momentum from the system in the form of a dense wind at a rate of $\dot{M} \sim 10^5 M_\odot$ yr^{-1}; this is however an order of magnitude or so less than the value for $\dot{M}$ derived from observed 'continuum' infrared flux densities (van Kerkwijk 1993b [69]). The period increase may alternatively be an observational manifestation of a precessing elliptical orbit (Elsner et al 1980 ([70]; Kitamoto et al 1992 [27]), in which case a slow-down in the rate of period increase may be expected - this may be the second-order period derivative mentioned above. The best fit parabolic ephemeris from van der Klis & Bonnet-Bidaud (1989 [26]) is described in Table 1.2. See chapter 5 for a new cubic ephemeris derived from previous X-ray observations combined with new OSSE hard X-ray data.

Cyg X-3 exhibits two relatively clearly defined X-ray states : the high-

Table 1.2 Parabolic ephemeris of van der Klis & Bonnet-Bidaud (1989)

$T_n = T_0 + P_0 n + c_0 n^2$	
Parameter	Fitted value
T_0	$2440949.89622 \pm 0.00094$ HJD
P_0	$0.19968354 \pm 0.00000015$ d
c_0	$(9.03 \pm 0.48) \times 10^{-11}$ d

and-soft state, and the low-and-hard state, ie. X-ray spectral hardness is anticorrelated with X-ray brightness (e.g. Hermsen et al 1987 [71]; Watanabe et al 1994 [36]). The changes in X-ray spectrum are primarily at lower energies (e.g. Willingale, King & Pounds 1985 [66]) : the spectrum below 15 keV is essentially flat in low-state, but in high state resembles a $\sim$ 1.2 keV black body. The hard X-ray tail is well described by a power-law and is not thought to exhibit the spectral variations of the soft X-rays though OSSE data at energies up to $\sim$ 300 keV (Matz et al 1994 [68]) may show an analagous spectral softening in high state. Matz et al (1994 [68]) also observed a significant decrease in the 47-120 keV flux from Cyg X-3 shortly before a radio flare in 1991 – observations made after the decline of the radio flare show Cyg X-3 had returned to a higher, steadier flux level. The transition between states at lower X-ray energies is smooth and takes typically days or weeks (e.g. Priedhorsky & Terrel 1986 [59]; see Fig 1.10). Watanabe et al (1994 [36]) have established a link between X-ray high state and enhanced radio activity – more specifically long-term data is consistent with Cyg X-3 always having been in a high X-ray state during periods of radio flaring. In its high state the X-ray luminosity of Cyg X-3, at a distance of 10 kpc, is $\geq 10^{38}$ erg s^{-1}, placing it at the Eddington luminosity limit for a solar mass object. Fig 1.10 plots 7 yr of X-ray monitoring of Cyg X-3 with the Vela 5B satellite, illustrating the smooth changes in mean X-ray flux, and also shows that the source was in a relatively bright state during the 1972 radio flares.

Shorter-period X-ray fluctuations are also observed (Kitamoto et al 1992

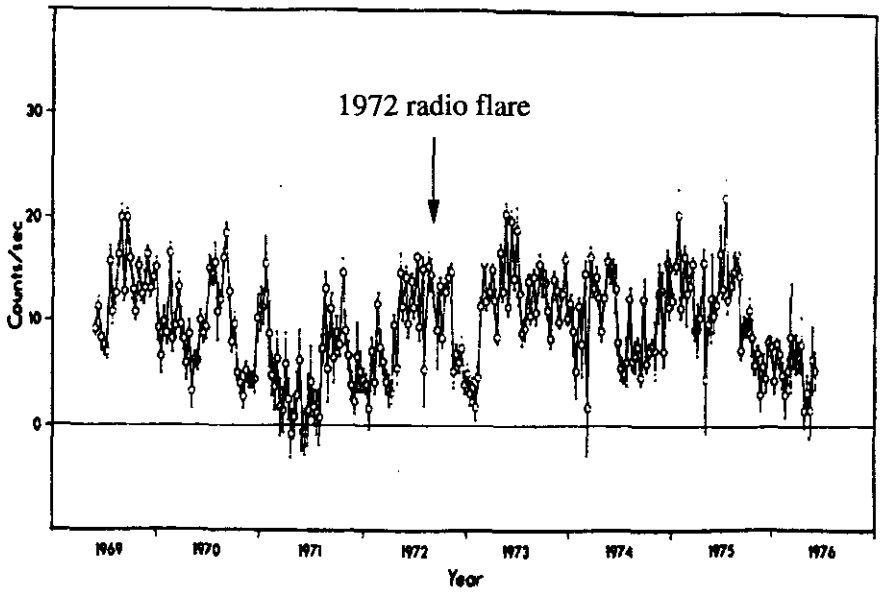

Figure 1.10 Seven years of X-ray lightcurve of Cyg X-3 from Vela 5B data, showing high and low states. Arrow indicates time of giant 1972 radio flare

[27]), most significantly on timescales of ten seconds or longer, with a limiting frequency of $\sim$ 1 Hz. Kitamoto et al (1992 [27]) also found that fluctuations in the 1.2 – 4.6 keV band lag those in the 4.6 – 9.3 keV band by about 3 sec, and those in the 9.3 – 18.5 keV band by about 10 sec. Several observations have suggested that short-timescale X-ray fluctuations occur preferentially near X-ray maximum (e.g. Willingale. Kind & Pounds 1985 [66]; Kitamoto et al 1992 [27]). The *Ginga* observations also recorded a 20% drop in X-ray brightness on a timescale of 16 sec, limiting the size of the emitting region to $\leq 4.8 \times 10^{11}$ cm.

From the earliest X-ray satellite observations it was clear that Cyg X-3 posessed an exceptionally strong iron line at $\sim$ 6.4 keV (eg. Kestenbaum et al 1977 [72]). Recent observations with the *Asca* satellite (Fig 1.11) have resolved this 'line' into three emission components and an absorption edge (Kitamoto et al 1994 [65]) – two of the emission components are from helium-like (6.67 keV) and hydgrogen-like (6.96 keV) ions whilst the third

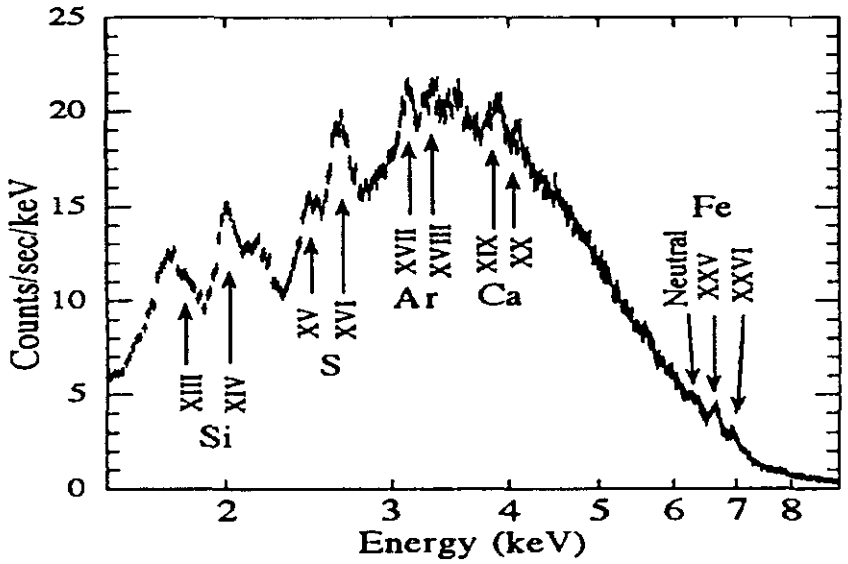

Figure 1.11 *ASCA* X-ray spectrum of Cyg X-3 (Kitamoto et al 1994)

(at 6.4 keV) comes from 'neutral' (i.e. low ionisation) iron, thus clearly indicating the presence of both extremely hot and relatively cool gases in the system. Phase-resolved observations of the highly-ionised lines find that they modulate in strength and width in **antiphase** with the continuum – i.e. maximum line strength at minimum light (Kitamoto et al 1994 [65]). The *Asca* spectrum also reveals the presence of emission lines of ionised sulphur, silicon, argon and calcium (Fig 1.11).

Kafuku et al (1994 [73]) have found that Cyg X-3 is surrounded on a scale of 2° by an X-ray scattering halo, similar to that found around SS433 (although it should be noted that in Cyg X-3 the halo is **not** aligned with the radio jets, as is the case with SS433). Predehl & Schmitt (1995 [63]) have also mapped the dust scattering halo around Cyg X-3 out to a distance of several hundred arcsec and have shown that up to 40% of the soft X-ray emission from the source may arise in the halo.

The complex observational characteristics of Cyg X-3 in the X-ray region alone have necessitated the development of some elaborate theoretical models in a bid to understand and explain what is observed (e.g. Davidsen

& Ostriker 1974 [74]; White & Holt 1982 [75]; Nakamura et al 1993 [76]). A feature common to all models is the requirement for emission from regions at different temperatures and the presence of several separate scattering media.

1.3.6 γ-rays and neutral particles

Cyg X-3 is clearly a strong source out to several hundred keV (e.g. Matz et al 1994 [68]; see also Bonnet-Bidaud & Chardin [77] for a good review of X- and γ-ray properties); however, above 0.5 MeV detections of the source become sporadic, possibly untrustworthy. In the early 70s, detections of Cyg X-3 at energies above 30 MeV were reported both from rocket flights (e.g. Galper et al 1975 [78]) and from the SAS-2 satellite (Lamb et al 1977 [79]). The SAS-2 data appeared to show modulation with the 4.8 h period, leading Lamb et al (1977 [79]) to claim that Cyg X-3 was a strong source at energies > 35 MeV. Susbsequent observations in the same energy regime by the COS-B satellite failed however to confirm the SAS-2 detection (Hermsen et al 1987 [71]). The COS-B group went on to suggest that the SAS-2 data had been misinterpreted and that their observations were consistent with no point source emission in the direction of Cyg X-3. However, a reanalysis of the SAS-2 data (Fichtel, Thomas & Lamb 1987 [80]) disputes the conclusions of the COS-B group and instead suggests that Cyg X-3 has declined in brightness at MeV energies. It should be noted that both the rocket flight and SAS-2 observations were made only a few months after the giant 1972 September radio flare, whereas the COS-B observations were made during a period of radio quiescence. However, more recent observations in the 20 MeV - 30 GeV range by the EGRET instrument onboard GRO, both shortly before and shortly after radio flare events, failed to make any detection of Cyg X-3 (Michelson et al 1992 [81]).

At energies of above $\sim$ 100 TeV (10^{14} eV), often referred to as the Ultra-High-Energy (UHE) regime, there have been many claimed but few confirmed, detections of Cyg X-3. In 1983 Samorski & Stamm (1983 [82]) claimed that archival data from the Kiel air shower array (designed to observe cosmic rays) showed a 4.4 σ excess from the direction of Cyg X-3 at

energies above 2 PeV. This claim prompted many further attempted observations of Cyg X-3 and other 'similar' sources (Her X-1, Vela X-1 etc) and many groups reported (albeit marginal) positive detections. UHE γ-ray emission seemed to come at a prefential phase in the 4.8 h period of Cyg X-3 (most commonly between phases 0.5 – 0.7) and many sites claimed enhanced PeV emission during, or shortly after, radio flare events. In 1985 Chadwick et al (1985 [28]) claimed a 12.6 ms period in TeV γ-ray emission from Cyg X-3, indicating the presence of a millisecond pulsar in the system. Subsequent observations by the same group (Bowden et al 1992 [83]) and by a group based at Woomera in Australia (Gregory et al 1990 [84]) appeared to confirm this detection. More recent attempted observations have however failed to detect Cyg X-3 at PeV energies. Protheroe (1994 [85]) claims that this is in fact unsurprising, given that the UHE γ-ray emission from Cyg X-3 was seen in a number of 'good' detections to be declining during the 1980s and he suggests that Cyg X-3 is at present in a γ-ray 'low' state. Other authors (e.g. Molnar 1985 [67]; Weekes 1991 [86]) draw more pessimistic conclusions, and cast doubt on the reality of any of the detections.

Cyg X-3 has also been claimed to be a source of emission at EeV (10^{18} eV) energies. Given that the decay length of a neutron at 1 EeV is $\sim$ 9 kpc, it has been suggested that Cyg X-3 is a source of high-energy neutrons (or even of some new neutral particle, the 'Cygnet' – e.g. Baym 1986 [87]) - see Protheroe (1994 [85]) for a discussion.

1.4 Location and distance

The distance to Cyg X-3 has been determined primarily by 21 cm HI spectroscopy while the source was in outburst. This was initially carried out by Laque, Lequeux & Nguyen-Quang-Rieu (1972 [18]) who discovered absorption components coincident with the velocities of the local and Perseus spiral arms. A third absorption component, effectively corresponding to the limit of the galactic disc in the direction of Cyg X-3 was later discovered (e.g. Laque, Lequeux & Nguyen-Quang-Rieu 1973 [43]). Further observations

using the VLA after a radio outburst in 1982 (Dickey 1983 [44]) confirmed the existence of the third absorption component and concluded that Cyg X-3 was at the edge of our galaxy if not further. Fig 1.12 illustrates the line of sight and minimum distance (from 21 cm radio observations) in the Milky Way.

The distance to Cyg X-3 has also been estimated from γ-day observations : Cawley & Weekes (1984 [88]) have shown that if the detections of γ-rays of energy $\geq 10^{15}$ are real (far from being universally accepted – see above) then Cyg X-3 is not likely to be much further than the minimum distance to the source (now $\sim$ 9 kpc; at the time of writing of their paper the galactocentric distance was believed to be $\sim$ 10 kpc and so their adopted minimum distance based upon the 21 cm observations described above was 11.4 kpc). This is because photon–photon pair production would cause signifcant absorption of such high energy γ-rays and, when this is taken into account, even at a distance of 30 kpc high–energy γ-rays would become the dominant energy channel with a luminosity of $\sim 10^{39}$ erg s^{-1}. At 100 kpc, Cyg X-3 would have a γ-ray luminosity in excess of 10^{43} erg s^{-1} !

A further very strong argument favouring the association of Cyg X-3 with our galaxy was made by Bonnet-Bidaud & Chardin (1988 [77]) who noted that in order that the observed expansion of Cyg X-3 following radio outbursts not be superluminal, the source can lie no further away than 30 kpc (although in the case of apparent superluminal motions this limit could be extended somewhat). Thus the association of Cyg X-3 with our galaxy is beyond doubt.

It should also be noted that some authors, including Schmutz (1993 [89]) have suggested that Cyg X-3 is in fact far closer than the lower distance limit implied by the 21 cm radio observations. He suggests that the absorption features may be due to circumstellar shells local to the source and that Cyg X-3 is in fact closer and less luminous than is generally accepted. It seems unlikely however that the velocities of circumstellar shells should mimic so well the known velocities of the spiral arms along the line of sight to Cyg X-3.

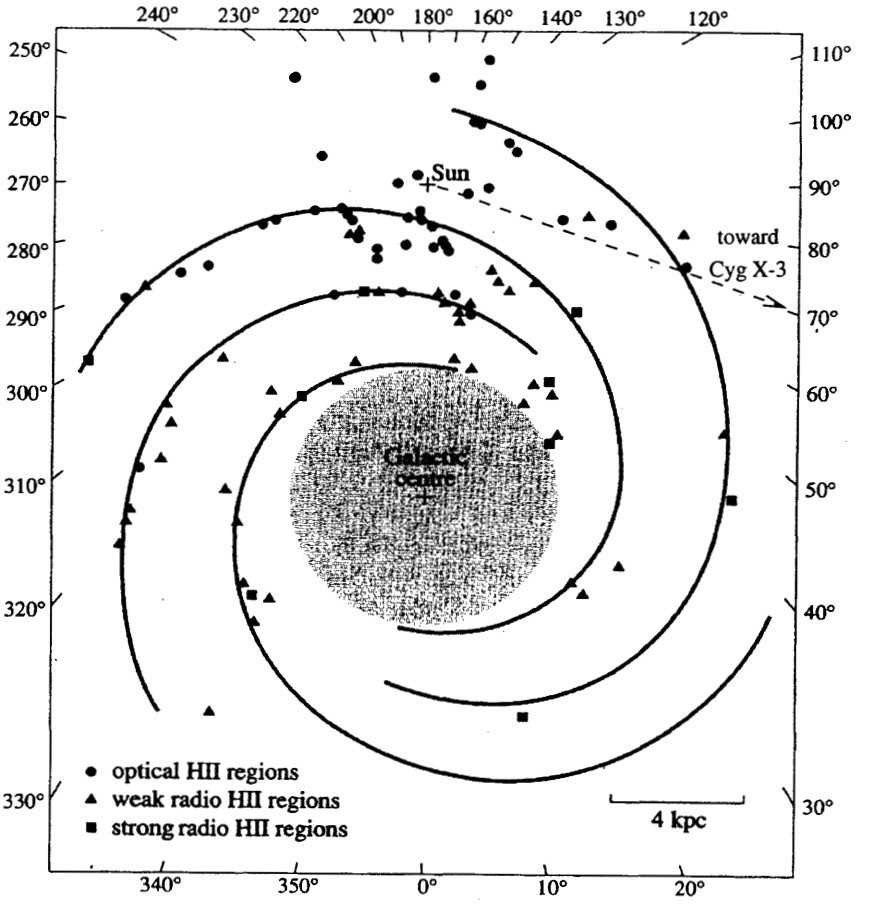

Figure 1.12 The location of the Sun and the direction to Cyg X-3 indicated on a plot of the distribution of HII regions in our galaxy and the inferred spiral arm structure. The minimum distance to Cyg X-3 places it roughly at the end of the arrow, the maximum distance calculated from observed expansion velocities (van der Klis & Bonnet-Bidaud 1989) places it about half as far again. Adapted from Adams et al (1994)

1.5 Some models

Many models have been put forward to explain the complex observational properties of Cyg X-3. We review three here in which Cyg X-3 has been described variously as a cocooned red dwarf + white dwarf system, an LMXRB system and as the first observed Wolf-Rayet + compact object system. It should be noted that no single model has attempted to explain the behaviour of Cyg X-3 across the spectrum. Physical models of the Cyg X-3 system tend to be driven by the need to explain the observed light curves and behaviour of spectral lines in the infrared and X-rays. Models for the radio jets and possible γ-ray emission generally exist somewhat independently from those concerned with the infrared and X-ray regimes.

Davidsen & Ostriker (1974 [74]) produced a comprehensive model in which the Cyg X-3 system comprised a white dwarf accreting matter from a red dwarf companion in the manner of U Geminorum. The phasing of the X-ray and infrared light curves was explained by placing the system within a cocoon of matter, possibly caused by a dense wind from the red dwarf. The cocoon absorbs UV and low-energy X-rays and reradiates in the infrared; higher energy X-rays scatter their way out. When the white dwarf is furthest from us the X-ray flux is naturally lower, and so, as a result, is the secondary infrared flux from the side of the cocoon facing us.

In 1982 White & Holt ([75]) proposed a model in which the Cyg X-3 system was a LMXRB with an accretion disc and accretion disc corona (ADC). The ADC is described as a corona of hot gas evaporated from the disc by radiation from the source, but still gravitationally bound, so corotating with it. Scattering of soft X-rays by the ADC was invoked to explain their modulation, and a bulge in the accretion disc (at the point where the accretion stream from the companion connects to it) invoked to explain the asymmetric minimum. The ADC model was very successful in describing the X-ray behaviour of Cyg X-3, and White & Holt (1982 [75]) concluded that the companion object to the compact object was either an extremely low-mass ($M \leq 0.05 M_{\odot}$) white dwarf or, more probably, a lower main sequence dwarf.

Following the discovery of broad emission features in I and K-band in-

frared spectra of Cyg X-3 (van Kerkwijk et al 1992 [29]), van Kerkwijk (1993b [69]) has proposed a model in which the Cyg X-3 system consists of a neutron star orbiting in a very tight (ie. almost 'grazing' the surface) orbit about a helium star core from which a hot dense wind originates. One of the cornerstones of this model, indeed of the entire identification of Cyg X-3 as a WR+c binary, is that Wolf-Rayet stars have small dense helium cores. This is in contrast to many widely-accepted models which would require a Wolf-Rayet star as luminous as that in the Cyg X-3 system to be larger than the orbital separation implied by a 4.8-hr period. Schmutz (1993 [89]) has in fact called into question the distance determination to Cyg X-3 as one solution to this dilemma. In the model of van Kerkwijk (1993b [69]) the observed modulation of the emission lines is due to the lines being observed primarily from that region of the wind shadowed from the X-ray emitting region by the helium star companion. This region, being cooler, also has a larger effective infrared photosphere and can obscure some of the smaller hotter photosphere in the X-ray irradiated region. This model neatly explains the modulation of the emission lines and the X-ray and infrared light curves being in phase.

Several other models have been put forward to describe the observed properties of Cyg X-3, and though very diverse, most share some common assumptions :

(i) The steady 4.8 h modulation in the infrared and X-rays is orbital in origin and is increasing with time (though see Molteni et al 1980 [90] for discussion of a possible 34.1 day orbital period).

(ii) The primary source of the X-ray emission is accretion onto a compact object (though see e.g. Lipunov et al 1994 [91] for models where the X-ray emission is rotation powered by the spin-down of a new pulsar).

(iii) The observed X-ray spectrum and variability (and probably infrared emission) requires a scattering medium (whether cocoon, ADC or stellar wind).

(iv) The radio emission is synchrotron in origin and the radio flares are associated with ejections of quantities of matter in a bipolar outflow at near-

relativistic speeds.

It should also be noted that some features of the models described above may be transferable to other models – e.g. a massive X-ray binary system with an accretion disc may produce an ADC, emission lines may come from the shaded region of a wind even if the companion is not a massive Wolf - Rayet star, etc.

1.6 This thesis

This thesis is based upon a series of observations of Cygnus X-3 across a wide range of wavelengths over a period of $\sim$ 10 years. Some of the observations were made by myself, some by others; nearly all involved collaborators across the world to a greater or lesser degree. Table 1.2 lists the various observations, along with the principal observer and chapter in which the data and analyses are presented.

The intention has been that this chapter serve as an introduction to XRBs in general, and Cygnus X-3 in particular. I shall conclude the chapter with an overview of the other chapters.

Chapter 2 describes observations made over three nights at UKIRT in 1984 August. These observations were made by others but the data reduction and the majority of analysis and interpretation is my own. Photometric and low-resolution spectroscopic observations provide much information on the orbital modulation, infrared flares and 1-5 μm infrared continuun of the source.

Chapter 3 presents observations made over a 48 h period in 1993 September, simultaneously with the MERLIN and Ryle Telescope radio interferometers in the UK, and the JCMT (sub)millimetre telescope in Hawaii. The JCMT observations were carried out by myself and S. J. Bell Burnell, and I performed the data reduction. I assisted in the reduction of the MERLIN data, and the drawing together of the different data sets, interpretation, and model developed are my own. These were the first observations at millimetre wavelengths during a period of radio quiescence in Cyg X-3 and revealed

unexpectedly high flux levels and steep spectral index at 2.0 and 1.1 mm.

Chapter 4 describes observations made during a $\sim$ 40 day period in 1994 February and March during which time Cyg X-3 underwent a series of medium-sized radio flares. While not directly involved in the observations, I was the driving force behind the UKIRT & JCMT observations, and performed the assimilation of the different data sets, analysis and development of models. We were able to obtain, at short notice (and as a result of the generosity of those people at the telescopes) (sub)millimetre and infrared observations during a period of intensive radio monitoring.

Chapter 5 presents the largest and most multi-wavelength data set, from a period in 1994 June-July when Cyg X-3 was observed in the radio, infrared and hard X-rays. I made and reduced the UKIRT observations personally. Other data was reduced by a variety of observers, but I was responsible for the analysis and interpretation of the data, except for the hard X-ray data which was primarily analysed and interpreted by S. M. Matz. Highlights of the data include a pseudo-simultaneous orbital light curves in four infrared bands displaying orbital colour changes, correlated hard X-ray and infrared behaviour and the discovery of much faint and complex infared structure within a few arc seconds of Cyg X-3.

Chapter 6 concludes the thesis with a look at the growing class of radio-jet X-ray binaries, including results from some preliminary multiwavelength observations of a number of them.

Table 1.3 Observation log

Date	Spectral regime	Instrument	Principal observer	Chapter
1984 Aug (Cyg X-3)	Infrared	UKIRT	S J Bell Burnell	2
1991 Aug (Cyg X-3)	Infrared	UKIRT (service)	S J Bell Burnell	5
1993 Sep (Cyg X-3)	mm	JCMT	R P Fender	
	Radio	Ryle Telescope	G G Pooley	
	Radio	MERLIN	R E Spencer	3
1994 Feb (Cyg X-3) (**radio flare**)	Infrared	UKIRT (T-of-O)	R P Fender	
	mm	JCMT (T-of-O)	R P Fender	
	Radio	Ryle Telescope	G G Pooley	
	Radio	NRL-GBI	E B Waltman	4
1984 Jun – Jul (Cyg X-3)	Hard X-ray	GRO (OSSE)	S M Matz	
	Infrared	INT (service)	R P Fender	
	Infrared	UKIRT	R P Fender	
	Infrared	TCS	P D Roche	
	Radio	NRL-GBI	E B Waltman	5
1994 (four candidate radio-jet XRBs)	mm	JCMT	R P Fender	6
1994 – 1995 (GT 2318+620)		Ryle Telscope	R P Fender	
	Radio	NRL-GBI	R P Fender	6
1995 Apr (GRS 1915+105)	Infrared	UKIRT	R P Fender	
	Radio	Ryle Telscope	R P Fender	
	Radio	NRL-GBI	E B Walman	6

Chapter 2

Flaring and quiescent infrared observations of Cygnus X-3 : 1984 August & 1991 July

2.1 Introduction

I present several sets of infrared observations of the galactic X-ray binary Cygnus X-3, possibly the first Wolf - Rayet plus compact object system discovered. High time resolution simultaneous H and K-band photometry over $\sim$ 1.5 orbital periods reveals the 4.79 hour orbital modulation, superimposed upon which are several extremely rapid flare events with rise times tens to hundreds of seconds. Analysis of the flaring component for both rapid flare events and for one prolonged period of very high infrared fluxes leads us to the conclusion that the emission mechanism of the flaring component is probably optically thin free-free, though synchrotron emission cannot be excluded. I find the infrared luminosity of Cyg X-3 can exceed 10^{36} erg s^{-1} during such periods. Data in the M, L′, L, K, H and J bands are combined with shorter wavelength data from the literature to produce a dereddened continuum from 0.8 - 4.8 μm. This is used to constrain the extinction to the source in the range $A_J = 6.0 \pm 1.5$ mag. Low-resolution K-band CVF spectra are consistent with the companion to the compact object in Cyg X-3 being a Wolf-Rayet object of the nitrogen-rich WN subclass. Flux densities of the nearby object 'Star Z' are found to be consistent with those

observed previously. A summary of the work presented in this chapter has been published in Fender & Bell Burnell (1994 [92]).

In section 2.2 I shall present our data from 1984 and 1991 UKIRT observations. In section 2.3 I shall look in more detail at the infrared flares and physical parameters which can be derived from them. In section 2.4 I shall discuss the nature of the infrared continuum, combining our data with I and R-band results from the literature and dereddening to account for the high degree of extinction by the ISM. Section 2.5 deals with the orbital modulation of the infrared light curves. Section 2.6 deals with our low-resolution K-band spectra which are consistent with a WNL classification.

2.2 Observations

I report here observations obtained with the United Kingdom Infrared Telescope (UKIRT) on Mauna Kea, Hawaii, between 1 - 5 μm on the nights of 1984 Aug 07-09. The observations comprise J, H, K, L, L$'$ and M-band photometry whilst the source was both in quiescent (Aug 07) and active states (Aug 09), plus high time-resolution simultaneous H and K-band photometry over 1.5 orbital periods whilst the source was again in an active state (August 08). Low-resolution K-band spectra obtained with a continuously variable filter operating in UKT9 (Aug 07) are also presented, along with H and K-band photometry obtained with IRCAM2 in 1991 of the Cyg X-3 field, including 'Star Z'.

2.2.1 1984 August 07 : UKT9

The UKT9 instrument is a common-user InSb photometer, operating in the 1-5 μm range. On the night of 1984 August 7 this instrument was used to perform photometry of Cyg X-3 in the J, H, K, L, L$'$ and M-bands with a 4.8 arcsec diameter aperture. Observations were all made between UT 07:23 and 07:56, corresponding to X-ray phases $\sim$ 0.7 to $\sim$ 0.8, during which the light curve is on a gradual increase to maximum at phase $\sim$ 0.85. Calibration was carried out on the nearby standard BS8143 and the data were

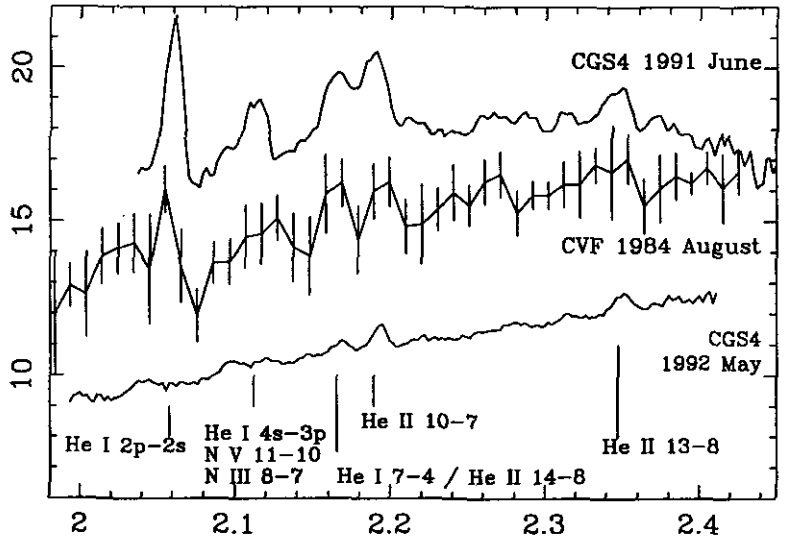

Figure 2.1 Mean K-band CVF spectrum of Cyg X-3 1984 Aug 07, shown with the strong-lined 1991 June and weak-lined 1992 May CGS4 spectra of van Kerkwijk (1993b) for comparison. Line identifications follow van Kerkwijk (1993b).

corrected for atmospheric absorption using standard values for Mauna Kea. The observations were of integration time 30 seconds, with observations at J, H, L, L′ or M typically being interleaved with an observation in the K-band. The K-band data were used to estimate the extent that flaring could have affected the photometry, from which I estimate flux increases of no more than 20% due to flares. In the M-band it was only possible to obtain a 3σ upper limit. The mean values obtained with this photometry are listed in Table 2.1.

On this night UKT9 was also used with a continuously variable filter (CVF) to obtain low resolution K-band spectra of the source. The CVF was used to scan the spectrum through 44 regularly spaced channels between 1.97 - 2.43 μm. Four Cyg X-3 spectra were obtained, during X-ray phases 0.81 - 0.95, corresponding to the fall from maximum to minimum flux density in the infrared and X-ray light curves. The spectra were normalised by dividing them by a spectrum of SAO 126643, which is an F5 star and should be essentially featureless in the K-band (apart from possible Brγ absorption

Table 2.1 Mean quiescent and flaring fluxes Aug 1984

Filter	λ_{eff} (μm)	Flux density (mJy) Aug 07 (quiet)	Flux density (mJy) Aug 09 (flaring)
M	4.8	< 41.6	134.5 ± 29.9
L′	3.8	24.7 ± 2.9	144.0 ± 38.1
L	3.4	23.9 ± 0.7	128.9 ± 4.6
K	2.2	16.6 ± 0.4	49.3 ± 7.4
H	1.6	7.5 ± 0.3	17.7 ± 2.1
J	1.2	1.9 ± 0.3	3.4 ± 0.2

which may contribute to the apparent HeI/HeII feature at $\sim 2.16\mu$m). The mean CVF spectrum is shown in Figure 2.1 alongside the strong-lined 1991 June and weak-lined 1992 May CGS4 spectra of van Kerkwijk (1993b [69]). Identification of the stronger He and N emission features follows van Kerkwijk (1993b [69]). The apparent emission feature at 2.058 μm cannot be confirmed as it is only one channel wide and the channel spacing is less than the instrument's spectral resolution; it may be as a result of flaring activity during the scan.

2.2.2 1984 August 08 : UKT10

The UKT10 'two-banger' instrument was an InSb photometer capable of operating simultaneously through the same aperture in the K and J or H bands. Between UT 06:20 and 14:20 August 8th this instrument was used to track Cygnus X-3 simultaneously in the H and K-bands with a 6.4 arcsec diameter aperture and 2 second integration times. The instrument was calibrated on four UKIRT standards, HD162208, GL748, Oph S-1 and HD161903 and data were corrected for atmospheric absorption using Mauna Kea standard values. Between UT 07:48 and 09:54 the instrument experienced battery problems and was unusable. It should be noted that the K-band filter used with UKT10 had a slightly different response to that used with UKT9, but the effect of this on absolute photometry is estimated to be less than 5% (P. M. Williams, private communication).

Figure 2.2 illustrates this data set, plus the (H-K) colour averaged over

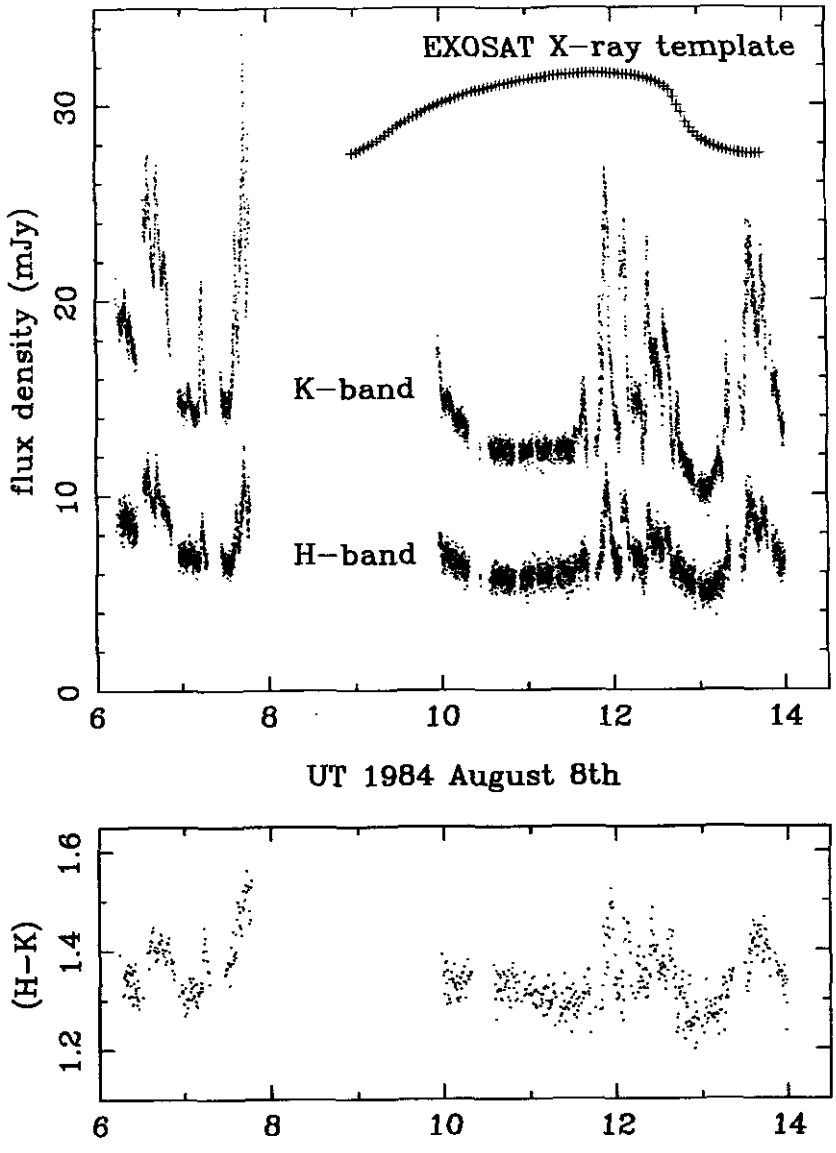

Figure 2.2 Simultaneous H and K band observations of Cyg X-3 with 2 second time resolution, obtained using the UKT10 instrument at UKIRT. The template EXOSAT X-ray light curve of van der Klis & Bonnet-Bidaud (1989) is shown for comparison. Orbital phase is calculated using the cubic ephemeris of Matz et al (in prep – see chapter 5) which agrees to within 2% with the ephemeris of van der Klis & Bonnet Bidaud (1989) at this epoch. The lower panel shows (H-K) colour index averaged over adjacent sets of six points – note the clear reddening during flares.

adjacent sets of 8 points (ie. 16 sec means). The mean EXOSAT X-ray template of van der Klis & Bonnet-Bidaud (1989 [26]) is plotted for comparison, with phase calculated using the ephemeris of Matz et al (1996 [93]) which agrees to within 2% with the ephemeris of van der Klis & Bonnet-Bidaud at this epoch. The most obvious feature of the data are the rapid large-amplitude flare events during which Cyg X-3 can more than double its flux in both bands on timescales of less than a minute. The (H-K) colour shows that the source gets significantly redder during these flares. The orbital modulation of the source is clearly visible in the interval $\sim$ 12:40 – 13:10 UT, though minimum light is hidden by the large flare complex at $\sim$ 13:30 UT.

2.2.3 1984 August 09 : UKT9

UKT9 (described above) was used again on this night to perform J, H, K, L, L′ and M-band photometry. The instrument was again used with a 4.8 arcsec diameter aperture, and the measurements were calibrated on BS8143 and corrected for atmospheric absorption using Mauna Kea standard values. In this data set the fluxes are extremely high, indicative of flaring behaviour even more violent than that observed on the previous night. Five K-band integrations were made during this $\sim$ 35 min period which measured flux levels consistently much higher than any observed previously, though there was a gradual decline near the end of the observations. These data are presented in Table 2.1. It should be noted that the quoted uncertainties in the K and L′-band fluxes are due to source variability.

2.2.4 1991 July 9 : IRCAM2

IRCAM2 was a 64 $\times$ 58 pixel InSb array camera used at UKIRT, operating in the 1 - 5 μm range. It was used in the 0.6 arcsec/pixel mode to study the Cyg X-3 field at H and K-bands. The instrument was calibrated on HD203856, and data were reduced using the IRCAM CLRED package. The mean Cyg X-3 flux densities were 5.1$\pm$0.1 mJy and 13.4$\pm$0.6 mJy at H and K respectively. This is both slightly lower and slightly redder than our

quiescent flux densities of 1984 Aug 07, with (H-K) = 1.55. The flux densities for the nearby infrared object 'Star Z' were 4.0±0.1 mJy and 6.3±0.6 mJy at H and K. Within the experimental uncertainties these values agree with Joyce (1990 [94]) and place constraints on any long-term variability in the infrared on timescales of $\sim$ 650 days.

2.3 Infrared flares

Cyg X-3 is known to exhibit in the infrared both short timescale rapid flare events (eg. Becklin et al 1973 [19]; Mason, Cordova & White 1986 [55]; Jones et al 1994 [47]) and prolonged states of increased flux density (eg. Becklin et al 1973 [19]). However, Cyg X-3 has also been observed in the infrared for several days without exhibiting such behaviour (Molnar 1988 [56]. Mason, Cordova & White (1986 [55]) envisaged the flares as due to free-free emission from a thermal plasma of temperature 10^6 K associated with the jets in the system. Apparao (1987 [37]) alternatively suggested that the flares may be due to interactions between a γ-ray beam associated with the compact object and clumps of matter orbiting in the binary system.

The dataset of infrared observations is at present too limited to determine which is the more common state for the source; there is certainly no evidence to suggest that the flares are a particularly rare occurence. Here I shall examine in detail both the rapid flare events of 1984 Aug 8 and the prolonged high flux state observed on 1984 Aug 9.

2.3.1 Evolution of rapid flare events

Figure 2.3 reveals several large flare complexes with durations of the order of 5–15 minutes and characteristic decay times of order 200 sec. Examination of the data reveals much fine structure within each of these flare events. In Figure 2.3, four flare events are shown with expanded axes. The H and K band flux values are normalised to their values at minimum light. It is evident that the flares do not follow any fixed morphology, and that within each flare complex there are many narrow spikes. A cross-correlation test

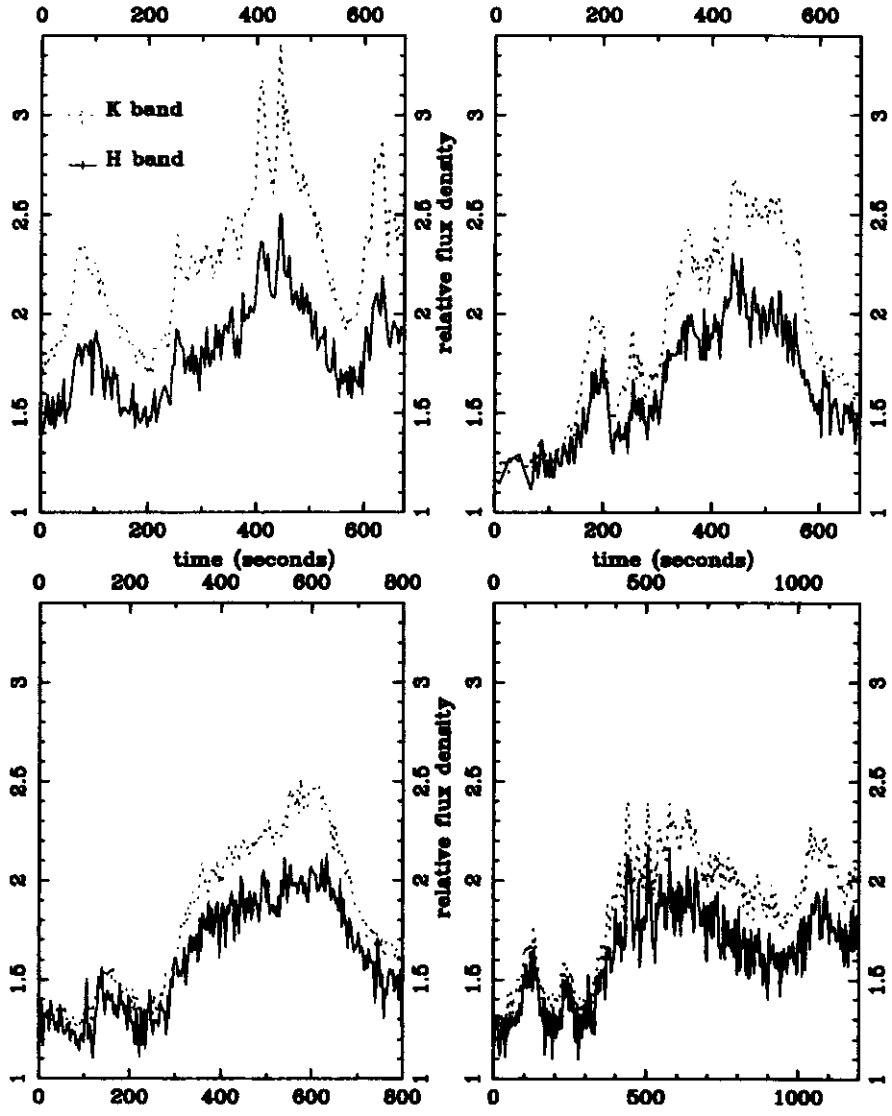

Figure 2.3 Cyg X-3 infrared flares, observed simultaneously in the H and K bands with 2 second time resolution. Note the differing abscissae scales.

found no significant delay between the emission at the two wavelengths. These spikes undergo very rapid time evolution; I find within the data at least five examples of the flux increasing or decreasing by $\sim 30\%$ in ≤ 15s. Such rapid rise times place an upper limit on the size of the emitting region of $\sim 15 \times c \sim 4.5 \times 10^{11}$cm ($\sim 6R_{\odot}$). For comparison, Cherepashchuk & Moffat (1994 [31]) place an upper limit on the orbital separation of the compact object and donor star of 5.6 $R_{\odot}$. Assuming a distance of 10 kpc and dereddening by $A_J = 6.0$ (see section 2.4) I derive a power output of $\sim 10^{35}$ erg s^{-1} across the K band (bandwidth $\sim 2 \times 10^{13}$ Hz). It is interesting to note that Mason, Cordova & White (1986 [55]), in observations made only one month after those reported here, also observed a large infrared flare event almost exactly at orbital minimum.

2.3.2 The nature of the flaring component

The 1.6 – 2.2 μm spectral index of the flaring component can be determined by subtracting an estimated quiescent flux level during periods of flaring. When doing so, and dereddening by $A_J = 6.0$ it is found that the flaring component tends toward a spectral index of $\sim +0.6$, in contrast to the 'quiescent' dereddened spectral index in this interval which is $\geq +1.5$ (section 2.4). Such a reddening in (H-K) is apparent in the lower panel of Fig 2.2. The likely emission mechanism for a hot ionised gas is free-free thermal bremsstrahlung, which has a spectral index of -0.1 when optically thin. A spectral index of this value can be recovered by introducing a small amount of local free-free opacity, associated not with the flaring component but with the dense stellar wind in which the system is embedded. An optical depth of $\tau_K \sim 0.3$ (giving $\tau_H \sim 0.2$) would be sufficient to produce the observed dereddened spectral index. Alternatively, we may be seeing a blend of emission from a dense, optically-thick (spectral index +2.0) region, possibly associated with the base of the jet or inner regions of accretion disc, combined with a majority of emission from an optically thin component. It should also be noted that uncertainties in the amount of extinction to the source are sufficient to change the derived spectral index for the flaring com-

ponent by $\sim \pm 0.5$ mag. However, optically thick emission (spectral index +2.0) is ruled out as the dominant process in the flaring component as the derived spectral index is too low and the introduction of local opacity from the stellar wind only widens the discrepancy.

On Aug 09 observations once again revealed flaring activity in Cyg X-3, but this time at a fairly stable level even higher than the peak fluxes observed on the previous night. On this occasion flux densities were measured across the J – M bands, ie. 1,2 – 4.8 μm. Again dereddening by $A_J = 6.0$ mag, the spectrum of the flaring component (completely dominating the flux in the K-band and longer, so subtraction of an accurately determined 'quiescent' component not so vital) was flat across all bands, consistent within estimated errors with optically thin free-free emission. This is significant as the lack of evidence of a self-absorption turnover at wavelengths at least as long as 4.8 μm places limits on the temperature and density of the flaring component. Dereddening and integrating the observed fluxes across the J – M-bands reveals an infrared luminosity in excess of 10^{36} erg s^{-1} during such periods.

If the flaring is indeed due to free-free emission from a hot optically thin plasma, the question arises *where is this plasma* ? This is difficult to answer precisely, though the small size implied by the rapid variability implies that the plasma is associated with the inner regions of the system. Wolf-Rayet winds are thought to be fairly clumpy (e.g. Brown & Richardson 1995 [95]), but it is difficult to see how a plasma with a typical temperature of order $1 - 5 \times 10^4$ K could be heated to temperatures in excess of 10^6 K. More likely, in my opinion, is that the plasma is associated with the inner regions of the accretion disc and base of the relativistic jets. Temperatures of order 10^6 K are not unlikely near the accreting compact object, and a thermal gas is already invoked by many models for jet emission (e.g. Marti, Paredes & Estalella 1992 [49]) to coexist with the relativistic synchrotron-emitting electrons.

Assuming free-free emission from a Maxwellian plasma, then given the observed luminosity of the flares, size limits imposed by the rapid flux changes, and the lack of appreciable free-free self-absorption at $\lambda \geq 4.8\mu$m,

some constraints can be placed upon the temperature and number density of the plasma :

Free-free emission from a plasma becomes optically thin at a frequency

$$\nu_T \sim 0.3(T_e^{-1.35} N_e^2 l)^{0.5} \quad \text{GHz}$$

where T_e is the electron temperature in K, N_e is the electron number density in cm^{-3} and l is the dimension of the source in pc (Lang 1980 [96]). From the rapid flaring $l \leq 4.5 \times 10^{11}$ cm (1.5×10^{-7} pc); and from the lack of self-absorption at 4.8 μm, $\nu_T \leq 6.3 \times 10^4$ GHz. This gives the following inequality :

$$\frac{N_e}{T_e^{0.7}} \leq 5.3 \times 10^8 \tag{2.1}$$

(Note that this is based upon the assumption that the rapid flares are, like their larger-amplitude counterparts, optically thin at 4.8 μm. This assumption is supported in part by subsequent observations, described in chapter 5, which demonstrate the rapid flares to be optically thin at least to the nbL band $\sim 3.6\mu$m).

The bremsstrahlung emissivity of a Maxwellian plasma is given by

$$\epsilon_\nu(\nu)\mathrm{d}\nu = 5.4\times10^{-39} Z^2 N_e N_i T_e^{-0.5} g_{ff} e^{-h\nu/kT} \mathrm{d}\nu \quad \text{erg s}^{-1} \text{ cm}^{-3} \text{ Hz}^{-1} \text{ rad}^{-1}$$

(Lang 1980 [96]) where Z is the mean atomic number of the plasma (2 for pure helium), N_e & N_i are the electron and ion number densities respectively, and g_{ff} is the Gaunt factor, assumed here to be 1.4 (good to within 10% for T > 10^6 K – Tucker 1977 [97]). For fully ionised helium (there is no evidence for the presence of hydrogen in infrared spectra of Cyg X-3 – van Kerkwijk et al 1992 [29]), $N_e N_i = N_e^2/2$. The monochromatic power expected from such a plasma is :

$$L_\nu = 4\pi V \epsilon_\nu \mathrm{d}\nu \quad \text{erg s}^{-1} \text{ Hz}^{-1}$$

where V is the volume of the plasma in cm^{-3} Assuming emission comes from a uniform sphere of radius 4.5×10^{11} cm, the maximum volume V = 3.8×10^{35} cm^3, this gives

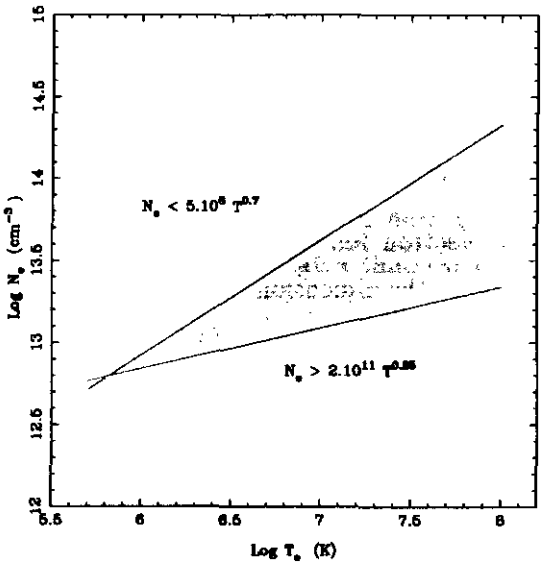

Figure 2.4 A plot illustrating the two functions described in the text. The shaded region indicates the allowed range of values for N_e and T_e. The upper curve is constrained by the requirement that the plasma be optically thin in the M-band and yet fit within the maximum size allowed by the rapid rise and decay times observed. The lower curve is constrained by the need for the plasma to be dense enough and hot enough to produce the observed luminosity within the size limit.

$$L_\nu = 0.07 N_e^2 T^{-}0.5 e^{\frac{h\nu}{kT}}$$

Equating with observed K-band monochromatic power ($\sim 4 \times 10^{21}$ erg s$-$1 Hz$-$1) I get the following inequality

$$N_e^2 \geq 5.1 \times 10^{22} T^{0.5} e^{\frac{h\nu}{kT}} \tag{2.2}$$

Combining equations 2.1 & 2.2 I get

$$2.3 \times 10^{11} T^{0.25} e^{\frac{h\nu}{kT}} \leq N_e \leq 5 \times 10^8 T^{0.7} \quad \mathrm{cm}^{-3} \tag{2.3}$$

(Note for K-band, at tempartures being discussed, $h\nu << kT$)

These two inequalities are plotted in Fig 2.4, illustrating the allowed range of values of T_e and N_e. This condition is only satisfied for $T \geq 7 \times 10^5$

K, which can be considered a lower limit on the temperature of the emitting plasma (below this temperature the electron number density required to produce the observed luminosity would result in emission at 4.8 μm being self-absorbed, given size constraints).

Assuming a reasonable range of temperatures to be $7\times10^5 \leq T \leq 5\times10^7$ K, equation 2.3 gives

$$6 \times 10^{12} \leq N_e \leq 1 \times 10^{14} \quad \mathrm{cm}^{-3}$$

It should be noted that a free-free plasma in such a temperature range would be bright across the optical and UV regimes, only fading in the EUV/soft X-rays. So while we may not expect to see X-ray analogues to the infrared flares, I predict strong optical counterparts.

The bremsstrahlung cooling time for a Maxwellian plasma is

$$t_{ff} = 1.8 \times 10^{11} \frac{T^{0.5}}{N_e} \quad \mathrm{s}$$

(Tucker 1977 [97]). Placing the constraints on N_e & T considered above, I expect bremsstrahlung cooling times for the plasma in the range 1 – 250 sec. This is consistent with the decay times observed for the rapid 'spikes' interspersed throughout the flaring periods.

Adiabatic cooling is also expected to be important for a hot dense plasma. As determined above, the luminosity of the plasma is related to the electron number density, volume and temperature by :

$$L \propto N_e^2 V T^{-0.5}$$

(assuming $h\nu << kT$)

For an adiabatically expanding plasma, $T \propto V^{-2/3}$ (Lang 1980 [96]). For a uniformly expanding sphere of radius r the following relations hold : $N_e^2 \propto r^{-6}$; $V \propto r^3$; $T^{-0.5} \propto V^{1/3} \propto r^1$. Thus

$$L \propto r^{-2}$$

Using the above relation I calculate that a reduction in flux by $\sim$ 30% requires an increase in radius of $\geq$ 15%. Assuming an initial radius of

4.5×10^{11} cm, this requires an expansion of $\sim 7 \times 10^{10}$ cm in 15 s – ie. an expansion velocity of 0.15 c ! A similar result is obtained for a cross-section of gas constrained by the jet envisaged by MPE92, which is inconsistent with their model fits. Although such lateral expansion velocities are observed in the jets (e.g. Schalinski et al 1995 [25]), the plasma would have cooled far earlier due to bremsstrahlung processes before this point was reached. Furthermore, a gas cannot expand due to its own internal pressure at a velocity greater than its own sound speed, which for a non-relativistic gas at 10^7 K is $\sim 3 \times 10^7$ cm s^{-1} (ie. 1/100 th of that required for observed decay time). I therefore favour bremsstrahlung as the dominant cooling mechanism.

Synchrotron radiation cannot be ruled out as the main emission mechanism responsible for the flares. However, it is difficult to add circumstellar absorption such that there is a consistent $\alpha \sim -0.6$ spectral index across the J to M bands in the 1984 Aug 09 data, as would be expected from an extrapolation of the spectral index in the optically thin radio regime (Waltman et al 1994 [21]). Polarization measurements would also be expected to show an increase in polarization during flare events (providing depolarisation by local gas eg. stellar wind did not destroy the effect) but this observation has not been made.

Becklin et al (1973 [19]) also observed a flaring period in which the fluxes became high enough to mask the modulation. This may have been a similar event to that observed by ourselves on 1984 August 9. Such events may represent particularly large and extended mass ejections in the relativistic jet and should be precursors of larger synchrotron flares than 'normal' infrared flares. There is a suggestion of a small radio flare (amplitude $\sim$ 100 mJy at 3.7 cm) at the time of the 1984 Aug 09 observations (Fig 2.4 – Elizabeth Waltman, private communication). This is far too limited evidence to claim any correlation between infrared and radio activity; however, given the very high infrared fluxes observed on 1984 August 9 and relatively modest nature of the radio flare, it seems likely that, were they in direct proportion, the infrared precursor of a major radio event would be extremely hard to miss.

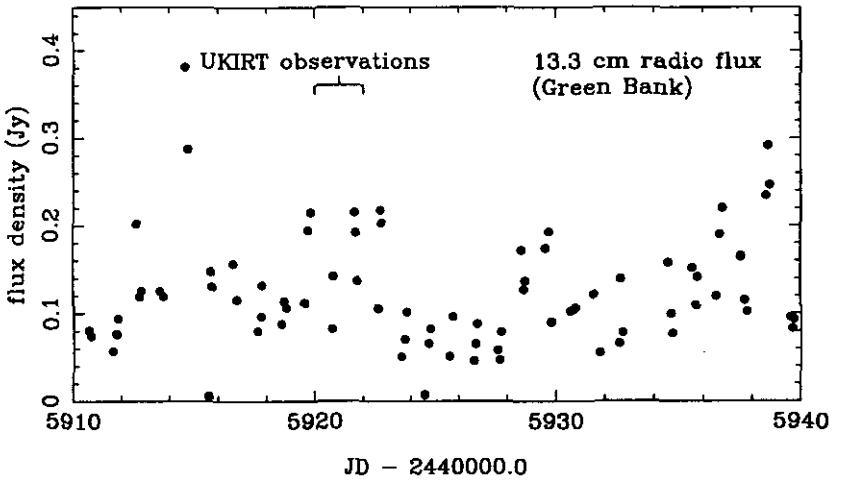

Figure 2.5 Green Bank radio monitoring of Cyg X-3 around the time of the 1984 UKIRT observations, showing the source to be in a small flaring state.

It should be borne in mind however, that there is, as demonstrated above, a limited period for strong emission in the infrared due to short bremsstrahlung cooling times for the kind of plasma envisaged, and that dynamical constraints may place a limit on the maximum rate of mass ejection. Thus during a large and prolonged ejection there would be a relatively stable maximum infrared flux corresponding to all the infrared-emitting region of the ejection cone being filled. This is a possible explanation for the very high but relatively stable fluxes observed on 1984 Aug 9. Any subsquent radio synchrotron emission would suffer a time delay before being observed, related to the time necessary for the ejecta to reach the radio 'photosphere' (see chapter 3).

2.4 The infrared continuum

Previous attempts to unravel the nature of the Cyg X-3 infrared continuum have concluded that it is due to a thermal bremsstrahlung spectrum becoming optically thick at ~ 2 μm (Molnar 1988 [56]) or that it is a power-law spectrum from the Wolf-Rayet wind (van Kerkwijk 1993a [30]). In order to

determine the nature of the infrared continuum inherent to Cyg X-3 is it necessary to (i) correct data for non-continuum emission (eg. flares, emission lines), and (ii) deredden the data to compensate for the large amount of extinction along the line of sight to the source. I shall address both these considerations briefly below, before considering the shape of our resultant dereddened continuum.

2.4.1 Normalising data

In addition to our own UKIRT data I shall use R and I-band broad band data (Wagner 1990 [58]) and a 0.925 μm continuum flux density (M.H. van Kerkwijk, private communication) to explore the Cyg X-3 continuum. The infrared flux received from Cyg X-3 in any band is highly variable and dependent upon (at least) : mean infrared luminosity at that epoch, orbital phase, flaring of source during integration and presence (or not) of emission lines. Here I assume that there are no major changes in the infrared luminosity of Cyg X-3 between the observations, and that flares contribute $< 20\%$ of the flux in any observation. I normalise the data to phase 0.75 and assume a modulation factor ξ = amplitude/mean of 0.25 for the I & R bands (Wagner et al 1989 [98]). To correct for emission lines, I use the following corrections, assuming the Wolf-Rayet nature of the wind : L & L′, (0.1 mag, He II line); K, (0.05 mag); H, (0.05 mag); J, (0.1 mag, He I line); I, (0.05 mag, estimate) and R, (0.05 mag, estimate) (P. M. Williams, private communication).

2.4.2 Dereddening the data

In order to deredden the data I used the $\lambda^{-1.7}$ extinction law of Mathis (1990 [99]), except for the R band data point where we used the 'outer cloud' dereddening ratio of Mathis (1990 [99]), as did van Kerkwijk (1993a [30]). Following these authors I shall use A_J as the reference extinction ($A_V = 3.55A_J$). I find that in order to obtain a spectrum that is neither falling off (too cool) nor too steep (unphyisically, i.e. significantly steeper than a black body) at higher frequencies I can constrain the extinction such

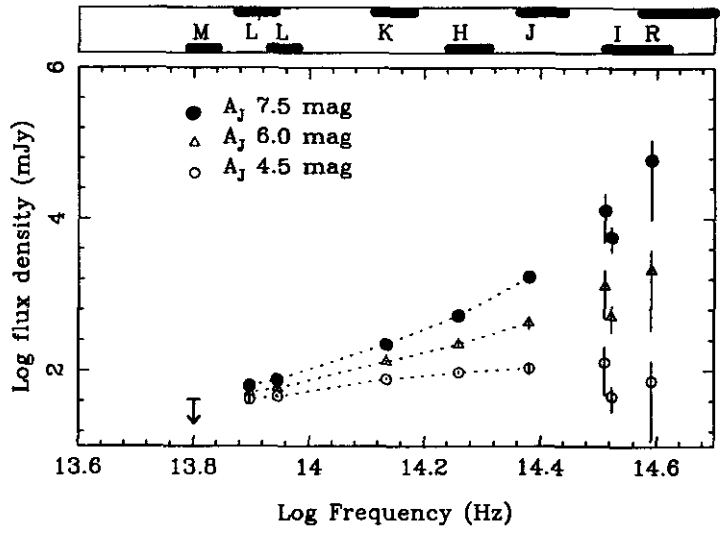

Figure 2.6 Cyg X-3 infrared continuum from 6.3×10^{13} to 3.9×10^{14} Hz (4.8 - 0.8 μm). Of the two data points in the I-band, the higher frequency point is is broad-band photometry from Wagner et al. (1989) and the other is the 0.925 μm continuum flux density from I-band spectra (M.H. van Kerkwijk, private communication). The R-band data point is from Wagner et al. (1990). Filter FHWM are indicated by horizontal bars - note that L & L' and R & I filters overlap. The data have been dereddened for 4.5, 6.0 and 7.5 magnitudes of A_J.

that $4.5 \leq A_J \leq 7.5$ mag. This is consistent with the range of values for A_J determined by van Kerkwijk (1993a [30]) from considerations of spectral indices of I-band spectra ($5 \leq A_J \leq 6$ mag). This estimate of the extinction in the infrared is significantly greater than that of Becklin et al (1972 [15]). Figure 2.5 shows the data set dereddened by 4.5, 6 and 7.5 magnitudes of A_J, illustrating in particular the sensitivity of the high-frequency range to the amount of dereddening applied.

2.4.3 The nature of the infrared continuum

Given the above range in values of A_J I choose $A_J = 6.0$ as a reasonable estimate of the extinction to Cyg X-3. Defining the spectral index $\alpha = (\Delta \log S_\nu / \Delta \log \nu)$ I find that shortwards of the K-band $\alpha \sim +2.0$ whereas longwards of this point $\alpha \leq +1.5$. Thus Cyg X-3 clearly has a significant

excess above the black-body continuum expected for a single hot star. Such an excess is typical of systems with dense stellar winds and/or cicrumstellar discs/shells. Van Kerkwijk (1993 a[30]) found that the spectrum could be fitted by a single power law of spectral index 1.4 ± 0.3 : my best-fit to a single power-law is in agreement, with spectral index $\sim +1.5$. This is at the top end of the range of spectral indices found for Wolf-Rayet winds by Morris et al (1993 [57]). See chapter 5 for a further discussion of the nature of the infrared continuum.

2.5 The infrared light curve

Here I shall briefly discuss the significance of a change in the (H-K) colour during a period of non-flaring activity, and the difference in minimum flux level at 2.2 μm between our observations on 1984 Aug 08 and those of [55], obtained on 02 September 1984, 27 days later.

2.5.1 Orbital colour changes ?

The bluest part of the light curve presented in Fig 2.2, as measured by the (H-K) colour, is during the decline toward minimum between $\sim$ 12:30 and 13:15 UT. This part of the light curve appears to be significantly bluer than during the interval $\sim$ 10:00 – 11:45 UT when again there was no obvious flaring activity, and may suggest that the source becomes bluer at orbital minimum (although unfortunately the large flare almost exactly at minimum made measurement of this region of the light curve impossible).

This conclusion was tentatively drawn by Becklin et al (1973 [19]), yet Molnar (1988 [56]) claimed no infrared orbital colour changes over several nights of observation. [69] suggests that orbital colour changes in the infrared could be due to bound-free opacity which would result in increased degree of modulation with frequency. Examination of the light curves at H and K suggest however that colour changes may result from something more complex than simply changes in the degree of modulation, ie. the *shape* of the light curve in the infrared may be a function of wavelength (see chapter

5).

The difference in the shapes of the infrared and mean X-ray light curves in the phase interval 1.1 - 1.5, where the infrared fluxes remain relatively constant whilst the X-ray light curve is increasing, should also be noted. A similar discrepancy is evident in the light curve of Mason, Cordova & White (1986 [55]) during simultaneous X-ray and infrared K-band observations. This may be due to geometrical differences between the media scattering the X-rays (electron scattering) and that scattering the infrared (free-free absorption).

2.5.2 Changes in the quiescent infrared flux level

Mason, Cordova & White (1986 [55]) obtained 5 hr of K-band infrared data clearly showing the orbital modulation (and flares - see section 6) only 27 days after our own UKT10 H and K-band observations. However, in their data the K-band flux density is $\sim$ 11.5 mJy at minimum, whereas in our data it is $\sim$ 10.0 mJy shortly *before* orbital minimum, presumably decreasing further at minimum. Such changes in minimum flux density are not unusual - van Kerkwijk (1993b) recorded a K-band flux density of $\leq$ 9 mJy at minimum from observations in 1992, whereas a light curve recorded in 1994 (chapter 5) shows a minimum K-band flux density of 10 mJy. Given the assumption that in the K-band the flux density is dominated by free-free emission from the stellar wind, this increase of base flux level must reflect some change in the physical characteristics of the wind. More recent infrared observations (chapter 5) suggest that monotonic flux trends may be superimposed upon the mean flux level in a similar manner to that observed in X-rays (see chapter 1). I find it unlikely that these changes can be attributed to photometric errors, and future imaging observations where Cyg X-3 can be ratioed against nearby stars of known magnitude should confirm the effect (see chapter 5).

Van Kerkwijk (1993a [30]) suggests that changes in the minimum or phase-averaged flux density of this kind may be related to the X-ray state of the source : when in X-ray high state the wind is heated more strongly,

bound-free opacity increases and observed flux decreases. Alternatively, the changes in base flux level may reflect changes in the density structure of the Wolf-Rayet wind. The flux density from free-free emission varies as $N_e N_i$, where N_e and N_i are the electron and ion number densities respectively. Thus an increase in minimum flux density from $\sim$ 10 mJy to $\sim$ 11.5 mJy could be produced by a global increase in the wind electron density of $\sim$ 7%. This could be due to clumping and/or narrow shells of enhanced density propagating through the wind (eg. see Waldron, Klein & Altner 1994 [21]), in which case the changes in base flux level would be on relatively short timescales. The apparent density enhancement could alternatively be due to a genuine increase in global wind density caused by, for example, an increase in the mass-loss rate or a decrease in the wind velocity. Kitamoto et al (1994 [65]) predicts that such an increase in wind density should lead to enhanced X-ray emission and, if the accretion rate reaches supercritical, subsequently to a radio outburst. It should be noted that there is no clear evidence for variability in infrared base continuum level in other Wolf-Rayet stars (P. M. Williams, private communication), though as Cyg X-3 is already in so many ways a seemingly unique object this may not make the choice between interpretations any easier.

2.6 The K-band spectra

Van Kerkwijk (1992 [29] and 1993b [69] have observed Wolf-Rayet emission features from Cyg X-3 in the infrared I- and K-bands. From these spectra they classified Cyg X-3 as belonging to the nitrogen-rich WN subclass, varying in states from WN7/8 to WN4/5. Schmutz (1993 [89]) confirms this classification from considerations of the radius, temperature and wind velocity of fits to the K-band spectra. However, Schmutz (1993 [89]) continues to state that the presence of such emission features is not conclusive evidence for the existence of a Wolf-Rayet star in the Cygnus X-3 system. Earlier Katz, Wright & Lawrence [100] had performed low-resolution CVF spectroscopy in the K-band in search of the Brγ recombination line, but had

failed to detect any emission lines due to the noisiness and poor spectral resolution of their data.

Our mean CVF spectrum is displayed in Fig 2.1 alongside two CGS4 spectra obtained at UKIRT (van Kerkwijk 1993b [69]). The spectrum is noisy and error estimation was difficult, but is consistent with Cyg X-3 having had a similar spectrum in 1984 to that observed in 1992 & 1993. This is significant, given the variable and controversial nature of the spectrum. The apparent HeI feature at 2.058 μm cannot be considered real, despite appearing in the spectra of van Kerkwijk (1993b [69]), as the resolution of the instrument was worse than one channel spacing. This consideration does not rule out the possibility that the feature may be related to a transient flare event occurring during the scan.

2.7 Conclusions

Cyg X-3 continues to exhibit much unusual and poorly-explained infrared behaviour. The orbital modulation, often observed in the infrared and X-rays is clearly present in our simultaneous H and K-band photometry. Further, the UKT10 observations reveal a clear reddening of the (H-K) colour during flaring activity, and some evidence also for the source becoming more blue in (H-K) at orbital minimum. The reddening during flare events is well described by the addition of an optically thin free-free component, possibly related to the relativistic jets known to exist in the system. Maximum size, optical depth and luminosity requirements have been combined to establish a lower limit to the temperature of the emitting plasma of 7×10^5 K. A reasonable upper limit to the temperature of 5×10^7 K constrains the electron number density of the flaring component in the range $6 \times 10^{12} - 1 \times 10^{14}$ cm^{-3}. Bremsstrahlung cooling, reasonably efficient at such relatively high densities, is likely to be the dominant cooling mechanism. Synchrotron emission, partly absorbed by the stellar wind, cannot however be ruled out as the flaring mechanism. Polarization measurements of infrared flares may help to resolve this, though depolarization by the absorbing wind material

may make this difficult. Periods of prolonged flaring correspond to infrared luminosities in the J to M-bands in excess of 10^{36} erg s^{-1}. Were the infrared flares related to the ejection process I might expect to see their analogues in other galactic jet sources: Hunt, Massi & Zhekov (1994 [101]) however found no significant fluctuations in the infrared flux from the 'jet' source LSI+61 303° on timescales of less than an hour; neither am I aware of any infrared flaring from other galactic jet sources. This may be a selection effect in that objects with optical counterparts are not in general studied in the infrared to the degree that Cyg X-3 has been. Alternatively, the flares may be a result of the particularly high densities present in the Cyg X-3 system due to the Wolf-Rayet wind, and may turn out to be a rare phenomena.

The 'quiescent' infrared continuum of Cyg X-3 is most naturally fit for interstellar extinctions of $A_J = 6.0 \pm 1.5$ mag. Given a distance to Cyg X-3 of ~ 10 kpc (which, it should be noted, is consistent with the reddening derived above using most distance : A_V relations) I find an absolute K-magnitude of ≤ -5 for the system. The CVF spectrum of 1984 August is consistent with that of a Wolf-Rayet object of late-WN subclass and so I find our data are compatible with the primary conclusion of van Kerkwijk (1993a [30]), ie. that the Cyg X-3 system contains a 'classical' massive Wolf-Rayet star. Such compatibility of data taken seven years apart is of significance given the observed tendency of Cyg X-3 to change its spectral class on timescales of a year or less (van Kerkwijk 1993b [69]). However, I also note that the infrared continuum may be better described by a spectrum steepening at shorter frequencies than by a single power-law. This may be due to our observing accelerating regions near the base of the wind, or possibly through to a small, extremely hot, black-body component. If we are seeing through to the base of the wind at infrared wavelengths shortward of $\sim 1.5\mu$m, then the model of van Kerkwijk (1993b [69]) for the modulation of the infrared continuum cannot be correct as there would not be sufficient optical depth in the J and I bands to explain the observed modulation. Note however that this would not affect the interpretation by this author of the location of the line-emitting region and hence the observed Doppler-shifts of the

infrared lines. Further (phase-binned, given possible orbital colour changes) spectroscopy across the infrared is now possible and would help to clarify the nature of the infrared continuum of Cyg X-3. The discovery of Wolf-Rayet emission features in other infrared bands would strengthen the case for the W-R + compact object nature of Cyg X-3, particularly in view of the recent discovery of W-R features in the infrared K-band spectra of Of stars (Conti et al 1995 [102]).

Chapter 3

Simultaneous millimetre and radio observations of Cygnus X-3 in a quiescent radio state : 1993 September

3.1 Introduction

Observations of Cygnus X-3 at 2.0 and 1.1 mm with the JCMT, partially simultaneous with radio flux measurements at 2 cm and 18 cm, are presented. These are the first known observations of Cyg X-3 at millimetre wavelengths whilst the source was in a quiet radio state. The observed millimetre fluxes are several times greater than those expected for the synchrotron tail of emission extrapolated from the radio, and the 2-mm flux exceeds that at 1.1 mm, suggesting a peak in the region of a few mm. The observations are interpreted using an extension of the model of Marti, Paredes & Estalella (1992 [49]) to repeated short injections of relativistic electrons in a region in the Cyg X-3 stellar wind which is optically thin to millimetre-wave photons, but optically thick at centimetre wavelengths. Centimetre-wavelength emission is not observed until the ejecta have travelled further out in the wind. A MERLIN radio map at 18 cm reveals the same elliptical asymmetry in the scattering medium around Cyg X-3 as found by Wilkinson, Narayan & Spencer (1994 [45]). A summary of the work presented in this chapter has been published in Fender et al (1995a) [103]. Further details of the model for quiescent emission, plus a summary of the search for strong millimetre

emission from other X-ray binaries (as presented in chapter 5), are to be published in Fender et al (1996a) [104].

3.2 Observations

3.2.1 JCMT

Observations were made with the James Clerk Maxwell telescope (JCMT) on Mauna Kea in Hawaii on the nights of 1993 September 02 and 03 UT. The radio-quiet mm fluxes were unknown, and it was not clear that Cyg X-3 would be detectable. The UKT14 common-user photometer was used with the 1.1-mm (central frequency 264 GHz, bandwidth 74 GHz) and 2.0-mm (central frequency 150 GHz, bandwidth 40 GHz) filters, with a throw of 60 arcsec at a frequency of 7.813 Hz. The aperture was 65 mm which corresponds to a beamwidth of 18 arcsec at 1.1 mm and 28 arcsec at 2.0 mm.

On September 02, relative flux-calibration for Cyg X-3 was made using the nearby standard W75N. Using Mars for absolute flux-calibration, we had previously determined for W75N flux densities of 11.6 and 2.9 Jy at 1.1 and 2.0 mm respectively. Pointing was checked on the source MWC349. The mean atmospheric optical depth at zenith τ was 0.16 at 1.1 mm and 0.1 at 2.0 mm. Observations of Cyg X-3 began at 04:50 UT using the 1.1-mm filter and individual integration times of 20 s. We subsequently reduced this integration time to 16 s in most cases as a compromise between reducing noise from a varying atmosphere during the integration and a desire to keep overheads to a minimum. We interleaved the target observations with those of the calibrator, with typically 50 min on Cyg X-3 followed by 10 min on W75N. By 09:30 we were confident that we had detected Cyg X-3 at 1.1 mm. So, to ascertain the spectral index of the emission, at 09:52 we began observations at 2.0 mm. It was decided to use this filter so that we could get as broad a range as possible over which to determine the spectral index. Observations were not attempted at shorter wavelengths than 1.1 mm because of the poor weather conditions. Observations concluded at

11:29.

On September 03 we had some difficulty flux-calibrating on Mars due to local weather conditions at low elevation, and so relied upon W75N. Pointing was again checked on MWC349. The mean atmospheric optical depth τ was 0.35 at 1.1 mm and 0.23 at 2.0 mm. Observations of Cyg X-3 again began at 04:50 and continued at 1.1 and 2.0 mm in a similar manner to the previous night, being interleaved approximately once every hour with calibration checks of W75N. Observations were terminated by fog at 13:15.

Fig. 3.1(a) shows the data from the two nights observations, averaged over bins of minimum length 20 min. Any single integration more than 3σ above the mean within a bin was removed and attributed to a random cosmic-ray event. The 1σ errors shown are the standard error for each bin. Due to the unexpected closure of the dome at the end of the second night, we were unable to end observations with a flux calibration, and so continued with the value of τ determined earlier.

3.2.2 MERLIN

Cyg X-3 was observed with all 8 telescopes of the MERLIN array (including the Lovell telescope) at 1658 MHz from 01:50 UT on 1993 September 02 to 01:15 UT on 1993 September 04. Both left and right circular polarizations were correlated, each with a bandwidth of 15 MHz, divided into 1-MHz channels. MERLIN provides interferometer spacings from 6 to 217 km corresponding to 35 $k\lambda$ to 1.2 $M\lambda$, though projection considerably reduces the shortest spacing.

Empirically determined corrections for the telescope sensitivities as a function of elevation were applied to the data. At very low elevations these corrections are large and become less reliable, since there is also an azimuthal dependence. Data for approximately 90 min either side of lower culmination where the elevation was less than 5° were deleted.

Initial calibration of the telescope and baseline complex gains for each 1-MHz channel was done using 2134+004, which is known to be unresolved. The flux density of 2134+004 was determined as 5.116 Jy by comparison on

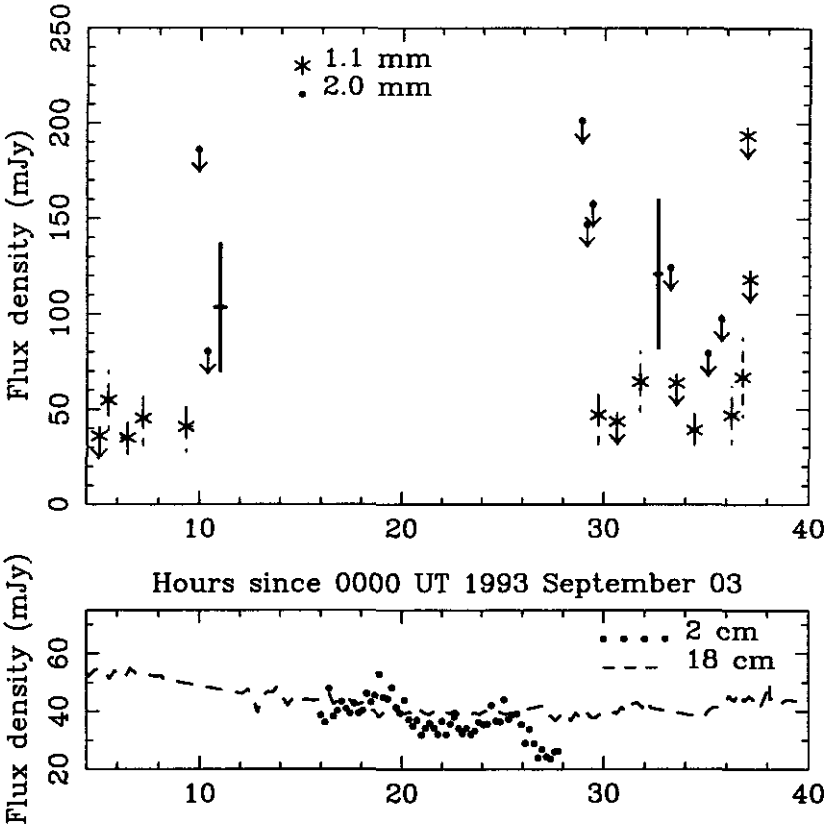

Figure 3.1 Observations at 1.1 mm, 2.0 mm, 2 cm and 18 cm of Cyg X-3. The errors on the cm data are smaller than the symbol size.

the shortest baselines with 3C286 for which a flux density of 13.639 Jy was used (Baars et al 1977 [105]). After the initial calibration the individual 1-MHz channels were averaged to a single 15-MHz band. The MkII – Lovell baseline, which is only 425 m and suffers severe confusion, was discarded at this stage. Subsequent calibration and mapping were done using the NRAO AIPS package running on SUN SparcStations at Jodrell Bank.

No attempt was made to interleave observations of a phase calibrator in case this precluded the detection of periodic behaviour on short timescales. Instead, the Cyg X-3 data were self-calibrated in phase using a circular Gaussian starting model with a FWHM of 0.15 arcsec (cf. Wilkinson et al 1994 [45]) and mapped. In order to remove the effects of variations in

the telescope gain from the map, an amplitude self-calibration was made and the corrections were smoothed over a timescale of 30 min. This will also have the effect of 'calibrating out' real variations in source strength, so this calibration was not applied to the data used to obtain the light curve (see below). Indeed, the similarity of the amplitude corrections for different MERLIN telescopes shows that the amplitude fluctuations are real and are similar on all baselines.

The resulting uniformly weighted map (Fig. 3.2) has a resolution of 0.15 arcsec and an rms noise of 38 μJy. A Gaussian fit to this map gives a major axis of 0.163 ± 0.007 arcsec and a minor axis of 0.124 ± 0.005 arcsec in position angle $63^\circ \pm 2^\circ$ degrees. This is slightly smaller than the fit by Wilkinson et al [45], but the axial ratio and position angle are consistent within errors. This confirms the suggestion by Jones et al (1994) [47] that the elongation of the scattered radio image is perpendicular to the orientation of the infrared polarisation in the direction of Cyg X-3. We note that there is no significant emission beyond the scattered image, which would be expected if a low level jet were present. There is no evidence that the variations depend significantly on baseline length, as expected if the scattering does not occur in the immediate vicinity of Cyg X-3.

The elliptical extension is due to interstellar scattering and the new data confirm that the scattering is similar when the source is quiescent (the previous data were obtained just after the outburst of 1989 June when the flux density at 18 cm was 5.1 Jy).

The light curve shown in Fig. 3.1(b) was produced using the phase-calibrated data since amplitude self-calibration smooths out real fluctuations. In order to remove the effects of the resolution, the data were first divided by the elliptical Gaussian model. All the baselines except those involving Defford and Cambridge (the two most distant telescopes) and MkII - Lovell were coherently averaged in 15-min bins. The data were then rescaled by the total flux density in the model. The variation in this light curve is clearly visible in the raw data in the shorter baselines. The noise errors are about 0.5 mJy per 15-min point, although telescope gain fluctuations could

give rise to errors of up to 2 mJy.

3.2.3 Ryle telescope

Cyg X-3 was observed over a period including the times of the JCMT observing, although the actual overlap is only an hour or so because of the difference in longitudes of the observatories, and the limited hour–angle coverage available. The observations, of Stokes $I+Q$, were at 15.1 GHz, using a bandwidth of 350 MHz. During each of the sessions, 16-min observations of Cyg X-3 were interleaved with 2-min observations of 2005+403, a bright unresolved calibrator a few degrees away. The calibration data were used to calibrate the instrumental phases, including slowly varying components of the atmospheric phase. The amplitude scale is calibrated with reference to 3C48, assumed to be 1.7 Jy at this frequency (consistent with the scale of Baars et al 1977 [105]).

The correlated signals on all of the baselines up to 100 m (involving 5 of the 8 aerials in this configuration) were added vectorially, to produce the equivalent of a phased array. Longer baselines are more liable to contamination by atmospheric phase changes, and have not been used in this analysis.

There were three observing runs made at 2 cm of Cyg X-3: the first was between September 01 16:31 UT and September 02 03:56 UT when the flux density varied in the range 11–78 mJy; the second was between September 02 15:55 UT and September 03 03:52 UT and is plotted in Fig. 3.1(b) as averages over 5 minutes; and the third was between September 03 23:36 UT and Sept 03 02:07 UT when the flux density varied between 27 and 64 mJy.

3.3 Interpreting fluxes

In this section we take some of the results of the successful model of Marti, Paredes & Estalella (1992) [49] (hereinafter MPE92), notably their predictions for peak flux density and peak flux time delay as functions of frequency, and apply them to repeated small injections within a dense stellar wind.

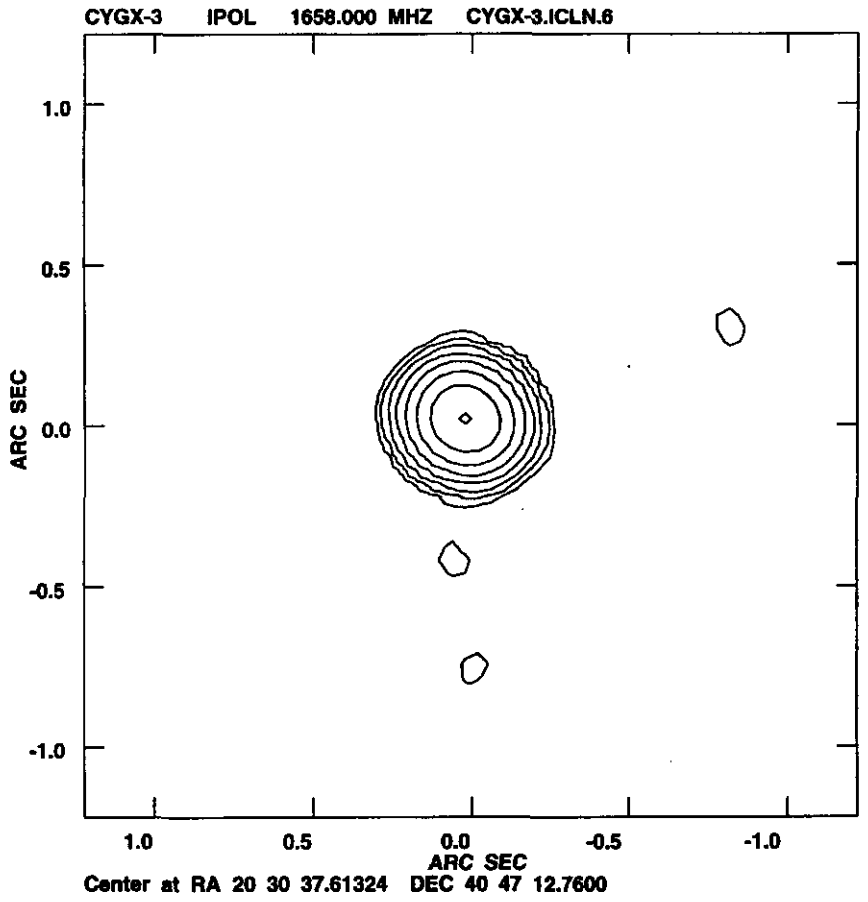

Figure 3.2 18-cm map of the asymmetric scattering by the ISM around Cyg X-3. Resolution is 0.15 arcsec and rms noise is 38 μJy (see Section 3.2.2).

Comparison of Figs 3.1(a) and 3.1(b) shows that the mm fluxes are higher than the cm fluxes, in contrast to predictions of the standard model of flares. The spectral index α, where $S_\nu \propto \nu^\alpha$, between 2 mm and 1.1 mm too is rather more negative than that predicted by the model of MPE92. By exploring the second point first we shall attempt to build a self-consistent picture to explain these properties, based upon repeated short, low-amplitude flares in a stellar wind. Note that in MPE92 it was assumed that the ejecta had travelled beyond the local opacity effects of the stellar wind (resonable for a major flare) - thus to use these results within the stellar wind requires

a consideration of its free-free opacity.

3.3.1 Behaviour in the millimetre region

We assume that the quiescent behaviour observed is a superposition of frequent low-amplitude flares, that these flares have the same spectral index as the major radio flares and that the material surrounding the emitting region is optically thin at these wavelengths. We ignore any contribution from line emission. For major radio flares the peak emission has a spectral index, in the absence of self-absorption, of $\alpha \sim -0.55$ (MPE92, using 408-MHz to 90-GHz data for the 1972 flare). The mean spectral index between 2.0 and 1.1 mm averaged over both nights is $\alpha = -1.2 \pm 0.4$.

Modelling repeated small injections

We assume the flares to be impulsive and neglect the rise times; we assume that the flares decay with a frequency-dependent time constant τ_ν and that flares recur after a typical time interval T. The peak flux at any frequency due to a single injection, $S_{\rm peak}$, gives us the mean flux density at that frequency

$$\langle S \rangle = S_{\rm peak} \times \tau_\nu / T$$

(sum of series) taking into account the flux from all previous injections.

The mean spectral index is thus a function of $\tau_{2.0\rm mm}/\tau_{1.1\rm mm}$, and solving for the observed spectral index we find $\tau_{2.0\rm mm} \sim 1.4\tau_{1.1\rm mm}$. The ratio τ_ν/T determines the amount of fluctuation (i.e. the noisiness of the data) about a flux level which is set by $S_{\rm peak}$. Since the observed fluxes neither are perfectly smooth nor show clear examples of individual flares, we deduce that τ_ν *is neither much greater than nor much less than* T.

We see average fluxes of $\langle S_{2.0\rm mm} \rangle \sim 100$ mJy and $\langle S_{1.1\rm mm} \rangle \sim 50$ mJy and peak to peak fluctuations around these values of ~ 40 mJy at 2.0 mm and $\sim$ 30 mJy at 1.1 mm. Decay times at 1.1 mm are consistent with $\tau \sim 120$ min. Given the $\tau_{2.0\rm mm}/\tau_{1.1\rm mm}$ ratio derived above, $\tau_{2.0\rm mm} \sim 170$ mins. We can simulate our observations at 2.0 and 1.1 mm with the following additional

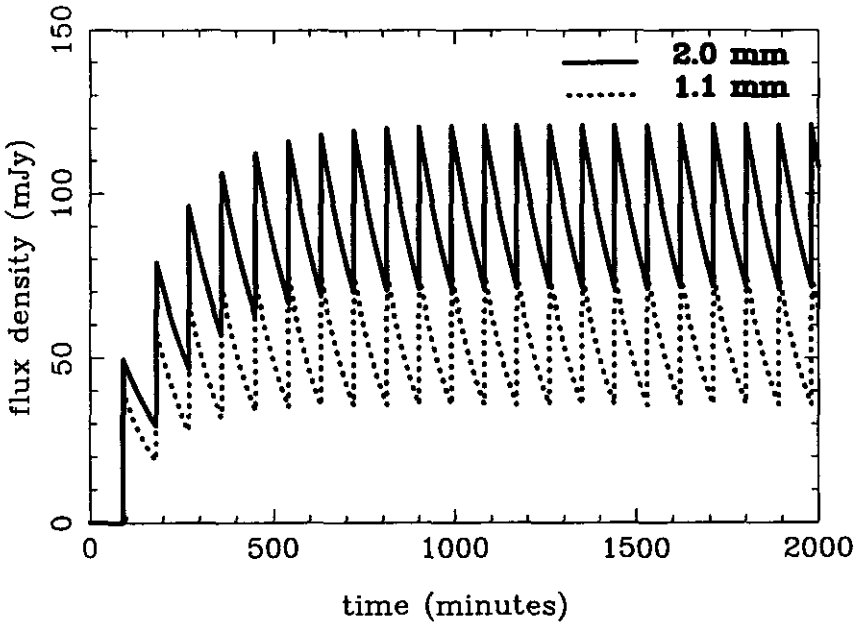

Figure 3.3 Model for emission at 1.1 and 2.0 mm, as described in the text. The plot illustrates how rapidly such a system, once initiated, will stabilise.

parameters: $T \sim 90$ min, $S_{\mathrm{peak(1.1mm)}} \sim 40$ mJy giving $S_{\mathrm{peak(2.0mm)}} \sim 50$ mJy (as $\alpha = -0.55$), and exponential decay. The model described above with these parameters would stabilise quickly, within 1000 min, as shown in Fig 3.3. Figs 3.4(a) & (b) show the predicted flux levels, degree and timescale of variability predicted by the model compared with the observed flux levels and variability.

Note that T should be regarded as a first order approximation of the variability timescale of the injection stream, typically a few hours; it is not a derived periodicity. Could the data be fitted with T equal to the orbital period of 4.8 h or the periodicity claimed by Molnar et al (1984) of 4.95 h ? Keeping $\tau_{1.1\mathrm{mm}} \sim 120$ min, this gives $S_{\mathrm{peak(1.1mm)}} \sim 120$ mJy. There is no evidence for an injection of such amplitude in our data. Alternatively, alteration of $\tau_{1.1\mathrm{mm}}$ to keep $S_{\mathrm{peak(1.1mm)}} \leq 50$ mJy (to agree with the observations) gives $\tau_{1.1\mathrm{mm}} \sim 290$ min which would appear to be too long to be consistent with the data. Note also that extrapolation of this model to the IR predicts quiescent fluxes that would lie below the IRAS detection

threshold. Thermal emission from a stellar wind, as seen in the IR, will contribute < 1 mJy longwards of 900 μm (see chapters 2 & 4).

3.3.2 Low-level radio emission

We turn now to the problem of the flux densities at centimetre wavelengths being significantly lower than those in the millimetre region.

The MPE92 model assumes synchrotron emission, with maximum emission from a single flare event (neglecting local opacity) at $\sim$ 6 cm. So if $S_{\mathrm{peak(1.1mm)}} \sim 40$ mJy then $S_{\mathrm{peak(2cm)}} \sim 200$ mJy and $S_{\mathrm{peak(18cm)}} \sim 100$ mJy. Note that MPE92 also predict a $\sim$ 24-hour delay after injection in reaching peak flux at 18 cm due to self-absorption by the ejecta.

A large body of evidence (e.g. Davidsen & Ostriker 1974; van Kerkwijk 1993a, Nakamura et al 1993) suggests that Cyg X-3 is embedded in a hot dense wind emanating from the companion to the compact object. Doppler-shifted Wolf-Rayet emission features have been found in the infrared spectrum (van Kerkwijk 1993b), though at present there are problems involved in physically fitting a 'classical' Wolf-Rayet star into a system with a 4.8-hour period. However, some parameters of this wind can be estimated and used tentatively to explain the observed low emission at centimetre wavelengths.

A radially symmetric wind with constant velocity is assumed; this assumption may not hold close in to the central source, but should be a good approximation in the regions where the wind is optically thin to mm and cm wavelengths. We envisage synchrotron-emitting ejecta travelling out through the wind and consider the effects of the optical depth of the embedding wind medium on the radio spectrum observed.

Wright & Barlow (1975) have shown that the medium becomes thin to successively lower frequencies as the radius from the central source increases; radii with equal optical depths at different frequencies are related by $R \propto \nu^{-0.7}$.

The steepness of our observed mm spectrum strongly suggests that the wind (as well as the synchrotron-emitting ejecta) is optically thin at mm wavelengths. We therefore assume that both the 1.1-mm and 2.0-mm emis-

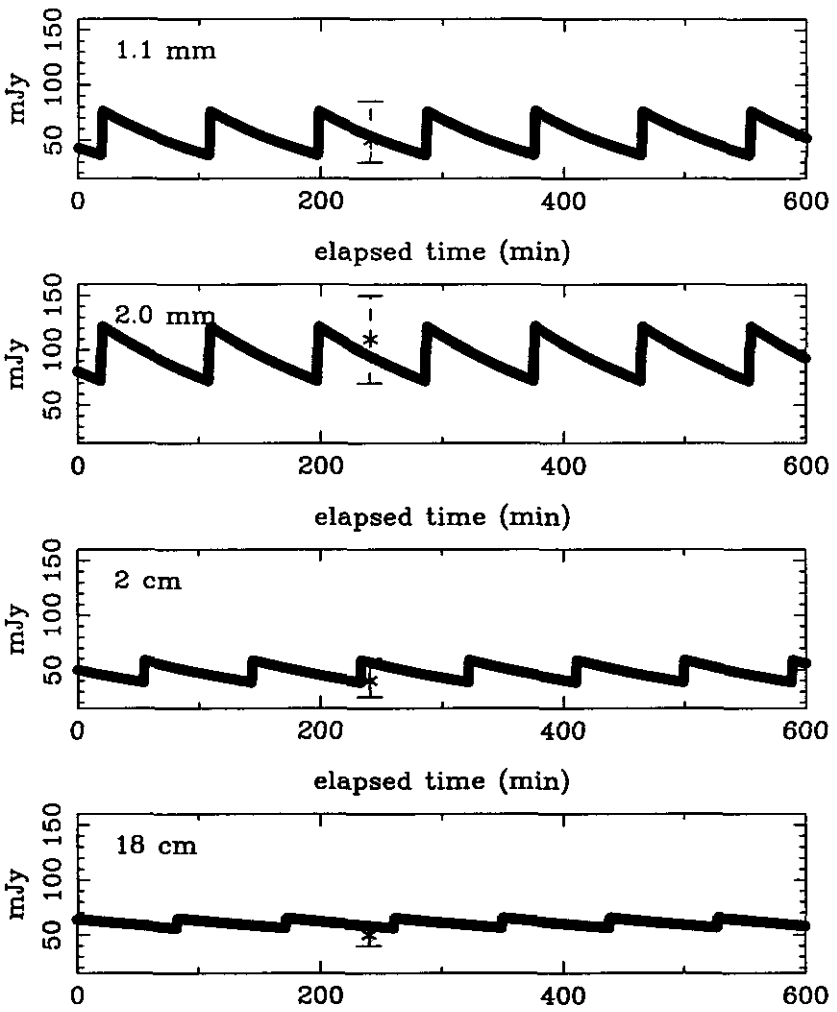

Figure 3.4 Predictions of model for quiescent emission at 1.1 mm, 2.0 mm, 2 cm and 18 cm (thick lines) in comparison with observed mean fluxes and degress of variability (stars with error bars)

sions come from ejecta in optically thin wind regions, and further that there is no synchrotron emission from within the 2.0 mm-photosphere. We assume this 'photosphere' to have a radius of $\sim$ 1000 $R_\odot$ (typical for a Wolf-Rayet wind, e.g. Williams et al 1990), i.e. the synchrotron emission starts when the ejecta reach 1000 $R_\odot$. This is far larger than the binary separation, for which Cherepashchuk & Moffat (1994) place a dynamical upper limit of 5.6 $R_\odot$.

Using the Wright & Barlow (1975) law the other relevant photospheres are: $R_{2\mathrm{cm}} \sim 5000\ R_\odot$ and $R_{18\mathrm{cm}} \sim 23000\ R_\odot$. The assumed geometry is illustrated in Figure 3.5. Previous observations of an expanding double-lobe structure associated with Cyg X-3 following radio outbursts have given ejection velocities of up to $\sim 0.3c$ (e.g. Molnar et al 1988). If the ejecta have a velocity of $0.3c$, travel times from 1000 $R_\odot$ to 5000 $R_\odot$ and from 1000 $R_\odot$ to 23000 $R_\odot$ are $\sim$ 8 hours and $\sim$ 50 hours respectively. During these travel times the peak fluxes will decay, except that there is a delay of 24 hours in the 18-cm flux reaching peak (MPE92) so the time available for decay at this frequency may be taken to be the travel time minus 24 hours. We shall assume here that decay of the flares is exponential.

Thus the observed fluxes and spectra in the cm range are a combination of two competing effects: (i) the decay of the peak fluxes as the ejecta travel out to the regions where the medium becomes optically thin, and (ii) the pile-up of the rapidly repeated injection fluxes as described in the previous section. Using the injection fluxes as predicted from MPE92 and the observed fluxes of $\sim$ 45 mJy at 2 cm and 18 cm, we can establish decay times for the flares of $\tau_{2\mathrm{cm}} \sim 210$ minutes and $\tau_{18\mathrm{cm}} \sim 600$ minutes. Thus we have a consistent pattern of increasing τ with wavelength from 1.1 mm to 18 cm.

The model also predicts peak to peak fluctuations of $\sim$ 15 mJy at 2 cm and $\sim$ 6 mJy at 18 cm, in reasonable agreement with observations. Figs 3.4(c) & (d) display the predicted emission at 2 cm and 18 cm.

A consequence of this model is that significant delay is predicted between the time when flares are seen at mm wavelengths and when they are seen at

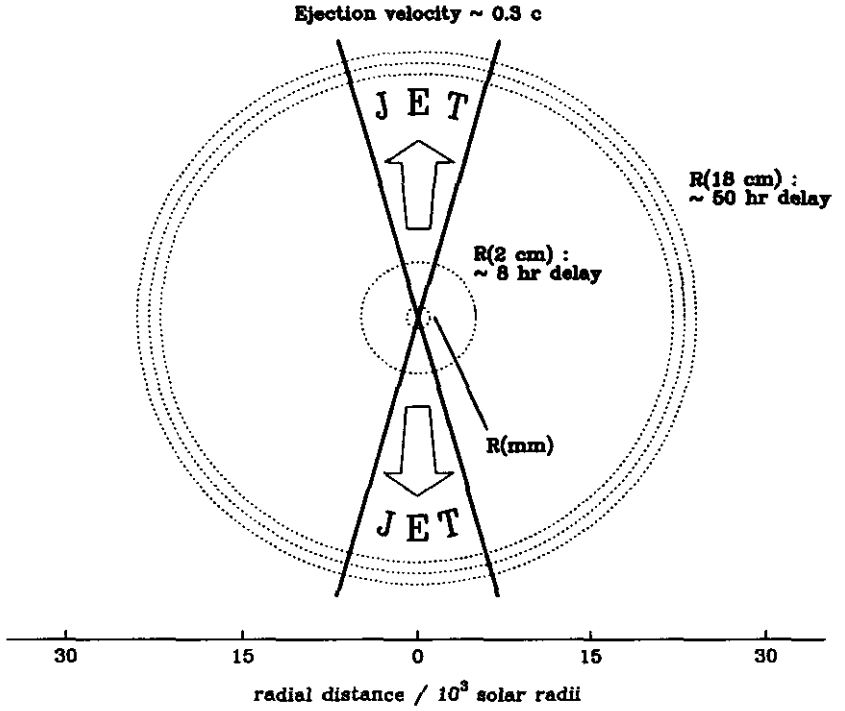

Figure 3.5 Simple geometry for Cyg X-3 system assuming $R_{\rm mm} \sim 1000 R_{\odot}$, and an isothermal, radially symmetric, constant velocity wind

cm wavelengths - when searching for correlations in behaviour the cm radio observations should continue after the the mm observations. Were the high millimetre fluxes observed the precursor of a radio flare? Data taken at 13.3 and 3.6 cm by the NRL - Green Bank Interferometer monitoring programme (Elizabeth Waltman, private communication) suggests not. The period from 30 d before to $\sim$ 60 d after was a period of stable quiescent radio emission with a mean flux density at 13.3 cm of 72 ± 22 mJy and a maximum of 104 mJy.

3.4 Conclusions

A self-consistent model has been developed to account for the observed quiescent behaviour of Cyg X-3 at 1.1 mm, 2.0 mm, 2 cm and 18 cm in terms of repeated small injections of synchrotron-emitting electrons in a region

in the Cyg X-3 wind which is transparent to millimetre-wave radiation but opaque at centimetre wavlengths. Fig 3.4 summarises the comparison of model & data. Though the model makes several crude simplifications (e.g. periodic injection at interval T, no rise-times taken into account, no account of evolution of ejecta as they approach the millimetre photospheres), we believe that the general conclusions stated above are valid. We take this to be further strong evidence for the existence of a hot dense wind within which the Cyg X-3 system is embedded. A further consideration not taken into account here is that the jet may be decelerating as it moves outwards in the wind. This would be due to increasing interaction between the wind and the ejecta as the density of the latter decreases during expansion. This would actually serve to reduce the consequences of neglecting a travel time from $R_{1.1mm}$ to R_{2mm} as between these two regions the ejecta would have been travelling with a velocity greater than the $0.3c$ observed with radio VLBI.

The ejection of streams of relativistic electrons is probably related to the accretion process at the heart of the system, for which the copious X-ray emission serves as evidence, though the exact mechanism remains unclear. It is also unclear as to whether or not all the active processes observed in this system (i.e. infrared flares, millimetre-wavelength emission and both quiescent and flaring radio emission) can be attributed to the near-constant ejection of matter from the accretion region. If it were so, then one would expect the chain of events ending in a large radio flare to have begun many hours earlier with infrared flares. However, there seems no evidence that infrared flares are necessarily the beginning of such a chain of events. Possibly the 'standard' infrared flares just die out before reaching the radio 'photospheres', in which case one would expect large radio flares to be pre-empted by especially large infrared flares, and so on. It should be noted that the consistency of the previous Cyg X-3 millimetre data with the model for a large radio flare is not opposed by this thesis, as those observations were not carried out until a radio flare had begun, by which time the ejecta would have travelled beyond the point at which free-free absorption by the wind was important.

The model presented here predicts that, during any resolvable 'event' observed simultaneously at millimetre and radio wavelengths (accounting for time lag as ejecta move outward), the spectrum should be flattest at the start of the event, steepening as the event evolves. This, and the steeper spectrum in the mm regime, may be due to radiative energy losses resulting in the electrons radiating at mm wavelengths having relatively short lifetimes. The model also predicts that, for the low-level emission, the observed light curve will be smoother with increasing wavelength at any epoch.

Chapter 4

Multiwavelength observations of the 1994 February – March Cygnus X-3 radio flares

4.1 Introduction

Cyg X-3 was first observed to undergo a sequence of radio flares in 1972 September (Gregory et al 1972 [12]), since which time over 20 outbursts of magnitude > 5 Jy have been observed. The 1972 activity remains however one of the most thoroughly monitored periods of strong radio flares from any galactic radio source (excepting possibly the Sun), with observations over the period at radio, millimetre, infrared and X-ray wavelengths (see Nature Phys. Sci. 239, 1972 and chapter 1 for more details).

Multiwavelength observations of Cyg X-3 during periods of radio flaring have however, since 1972, been rare. The majority of flare events have been observed only at the two radio frequencies operated by the NRL-Green Bank monitoring program. Millimetre observations have been performed only on one occasion during a radio flare since 1972 (Baars et al 1986 [52]). Despite several models for infrared flares predicting some correlated infrared : radio behaviour (eg. Mason et al 1986 [55], Apparao 1987 [37]) there has been no concerted campaign to search search for such a correlation (due presumably, in part, to the difficulty of obtaining target-of-opportunity observations on infrared telescopes). X-ray behaviour has been found to correlate with radio flares, (Watanabe et al 94 [36]) but this was as a result of the comparison of

two large long-term data sets and not due to specific coordinated observations. Weak evidence for enhanced UHE γ-ray emission during radio flares (eg. Protheroe 1994 [85]) has not been confirmed.

I present in this chapter observations of Cyg X-3 during a 60 - day active period in 1994 February – March. The source was monitored intensively in the radio at 13.3 & 3.6 cm (NRL-Green Bank, USA) and at 2.0 cm (Ryle Interferometer, Cambridge, UK). I also managed to obtain, with the cooperation of several others, (sub)millimetre and infrared data at several epochs from the JCMT and UKIRT respectively, providing a valuable multi-wavlength aspect to the observations.

A brief summary of the work presented in this chapter is to be published in (Fender et al 1996b [106]).

4.2 Observations

4.2.1 NRL-Green Bank : 13.3 & 3.6 cm

Cyg X-3 has been observed by the NRL-GBI Monitoring Program on a daily basis since 1982. The Green Bank Interferomter (GBI) is currently operated by the National Radio Astronomy Observatory for the Naval Research Laboratory (NRL). In Autumn 1989, the National Radio Astronomy Observatory installed cryogenic receivers on the Green Bank Interferometer. Since October 1989, Cyg X-3 and the calibration sources were observed for approximately ten minutes each, simultaneously at two frequencies, 2.25 and 8.3 GHz. Prior to October 1989, the frequencies were 2.7 and 8.1 GHz, and the observations alternated between the two frequencies every 30 seconds. The flux densities were measured on the 2.4 km baseline and are the average of the left-left and right-right circular polarizations. Cyg X-3 is observed five to 15 times a day (three times daily before 1990.6) on two different gain codes to facilitate accurate measurements over a range of possible, and occasionally rapidly changing, flux densities from 100 mJy to almost 20 Jy.

A flux density calibration procedure similar to that reported in Waltman et al (1994) [21] was employed here. Three secondary calibration sources

(0237−233, 1245−197, and 1328+254) were used to produce flux densities for Cyg X-3 and 2005+403. The flux densities of 0237−233, 1245−197, and 1328+254 were determined using observations of 1328+307 (3C 286). The flux density of 3C 286 was based on the scale of Baars et al (1977) [105], and the assumed values were 11.85 Jy at 2.25 GHz and 5.27 Jy at 8.3 GHz.

The quiescent flux densities for Cyg X-3 were calibrated using the four calibration sources listed above, weighted by the difference in time between the observations of Cyg X-3 and calibrator sources observed within 24 hours of the Cyg X-3 observation. However, during flares when Cyg X-3 was observed almost continuously from 5 hours east to 5 hours west of the meridian, scans of Cyg X-3 were paired with scans of 2005+403 in order to remove hour angle gain effects in the flux densities. These may exceed 20% at 8.3 GHz. In this case, the meridian observation of 2005+403 was calibrated using the three calibrators above. Then, paired scans with 2005+403 were used to calibrate Cyg X-3.

Errors in the GBI data are flux dependant: 4 mJy (2 GHz) or 6 mJy (8 GHz) for fluxes < 100 mJy, 15 mJy (2 GHz) or 50 mJy (8 GHz) for fluxes ~ 1 Jy, and 75 mJy (2 GHz) or 250 mJy (8 GHz) for fluxes ~ 5 Jy.

4.2.2 Ryle Interferometer : 2.0 cm

The Ryle Telescope (Jones 1991 [107]) has been used to monitor variable sources, primarily during gaps in the main observing programmes of the telescope apart from the coordinated observations for which observations were specifically scheduled.

During the period discussed here, the telescope operated at 15 GHz with a banFROM GUYdwidth of 350 MHz. The Stokes' parameters I+Q were measured in all cases. Data from each interferometer pair are collected, together with interleaved calibration observations of 2005+403, a nearby quasar which is unresolved at all baselines in use here. The calibrations were used to correct for the instrumental phases of the system; the amplitude scale was calibrated by nearby observations of 3C48 or 3C286. Atmospheric refractive-index fluctuations introduce phase errors which increase

with baseline; the time-scales of these are such that it is not possible to remove them by using the interleaved calibrator. The optimum procedure is to use only the shorter baselines, for which the phase uncertainties are small, except in the few cases where the flux is exceptionally low (before major flares) when it may be desirable to use all the available data. During the observations described here, the telescope was in its 'compact array' mode with 5 aerials in a group having maximum baseline of about 100m; in practice nearly all data use only this set of aerials.

Once the instrumental phases have been removed, the data for all the baselines selected are added vectorially, producing the effect of a phased array. This vector sum is smoothed vectorially in time and its amplitude is taken as the flux of the source. (In the rare cases of very low flux density, this procedure overestimates the flux; the in-phase component of the vector sum is used to give an unbiased estimate.)

4.2.3 JCMT : 1.1, 0.8 & 0.45 mm

Following the detection of radio flaring from Cyg X-3 at Green Bank and Cambridge, target-of-opportunity observations were requested and made at the James Clerk Maxwell Telescope (JCMT) over a three day period between the first and second flares. All observations were made using UKT14, a photometer operating in the 0.45 - 2.0 mm wavelength range. The JCMT observations are summarised in table 4.1. On 1994 Feb 26 we obtained a 3σ upper limit at 1.1 mm and shortly afterwards a 3.9σ detection of Cyg X-3 at 0.8 mm. Observations on the following two days at 0.45 mm provided initially a 3σ upper limit and then a 4.8σ detection. The detections at 0.8 and 0.45 mm are the first reported detections of Cyg X-3 at these frequencies.

4.2.4 UKIRT : 2.2 & 1.6 μm

At the same time as requests were being made to the JCMT for observations, similar requests were being made to the United Kingdom Infrared Telescope (UKIRT). Observations were made at very short notice on two occasions between the first and second flares, due largely to the kindness of observers

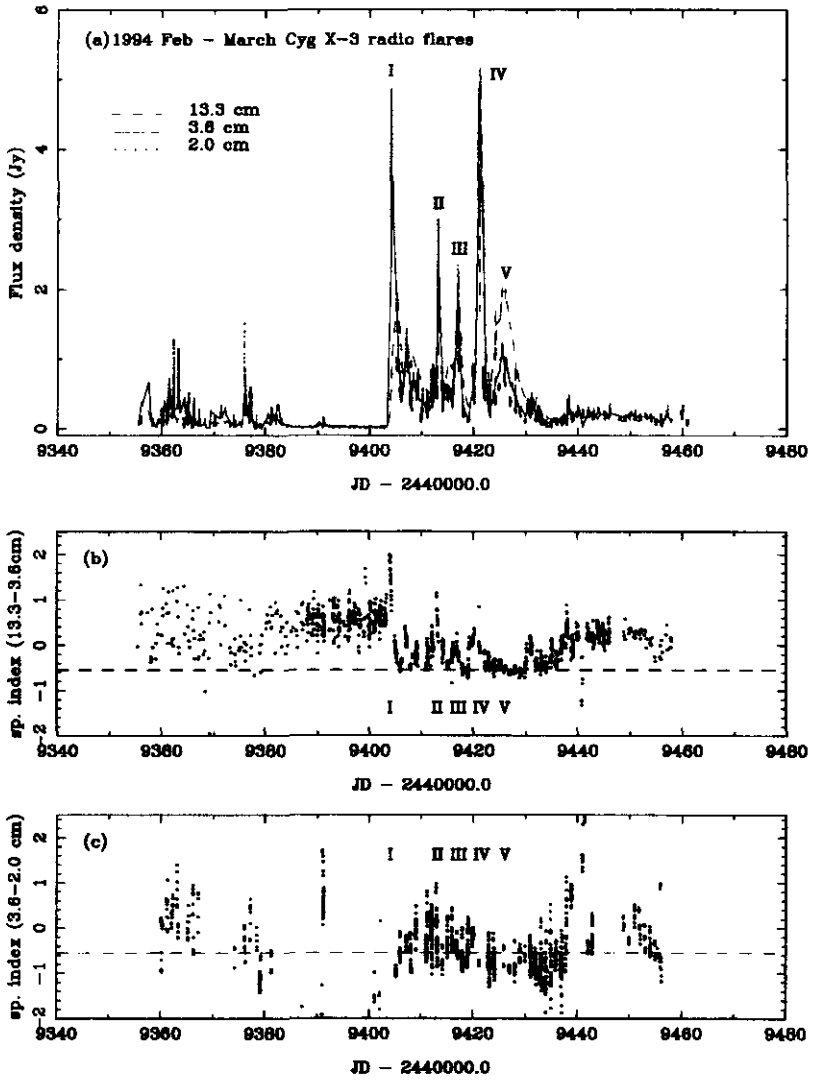

Figure 4.1 Monitoring of the 1994 Feb-March radio flares at 13.3, 3.6 & 2.0 cm. The five major flare events have been labelled I – V. Figs 1(b) & 1(c) show how the spectral indices from 13.3 - 3.6 cm & 3.6 - 2.0 cm respectively evolved with time.

Table 4.1 JCMT observations during 1994 Feb – March

JD - 2440000.0	Filter	Flux density (mJy)
9410.32	1.1 mm	< 40 (3σ)
9410.33	0.8 mm	77 $\pm$20
9411.34	0.45 mm	< 430 (3σ)
9412.36	0.45 mm	330 $\pm$69

Table 4.2 UKIRT observations during 1994 Feb – March

JD - 2440000.0	K band (mJy)	H band (mJy)
9406.76		16.1 $\pm$1.0
–	32.5 $\pm$2.0	
–		16.8 $\pm$1.0
–	39.5 $\pm$2.0	
9407.75	25.1 $\pm$1.0	
–	23.7 $\pm$1.0	
–	23.4 $\pm$1.0	
–	21.8 $\pm$1.0	
–	19.8 $\pm$1.0	

at the telescopes who gave up some valuable PATT time. All observations were made using IRCAM2 (now superceded by IRCAM3), a 58 x 62 imaging array operating in the $1-5\mu$m wavelength range. On 1994 February 23, less than five days after the onset of the first radio flare, observations were made twice each in the H (1.6 μm) and K (2.2 μm) bands with an integration time of 10 s and flux calibrated using HD136754. On the following night a series of five observations in the K band were made, each with 15 s integration time and flux calibrated using HD162208. During all UKIRT observations Cyg X-3 was significantly brighter than during 'quiescence' (see chapters 3 & 5); however on both nights observations were made near the end of the shift as dawn approached and the error bars are larger than usual. The (H-K) colour for JD 2449406 of $\sim$ 1.3 was slightly redder than the mean observed in 1984 (Chapter 2, Fender et al 1995b) but not as red as during the strong rapid infared flares observed in that period. The UKIRT observations are summarised in table 4.2.

4.3 The radio flares

On approximately 1994 Feb 20 Cyg X-3 underwent the first of a series of five medium-sized radio flares, reaching $\sim$ 5 Jy during two of the events. This activity had been preceded by $\sim$ 19 days of very low flux densities from Cyg X-3. Figure 4.1(a) summarises the observations at 13.3, 3.6 & 2.0 cm of the sequence of five radio flares, which I have chosen to label I – V. A rise to $\sim$ 5 Jy at 2 - 4 cm on a timescale of $\sim$ 24 h (as observed for flares I and IV) gives a brightness temperature $T_b \geq 10^9$ K, typical for radio emission from X-ray binaries and as found for sources of nonthermal synchrotron emission.

Parts (b) & (c) of Fig 4.1 plot the spectral index α (where $S_\nu \propto \nu^\alpha$) in the two wavelength intervals 13.3 - 3.6 cm and 3.6 - 2.0 cm. The former is trivial to calculate, as the observations at 13.3 & 3.6 cm are performed simultaneously at Green Bank. In order to calculate the index from 3.6 - 2.0 cm however, I have used the following method : for each 2.0 cm data point, I have averaged all (if any) of the 3.6 cm data points within 15 min of it, and used this value to calculate the spectral index. Smaller time intervals reduced the effective overlap of the two data sets, giving fewer values for the index, whereas larger time intervals are approaching the typical timescale of change at high radio frequencies and would be untrustworthy. Experimentation with the time interval between 5 and 20 min however revealed the same broad trends as plotted in Fig 4.1 (c) as a result of using a 15 min interval.

4.3.1 Quenched emission preceding flares

Waltman et al 1994 [21] have shown that periods of radio flaring in Cyg X-3 tend to be preceded by periods of very low (< 30 mJy) or 'quenched' flux densities. It has been suggested in Waltman et al 1995 [50] that such quenching is due to the presence of an increased proportion of thermal gas in or near the binary system, possibly due to an enhanced mass loss/transfer rate from the companion to the compact object (see also Kitamoto et al 1994 [65] and Watanabe et al 1994 [36]).

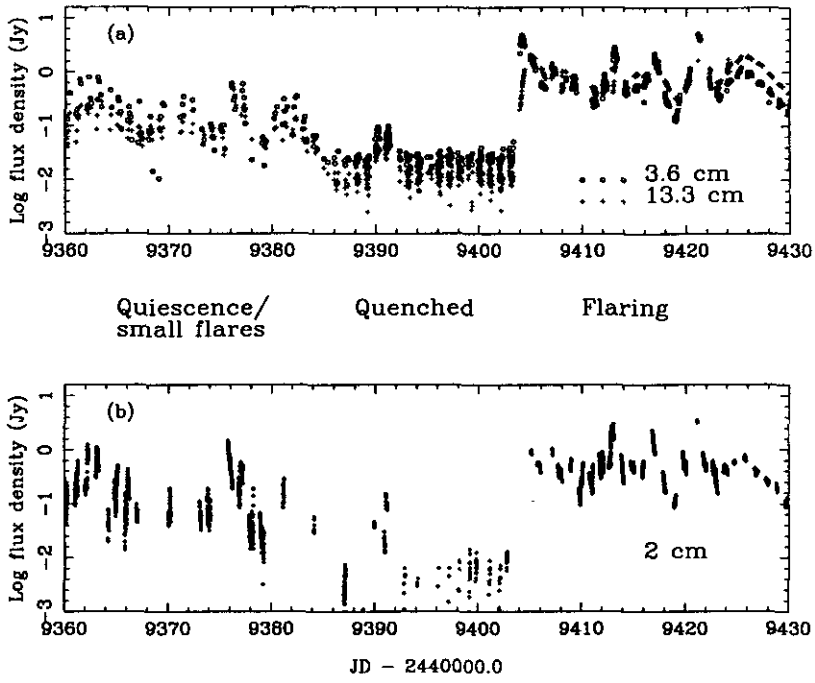

Figure 4.2 Quenched radio emission preceding flares : Fig 4.2(a) shows the NRL-Green Bank monitoring revealing unusually low flux densities for $\sim$ 19 days preceding flare I. Fig 4.2(b) presents independent confirmation of this effect, in the 2.0 cm Ryle Telescope data. During the quenched period the mean flux density at 13.3 cm appears to be less than that at 3.6 cm, suggesting opacity is important during this period (but see discussion below).

The NRL-Green Bank data reveal a period of $\sim$ 19 days of unusually low flux densities preceding flare I on 1994 Feb 20 (except for a small event on JD $\sim$ 2449391). The 2.0 cm Ryle Telescope data provide independent confirmation of this period of quenched radio emission (Figure 4.2), with flux densities as low as a few mJy recorded.

The mean spectrum of the quenched emission is interesting in that there is still evidence for some opacity at 13.3 cm - ie. the emission is not simply optically thin afterglow from previous injections during a period when no fresh particle injection is taking place. Such emission would be expected to

be optically thin as opacity from thermal electrons mixed with the ejecta and/or from a dense stellar wind should not be important in remnant ejecta which would be of a relatively low density and far from the system. The beam sizes of both the Green Bank and Ryle Telescopes are greater than several arcsec (Elizabeth Waltman & Guy Pooley, private communications) and so would include the faint radio lobes detected by Strom, van Paradijs & van der Klis (1989) [38]. These lobes may be tracers of the outermost regions from which synchrotron emission from the Cyg X-3 jets may be detected, representing $\sim$ 200 days of travel time for a constant jet velocity of 0.3 c and a distance to Cyg X-3 of 10 kpc.

Instead it seems that the emission during this period originates in an environment with some significant opacity, possibly some standing shock (see eg. Icke 1991 [108]) deep within the wind near the base of the jets. Alternatively, continuing low-level injection into the jets deep in the wind and/or with a significant proportion of thermal electrons mixed with the relativistic electrons, could be responsible. Elizabeth Waltman at NRL (private communication) however cautions that the NRL-Green Bank data are noisy at this level and observations with a more sensitive instrument (eg. VLA) during a quenched period are necessary to confirm this effect.

4.3.2 Evolution of the radio spectrum

There are several clear trends evident in the 13.3, 3.6 & 2.0 cm radio data during the sequence of events I – V. The first and most obvious is the turn around of the radio spectrum : ie. flare I peaks at $\lambda \leq 3.6$ cm and appears to be heavily absorbed at 13.3 cm, wheras flare V is effectively an optically thin event, brightest at 13.3 cm and with no turnover evident in the radio spectrum. The transition between these two extremes, through flares II – IV, is fairly smooth. Figures 4.1(b) & (c) show how the spectral indices from 13.3 – 3.6 cm & 3.6 – 2.0 cm respectively evolve with time : $\alpha_{13.3-3.6cm}$ seems to evolve towards the mean optically thin value (for Cyg X-3) of -0.55, whilst $\alpha_{3.6-2.0cm}$ seems to reach even more negative values, suggestive of radiation losses playing a role (see sect 4.6.1). Figure 4.3 illustrates how

the spectrum of the flare events changes in the sequence I – V, using the peak flux densities for each event (ignoring time delays, see below).

The transition towards lower opacity along the sequence I – V is also evident in the decreasing time delay between peak emission at 2.0 & 3.6 cm and that at 13.3 cm. A delay in peak emission at wavelengths greater than $\sim$ 6 cm is often observed in Cyg X-3 flares and can be explained as being due to emission at the longer wavelengths being significantly absorbed at the time when the shorter wavelengths are peaking. Only at later times when the ejecta have expanded significantly for self-absorption (synchrotron or free-free, see eg. MPE92 [49]) to be unimportant, or for the ejecta to have travelled further out in stellar wind (see chapter 3, Fender et al 1995a) does the longer wavelength emission peak. A decreasing time lag at 13.3 cm is thus a clear indicator of decreasing opacity affecting the flares as the sequence I – V progresses.

Table 4.3 clearly illustrates the decreasing time delay of peak emission at 13.3 cm relative to that at 3.6 cm in the sequence I – V.

Table 4.3 Time lag between peak emission at 3.6 & 13.3 cm

Flare	Δt
I	$\sim$ 24.5 h
II	$\sim$ 12 h
III	$\geq$ 5 h
IV	insufficient coverage
V	zero (no lag)

There is a hint at times in the data set of a small time lag between emission at 2.0 cm and that at 3.6 cm, but this effect is marginal and is not often observed and so no systematic trend can be detected.

4.3.3 Decay of radio flares

Hjellming, Brown & Blankenship (1974) [48] found that for the 1972 September radio flares the decline after peak could be well described during the initial few days by an exponential decay. However, these authors found that after $\sim$ 4 days the decline in the radio was better fitted by a power-law

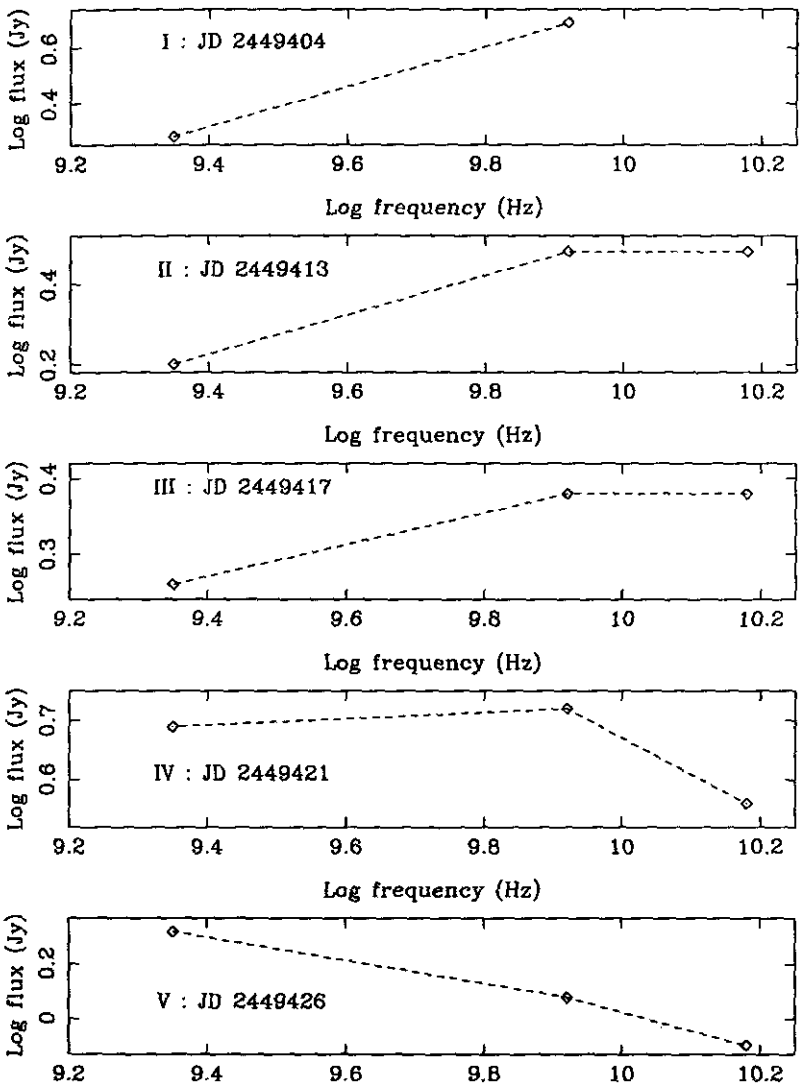

Figure 4.3 The evolution of the radio spectrum of the flare peaks in the sequence I – V. Time delays, as discussed below, are ignored. A clear trend from a state with significant opacity at 13.3 cm (and possibly also at 3.6 cm) towards one which is effectively optically thin, can be seen.

decay of index ~ 4.9. The exponential decay proved troublesome for those applying the simple van del Laan (1966) [34] model for an adiabatically expanding cloud of relativistic electrons, which predicts a power-law decay at all times.

Martí et al 1992 [49] have tackled this problem in their model for the Cyg X-3 radio flares by invoking twin radio jets which expand in the lateral direction exponentially at first, and then linearly at later times. This reproduces well an initial exponential and subsequent power-law decay.

In order to investigate the form of the decay of the radio flare events the entire radio data set was searched by eye to look for periods of relatively smooth flux decline. The least-squares fitting routine *Gnufit* was then used to find a best fit to the decay using one of the following two laws :

Exponential decay :

$$S_\nu(t) = S_0 \times e^{-\Delta t/\tau}$$

where S_0 and τ are free parameters, and

Power-law decay :

$$S_\nu(t) = S_0 \times (\Delta t \pm t_0)^{-\alpha}$$

where S_0, t_0 and α are free parameters.

Radio observations of Cyg X-3 tend to show clearer variability at higher frequencies : this, coupled with ~ 3 times more intensive coverage by the Ryle Interferometer during this period than at Green Bank, meant that there are considerably more clear decays fitted at 2.0 cm than at 3.6 or 13.3 cm. I fitted in total 9 clear decays at 13.3 cm, 12 at 3.6 cm and 27 at 2.0 cm.

In general the goodness of fit was very similar for both the exponential and power-law decays. However, whereas the exponential fits generally yielded fairly consistent decay constants τ at each of the three frequencies, the power-law fits yielded an extremely wide range of values for α, the power-law index. Because of this, and the extremely unphysical nature of some of the power-law fits (ie. $\alpha > 10$), I concluded that the exponential fits were

the most realistic in most, perhaps all, cases. There is no clear evidence for a change from exponential to power-law decay at a certain time after flare peak, as observed by Hjellming et al 1974 [48], and no clear trend toward a power-law index of ~ 4.9, as observed twice by those authors. However, it should be borne in mind that clear decays after ≥ 4 days are difficult to observe as the mean interflare interval was 4 – 5 days.

MPE92 relate the electron energy distribution index p (where the number of electrons of energy E varies as $N(E) \propto E^{-p}$) to the power-law decay index by

$$\alpha = \frac{7p - 1}{6}$$

For $p \sim 2.1$ (calculated from optically thin tail of index -0.55 : see eg. MPE92), $\alpha = 2.29$.

Table 4.4 tabulates the times and best-fit values of τ for an exponential decay, for each of the three frequencies. These data are plotted in Figure 4.4. Flare V, as can already be seen from its shape in Fig 4.1, is clearly an anomalous event, with a much slower decay (and rise) at all three frequencies than any of the previous events. Nevertheless, flare V can be fit satisfactorily by an exponential decay. Flare V can also be fit reasonably well by a power-law, though the exponential law fit is formally better. Is it interesting to note however that for flare V the values obtained for α from power-law fits are similar at all three wavelengths (**not** the situation for most decays), being 2.88 ± 0.35, 2.41 ± 0.77 & 2.59 ± 0.96 at 13.3, 3.6 & 2.0 cm respectively. This is intriguingly close to the value of ~ 2.29 predicted by MPE92. Both exponential and power-law fits to the decay of flare V are illustrated in Fig 4.5.

The mean values for τ are 0.18 ± 0.09, 0.548 ± 0.37 & 1.01 ± 0.26 at 2.0, 3.6 & 13.3 cm respectively. Although the errors on the fits to the Green Bank data are large (particularly at 3.6 cm), there remains strong evidence for consistently longer decay times at longer wavelengths.

Table 4.4 Exponential decay fits

Time interval (JD-244000.0)	τ(2.0 cm)	τ(3.6 cm)	τ(13.3 cm)
Flare I : peak 9404.1			
9404.122 - 9404.372		0.564 ± 0.030	
9404.935 - 9405.368		0.764 ± 0.050	
9405.161 - 9405.191	0.268 ± 0.024		
9405.903 - 9406.010	0.291 ± 0.016		
9406.117 - 9406.366		1.350 ± 0.166	0.883 ± 0.028
9407.157 - 9407.185	0.089 ± 0.005		
9407.723 - 9407.778	0.115 ± 0.002		
9407.981 - 9408.030	0.142 ± 0.004		
9409.223 - 9409.357		0.215 ± 0.024	
9410.860 - 9410.890	0.130 ± 0.010		
9410.992 - 9411.035	0.092 ± 0.002		
9410.918 - 9411.072		0.475 ± 0.060	0.867 ± 0.045
9411.145 - 9411.174	0.076 ± 0.002		
9411.771 - 9411.800	0.088 ± 0.003		
9411.822 - 9411.880	0.109 ± 0.002		
9412.226 - 9412.287		0.186 ± 0.010	0.849 ± 0.105
Flare II : peak 9413.0			
9413.043 - 9413.169	0.183 ± 0.004		
9413.098 - 9413.313		0.491 ± 0.035	
9413.874 - 9414.020	0.178 ± 0.006		
9414.063 - 9414.345			1.080 ± 0.096
9414.774 - 9414.800	0.227 ± 0.023		
9414.855 - 9414.897	0.159 ± 0.008		
9414.930 - 9414.997	0.299 ± 0.029		
9415.053 - 9415.113	0.299 ± 0.029		
9416.162 - 9416.276	0.438 ± 0.030		
Flare III : peak 9416.8			
9416.922 - 9417.106	0.206 ± 0.007		
9416.931 - 9417.056		0.236 ± 0.010	
9417.864 - 9417.997	0.181 ± 0.005		
9417.897 - 9417.988	0.166 ± 0.006		
9417.896 - 9418.105			1.170 ± 0.130
9417.896 - 9419.330			1.480 ± 0.030
9419.781 - 9419.846	0.114 ± 0.002		
9420.053 - 9420.090	0.084 ± 0.005		
Flare IV : peak 9421.2			
9421.071 - 9421.122	0.407 ± 0.030		
9421.108 - 9421.324		0.833 ± 0.087	
9421.696 - 9421.997	0.374 ± 0.004		
9422.198 - 9422.322		0.268 ± 0.013	
9422.261 - 9422.322			0.707 ± 0.040
9422.655 - 9422.697	0.089 ± 0.003		
9422.837 - 9422.927	0.134 ± 0.003		
9422.982 - 9423.060	0.103 ± 0.003		
Flare V : peak 9425.5			
9425.699 - 9429.894	2.110 ± 0.025		
9425.874 - 9429.989		2.400 ± 0.050	2.630 ± 0.050

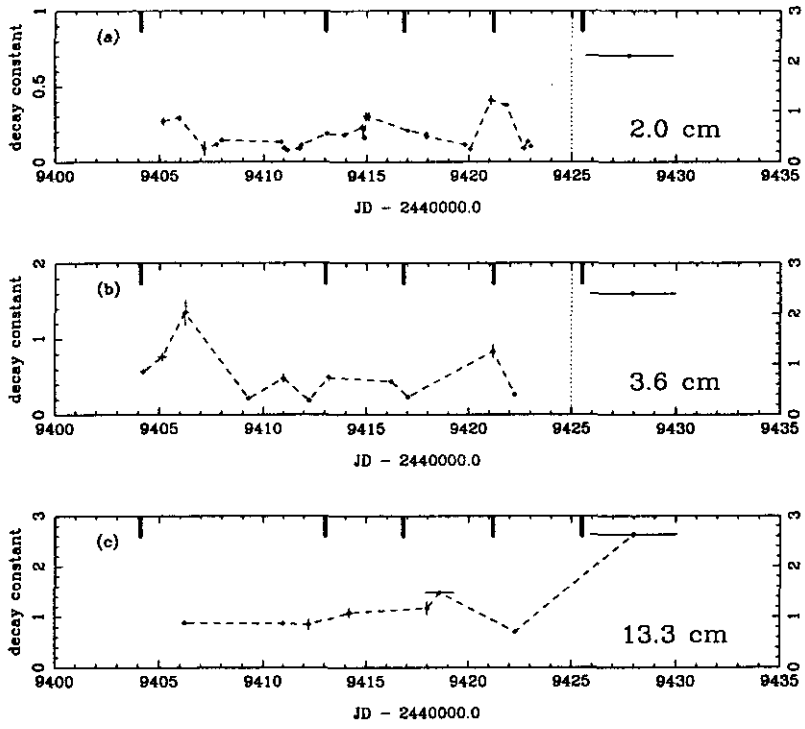

Figure 4.4 Fits to τ for exponential decay models (ie. the data from Table 4.4 plotted. The five solid bars at the top of each box indicate the approximate time of peak flux of flares I - V. The vertical dotted lines in parts (a) & (b) indicate a change of scale to accomodate the longer decay time for flare V more easily.

4.4 (Sub)millimetre behaviour

The (sub)millimetre observations during the flaring period are summarised in Table 4.1 and Fig 4.6. There appears to be a fresh injection of particles between the two observations on JD 2449410, with a detection at 0.8 mm of 77 ± 20 mJy less than 20 min after a 3σ upper limit at 1.1 mm of 40 mJy was established. Note that Fender et al 1995 (chapter 2 [103]) found a mean flux density of 50 - 60 mJy at 1.1 mm during radio quiescence, Assuming a significant increase in flux density at $\sim$ 1 mm did occur on a timescale of $\leq$ 20 minutes, this implies a limiting size for the emitting region from light-travel times of $\leq 3.6 \times 10^{13}$ cm, which, at a distance of 10 kpc gives a

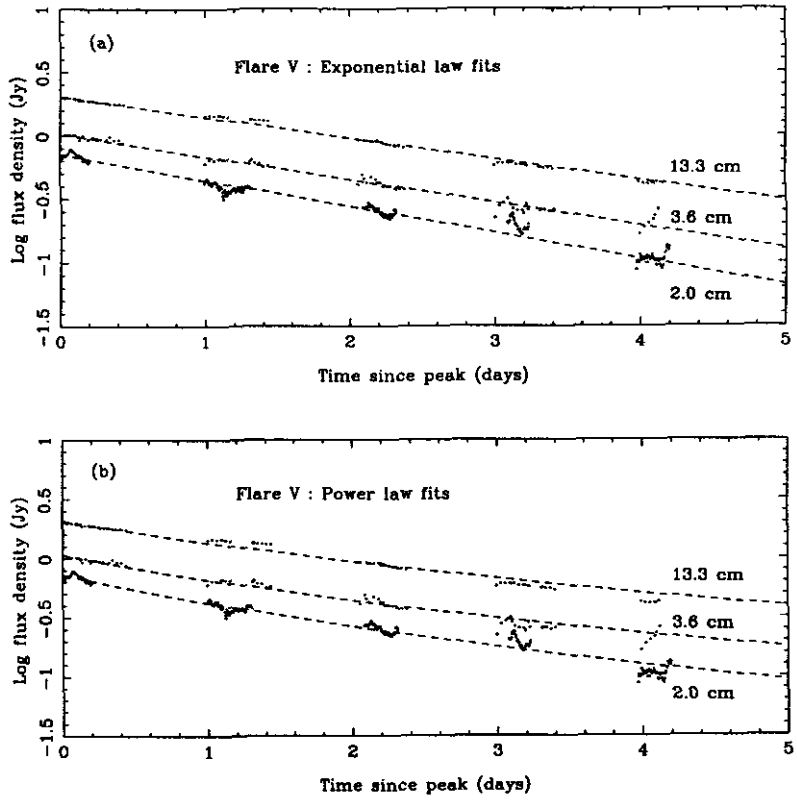

Figure 4.5 Fits of exponential and power-law decays to the decline of flare V at all three frequencies. Part (a) illustrates the exponential fits, which are formally better, and have decay constants τ of 2.63 ± 0.05, 2.40 ± 0.05 and 2.11 ± 0.025 at 13.3, 3.6 and 2.0 cm respectively. Part (b) shows best fits to a power-law decay, with indices α of 2.88 ± 0.35, 2.41 ± 0.77 and 2.59 ± 0.96 at 13.3, 3.6 and 2.0 cm respectively.

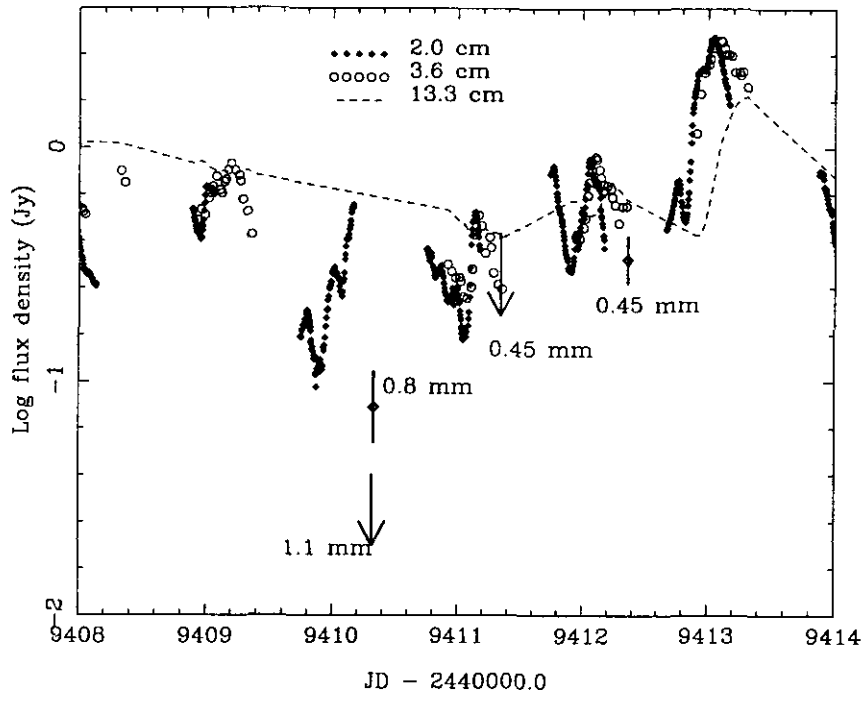

Figure 4.6 (Sub)millimetre observations with the JCMT during the flaring period. Note the 13.3 cm observations were not continuous, the dotted line is simply used to distinguish them more clearly.

brightness temperature $T_b \sim 2 \times 10^6$ K (for an increase of 20 mJy). This brightness temperature is significantly lower than that for the 2.0 & 3.6 cm emission and is in fact far more like that derived for the rapid infrared flares in Cyg X-3, as discussed in chapter 2 (Fender et al 1995b). This is a result of the frequency dependence of T_b however — the dimensions of the emitting region make a thermal origin for the (sub)millimetre emission highly unlikely, which is not the case for the infrared flares which have rise times of order a few seconds.

The size constraint places the emitting material either within a fairly well-collimated jet or deep within the centimetre photosphere of the stellar wind, using the geometry adopted in Chapter 3 (which places R_{2cm} several light-hours out in the wind). If the second interpretation is correct then any

correlated behaviour at centimetre wavelengths would not be expected to be observed for several hours, if at all (due to it having decayed during the time of flight - see chapter 3).

Although no directly simultaneous cm observations were made during the JCMT observations of JD 2449410, I estimate a flux density of $\leq$ 1 Jy at 2.0 cm during this period (from Fig 4.6). Simply extrapolating an optically thin tail of the synchrotron emission (spectral index $\alpha = -0.55$) out to 0.8 mm predicts a flux density of $\sim$ 170 mJy at this wavelength. Thus on this date the (sub)mm emission is not anomalously strong and may even be showing evidence for radiation losses (certainly to be expected at mm wavelengths if significant at 2.0 cm).

In contrast, the flux density at 0.45 mm on JD 2449412 **does** appear to be anomalously strong, at a level of 330 ± 69 mJy. I estimate the 3.6 cm flux density at this time to be $\sim$ 500 mJy, which would predict a flux density of $\sim$ 45 mJy at 0.45 mm when again simply extrapolating the optically thin tail with spectral index $\alpha = -0.55$. This high flux density may be a precursor to flare II, which occurred $\sim$ 1 day later, or may be showing signs of a contribution from a thermal gas. Note that the upper limit at 0.45 mm of < 430 mJy (3σ) on the previous day also leaves plenty of room for an anomalously strong flux density as I estimate the contribution from the optically thin tail to be $\sim$ 22 mJy at this time (from an estimate of $S_{3.6cm} \sim 250$ mJy).

4.5 Infrared behaviour

The mean flux densities of Cyg X-3 in the infrared K (2.2 μm) and H (1.6 μm) bands are $\sim$ 14 mJy and $\sim$ 9 mJy respectively (see chapters 2 and 5). Thus the data presented in Table 4.2 clearly show that during the UKIRT observations, between flares I and II, Cyg X-3 was brighter than usual in the infrared by a factor of 2 – 3. This is as bright as the strongest infrared flares, yet the data appear to be consistently at this level, unlike infrared flares which typically decay on timescales of minutes or less (though see

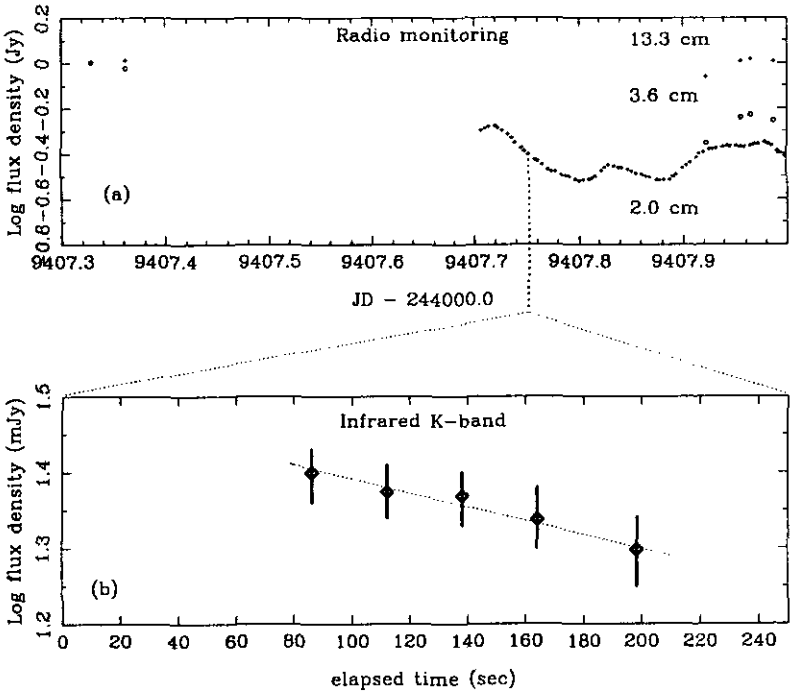

Figure 4.7 Simultaneous decays at 2.0 cm and 2.2 μm. The dotted line in part (a) indicates the time of the infrared observations. The solid line in the part (b) is a fit to an exponential decay of time constant 0.0059 ± 0.005 d. The simultaneous decay at 2.0 cm is well fit by a decay with time constant 0.115 ± 0.002 d, ie. $\sim$ 20 times slower

chapter 2 for a description of a prolonged period of high infrared fluxes observed in 1984).

Another striking point about the infrared data is that during the second night of observations at UKIRT, K band observations showed a clear gradual decline in flux density simultaneous with which there was a clearly observed decay at 2.0 cm (over a longer period). Fitting of an exponential decay to the infrared data (albeit with a very limited data set) gave a decay constant $\tau = 0.006 \pm 0.005$ d (ie. $\sim$ 8.5 min) in contrast to the 2.0 cm data which was well fit by an exponential law of time constant $\tau = 0.115 \pm 0.002$ d, ie. the infrared flux decayed $\sim$ 20 times faster. This simultaneous decay

at 2.0 cm & 2.2 μm is illustrated in Fig 4.7. Note that a single law cannot fit the decay observed on this day in the infrared combined with the flux density of the previous day (although it was higher) as this would require an accelerating decay process. Instead, I believe that this relatively rapid (at least in comparison to the cm flux) decay rate at 2.2 μm indicates that some process must be replenishing the infrared flux to maintain it at such high levels over two (and in all likelihood more) days.

4.6 Discussion

Here I address the two most important features to have arisen from the analysis of the data, the dramatically decreasing opacity in the sequence of events I - V, and the unexpected importance of radiation losses even at cm wavelengths. I address the issue of radiation losses first, as this has some impact on the discussion in section 4.6.2.

4.6.1 Radiation losses

In the model of MPE92, synchrotron and inverse Compton radiation losses were not considered to be significant when compared to the adiabatic expansion losses suffered by the exponentially expanding jet. However, there is strong evidence presented here that radiation losses are in fact important.

This evidence is in the form of repeated examples in the data set of more rapid flux density decays at shorter wavelengths (sect 4.3.3). It is particularly important that two wavelengths on the optically thin branch of the synchrotron emission (ie. 3.6 cm & 2.0 cm) consistently show different decay rates, as decays at 13.3 cm can be clouded by evolution of the opacity of the ejecta itself (MPE92 find a turnover wavelength of $\sim$ 6 cm between the optically thin and initially self-absorbing branches of the emitted spectrum). The same interpretation can be drawn from observing that $\alpha_{3.6-2.0cm}$ decreases below the optically thin branch value of ~ -0.55 (Fig 4.1(c)).

As radiation losses do appear to be important, it is important to calculate

the relative importance of synchrotron and inverse Compton losses, and to consider under what physical conditions radiation losses by these two mechanisms would prove significant.

Following the work of MPE92, I retain their jet geometry and formulation governing the evolution of the lateral expansion velocity, jet radius and hence magnetic field (via conservation of magnetic flux) with time. From this the relative contributions from adiabatic expansion losses and synchrotron losses can be calculated. I futher make an approximation to the radiation field and calculate the relative contribution of inverse Compton losses also. Details of the equations governing the model are given in Appendix A. The model parameters to be fit are :

B_0, the magnetic field at the base of the jet

t_c, the time at which the lateral expansion changes from exponential to linear

t_e, the time constant for the exponential expansion, related to the observed decay constant τ by $t_e = \tau(7p-1)/6$

T_* & R_*, the temperature and radius of the black-body being used to approximate the radiation field from the companion to the compact object.

From the observed change from exponential to power-law decay in the 1972 flares, we take t_c to be 4 days, as did MPE92 (although there is no evidence for this in the data, it may still have occurred, at least for flares I - IV, and been lost in the rise of the following flare). Assuming radiation losses to be of least significance at 13.3 cm, we take the observed decay mean constant $\tau = 1.005$ at this frequency and use it to derive a value for t_e of 2.29 d. Infrared observations (Chapter 2, Fender et al 1995) indicate that the companion to the compact object has an absolute magnitude in the near IR of ≤ -5. An approximation to such a luminous object can be made by taking a black-body of $T_* = 40\ 000$ K and radius $R_* = 10 R_\odot$. Note that although the radiation field from the companion star almost certainly comes from a far more extended region (ie. a bright stellar wind, particularly in the case of the companion being a Wolf-Rayet star), given the high ejection velocity of 0.3 c, the approximation to a relatively small black-body should

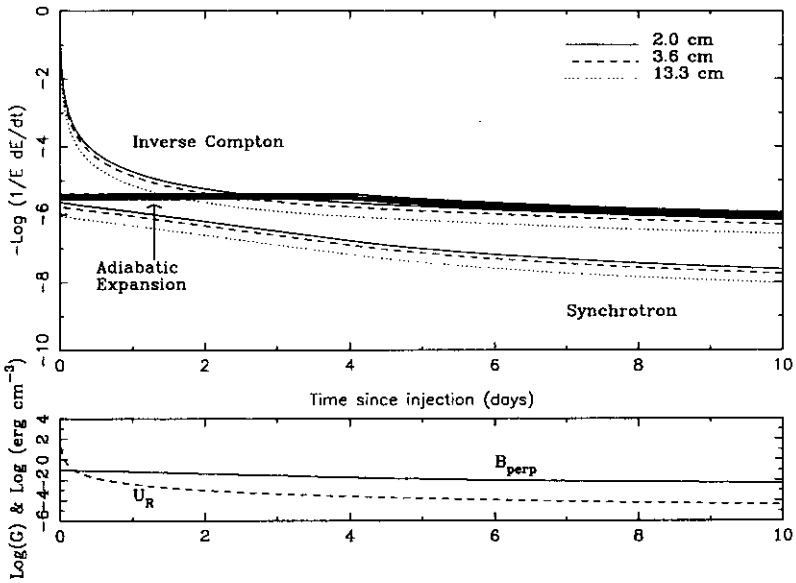

Figure 4.8 A comparison of loss mechanisms in Cyg X-3 jet. Adopted jet geometry follows MPE92; magnetic field at injection $B_0 = 0.1$ G, luminous companion star (10 $R_\odot$, T = 40 000 K). Top panel plots E^{-1} dE/dt (a measure of number of electrons of energy E lost) as a function of time as a result of adiabatic expansion, inverse Compton, and synchrotron losses. The bottom panel plots the evolution of B_{perp} (component of magnetic field perpendicular to jet axis) and U_R (radiation energy density local to ejecta) with time.

be adequate.

We use $B_0 \sim 0.1$G as fit to the data by MPE92 and also obtained from applying equipartition theory to the Cyg X-3 radio jets by Spencer et al 1986 [23] (we note however that there are no a *priori* reasons for energy equipartition to be a valid assumption - see eg. Leahy 1991 [109]).

Using the above parameters, we find that inverse Compton losses dominate the loss mechanisms for the first two days of jet expansion, and after this time remain important at between 10 – 50 % of the level of the expansion losses, which dominate from this point onwards. The exact proportion of the contribution from inverse Compton losses is wavelength depen-

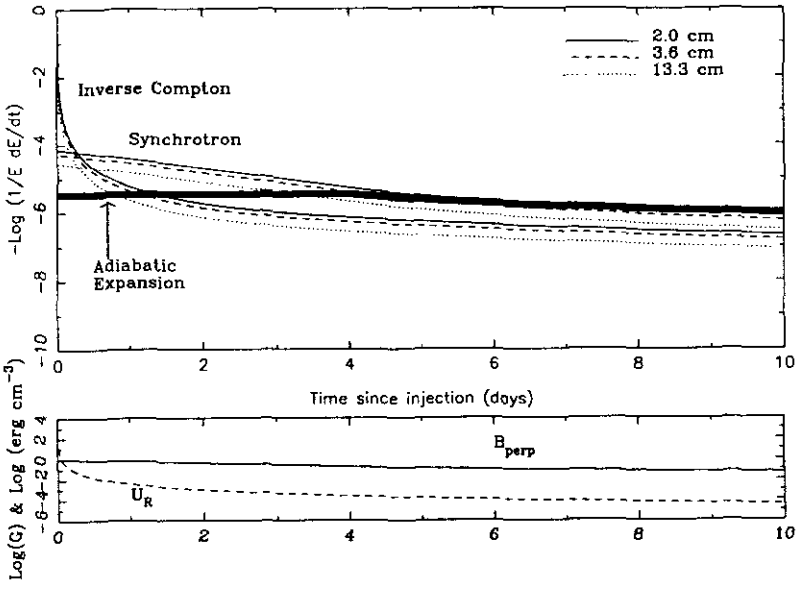

Figure 4.9 As Fig 4.9, but for initial magnetic field B_0 = 1.0 G.

dent, with it being most important at shorter wavelengths. Fig 4.8 plots $E^{-1}(dE/dt)$ (which is proportional to the number of electrons of energy E lost and is therefore a measure of the relative importance of each loss mechanism) against time for this model.

Synchrotron losses do not play a major role, although increasing B_0 to 1.0 G is sufficient to make them important (see Fig 4.9). This is not an unphysical amount and synchrotron losses should be considered in future models of radio emission from Cyg X-3.

Several authors dispute the high-mass, luminous nature of the companion star to Cyg X-3, preferring a low-mass X-ray binary (or similar) scenario. The relative contributions of the three loss mechanisms in such a scenario (where I represent the companion star in this case by a 1 $R_\odot$, T = 4000 K object) are illustrated in Fig 4.10. Given that radiation losses **are** observed, if the LMXRB scenario is correct, then $B_0 \geq 1.0$ G.

We have found here that adopting the geometry of MPE92 but including

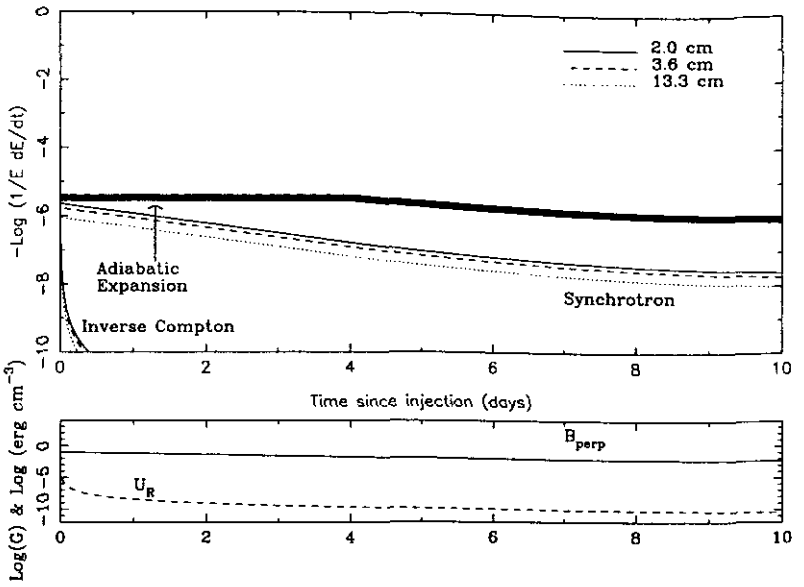

Figure 4.10 As Fig 4.9, but for main sequence (1 $R_\odot$, T = 4000 K) companion, as in LMXRB scenario.

a massive luminous companion star, inverse Compton losses dominate for $\sim$ the first two days after injection. This is inconsistent with the model fits put forward by MPE92 and in turn casts some doubt upon their fits and geometry. However, it should be noted here that inverse Compton losses are the most geometry-independent of the loss mechanisms considered here and are not strongly affected by small changes in assumed jet configuration. In particular, a model was run for constant lateral expansion immediately after injection (ie. no period of exponential lateral expansion) – again inverse Compton losses dominated over adiabatic and synchrotron losses when a highly luminous companion was considered.

In the inverse Compton process, electrons of energy $\gamma m_e c^2$ will scatter photons of frequency ν to a mean frequency of $\sim \frac{4}{3}\gamma^2\nu$ (eg. Hughes & Miller 1991 [110]) Electrons radiating synchrotron emission at 2.0 cm at the base of the jet (ie. where B=0.1 G) will have energies of $\sim$ 0.1 GeV and hence

Lorentz factors $\gamma \sim 200$. Thus inverse Compton losses suffered by these electrons will cause photons in frequency range $10^{14} - 10^{16}$ Hz (ie. infrared through UV, where emission from luminous companion should be concentrated) to be reemitted after interaction with the electrons in the frequency range $5 \times 10^{18} - 5 \times 10^{20}$ Hz (ie. 20 keV - 2 MeV) : hard X-rays through γ-rays. Based upon this, and the observed importance of radiation losses, probably inverse Compton, at 2.0 cm, I predict hard X-ray/γ-ray bursts associated with radio flares. There may also be some constant contribution to the hard X-ray/γ-ray flux from the inverse Compton mechanism if the jet is continuous (but with a lower injection rate) during quiescence.

4.6.2 Decreasing opacity

As has been demonstrated in section 4.3.2, the evolution of the five flare events in the sequence I - V is strongly indicative of decreasing opacity with time. We consider below two scenarios in which this decreasing opacity is due to (A) events I - V taking place in locations increasingly distant from the absorbing effects of the Cyg X-3 wind, and (B) events I - V having different physical parameters due to evolving conditions at or near the base of the jet.

A : Single injection, multiple shocks

In this scenario we consider the likelihood that the events I - V were caused by five shocks occuring at different times but all associated with a single ejection event. Events I - V take place at times when the ejecta, travelling at 0.3 c, are increasingly distant from the base of the jet and the absorbing effects of the dense stellar wind.

Assuming injection into the jet to have occurred at the time when event I began to rise, and assuming a constant ejection velocity of 0.3 c, we find events I - V to have occurred at distances from the system of $\sim 7.8 \times 10^{14}$ cm, $\sim 7.7 \times 10^{15}$ cm, $\sim 1.1 \times 10^{16}$ cm, $\sim 1.4 \times 10^{16}$ cm & 1.7×10^{16} cm respectively. A laterally expanding jet geometry (eg. MPE92) is consistent with observations for the Cyg X-3 system (eg. Spencer et al 1986 [23],

Schalinski et al 1995 [25]). So, further from the base of the jet, the ejecta will have expanded considerably at right angles to the jet axis, and will be at considerably lower densities than at the point of injection. Assuming the jet geometry of MPE92 (see Appendix 1), which produces a jet opening angle of 90° far from the base, the ejecta density should be reduced by a factor of $\sim$ 1000 by the time event III rises. Absorption effects from the Cyg X-3 stellar wind will also be decreasing rapidly with time as the ejecta move away from the system. So, qualitatively at least, we have a scenario in which we might expect shocks to show decreasing evidence of opacity as time progresses. However, there are problems with this simple model :

(i) an increasingly large volume of ejecta should show increasingly long rise times in the sequence I - V, but flares I - IV show approximately equal rise times, suggesting a similar sized region is resposible for the emission; only event V deviates and shows a longer rise time.

(ii) In the model of MPE92, after a few days all cm wavelengths are optically thin to self-absorption. Using the geometry of Chapter 3 & Fender et al 1995a [103], after a similar amount of time the ejecta should be beyond the absorbing effects of the stellar wind. This implies that within $\sim$ five days of injection into the base of the jet, no absorption effects should be significant. However, as Fig 4.3 clearly illustrates, there is significant absorption of emission at 13.3 cm certainly as far down the sequence as event III, $\sim$ 13 days after event I.

(iii) (Perhaps most importantly) what is causing the shocks ?

Regions of high synchrotron brightness a considerable distance along the jets of AGN (eg. Muxlow & Garrington 1991 [111]) appear to demonstrate that particle reacceleration can take place far from the point of particle injection at the base of the jet. Such shocks may be caused by reconfinement due to the magnetic field of the ejecta or as a result of interactions with a dense medium (in this case the Cyg X-3 stellar wind) (see eg. Leahy 1991 [109]). If event I was an initial shock deep within the stellar wind, and events II - IV recombination shocks further along the jet, then some of the problems mentioned above disappear. Firstly, if reconfinement is occurring, then we

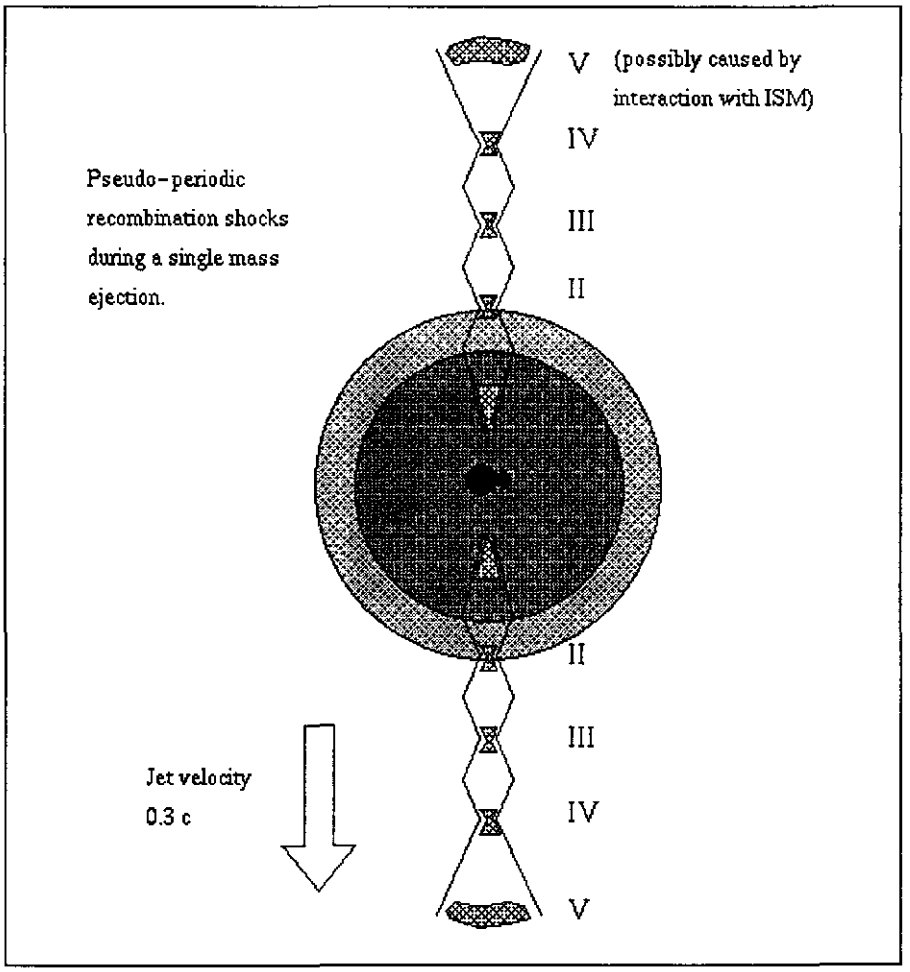

Figure 4.11 Scenario A. The initial, high opacity flare (I) occurs during initial injection into the jets, whereas events II – IV are due to reconfinement shocks (possibly magnetic or caused by the dense stellar wind). The reconfinement shocks occur in regions of decreasing local opacity on a pseudo-periodic timescale. An optically thin, slow rise-time event (V) may be due to an interaction of the ejecta with part of the ISM.

would expect all the shocks to be of a similar dimension and thus have similar rise times (this may also be consistent with the pseudo-periodic event separation of $\sim$ 5 days as the ejecta oscillate between shocked expansion and reconfinement). Reconfinement would clearly also keep the opacity high, though some leakage of material into the surrounding medium and/or slight overall lateral expansion could result in a decreasing opacity with time. In this scenario, flare V would not be a reconfinement shock, but rather a shock caused at a time when reconfinement was no longer occurring and the ejecta had expanded significantly – possibly due to some interaction with the ISM – thus long rise time and low opacity. This scenario is summarised in Fig 4.11.

A major problem with this scenario is the clear evidence for radiation losses all along the sequence I – V (section 4.3.3.). After the initial flare event inverse Compton losses would be far less important, as the radiation energy density falls off as r^{-2}; yet the evidence for radiation losses is comparable along the sequence (at least for flares I – IV).

B : Multiple injections, evolving conditions

In this scenario we consider that events I - V (or at least I - IV) are as a result of five (or four) separate injection events, and that the evolving characteristics reflect changing condition in the region of injection. The scenario is envisaged as follows :

Initially Cyg X-3 is in a quiescent state, with a low-level jet responsible for the quiescent radio emission. A period of increased mass-loss from the companion star results in an increasing density of thermal electrons in the region of the accreting compact object. This causes the quenching of the jet and thus radio emission is reduced. At the same time the infrared flux (proportional to $n_e n_i$ where n_e & n_i are the electron and ion number densities) increases due to the higher electron and ion number densities, as does the X-ray flux, due to a higher accretion rate.

Radiation and/or magnetic pressure builds up in the inner regions of the disc (the exact mechanisms for producing jets remain unclear) and finally

there is an explosive injection of relativistic particles into the jet. This produces a radio flare, with considerable associated opacity due to a high proportion of absorbing thermal particles (located both in the local stellar wind and entrained in the jet).

Subsequently the mass-loss rate from the companion star subsides towards its normal levels and a sucession of injections with decreasing proportions of absorbing thermal electrons occur. During this period the infrared and X-ray brightness begin to decline toward their normal levels (although there may still be X-ray/γ-ray flares due to inverse Compton losses from later flares). Flare V remains anomalous and may, as in the previously described scenario, be due to an interaction between the ejecta and part of the ISM. If not, then it would appear that the rate of injection of relativistic particles into the jet had declined dramatically by the time this event occurred, which seems feasible.

This scenario has a lot of attractions in that it seems to explain the observed evolution of the opacity in the sequence I – V, **plus** the strong infrared brightness and observed correlation between radio flares and bright X-ray states (Watanabe et al 1994 [36]). It is also consistent with the suggestion from the infrared and (sub)mm data that continued injections were taking place *at least* between flares I & II. Although scenario B does not contradict the quenching and other aspects of a denser local medium before a radio flare, I feel that as the evidence is in favour of changing conditions near the base of the jet, then it is most natural to invoke these changes as being responsible for the evolving properties of the sequence of radio flares; thus I find B the more plausible of the two scenarios described here.

4.7 Conclusions

The multiwavelength observations of Cyg X-3 during a sequence of radio flares in 1994 Feb – March have revealed new properties of the system giving further clues as to its nature.

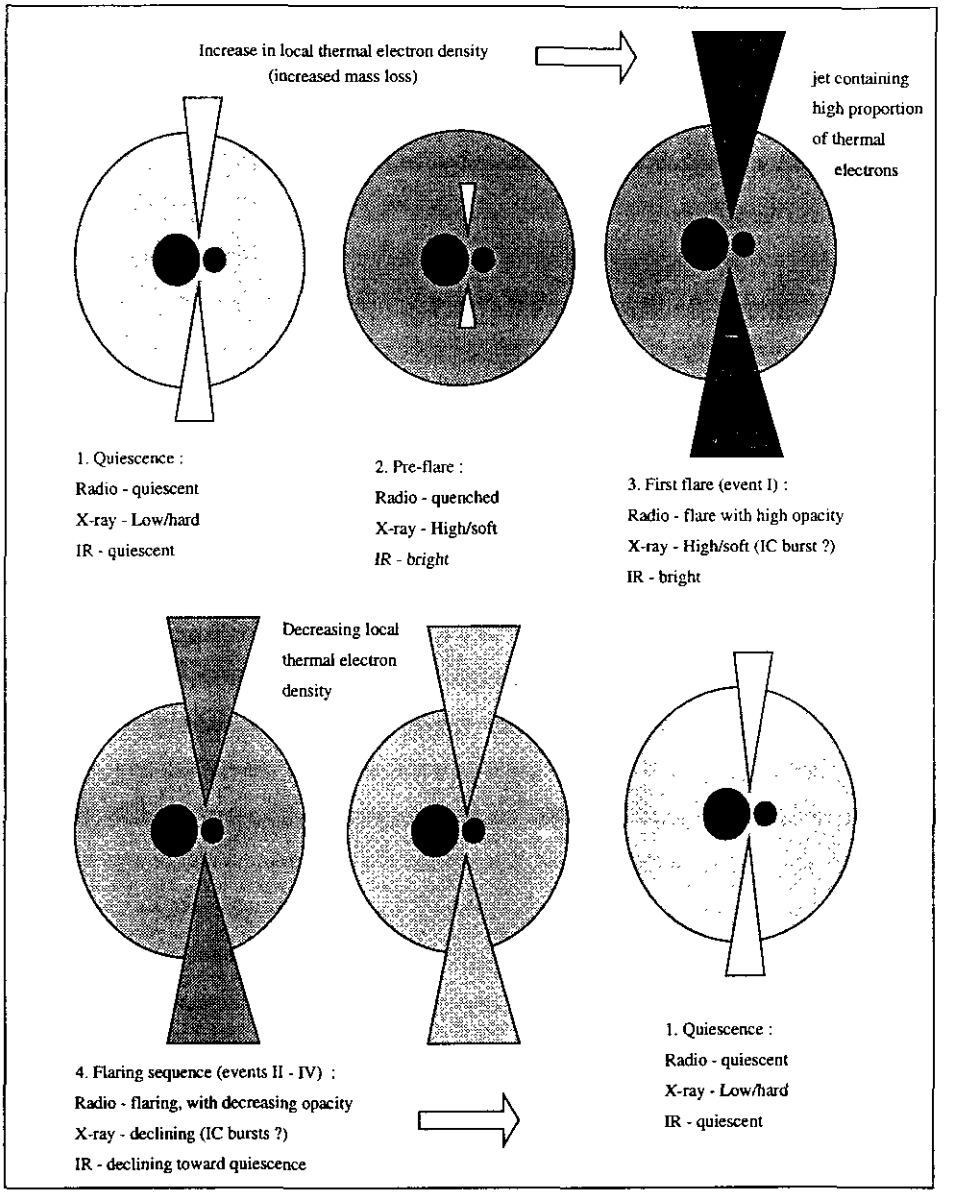

Figure 4.12 Scenario B. Increased mass-loss by the companion star causes quenched radio emission but bright infrared and X-ray fluxes. Eventually a large injection of relativistic particles into the jet occurs, entrained with which are a high proportion of absorbing thermal electrons. As $\dot{M}$ declines toward its 'normal' level, a series of radio flares with progressively lower opacity occur. During this period the infrared and X-ray brightnesses decline gradually toward their quiescent levels. Radio flares may also be accompanied by X-ray/γ-ray bursts due to the interaction of optical photons from the companion star with high energy electrons in the jet (see section 4.6.2).

Intensive radio monitoring at three wavelengths has provided a wealth of information on the evolution of a flare sequence. It is clear that radio flaring sequences progress in a manner which is strongly suggestive of an initial increase and then steady decrease of local opacity. The fact that radio flares are correlated with increased X-ray brightness (Watanabe et al 1994 [36]) strongly favours a scenario whereby an increased mass loss rate from the companion star triggers a period of 'quenching' and subsequent violent mass ejections, and heightened X-ray activity is due to an increased accretion rate. Scenario B described in section 4.6.2 encompasses such behaviour and makes some predictions which can be tested in future (in particular the infrared brightness from the quenched period along a flare sequence).

The observed importance of radiation losses as the flares in Cyg X-3 decay has led to the conclusion that the dominant radiation loss mechanism is the inverse Compton losses. This would not have been considered in the past as until 1992 Cyg X-3 was assumed (by most) to be a low-mass X-ray binary in which the radiation field from the companion star would have been orders of magnitude less than that approximated here, and *not* a hot & massive Wolf - Rayet star as asserted by van Kerkwijk and others since the discovery of emission lines in infrared spectra (van Kerkwijk et al 1992 [29]). It is interesting to note that if Cyg X-3 *is* a low-mass X-ray binary then synchrotron losses would need to be invoked to explain the observed decays, requiring a jet initial magnetic field greater than 1.0 G. The domination of inverse Compton losses over adiabatic losses for the first two days after injection suggests strongly that there should be correlated X-ray/γ-ray behaviour during radio flares (and perhaps, at a lower amplitude, during quiescence) - as found for SS433 by Martí (1993 [112]). The similarity in importance of inverse Compton losses between SS433 & Cyg X-3 during radio flares is not surprising given the similarity of their jet velocities and companion star luminosities (asssuming Cyg X-3 has a luminous companion – SS433 has a bright OB companion). J. Martí (private communication) comments that there is evidence for similar inverse Compton losses, and also for high-frequency flare precursors in the periodic radio-emitting X-ray

binary LSI +61° 303.

Further modelling is required to see whether the emergence of inverse Compton losses as important removes the need for the initial exponential lateral expansion phase of MPE92. Note that exponential lateral expansion is physically consistent with models of free jets ploughing into a medium of rapidly decreasing density (see eg. Leahy 1991 [109]), in which constant lateral expansion occurs only after the lateral expansion velocity is $\sim$ the internal sound speed of the jet (which in this case may be the relativistic sound speed of $c/\sqrt{3}$). Note also however, that the laterally expanding cone-shaped jet observed in Cyg X-3 may in fact be due to a relatively *well-collimated* jet whose axis is not perpendicular to the orbital plane and so sweeps out a cone every 4.8 hr. This is less than the injection period for a major flare and so all such events would be expected, at today's resolution, to show a cone, not a well-collimated jet. If this *is* the case then future higher resolution radio mapping may reveal a corkscrew-like structure as observed in SS433.

The shorter wavelength observations at (sub)millimetre and infrared demonstrate that there is rapidly varying behaviour related to the radio flares which cannot be directly observed at centimetre wavelengths, probably due to the absorbing effects of the dense stellar wind. The strong (sub)mm fluxes demonstrate particle injection to be going on deep within the jet between flare events. The enhanced infrared brightness on both occasions observed between events I & II agrees with scenario B described in sect 4.6.2. This, and the simultaneous flux decay at 2.0 cm & 2.2 μm (sect 4.5, Fig 4.7) may be the first evidence for some correlated radio - infrared behaviour in Cyg X-3.

I conclude that the multiwavelength approach has shed new light on the Cyg X-3 system, definitively revealing the presence of a trend towards decreasing opacity and the importance of radiation losses (probably inverse Compton) during a sequence of radio flares. I would encourage further multiwavelength campaigns on this and similar sources to be undertaken.

Chapter 5

Multiwavelength observations of Cygnus X-3 in June–July 1994

5.1 Introduction

The multiwavelength observing campaign is a powerful tool in the quest to understand what is going on in the more unusual of astrophysical objects. Cyg X-3 certainly counts as an unusual object, and several sets of multiwavelength observations of the source have been published, often shedding valuable new light on the physical processes responsible for the system's enigmatic behaviour.

In 1972, a concerted campaign following the first recorded radio outbursts included observations at centimetre, millimetre, infrared, optical (unsuccessfully) and X-ray wavelengths (Gregory et al 1972 et seq. [12]). Simultaneous soft X-ray and infrared observations (eg. Mason et al 1976 [54]; Mason, Cordova & White 1986 [55]) have demonstrated not only that the same 4.79 h periodicity is observed in both regimes, but that it is *in phase* which is a crucial factor for physical models of the system to explain. The radio monitoring program conducted at NRL-Green Bank (which has monitored Cyg X-3 daily since 1988, and in some form since 1984 - see eg. Waltman et al 1994 [21], 1995 [50]) provides radio data during all observations of Cyg X-3 in other bands. This has allowed a link to be established between X-ray & radio activity (Watanabe et al 1994 [36]) and was impor-

tant in establishing a link between bright X-ray & radio states and strong infrared emission lines (Kitamoto et al 1994 [65]).

Work by myself in collaboration with others has also used the multiwavelength aspect well - in showing that millimetre flux densities were anomalously strong during radio quiescence (chapter 3, Fender et al 1995a [103]), and in providing valuable clues to the state of the source during a sequence of radio flares by combining observations at three radio frequencies with some (sub)millimetre and infrared observations (chapter 4, Fender et al 1996a [104]).

In this chapter I present observations from a concerted campaign in June–July 1994 when, both by planning and coincidence, observations of Cyg X-3 were being performed at hard X-rays (GRO : OSSE), red-optical (INT), infrared (UKIRT) and radio (Ryle Telescope, NRL-Green Bank). A deep K-band finder chart constructed from the infrared observations is to be published in Fender & Bell Burnell (1996c [113]) and a comparison of the hard X-ray and infrared K-band light curves is being published in Matz et al (1996 [93]). Further publications detailing the other work presented in this chapter are to follow.

5.2 Observations

The most thorough monitoring of Cyg X-3 was again in the radio, from both Green Bank and Cambridge (sections 5.2.1 & 5.2.2 below) Fig 5.1 summarises the radio observations during the period discussed here, and uses them as a backdrop to indicate when the observations at other frequencies took place.

5.2.1 NRL-Green Bank : 13.3 & 3.6 cm

Details of the Green Bank monitoring program, calibration procedures and errors are as for Chapter 4. Monitoring of Cyg X-3 was stepped up during the period of multiwavelength observations. The data from 1994 June – July is plotted in Fig 5.1.

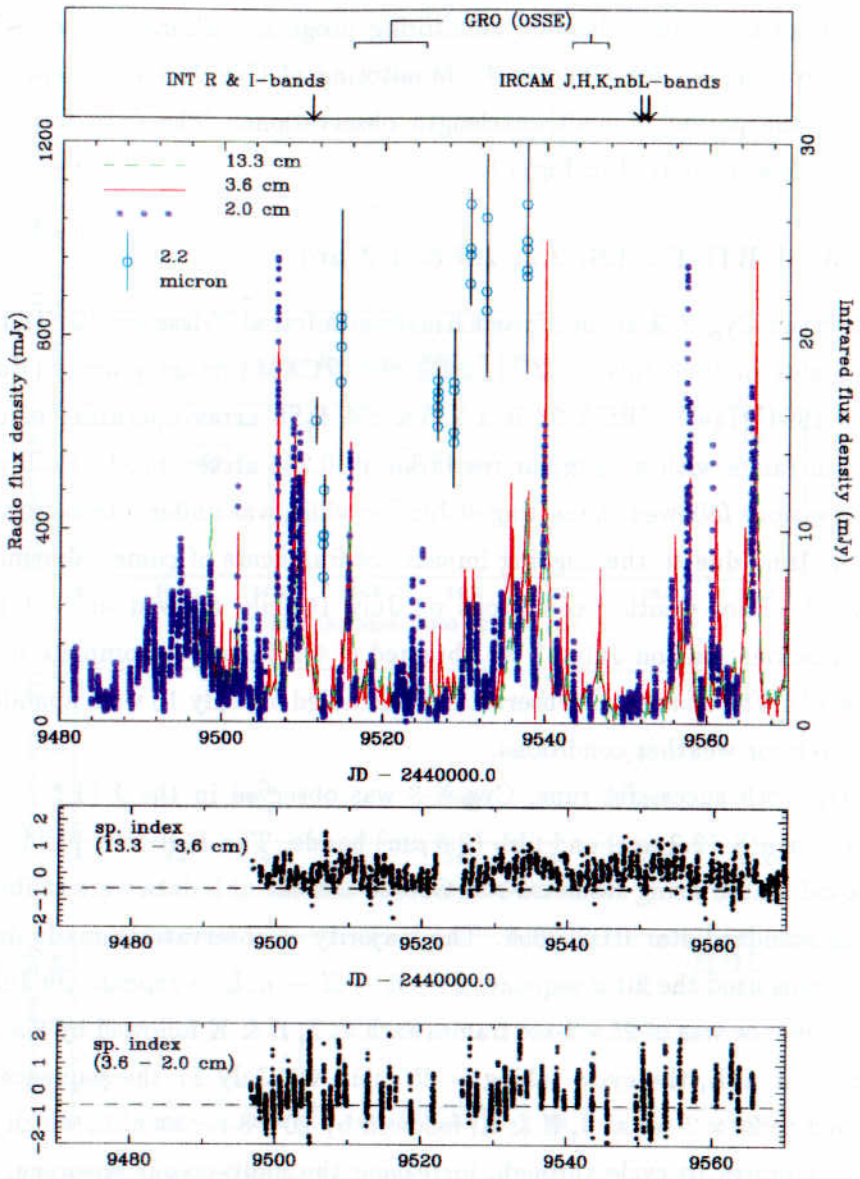

Figure 5.1 Multiwavelength observations of Cyg X-3 in 1994 June – July. The radio monitoring at Green Bank and the Ryle Telescope is plotted here, along with the infrared monitoring from the TCS. The lower two panels show the spectral index α between 13.3 – 3.6 cm cm & 3.6 – 2.0 cm. Periods of observations in other wavelength regimes are indicated in the top panel of the plot.

5.2.2 Ryle Telescope : 2.0 cm

Details of the Ryle Telescope monitoring program, calibration procedures and errors are as for Chapter 4. Monitoring of Cyg X-3 was stepped up during the period of multiwavelength observations. The data from 1994 June – July is plotted in Fig 5.1.

5.2.3 UKIRT : 3.6, 2.2, 1.6 & 1.2 μm

I observed Cyg X-3 at the United Kingdom Infrared Telescope (UKIRT) on the nights of 1994 July 16 & 17, using the IRCAM3 imaging array (Puxley et al 1994 [114]). IRCAM3 is a 256 × 256 InSb array operating in the 1 - 5 μm range with an angular resolution of 0.286 arcsec/pixel. Each night observations followed the setting of Jupiter which was under intense scrutiny at the time due to the ongoing impacts of fragments of comet Shoemaker-Levy 9. Poor weather conditions on July 16 only allowed us $\sim$ 1 hr of observations, but on July 17 we obtained $\sim$ 4 h (nearly a complete orbital cycle of 4.8 h) on source. Observations scheduled for July 18 were abandoned due to poor weather conditions.

On both successful runs, Cyg X-3 was observed in the J (1.2 μm), H (1.65 μm), K (2.2 μm) and nbL (3.6 μm) bands. The J, H & K bands were flux-calibrated using standard star G93-48 and the nbL data were calibrated using standard star HD203856. The majority of observations made during both runs used the filter sequence J → H → K → nbL → *repeat*. On July 16 the sequence was of 25 × 2-sec frames each at J, H & K followed by 9 × 8-sec frames at nbL, the cycle taking $\sim$ 25 min. On July 17 the sequence was altered to 20 × 2-sec at J, H & K, followed by 20 × 8-sec at nbL, which took $\leq$ 15 minutes to cycle through, increasing the multi-colour coverage. The 8-sec frames at nbL were a composite of 229 × 0.035-sec integrations (where 0.035 sec is maximum exposure at nbL before array saturates). Within each set of frames the pointing was jittered in a five-point or nine-point offset to allow median flat-fielding during the data-reduction stage. In all observations the array was stopped down to 128 × 128 which reduced the amount of stored data whilst still allowing accurate relative photometry (if

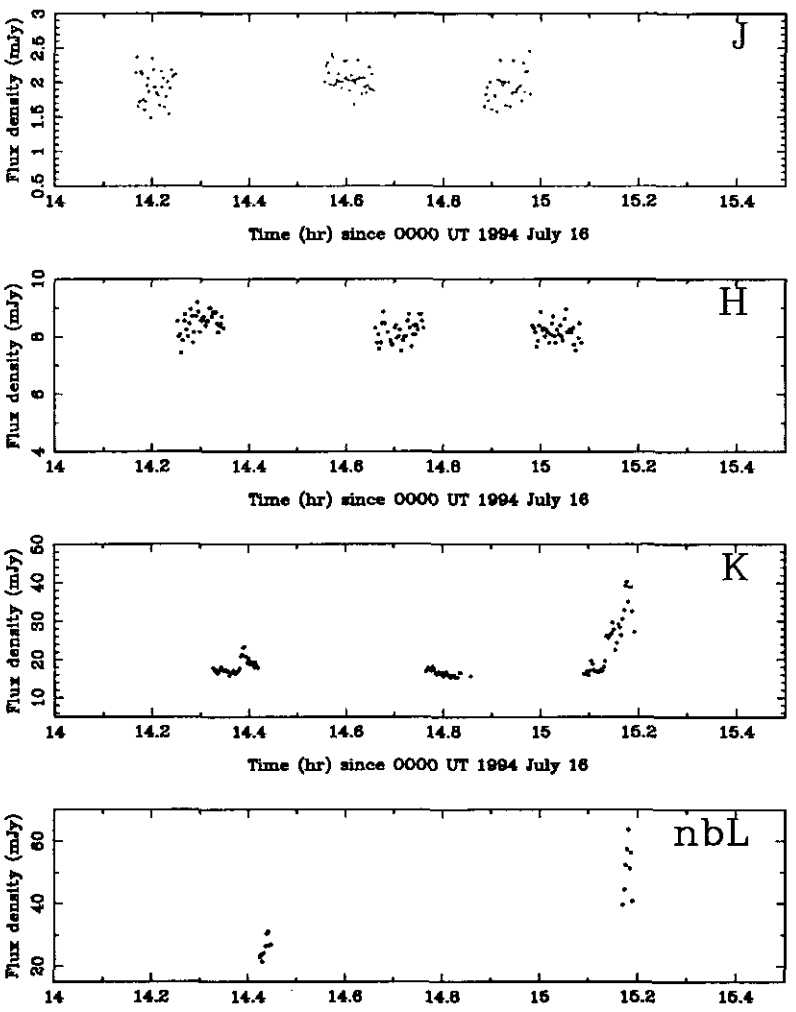

Figure 5.2 IRCAM3 J, H, K & nbL Cyg X-3 light curves obtained on 1994 July 16. The source is much brighter than its 'quiescent' level - see also fig 5.4

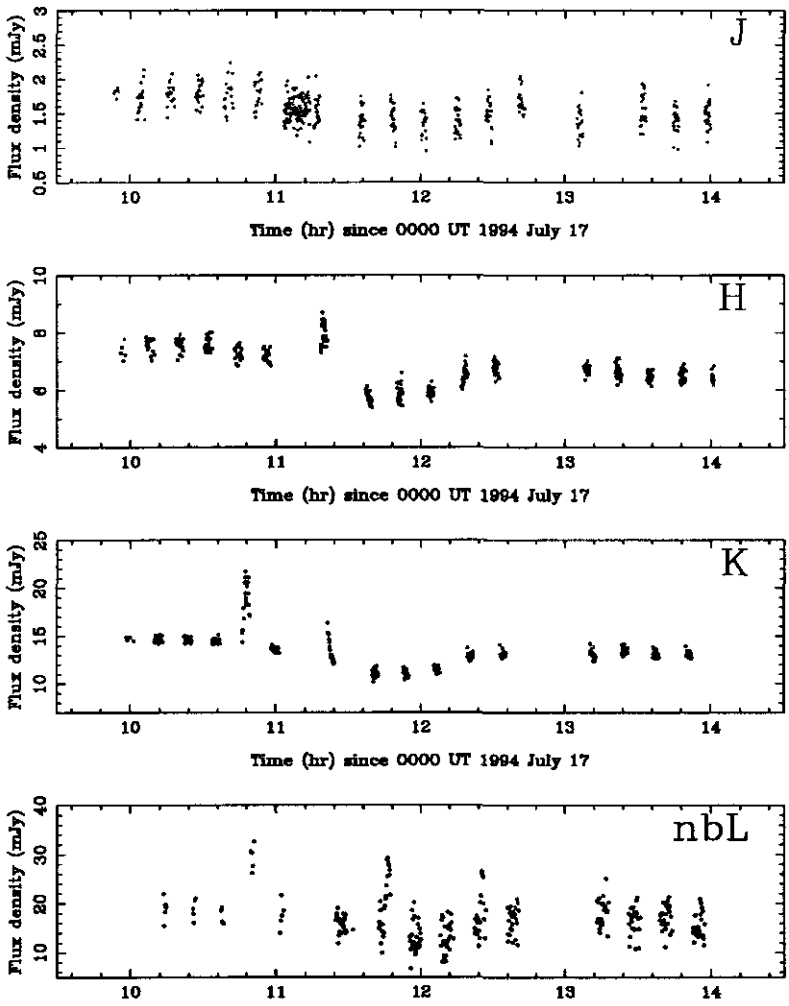

Figure 5.3 IRCAM3 J, H, K & nbL Cyg X-3 light curves obtained on 1994 July 17. Orbital minimum and a number of rapid infrared flares are clearly observed.

needed) using nearby stars Z & D which lie within 10 arcsec of Cyg X-3. Data were reduced and manipulated using the CLRED software.

Photometry was performed on each of the frames obtained in the observing run, a total of 330 frames on July 16 and 1532 frames on July 17. A 5 arcsec software aperture was used to obtain magnitudes for Cyg X-3, Star Z and Star D (using the same region for sky subtraction) for each frame at J, H and K. This allowed allowed accurate checking of sky brightness/transmission variations. It was found from this that at H & K the data was photon–noise dominated and no corrections for sky variations needed to be made. At J however sky variations were significant and for each frame Cyg X-3 was ratioed with stars Z & D (assuming their mean magnitudes over the night to be correct) to obtain a more accurate measurement. At nbL Stars Z & D were too faint to be used in each frame and only appear on composite images. In this band I used three separate regions for sky subtraction and averaged them. However, this does not compensate for large changes in sky brightness and photometry in this band is consequently not as accurate as that at J, H & K.

Fig 5.2 plots the J, H, K & nbL light curves for July 16, and fig 5.3 for July 17. During the short period of observations on July 16, Cyg X-3 was clearly much brighter in all four bands than on the following night (see fig 5.4). The July 17 data reveal the orbital modulation with minimum light clear in all four bands, as well as a few rapid flaring events, similar to those observed in 1984 (chapter 2).

5.2.4 TCS : 2.2 μm

The Telescopio Carlos Sanchez (TCS) is a 1.5m infrared telescope at the Izana observatory, Tenerife. Observations were carried out in the K-band (2.2 μm) using a continuously variable filter with a single-channel photometer. The observations were made at irregular intervals during the period 1994 June 7 – July 4 for typically one hour at a time. Cyg X-3 is seen to be a highly variable K-band object over this period. Phase-binning of the data showed no evidence for the orbital modulation due to the large varia-

tions in source brightness and sparseness of the sampling. Fig 5.1 plots the TCS data set with the radio monitoring over the 1994 June – July period. A possible correlation between activity in the infrared and radio (and hard X-ray) is discussed in more detail in section 5.3.

5.2.5 INT : 0.9 & 0.8 μm

Observations were made at the Isaac Newton Telescope (INT) on the nights of 1994 May 31 and June 1 as part of the service observing program. The observations of May 31 were troubled by problems with the instruments and are not used here. On June 1 however, the Cyg X-3 field was successfully imaged in the R (0.77 μm) and I (0.9 μm) bands using the TEK1 CCD chip (1124 $\times$ 1124 pixels) at prime focus. Four 10-min R-band frames and four 5-min I-band frames were obtained. Fig 5.4 shows a typical I-band image, cut down to a similar size and scale as the deep infrared images presented later in the chapter. The field within ten arcsec of Cyg X-3 is dominated by Star D, which infrared colours confirms is at significantly lower reddening than Cyg X-3 or Star Z (section 5.4). In the R-band Star D is even more dominant and Cyg X-3 is hard to discern.

Co-adding all the frames in each band allowed a $\sim 6\sigma$ detection at I, but unfortunately the R-band detection was only at $\sim 2\sigma$. Flux calibration was performed using stars in the field of PG1657+078, and the following colour corrections (Brian Boyle, private communication) were used to compensate for the extreme reddening of the source :

$$R_{\rm true} = R_{\rm inst} + 0.013(R-I)_{\rm inst}$$

$$I_{\rm true} = I_{\rm inst} + 0.055(R-I)_{\rm inst}$$

The mean I-band magnitude obtained from the observations, after applying the reddening colour correction, is I= 19.5 ± 0.2 mag. The lower limit obtained from the R-band observations is R> 21.1 mag. The I-band magnitude is slightly brighter than the mean of I= 20.0 ± 0.2 reported by Wagner et al (1989 [98]) but is consistent with their estimation of 90% modulation/variability in this band. Note also that the INT observations were

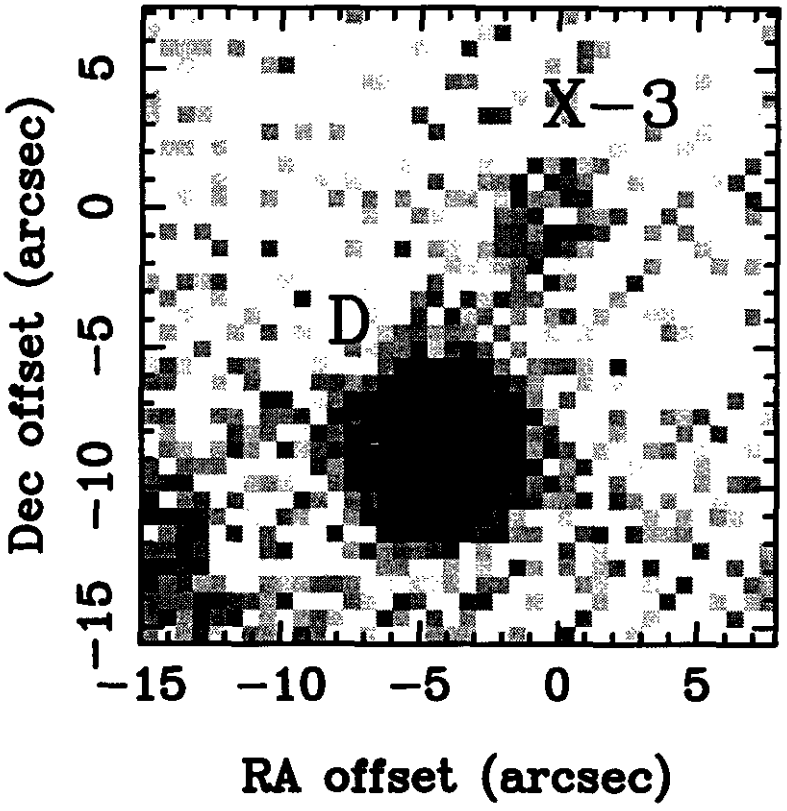

Figure 5.4 A portion of a typical 300 sec exposure I-band frame of Cyg X-3 obtained at INT. Image has been cut down to be the same size and scale as the deep infrared images presented below. Only Star D and Cyg X-3 are visible.

made during a period of small flaring and there may have been significant brightnening of the source at this time. The R-band upper limit is consistent with the result of Wagner (1990 [58]).

5.2.6 GRO - OSSE : 50 - 150 keV

The Oriented Scintillation Spectrometer Experiment (OSSE) instrument (Johnson et al. 1993 [115]) on the Gamma-Ray Observatory (GRO) consists of 4 cylindrical NaI/CsI phoswich detectors, each surrounded by an active NaI shield. Each has a tungsten collimator which defines a rectangular field of view, approximately $3.8° \times 11.4°$ FWHM. The detectors can be indepen-

Table 5.1 Preliminary best-fit cubic ephemeris from OSSE data

$T_n = T_0 + P_0 n + c_0 n^2 + d n^3$

Parameter	Fitted value
T_0	2440949.8999 ± 0.0014 HJD
P_0	$0.19968240 \pm (2.8 \times 10^{07})$ d
c_0	$(1.81 \pm 0.16) \times 10^{-10}$ d
d	$(-2.04 \pm 0.25) \times 10^{-15}$ d
χ^2 (d.o.f.)	114.68 (84)

dently pointed and can be rotated through 192° about the spacecraft y-axis, which is parallel to the long direction of the collimator. The normal observation mode is to alternate source and background pointings with each detector every 2 minutes. The background measurements are used to interpolate the level of background during the source observations. The normal spectral energy range of the OSSE detectors is $\sim$ 50 keV to $\sim$ 10 MeV.

OSSE observed Cyg X-3 twice in the summer of 1994: from June 7 to 17 (JD 2449510–20) and from July 7 to 12 (2449540–45). The principal investigator on this program was Steve Matz.

Derivation of a new ephemeris from OSSE data

As well as comparison with both day-to-day and orbital infrared light curves, the OSSE observations of 1994 June – July were combined with previous soft X-ray data to determine a new cubic ephemeris for Cyg X-3. The method employed was to fit the mean EXOSAT light curve of van der Klis & Bonnet-Bidaud (1989 [26]) to the binned OSSE data, allowing phase, amplitude and background (DC) to vary – though note that both the OSSE and UKIRT data are in fact marginally *inconsistent* with the EXOSAT template. In all cases however the EXOSAT template was a significantly better fit than a simple sine function, which is commonly used to fit light curves. The preliminary best-fit cubic ephemeris is described in Table 5.1.

The ephemeris derivation was carried out by Steve Matz and is described in more detail in Matz et al (1996 [93]).

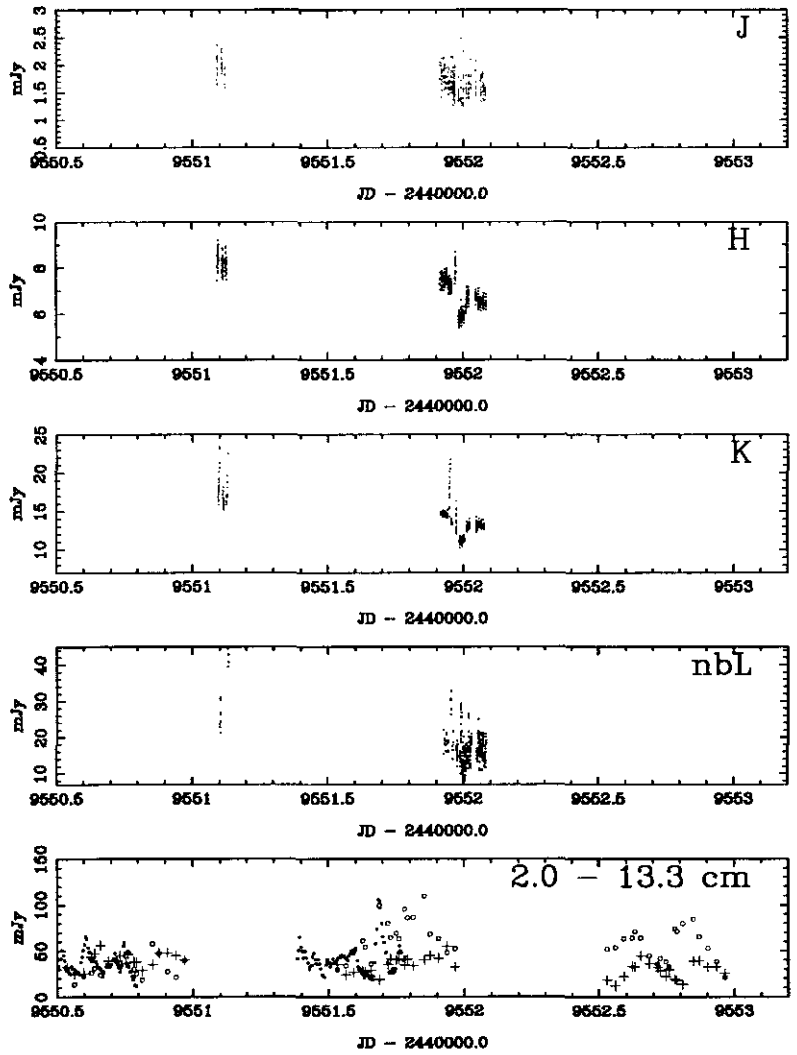

Figure 5.5 IRCAM3 J, H, K & nbL Cyg X-3 light curves compared with radio monitoring at Green Bank & Ryle Telescope in interval 1994 July 16 -17. Cyg X-3 was clearly brighter in the infrared on July 16. Lack of simultaneity in observations makes comparisons difficult, but there is no clear correlation between radio & infrared activity.

5.3 Comparison of variability at different wavelengths

5.3.1 Radio – Infrared correlation ?

Fig 5.1 clearly shows that Cyg X-3 was in a small flaring state in the radio throughout the period of multiwavelength observations. This state is characterised by low-amplitude ($\leq$ 1 Jy) radio flares typically every 5-15 days, and rapid variability at all wavelengths. The 3.6 – 2.0 cm spectral index was calculated using the method described in chapter 4, and the 13.3 – 3.6 & 3.6 – 2.0 spectral indices are plotted as the lower two panels in Fig 5.1. There is no evidence for a systematic trend in the spectral indices such as that found for the 1994 Feb – March flaring sequence (although the most active periods are, as in 1994 Feb – March, characterised by an increase in $\alpha_{13.3-3.6}$, indicative of increased opacity).

Combination of the UKIRT & TCS data sets has allowed me to check for both short-term and long-term correlation of radio & infrared activity. Unfortunately, large differences in both longitude & latitude between UKIRT (at Mauna Kea, Hawaii) and the radio telescopes (at Green Bank, Virginia, USA & Cambridge, UK) meant that radio coverage was not simultaneous with the UKIRT observations. Nevertheless, the clear difference in infrared brightness between July 16 & July 17 allowed some hope of finding perhaps a correlated decline in radio flux strength. Unfortunately, this was not observed – as Fig 5.1 shows clearly, the UKIRT observations fell during possibly the quietest period (in terms of radio actvity) during the entire campaign, with flux densities at centimetre wavelengths of typically 40 – 60 mJy. Furthermore, Fig 5.5 plots the two sets of UKIRT observations in all four bands, in comparison with the radio flux immediately before, between, and immediately after. There is certainly **no** obvious correlated activity, and if anything Cyg X-3 appears to be in a slightly more active radio state around the time of the July 17 observations ie. infrared quiescence. However, time delays in emission at centimetre wavelengths due to both self-absorption and absorption by the stellar wind, could cause lags in

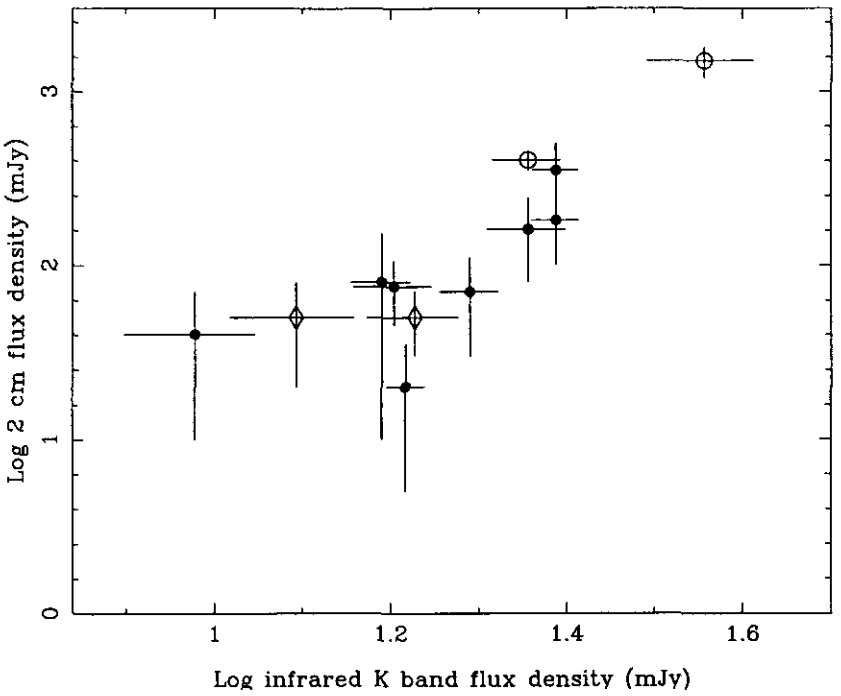

Figure 5.6 Comparison of long-term infrared and radio flux variability. $\log(S_{2.0cm})$ is plotted against $\log(S_{2.2\mu m})$ for data from the TCS (filled circles), UKIRT during 1994 Feb – March radio flares (clear circles) and UKIRT on 1994 July 16 & 17 (diamonds). There is a hint of a correlation for infrared K-band flux densities > 20 mJy.

correlated behaviour (see e.g. discussion in chapter 3).

Comparison of medium and long-term brightness variations in the infrared and radio proved slightly more fruitful. In Fig 5.6 I have plotted $\log(S_{2.0cm})$ against $\log(S_{2.2\mu m})$ and there may be a weak correlation, at least for $S_{2.2\mu m} > 20$ mJy. The Infrared flux densities are the mean from a night's observing and are drawn from the TCS data from 1994 June – July, UKIRT data from the period of infrared flaring in 1994 Feb – March (chapter 4) and the UKIRT data from 1994 July 16 & 17. The 2 cm flux densities are in most cases estimated daily means with error bars judged by eye to equal the variability on that day; in one case an estimate of S_{2cm} was made from the 3.6 cm flux density with which it is well-correlated.

5.3.2 Orbital colour changes in the infrared ?

In this section I investigate the infrared data for orbital colour changes across the J-H-K-nbL bands. Given that the data are not simultaneous, it is necessary to bin the data. In order to do so I tried to make the bin size as small as possible whilst still being larger than the typical period spent in one band (in order to smear out the effects of non-simultaneity). A compromise was made at binning the data into 16 phase bins (some of which turn out to be empty for one or more filter). Flare events have been removed by eye. The binned light curves are plotted in Fig 5.7.

Note that in calculating the error within each bin the *average deviation*

$$\mathrm{ADev}(x_1 ... x_N) = \frac{1}{N} \sum_{j=1}^{N} |x_j - \overline{x}|$$

was used as opposed to the *standard deviation*. This error calculation is better ('more robust') for data sets with 'broad distributions and a significant number of outlier points' (Press et al 1992 [116]) – this is particularly relevant where removal of large flares by eye may still have left small flare events within the data. The overall effect of this method is to make the errors at J slightly larger and those at nbL significantly smaller as compared to a standard deviation error. Note that (particularly at H & K) the 'error bars' calculated here reflect the intrinsic variability of the source within the phase bin.

The binned data were then used to calculate the (J–H), (J–K), (H–K) and (K–L) colours. These are plotted in Fig 5.8.

The infrared colours do not appear to show any particular phase-dependent trends (although all have their bluest points within 0.1 phase of orbital minimum). A tendency toward the red or blue at a particular phase would show up best in the (J–L) colour, but unfortunately the combined errors of these two data sets would hide any colour changes less than 40% ! It should be noted that small colour changes, such as the apparent changes in (H–K) outside of flares described in chapter 2 would not necessarily show up in the data here due to both poorer phase coverage and non-simultaneity of data.

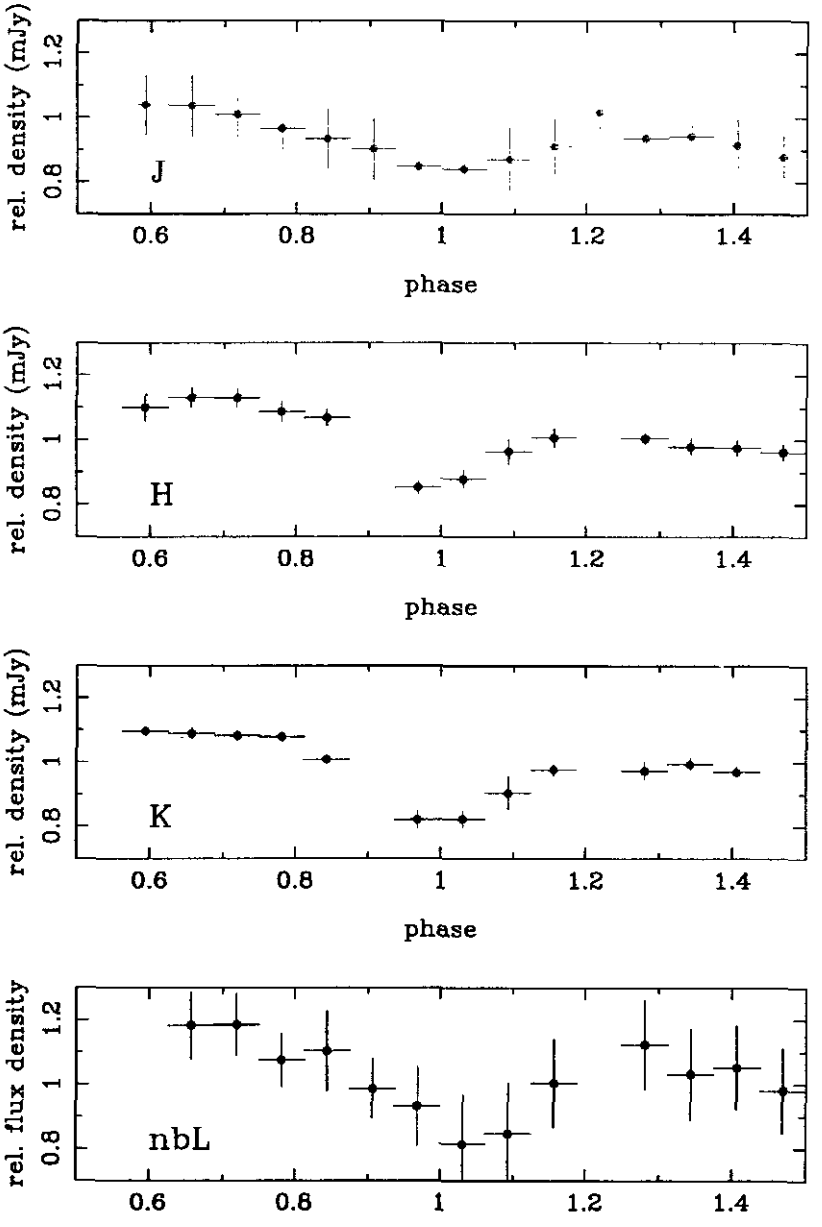

Figure 5.7 J, H, K & nbL data binned into 16 equally spaced phase intervals, and normalised to their mean values as determined from deep mosaics. Errors shown are *average deviation* within each bin.

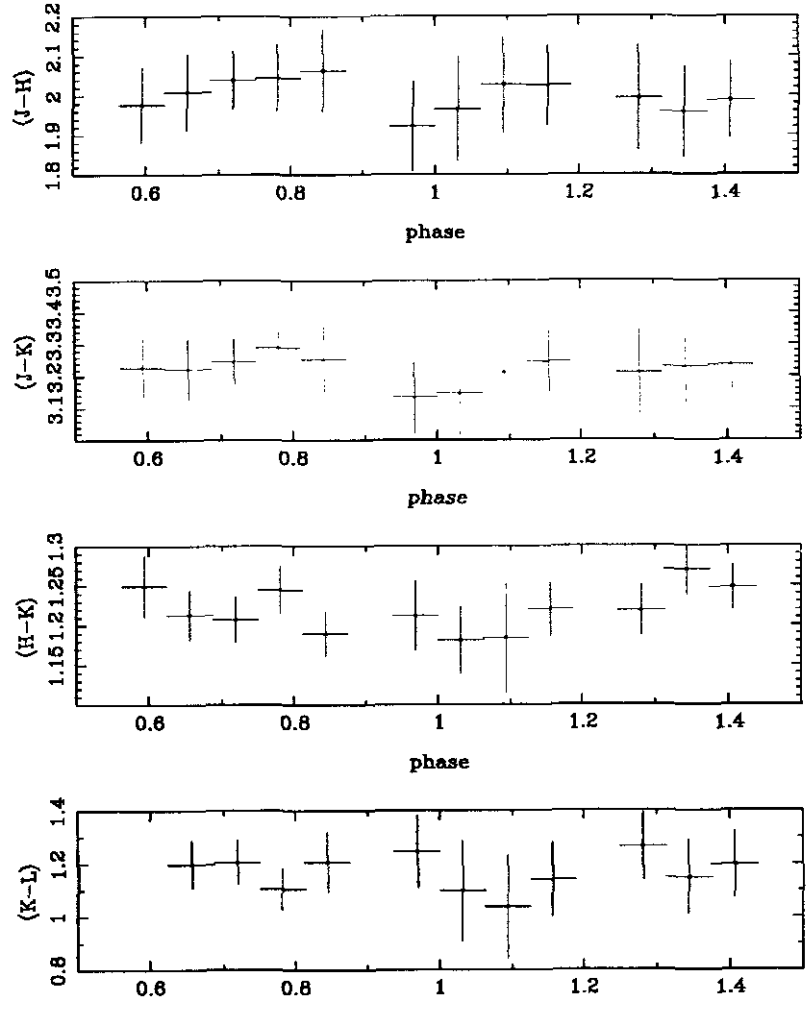

Figure 5.8 Infrared colours of Cyg X-3 in 16 equally spaced phase bins. There is no evidence for any strong phase-dependent trends, though the minimum value of all the colours lies near orbital minimum.

The suggestion that the source may be getting slightly bluer at minimum is worth investigating as it may shed light upon the process responsible for the orbital modulation in the infrared. To this end, two methods were employed. Firstly, the colours of the two data bins near orbital maximum and orbital minimum respectively were plotted in the JHK colour-colour diagram, thus utilising three measurements simultaneously instead of just two used in a simple (M_1 - M_2) colour. The result is plotted in Fig 5.9. Both points near orbital minimum are clearly bluer than those obtained near maximum, but the size of the error bars precludes any definite conclusions. I can simply say that the JHK colours are consistent with the source getting bluer at minimum.

A second method, utilising all four JHKnbL measurements was then employed. For this I took the mean of the JHKnbL colours in the two phase bins nearest orbital minimum, and similarly took a mean of the two phase bins nearest orbital maximum. I then dereddened each by $A_J = 6.0$ mag using the dereddening law of Mathis (1990 [99] – see chapter 2). The results are plotted in Fig 5.10, normalised at the J-band to allow easier comparison. It can be seen that at maximum the source does appear to be redder; and that although the result is marginal when considering error bars, it is consistent across all four bands. If, instead of the more elaborate models of e.g. van Kerkwijk et al (1993b [69]), some component in the system is being (partially) eclipsed at orbital minimum, then the colours of the eclipsed component could be deduced from the difference between the dereddened spectrum at maximum light and that at minimum. This component is also plotted in fig 5.10. The spectral index of the 'eclipsed' component is $\sim +1.9$, far steeper than the $+\frac{1}{3}$ predicted for a 'classical' accretion disc (Beall et al 1984 [117]); but may be consistent with the partial eclipse of the outer, redder, optically thick portions of a disc.

A simple calculation of the modulation factor ξ = amplitude/mean (table 5.2) based upon maximum and minimum flux bins in each band, indicates a greater degree of modulation at *longer* wavelengths. Earlier simple fitting of the H & K light curves presented in chapter 2 (Fender & Bell Burnell 1994

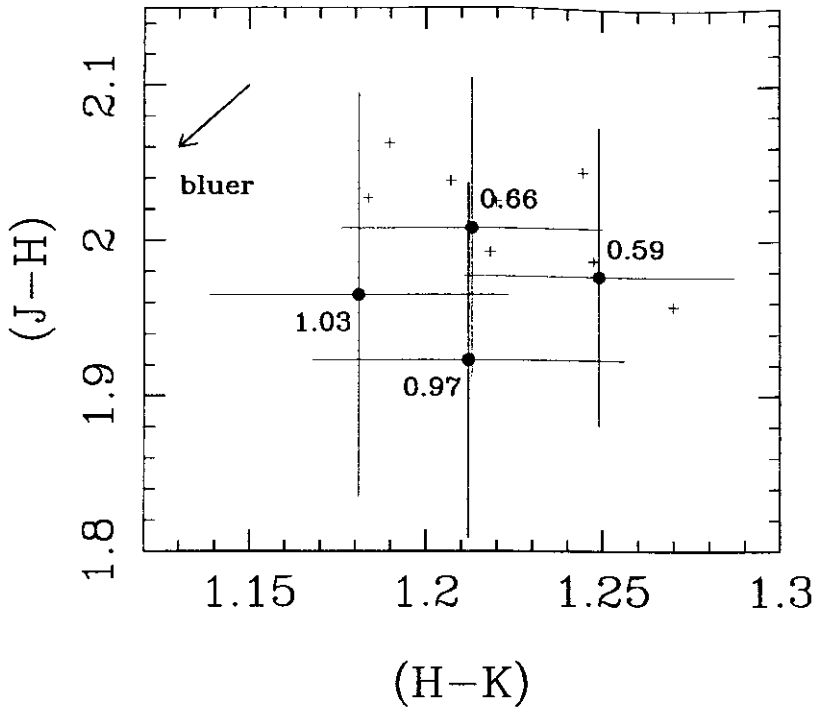

Figure 5.9 JHK colour-colour diagram for the phase-binned orbital data. The colours are plotted with errorbars for the two points nearest orbital minimum and those nearest orbital maximum (central phase of bin indicated) Small crosses (size not representative of error bars) indicate loci of other phase bins. It is clear that the phases near orbital minimum are the bluest in JHK, but given the size of the error bars this result must be treated with caution.

[92]) in fact suggested greater modulation at H than at K, but this was due to different apparent shapes at phases other than orbital minimum, which is in fact not clearly observed in that data set.

5.3.3 Infrared flares

Several infrared flares are clearly visible superimposed upon the orbital modulation in the infrared light curves. I investigate two in detail in which the flaring activity continued across one or more filter changes, thereby providing some information on the spectrum of the flaring component. In both cases I have first removed an estimated quiescent component appropriate

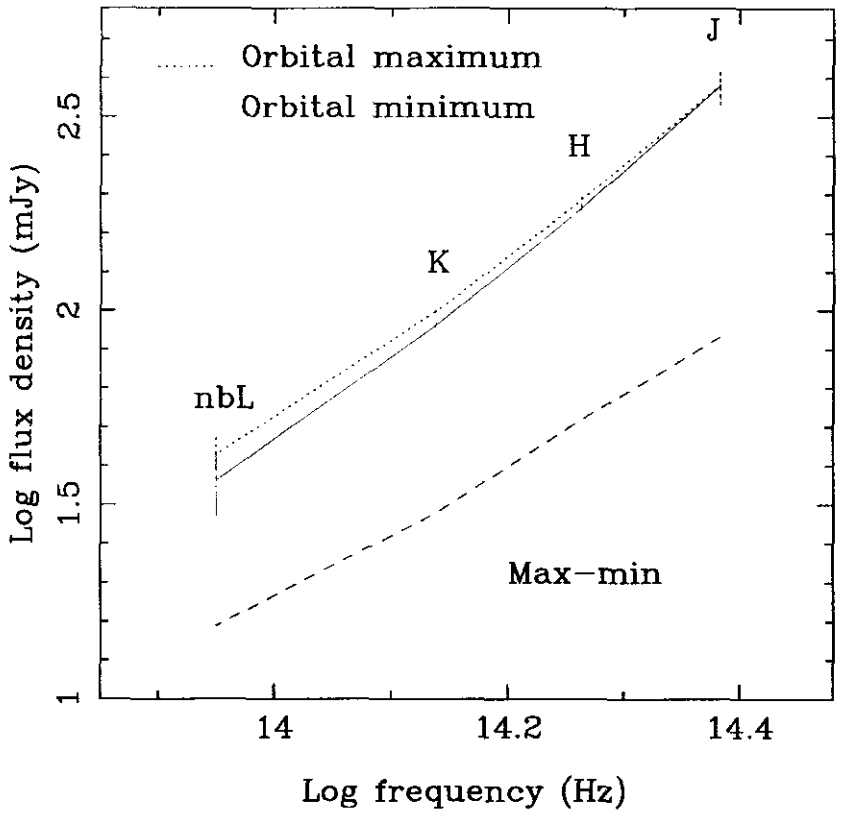

Figure 5.10 1.2 – 3.6 μm spectrum dereddened by $A_J = 6.0$ for minimum and maximum light. The fluxes at orbital maximum have been normalised to those at minimum in the J-band. The spectrum appears to be marginally, though consistently, redder at maximum.

Table 5.2 Modulation factor ξ = amplitude/mean

J	0.107 ± 0.107
H	0.140 ± 0.028
K	0.143 ± 0.020
nbL	0.185 ± 0.127

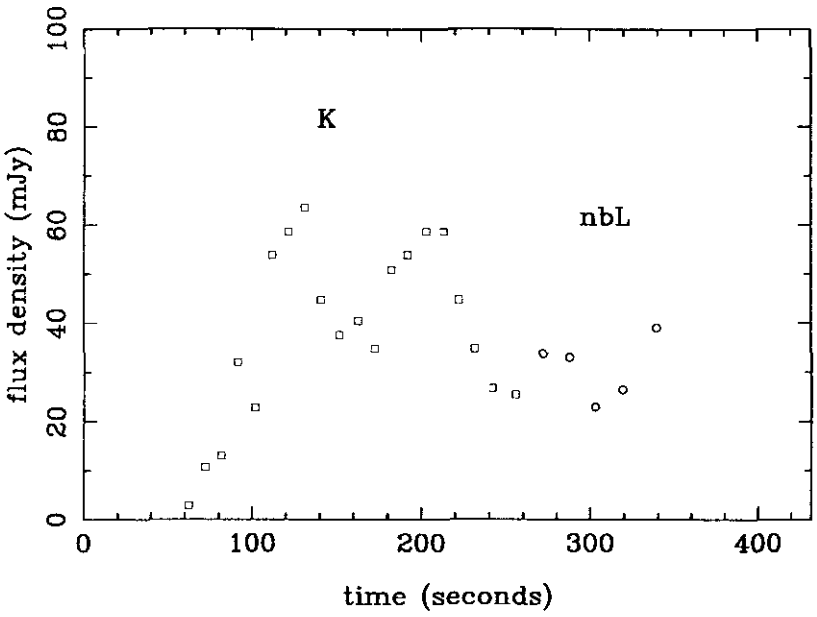

Figure 5.11 Infrared flare observed in both K and nbL bands. Flux densities have had estimated quiescent fluxes removed and been dereddened by $A_J = 6.0$ mag. The consistency in flux levels across the two bands indicates a flat spectrum (optically thin free–free) for the flaring component.

for the filter at the relevant phase, and have then dereddened the residual flaring component by $A_J = 6.0$ mag using the dereddening law of Mathis (1990 [99] – see above and chapter 2).

In the first flare, shown in fig 5.11, the event is seen to rise in around 50 sec in the K-band and there appears to be a second event superimposed before the first has faded away. During the decay of the second event the filter changed to the nbL band where the activity was seen to continue for a further 80 – 90 seconds. The consistency of flux levels in both bands for the flaring component is heavily in favour of a flat spectrum i.e. optically thin thermal bremsstrahlung, as suggested in chapter 2.

An even better example is the second highlighted flare event, plotted in fig 5.12. In this case a flare rises in about 35 sec at H, with a secondary event observed in the same band some 50 sec later. During the decline of this second event (possibly incorporating a smaller third event) the filter

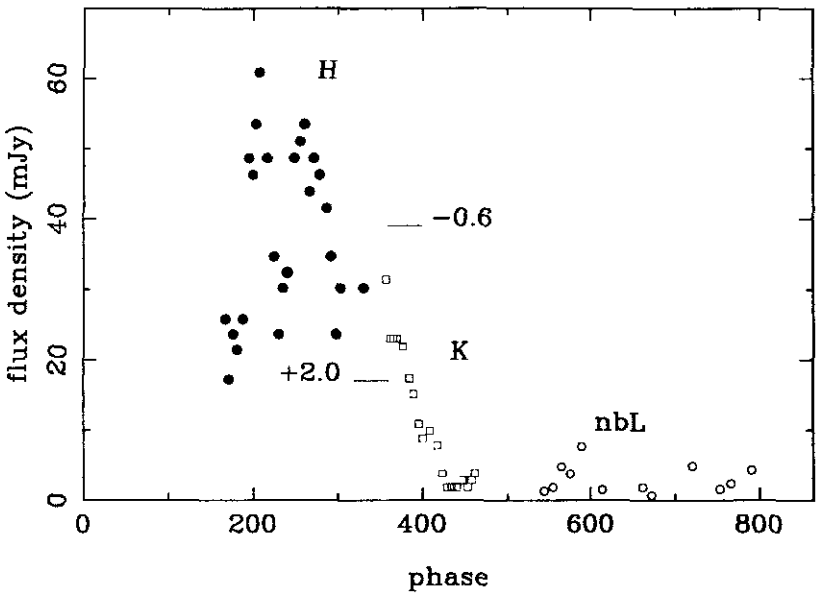

Figure 5.12 A second infrared flare, this time observed in H, K & nbL bands. Fluxes have had quiescent estimates removed and been dereddened as in the previosu figure. Consistency of flux levels across the bands, in particular from H to K, is again strong evidence for a flat spectrum for the flaring component. The positions are indicated of the K-band flux expected at the point of H → K filter change in the case of the flaring component having a black-body (index +2.0) or optically thin synchrotron (index -0.6). Clearly a flat spectrum is more consistent with the data.

changed to the K-band. The almost perfect continuity of the decay rate and flux levels across H − K again argues strongly for a flat spectrum for the flaring component. Further activity at a lower level continued in the nbL band only $\sim$ 90 sec later, at a roughly consistent level. Note also that during the interval between the first and second events, observed in the H-band, there were at least two *significant* flux variations at the time resolution of the data, ie. $\sim$ 10 sec. This, and other such rapid variations in the data, confirms the report in chapter 2 of flares with rise times $\leq$ 15 sec. A rise time of $\sim$ 10 sec indicates flaring activity on size scales of $\sim 3 \times 10^{11}$ cm.

The continuity across filter changes provides strong support for the suggestion (Mason, Cordova & White 1986 [55]; chapter 2) that the flaring component is hot optically thin free-free; any significantly wavelength-

dependent spectrum (e.g. optically thin tail of synchrotron with spectral index $\alpha = -0.6$ or the Rayleigh-Jeans tail of a black-body with $\alpha = +2.0$) would have shown up as a discontinuity in the plots at the point of filter change – this is illustrated in fig 5.12.

5.3.4 Infrared & hard X-ray light curves

The infrared observations of 1994 July can be compared with the OSSE hard X-ray observations in two ways : firstly, day-to-day variations observed at the TCS can be compared with day-to-day varaitions in the hard X-ray flux, and secondly the mean OSSE orbital light curve can be compared with the UKIRT orbital light cuvre of July 17.

Comparison of day-to-day infrared & hard X-ray variability

There is no clear correlation between the TCS and OSSE day-to-day data sets, plotted together in fig 5.13, although the errors in the measurements are large enough that no strong conclusions can be drawn either way. Both data sets show a large degree of day-to-day variability, up to 100% on timescales of 2 days or less. The X-ray observations are however just about consistent with orbital modulation at a random phase plus a small change in base level, and do not require a change of X-ray state. The infrared observations however show a comparable, if not larger spread in flux, despite the modulation in this band being less than half that in the OSSE band (see below) – so there was some infrared flaring going on during the observations (though whether of the rapid second-timescale or more prolonged varieties it is impossible to tell).

Comparison of infrared & hard X-ray orbital light curves

Fig 5.14 presents the mean binned hard X-ray OSSE light curve with the K-band UKIRT light curve (obtained just days after the final OSSE observation) for comparison. The OSSE light curve is significantly more symmetric than the mean EXOSAT soft X-ray template of van der Klis & Bonnet-Bidaud (1989 [26]).

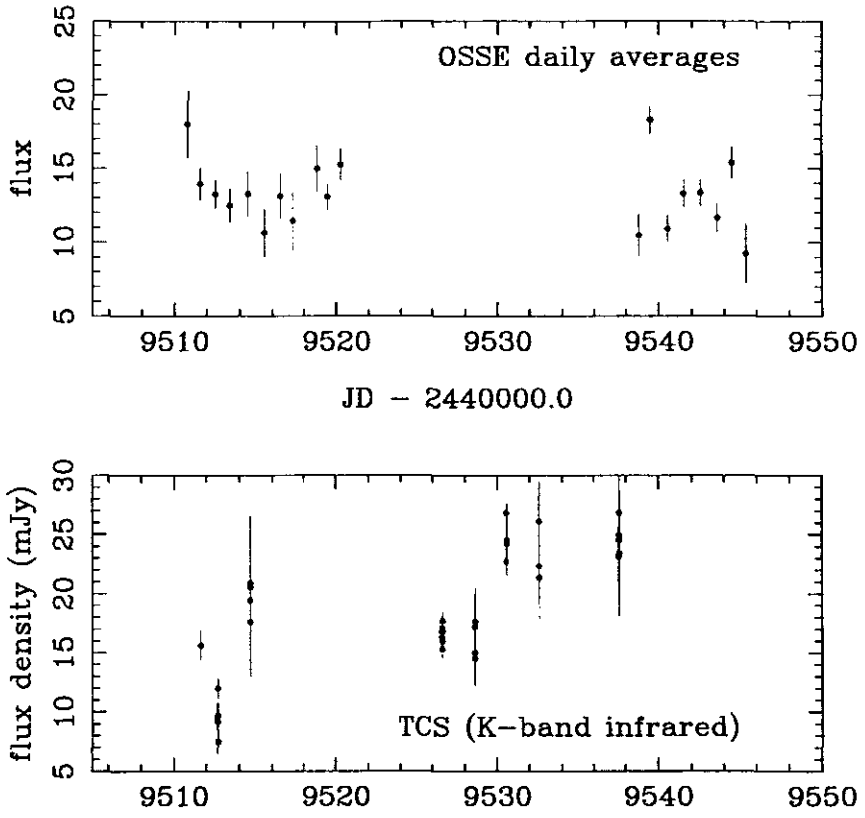

Figure 5.13 Comparison of OSSE (> 50 keV) daily average fluxes with infrared observations at the TCS over the same period. Unfortunately the poor coverage can neither confirm nor rule out the possibility of day-to-day correlated activity in the two regimes.

This is the first time that quasi-simultaneous observations of an orbital cycle of Cygnus X-3 have been made both at hard (> 50 keV) X-rays and the infrared. Confirmation that the light curves in the two energy regimes are in phase (tested formally in the pulse-fitting by Steve Matz during the derivation of the new ephemeris described in section 5.2.6) is very important. This is because it was already known that the soft X-ray and infrared light curves were in phase, and so it can now be safely assumed that hard and soft X-ray data can be combined in the derivation of ephemerides. Given future planned hard X-ray observations using OSSE (Matz, private communication) and SAX (Del Fiume, private communication) this becomes a

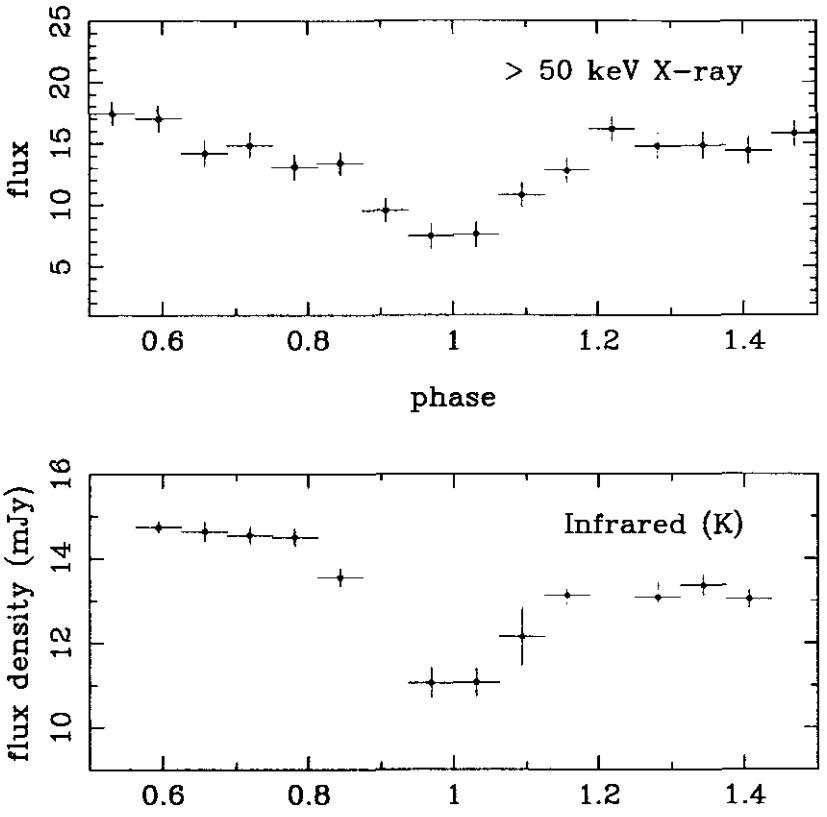

Figure 5.14 Comparison of mean OSSE hard X-ray (> 50 keV) lightcurve in interval JD 2449510 – 45 with UKIRT K-band lightcurve of JD 2449550 (1994 July 17). The light curves are clearly in phase and of similar shape.

most useful result.

That light curves from the infrared nbL band to hard X-rays are in phase implies a common mechanism which is of importance (if not dominant) across seven decades of energy. The degree of modulation $\xi_X = 0.401 \pm 0.044$, two to three times that observed in the infrared. This degree of modulation is comparable to, if not greater than that observed at lower X-ray energies, contrary to previous reports.

5.3.5 Comparison of 1984 & 1994 infrared light curves

Jones et al (1994 [47]) have claimed that infrared light curves obtained by them show that the minimum in Cyg X-3 is getting broader and more

symmetrical. Matz et al (1996 [93] and previous section) has also shown that the hard X-ray light curve obtained in June – July 1994 is more symmetrical than the mean EXOSAT soft X-ray template of van der Klis & Bonnet-Bidaud (1989 [26]). An evolution of the light curve from the asymmetric EXOSAT template toward a more symmetric form is to be expected in the case of precession of the line of apsides of the orbit ('apsidal motion'). Such a process has been proposed by eg. Elsner (1980 [70]) to explain the observed lengthening in the 4.8 hr orbital period. This process predicts a reversal in the sign of $\dot{P}$, and the longer before this is observed, the longer the derived precession period.

In order to explore the claim of Jones et al (1994 [47]) that the infrared light curve had evolved, particularly in light of the importance of the apsidal motion model, I have compared K- & H-band orbital light curves obtained at UKIRT in 1984 (chapter 2) and 1994 July. Fig (5.15) shows the light curves from both epochs superimposed upon each other. Note that no normalisation has been applied to the flux densities – these are the calibrated values in both cases – indicating little very-long-term (years) variability in the infrared output of the source (in stark contrast to e.g. X-ray transients and to the jet-source Cir X-1 – see chapter 6).

The phase was calculated using the new ephemeris of Matz et al (1996 [93], see section 5.2.6). This ephemeris provides an excellent fit to the 1994 data and is also consistent within a few percent with the ephemeris of van der Klis & Bonnet-Bidaud (1989 [26]) for observations in 1984.

Though the data, in particular that from 1984, are heavily clouded by flares, there is enough clear orbital modulation for some comparison to be made, especially around orbital minimum. The decline toward orbital minimum for both light curves appears to be well underway by phase 0.8. However, in 1984 the fluxes appear to be declining much more rapidly and are already as low as those at minimum in 1994 when flaring interrupts the light curve some 0.1 phase before minimum. This suggests that the minimum in 1984 was substantially deeper than that in 1994. However it should be remembered that, in X-rays at least, one orbital light curve is often dissimilar

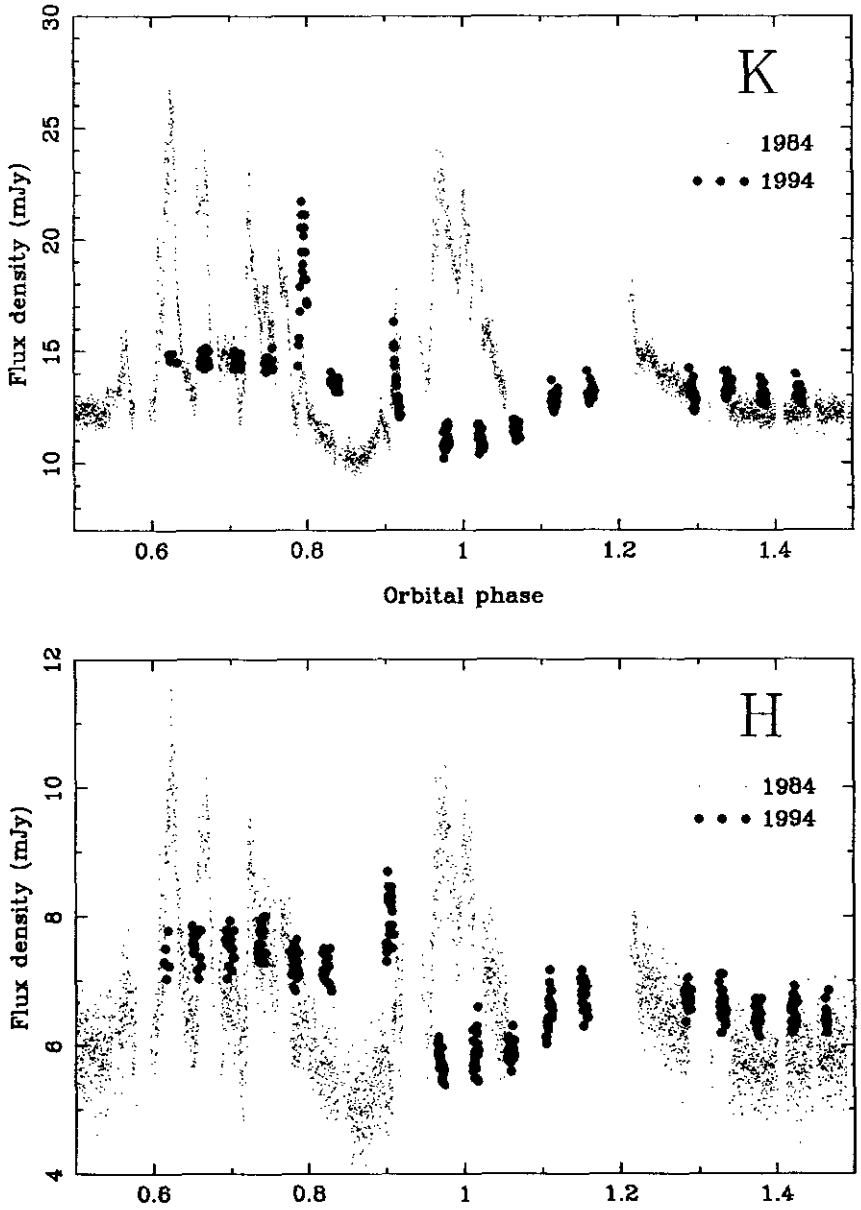

Figure 5.15 A comparison of H & K band infrared light curves taken 10 years apart. Phase is calculated for the 1994 data using the ephemeris of Matz et al 1996 (this chapter).

to the next and it is only when averaged over five or more orbits that the mean light curve shape becomes apparent. The idea that the situation in the infrared might be similar is supported by the apparent DC downwards trend from the 1994 July 16 to July 17 observations.

Has the light curve become more symmetric ? This is extremely hard to judge and I would say that although the data are consistent with an evolution toward a broader, shallower light curve, more data (preferably without flares) is needed before conclusions can be drawn.

5.4 Deep imaging in the infrared

One of the advantages of IRCAM3 as an imaging array is that as well as extracting the light curve from photometry of each frame, the frames can be added together and the result is a deep image of your field.

Figs 5.16 to 5.19 presented here represent the deepest infrared imaging yet of the Cyg X-3 field and reveal the existence of *at least* ten previously undetected objects withing a few arcseconds of the source. I have labelled these new sources '1' to '10' and indicated them on the J, H and K-band images (though object '7' only appears in the K-band). Only Cyg X-3, Star Z and Star D appear on the nbL-band image. The smoothness of an image is a rough measure of the signal to noise of the measurement in that band – thus it is clear from inspection of Figs 5.16 to 5.19 that the highest S/N was achieved at H & K, with that at J being significantly poorer and that at nbL much worse. Possible extended emission around Cyg X-3 is highlighted in Fig 5.20, a K-band contour image of the field.

There are considerable difficulties associated with performing accurate photometry of faint objects so close to bright sources and as a result the estimated errors in the photometry are larger than would be predicted for a source of comparable brightness in a less crowded field. For example, star '1' lies so close to the point spread function (psf) of Cyg X-3 that a software aperture no larger than 2 arcsec could be used, despite the recommended software aperture being 5 arcsec. In order to compensate for this effect,

the psf of the brighter objects in the field (ie. Cyg X-3, Star Z & Star D) was investigated. It was found that for these objects the psf could be well approximated by a circular Gaussian with a standard deviation of $\sim$ 1.5 pixels (though it was in fact found that the psfs were slightly east-west elongated, probably due to telescope wobble in RA – Phil Puxley, private communication). Using this approximation, and assuming a similar standard deviation for all objects in all bands, it is possible to calculate the amount of total light falling within a certain software aperture. For a 5 arcsec aperture this value is $>$ 99% (see Fig 5.21). However, for a 2 arcsec aperture only 82% of the light from a point source falls within the aperture (see Fig 5.22) – therefore a -0.18 mag correction was applied to all magnitudes obtained within 2 arcsec aperture. This value is consistent with, though at the lower end of, empirical estimations of this correction made by placing both 2 arcsec and 5 arcsec apertures on relatively isolated objects in the frame. Table 5.3 presents J, H & K (and nbL for Cyg X-3, Star Z and Star D) magnitudes (where measurable) for all objects in the frame. Exact errors in the magnitudes are hard to quantify, but good estimates are :

$\pm$0.05 mag for J$<$16, H$<$ 14 or K$<$ 13

$\pm$0.10 mag for 16$\leq$J$\leq$19, 14$\leq$H$\leq$18 or 13$\leq$K$\leq$17

$\pm$0.50 mag for J$>$19, H$>$18 or K$>$17

Errors at nbL are $\sim$ 0.05 mag for Cyg X-3 & Star Z (though Cyg X-3 is of course variable), and $\sim$ 0.1 mag for Star D.

The JHK colours can be used to plot these objects in the JHK colour-colour diagram (see Fig 5.23). From this it is clear that all of the objects in the frame except Star D and '3' are significantly reddened. Star D, as expected from its dominance in the I and J-bands (see Figs 5.4 and 5.19) appears to be a foreground main-sequence object suffering little or no interstellar extinction. Object '3' may be similar, though within the rather large error bars it could conceivably be reddened by up to $A_J = 1.0$ mag – given its relative faintness in the frame this may well be the case. Because of the similarity in the JHK colour-colour diagram of the gradients of the main sequence and the reddening line, it is rather difficult to estimate the spectral

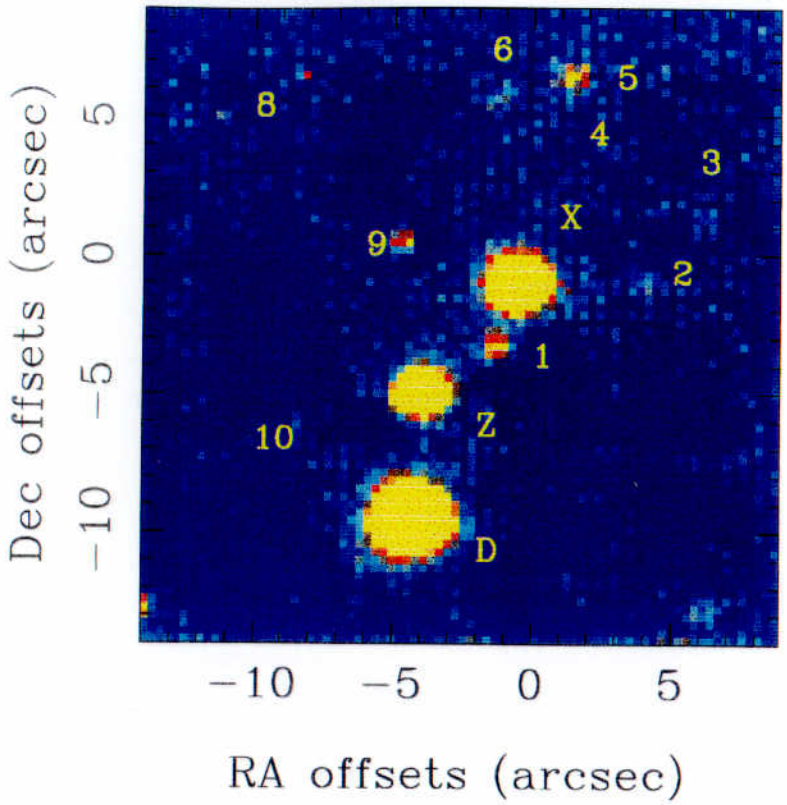

Figure 5.16 Composite J band (1.2 μm) image of Cyg X-3 field with total integration time of 1100 sec

class of a reddened star from its JHK colours, and little can be said about objects '2', '5', '6' and '9' from their placing in the diagram except that they are heavily reddened. Object '1', Cyg X-3 and Star Z all lie at extremely high reddenings, with $A_J > 3.0$ mag for all three objects, possibly much higher depending on their dereddened positions on the main sequence. It is interesting that Stars Z and D have comparable brightnesses in the infrared when one is clearly very distant and heavily reddened (a red giant ?) while the other is a relatively nearby star undergoing little or no extinction. Given the significantly lower (H-K) of Star '1' compared to Cyg X-3 it is likely that this object is suffering less extinction than Cyg X-3 and is therefore closer – I do not think there is much likelihood of these two stars being associated,

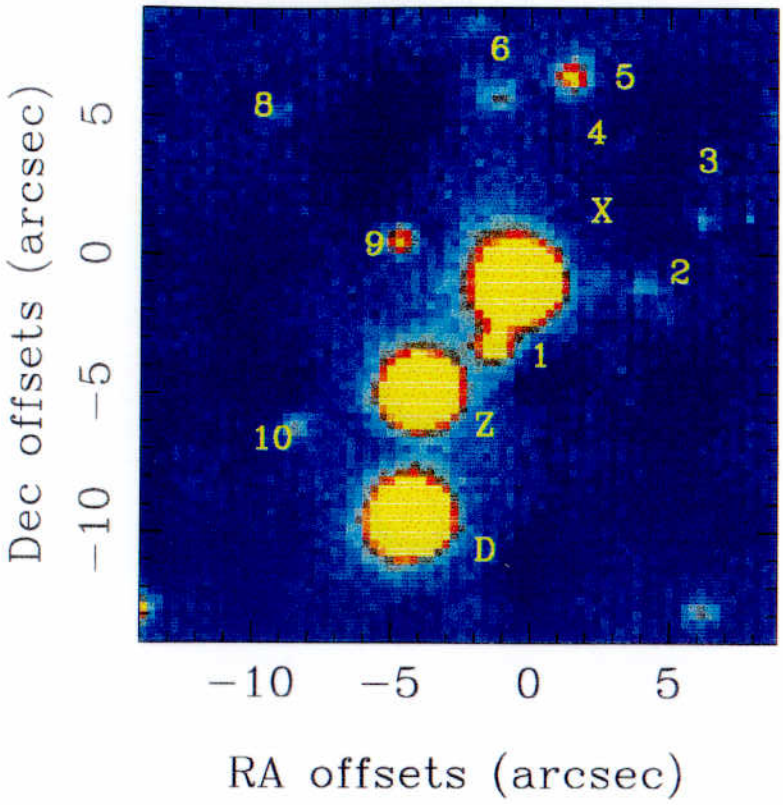

Figure 5.17 Composite H band (1.65 μm) image of Cyg X-3 field with total integration time of 760 sec

Source profiles

Further information on the nature of the field objects can be otained from investigation of crosscuts in the image which are used to reveal their profiles in the South-North and East-West directions (Fig 5.24). Cyg X-3 and stars 'Z' and 'D' clearly have very similar, smooth, profiles which we shall take as being representative of a point source (ie. unresolved star). As noted earlier, these profiles are reasonably well fit by circular Gaussians.

Of the newly-discovered objects, '1', '5', '8' & '9' all have reasonably well-defined Gaussian profiles. Of these four objects, the first three have JHK colours indicative of a reddened star and so I conclude they are stellar sources. Object '8' has a (H-K) colour of $\sim$ 1 and yet is not clearly measurable in the J-band : this suggests this object is also at extremely high

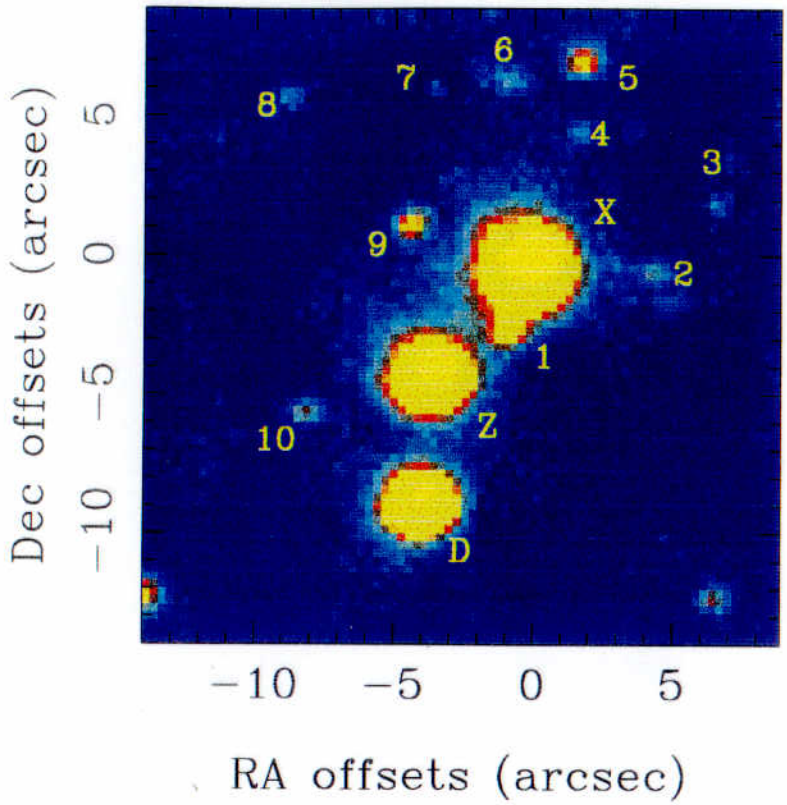

Figure 5.18 Composite K band (2.2 μm) image of Cyg X-3 field with total integration time of 800 sec

reddening comparable to that of Object '1' or Star Z.

Object '3' may well have two components, aligned roughly North-South. Its profile is very noisy but may be consistent with a Gaussian. Objects '6' and '7' are also rather noisy, and '6' in particular appears to be somewhat extended, though at this low S/N it is impossible to draw strong conclusions, Object '10' again is faint but is probably fit reasonably well by a Gaussian.

Object '2' is of interest as it appears to be both somewhat extended and also connected to Cyg X-3. Object '4', and to a lesser extent object '6' are also curious, as they may be extended and appear to lie in a region of slight excess emission (compared with other regions of sky nearby) lying between Cyg X-3 and object '5' to the north. At a distance of 10 kpc, an extended region of angular size 2 – 3 arcsec would be $\sim$ 0.1 pc in extent. Further deep

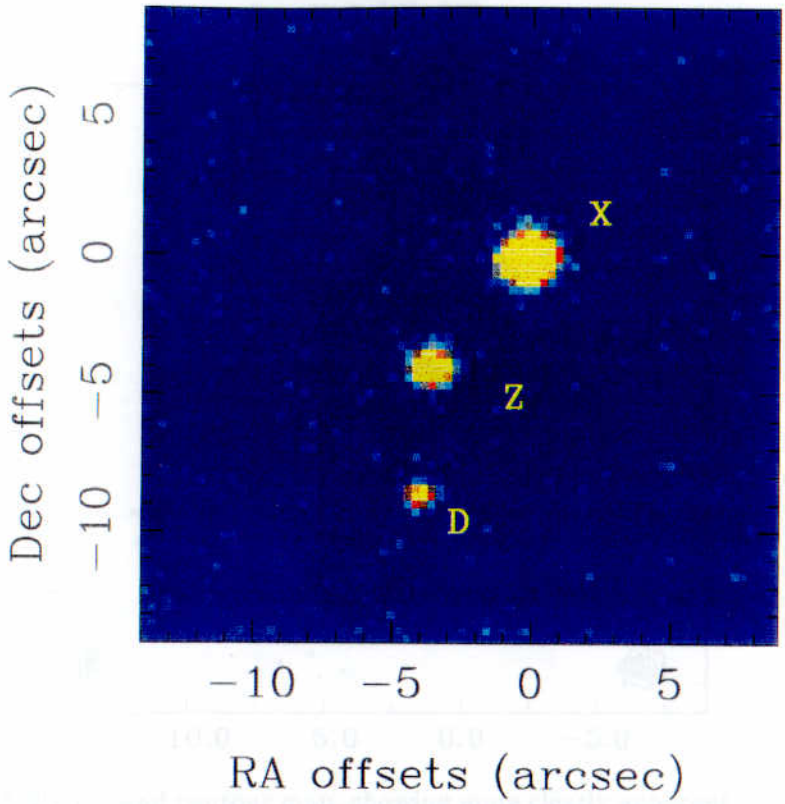

Figure 5.19 Composite nbL band (3.6 μm) image of Cyg X-3 field with total integration time of 2200 sec

imaging is required to determine the nature of these objects.

5.5 Discussion

Here I discuss the possible origin of a radio : infrared correlation, the tentative evidence for the source becoming bluer at minimum, and possible origins of any extended emission around Cyg X-3.

5.5.1 Correlated radio : infrared behaviour ?

Although fig 5.5 shows that there is no clear correlation between radio and infrared flux levels on short timescales, fig 5.6 does appear to show that periods of strong radio emission are generally accompanied by an increased

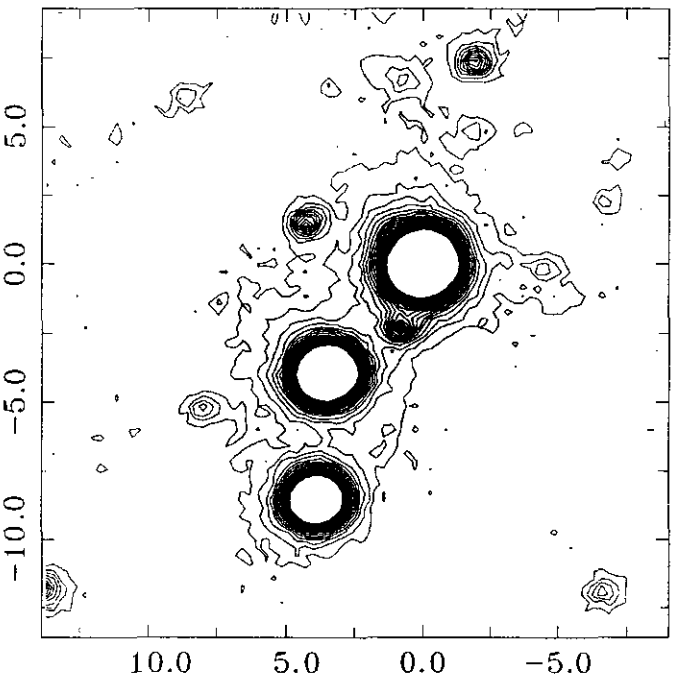

Figure 5.20 K-band contour map, showing more clearly apparent extended emission to north and west of Cyg X-3

Table 5.3 Infrared magnitudes of objects in Cyg X-3 field from composite deep imaging

Source	J mag	H mag	K mag	nbL mag
Cyg X-3	14.83	12.89	11.66	10.38
Star Z	15.64	13.40	12.42	11.76
Star D	13.81	13.16	12.95	12.7
'1'	18.3	16.4	15.5	–
'2'	19.8	18.2	17.9	–
'3'	19.7	18.6	18.6	–
'4'	–	–	17.7	–
'5'	18.5	17.3	16.7	–
'6'	19.4	17.8	17.3	–
'7'	–	–	18.4	–
'8'	–	18.8	17.8	–
'9'	19.4	17.5	16.9	–
'10'	21.9	18.1	17.4	–

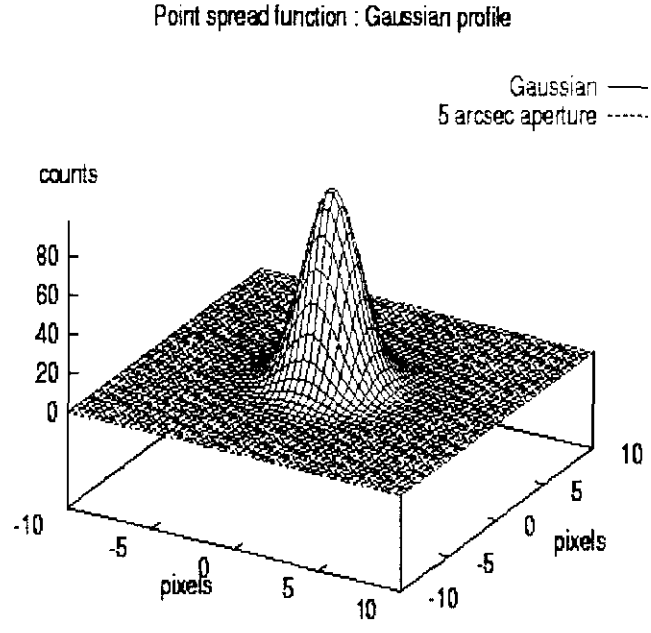

Figure 5.21 Gaussian point spread function with $\sigma = 1.5$ seen through a 5 arcsec software aperture. More than 99% of flux is captured within aperture.

output in the infrared. In the model (scenario B) proposed in chapter 4, this is to be expected as a result of enhanced emission from the stellar wind in the system during a period of increased mass-loss which triggers radio flaring.

As well as overall trends such as scenario B of chapter 4, it might also be expected that there would be correlated radio – infrared behaviour on shorter timescales due to thermal gas injected into or entrained with the jet. However, as discussed in chapter 3, there may be significant delays between the ejecta passing the infrared 'photosphere' (likely to be very close to the system) and travelling far enough out in the wind for radio emission to be observable. Activity might only be recognised as being correlated when this time lag is taken into account, but the data set here is not sufficient for such an analysis.

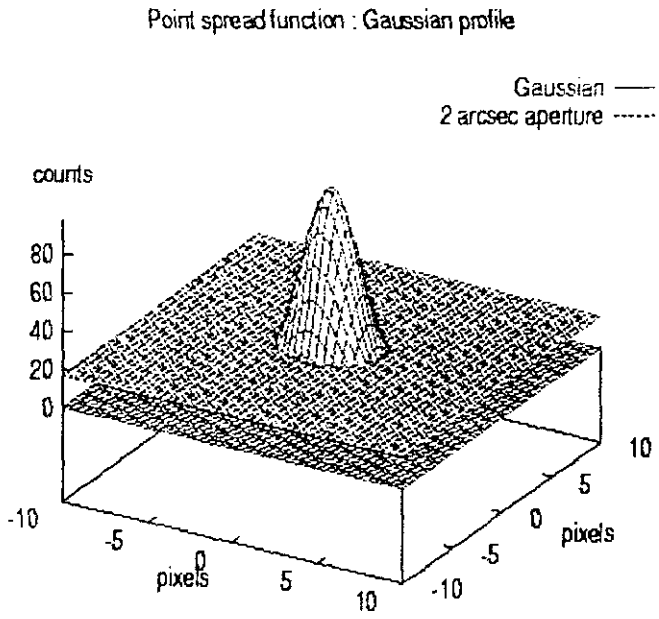

Figure 5.22 Gaussian point spread function with $\sigma = 1.5$ seen through a 2 arcsec software aperture. Only 82% of flux falls within aperture; some 18% is lost.

5.5.2 Bluer at minimum ?

The marginal evidence in the infrared data of the source becoming bluer at minimum supports the (again marginal) evidence for a similar effect in (H-K) in the 1984 data (chapter 2), and also the earlier tentative conclusion drawn by Becklin et al (1973 [19]). A simple measure of the modulation factor ξ for each band supports this conclusion by suggesting that the degree of modulation in the infrared is an *increasing function of wavelength.* Such an effect was in fact predicted by the cocoon model of Milgrom (1976 [118]), in contrast the contemporary model of Davidsen & Ostriker (1974 [74]) which predicts the opposite effect. The more recent model for the orbital modulation of van Kerkwijk (1993b [69]) makes no strong prediction regading degree of orbital modulation as a function of frequency, but notes that

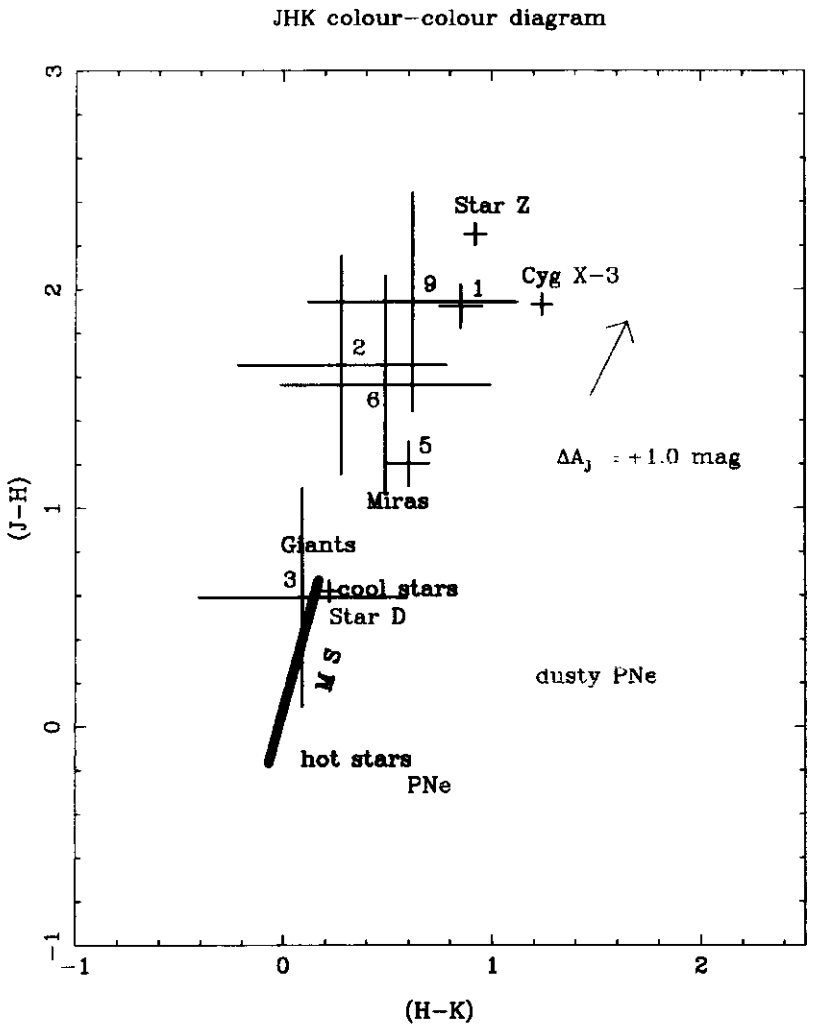

Figure 5.23 JHK colour–colour diagram of objects in Cyg X-3 field

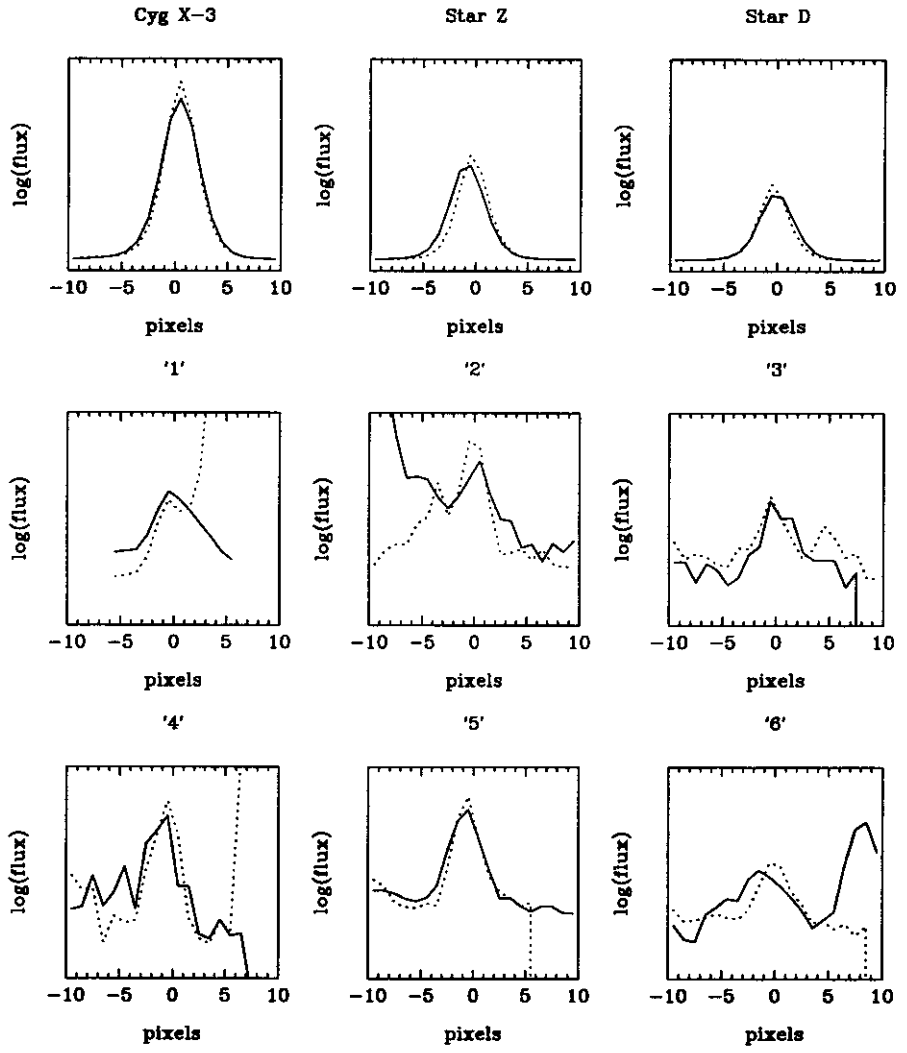

Figure 5.24 Crosscut profiles of objects in Cyg X-3 field obtained from composite 800 sec K-band image. Solid lines indicate a south – north cut, dotted lines indicate an east – west cut about the same centroid. Flux units are arbitrarily scaled to show maximum detail. The large scale crosscut (over) shows that Cyg X-3 completely dominates the flux within 30 pixels north-south and east-west of its cenroid.

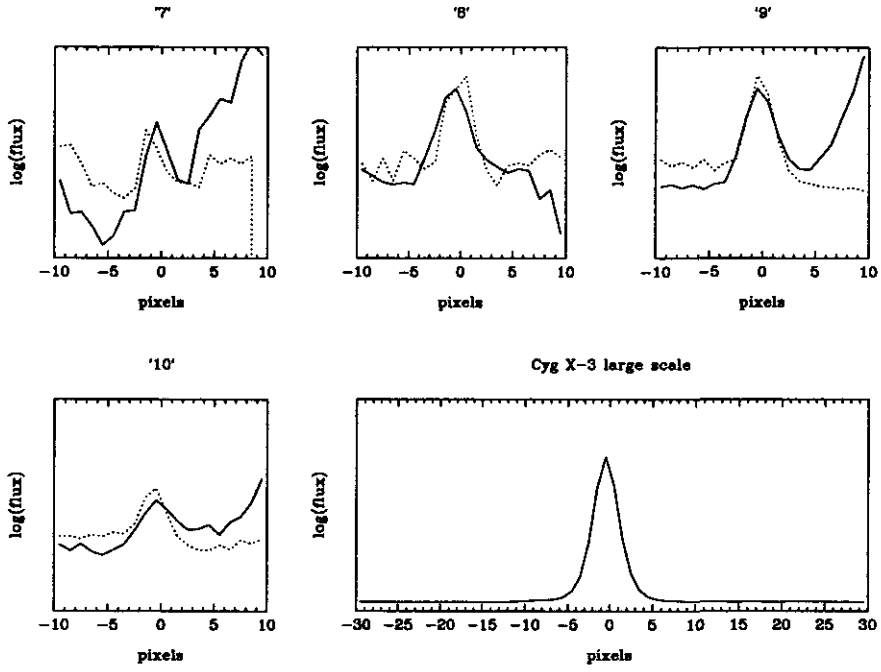

Figure 5.24 (continued)

bound-free absorption, which is frequency dependent, may be important.

In a simple scenario whereby there was some modulating component embedded in a wind with significant optical depth, one would expect the degree of modulation to decrease with increasing wavelength as phase-smearing was caused by scattering. The degree of modulation would decrease until it was no longer detectable, ie. when photons of a certain wavelength would undergo multiple scattering events in the wind and lose all phase information. However, given that the opposite effect appears to be occurring, the central modulating component must inherently become bluer at minimum. This could be caused by the eclipse of a red component or possibly by the cocoon of Milgrom (1976 [118]).

In the eclipse scenario, subtraction of minimum from maximum infrared fluxes (dereddened, see fig 5.10) would indicate an eclipsed component with spectral index $\sim +1.9$, only slightly less steep than a black body. As already noted, this is steeper than the theoretical $+\frac{1}{3}$ spectrum predicted for an

accretion disc in the infrared. A good data set of infrared observations of accretion discs does not however exist and the true infrared colours of an accretion disc in an X-ray binary are not well known.

Alternatively, without any eclipse, the source could appear to become bluer as a hot component (again, possibly an accretion disc) moved further away from us at the far side of the system. Absorption by a larger mass of the stellar wind would be stronger at longer wavelengths and thus cause an apparent shift to the blue in the colour of the source (absorption by differing column densities around the orbit is essentially the basis of most models for the X-ray modulation, though in that case the scattering is Thompson, whereas in the infrared it is free-free). The free-free optical depth τ is proportional to $\nu^{-2.1}$, so $\tau_{\rm nbL} = 2.8\tau_{\rm K} = 5.1\tau_{\rm H} = 9.2\tau_{\rm J}$. A change in optical depth of $\Delta\tau_{\rm J} = +0.11$ between orbital maximum and minimum could produce the observed $\sim 10\%$ modulation at J. However, this simple model would predict modulations of 17, 30 & 36% at H, K & nbL respectively. While that at H is approximately accurate, the modulations predicted at K & nbL are way too high (though maybe phase-scattering by the wind is becoming important at these wavelengths and is offsetting the greater optical depth changes).

Other possible mechanisms which would produce a bluer spectrum at minimum include partical eclipse of the (presumably) hot blue companion to the compact object by an accretion disc at maximum, and (perhaps more speculatively) a red modulating component associated with thermal gas entrained in a constant low-level jet (which would be centred on the compact object). Something like the cocoon scenario of Milgrom (1976 [118]) may also be partly applicable to the more involved wind scenario of van Kerkwijk (1993a [30]). Clearly the mechanism for the orbital modulation in the infrared is not yet clearly understood and further study is necessary.

5.5.3 Extended emission ?

There are two patches of apparent extended emission in the Cyg X-3 field. A diffuse patch of apparent enhanced emission appears to extend to the north,

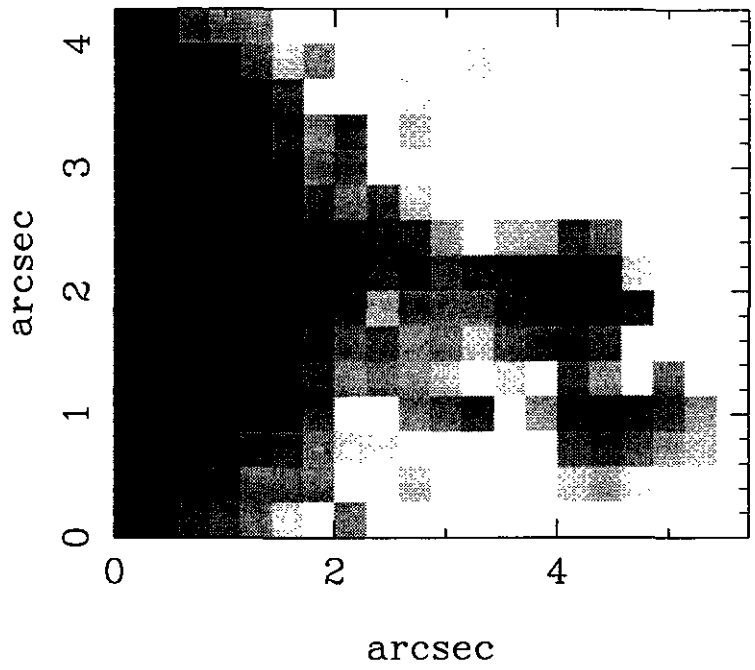

Figure 5.25 Close-up detail of possible westerly extension from Cyg X-3 to object '2'

toward object '5' and including objects '4' & '6'. A thin strip also appears to extend westwards toward object '2'. These patches are highlighted by regions of very low emission lying to the east and south west of Cyg X-3, Star Z & Star D. In fact it is peculiar that all the new objects (excepting possibly '10') appear to cluster around Cyg X-3 and are not evenly distributed across the frame. It may also be that the 'quiet' patches to the E & SW are regions of high gas/dust density, possibly interstellar clouds.

If the apparent extended emission to the north of Cyg X-3 is real then a connection with the radio jets (which are aligned roughly north–south) is tempting. However, the immediate question is 'where is the southern component ?' and this is not easily answered. Furthermore, there are problems with the emission mechanism : free-free emission from thermal electrons associated with the jet would have cooled by the time such large distances had been reached, so emission at this distance would have to be from the relativistic electons, ie. synchrotron. However, the radio map of Strom, van

Paradijs & van der Klis (1989 [38]) implies that strong emission from the radio lobes fades off at an angular distance of about $\sim$ 1 arcsec from Cyg X-3. These apparent radio lobes are also bipolar, seemingly unlike the infrared emission observed here. Synchrotron emission in the infrared would imply very bright emission at radio wavelengths, and this is simply not observed. So, direct association of the apparent enhanced infrared emission north of Cyg X-3 with the radio jets is unlikely, though some secondary mechanism, eg. a local jet–cloud interaction is not inconceivable.

The possible westerly extended emission toward object '2' is also intriguing, and is shown in close-up in fig 5.25. It seems quite possible that this is the orientation of the equatorial plane of the companion star to the compact object. This is because an accretion disc is likely to form from wind accretion in (approximately) the plane of densest material, and this accretion disc is the likely source of collimation for the radio jets along its rotation axis. Since the jets are seen to propagate roughly north–south, in this scenario the equatorial plane of a massive mass–losing companion would be roughly east–west. So, there may just be a small chance that emission from an equatorially-enhanced wind may be imaged here. There is already very strong evidence for anisotropy in the winds of Wolf–Rayet stars (e.g. Schulte-Ladbeck 1995 [119]), and the interactions of the winds of these objects are known to form structures several parsecs in extent (e.g. Smith 1995 [40]; Nichols 1995 [41]). An orbit in or near to an equatorially enhanced plane may serve to explain some of characteristics of Cyg X-3 such as the steady high γ-ray (probably), X-ray and radio brightness. Unfortunately the detection is again marginal and there is no strong evidence for an easterly extension and so future deeper imaging is required in order to progress.

5.6 Conclusions

In this chapter I have described the observations at radio, infrared, red–optical and hard X-rays of Cyg X-3 in 1994 June – July. The multiwavelngth nature of the campaign allowed some hitherto impossible comparisons to be

made, some of which turned up new correlations and discoveries, some of which gave negative results; all were interesting.

A correlation between radio and infrared behaviour on relatively short (hours – days) timescales remains elusive, possibly due to time-delays introduced before local opacity (in the form of a dense stellar wind) can be bypassed by outwards travelling ejecta. However, there is some evidence for correlated activity on longer (weeks – months) timescales. This result agrees well with the findings of chapter 4 that during radio flares there is enhanced infrared emission. Clearly there is more thermal gas around during radio flaring, but its exact source and location in the system remain to be determined.

The red–optical observations were not highly successful, being of too low S/N. However, the I-band measurement was in rough agreement with previous observations (though at the bright side of the range), and frames at I and R confirmed that Star D is a foreground star which dominates the close field in these filters.

The infrared observations revealed the 4.8 – hour orbital modulation in 4 infrared bands, both at longer (nbL) and shorter (J) wavelengths than recorded previously. For the third time marginal evidence suggests that Cyg X-3 gets slightly bluer in its infrared clours during orbital minimum – in fact, the fractional modulation seems to increase with wavelength from 1.2 – 3.6 μm. The cause of this apparent colour change, if confirmed, remains unclear – but this is not surprising since the mechanism for the orbital modulation in the infrared is not yet well understood at all.

Rapid infrared flares were observed again, and comparison of flares which overlapped filter changes is strongly in favour of an approximately flat (probably optically thin free–free) spectrum for the flaring component. A state of abnormally high infrared emission without obvious rapid flares was also again observed, suggesting that two distinct (though not exclusive) modes exist for brightness fluctuations in the infrared.

Hard X-ray observations have allowed a new cubic orbital ephemeris to be derived, and comparison of hard X-ray and infrared light curves confirm

that the orbital modulation in these two extremely different wavelength regimes is in phase. The X-ray observations show the light curve at energies > 50 keV to be more symmetrical than the mean soft X-ray template constructed from EXOSAT soft X-ray observations in the 1980s. This suggestion that the light curve may be evolving was tested by comparing H & K-band infrared light curves from 1984 (see chapter 2) and 1994 – the results are not conclusive due to heavy obscuration by flares, but the orbital minimum in 1994 does appear to be shallower and possibly broader than that in 1984.

The infrared observations had the additional benefit of providing the deepest yet composite images of the Cyg X-3 field. This allowed the discovery of ~ 10 new infrared objects within a few arcseconds of the system. While most a probably stars reddened in the galactic plane, several display intriguing hints of extended emission and warrant further study when more sensitive instruments become available.

Chapter 6

Related objects : galactic radio-jet X-ray sources

6.1 Introduction

Cygnus X-3 is a member of a small, but growing, class of galactic X-ray sources with some form of associated radio structure which can be interpreted as being due to a jet or jets. Here I review our understanding of these sources, present some new radio/mm/infrared data, and discuss the similarities/differences between these objects.

Included in the class are the X-ray binaries SS433, Cir X-1 and LSI+61° 303. Also included are two recently discovered bright X-ray transients with apparent superluminal jets, GRS 1915+105 (Mirabel & Rodriguez 1994 [120]) and GRO 1655-40 (Tingay et al 1995 [121]). These sources are both interpreted as being X-ray binaries, GRO 1655-40 being a strong candidate black hole system. I also include within the class the galactic centre hard X-ray sources 1E 1740.7-2942 (Mirabel et al 1992 [122]) and GRS 1758-258 (Martí 1993 [112]). Both these sources have been found to have associated large-scale collimated radio structures, interpreted as resulting from interactions of jets with the surrounding ISM. Finally, I include the source GT 2318+620 which has been shown to be probably galactic in origin, with an associated radio jet and a possible identification with an UHURU X-ray source. I do not include in the class the young stellar objects known to

have associated outflows (eg. HH80-81 – Martí, Rodriguez & Reipurth 1995 [123]), nor candidate outflow-systems amongst the symbiotic stars and novae (eg. CH Cyg, RS Oph – Iijima et al 1994 [124])

Table 6.1 summarises the primary system characteristics of the nine sources considered here : spectral classification (if any) of companion to compact object, confirmed periodicities and estimated system distance. Models have been proposed for the two galactic centre sources, 1E1740.7-2942 & GRS 1758-258, in which they are not in fact X-ray binary systems but solitary neutron stars or black holes accreting from the ISM (see eg. Mirabel 1994 [125]; Chen & Gehrels 1994 [126]). For none of the sources has the nature of the accreting object been indisputably determined, though there is strong phenomenological evidence that Cir X-1 contains a neutron star (because of its very definite LMXRB X-ray characteristics), and the two 'superluminal sources', GRS 1915+105 & GRO 1655-40, are strong black-hole candidates (GRO 1655-40 due to optical determination of the mass function, GRS 1915+105 both by analogy to GRO 1655-40 and because of the similarity of its hard X-ray tail to black-hole candidates such as Cyg X-1). X-ray pulsations, a sure indicator of strong neutron star magnetic fields, have not been observed from any of the sources.

It should be noted that for some 20 years or so a bipolar radio structure was believed to be associated with the LMXRB Sco X-1 (eg. Hjellming & Wade 1971 [127]) which has only recently been demonstrated to be a chance alignment with a background radio galaxy. The Sco X-1 'radio lobes' in fact prompted an unsuccesful search for radio lobes associated with the LMXRB GX 17+2 which is an 'Atoll' LMXRB like Sco X-1 (Penninx, van Paradijs & Zijlstra 1990 [128]).

In this chapter I shall discuss the observational properties of the nine sources, based upon previously published results, and shall then present some new results in the radio, millimetre and infrared bands relating to several of them.

Table 6.1 Radio-jet X-ray sources : system properties

Source	RA & Dec (J2000)	spectral class of companion	periodicities ('o' = orbital)	distance (kpc)
SS433	19 11 49.5 +04 58 58	OB	13 d (o) 164 d	8
Cyg X-3		WNL (?)	4.8 h (o)	8.5–12
LSI+61° 303	02 40 31.6 +61 13 41	Be	26.5 d (o) 4 yr	
Cir X-1	15 20 40.8 -57 10 00	MS	16.6 d (o)	≥ 6.5
GRS 1915+105	19 17 37 +11 03.6	Red giant ?		10 – 12.5
GRO 1655-40	16 55 -40.5	F or G	2.6 d (o)	3 – 6
1E 1740.7	17 44 02.6 -29 43 25	binary ?		8.5 (g.c.)
GRS 1758-58	18 01 12.2 -25 44 36	binary ?		8.5 (g.c.)
GT 2318+620	23 20 34.0 +62 17 33	lower MS		8

6.2 Observational properties

In this section I shall briefly review the observational properties of the class across the spectrum, from radio to X-ray. Observations in the γ-ray regime shall not be discussed here as, though several of the systems are claimed by various groups to be sources of high-energy γ-rays, the detections are often marrginal and not confirmed (similar to the situation for Cyg X-3). Cyg X-3 shall not be discussed in any detail, having already been covered very extensively in chapters 1-5.

6.2.1 Radio

I shall divide the discussion of the radio properties of the sources into two parts - initially I shall discuss the morphology of radio maps which reveal the jet structures, and subsequently I shall discuss the radio light curves of the sources.

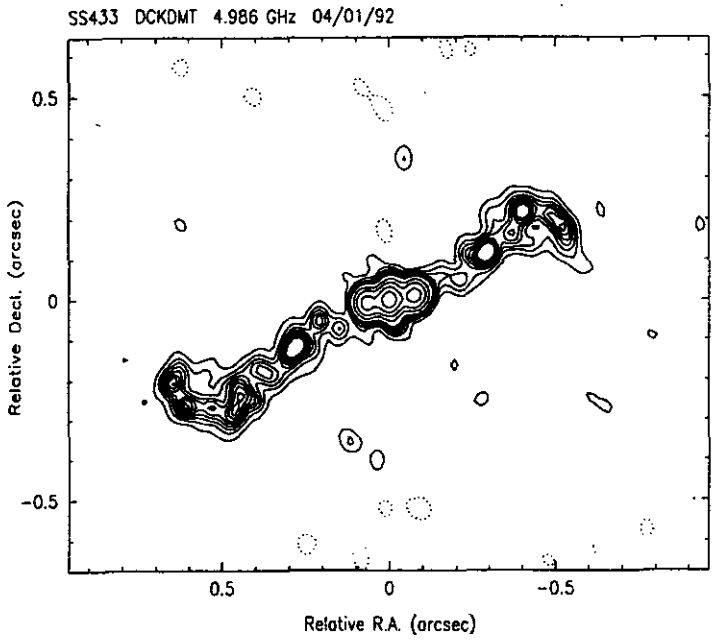

Figure 6.1 (a) SS433 : twin jets and 'corkscrew' structure mapped by MERLIN (Jowett 1995)

Radio imaging

The most irrefutable criterion for classing an object as a radio-jet source is the observation of collimated structure in radio maps. There is however a large variety in the quality of the mapped structure, and by no means all of the structures have shown any direct evidence of motion.

SS433, GRS 1915+105 and GRO 1655-40 undeniably have collimated radio structures along which blobs of radio-emitting material ('plasmons') travel at relativistic or near-relativistic velocities. In the case of SS433 the ejecta are seen to consistently travel at 0.26 c (eg. Vermeulen et al 1993a [129]), and high-resolution images reveal a 'corkscrew' pattern indicative of jet precession with a period of $\sim$ 164 days (eg. Jowett 1995 [130]). VLA observations of GRS 1915+105 reveal blobs to be moving away from the central source with a much greater velocity, 0.92 ± 0.08 c (Mirabel &

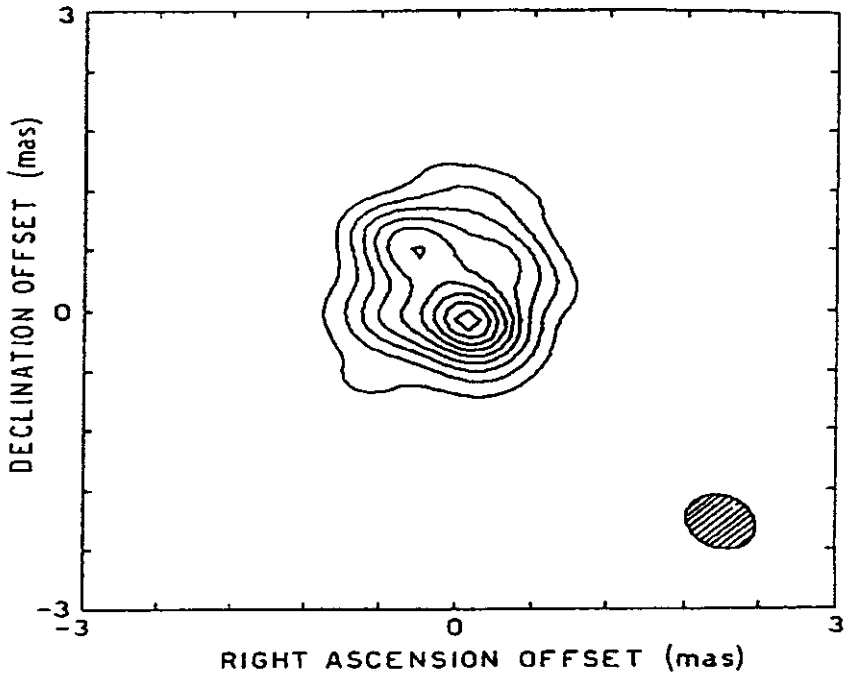

Figure 6.1 (b) LSI+61° 303 : an expanding radio source following radio outbursts (Massi et al 1993)

Rodriguez 1994 [120]). Similarly, apparent superluminal motions in GRO 1655-40 are interpreted as arising from true ejecta velocities of 0.92 ± 0.02 c in oppositively-directed precessing jets (Tingay et al 1995 [121]; Hjellming & Rupen 1995 [131]). Furthermore, the jets in SS433 are seen to be aligned with a larger structure in the surrounding supernova remnant W50 (e.g. Watson et al 1983 [132]).

LSI +61° 303, like Cyg X-3, has been seen to become an expanding radio source after radio flares (Massi et al 1993 [133]), though no individual knots of material have been resolved, making determination of an outflow velocity difficult. A preliminary interpretation by Massi et al (1993 [133]) finds the outflow velocity to be only 440 km s^{-1} (0.001c), ie. much slower than for the other systems for which outflow velocities have been estimated. However, further work is underway to clarify the situation (M. Peracaula, private communication).

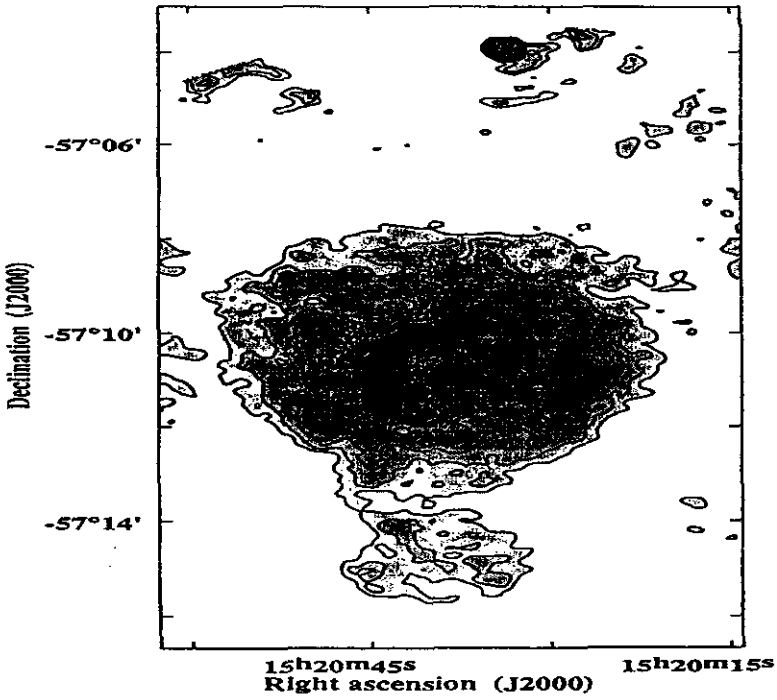

Figure 6.1 (c) Cir X-1 : large scale swept-back jets suggestive of a runaway radio-jet system (Stewart et al 1993)

The remaining sources, Cir X-1, 1E 1740.7-2942, GRS 1758-258 and GT 2318+620 have shown no evidence to date for evolution of their radio structures (see Tsutsumi 1994 [134] for details of an unsuccessful search for motion in radio maps of GT 2318+620). Cir X-1 appears to reside within a synchrotron nebula and maps made with the AT compact array appear to show swept-back radio jets originating in the central source (Stewart et al 1993 [135]). The two galactic centre sources, 1E 1740.7-2942 and GRS 1758-258, both show large ($\geq$ parsec) collimated structures roughly symmetric about their radio positions (Mirabel et al 1992 [122], Marti 1994 [112]). Finally GT 2318+620 also displays a well-collimated radio stucture symmetric about the radio location of the source (Taylor et al 1991 [136]).

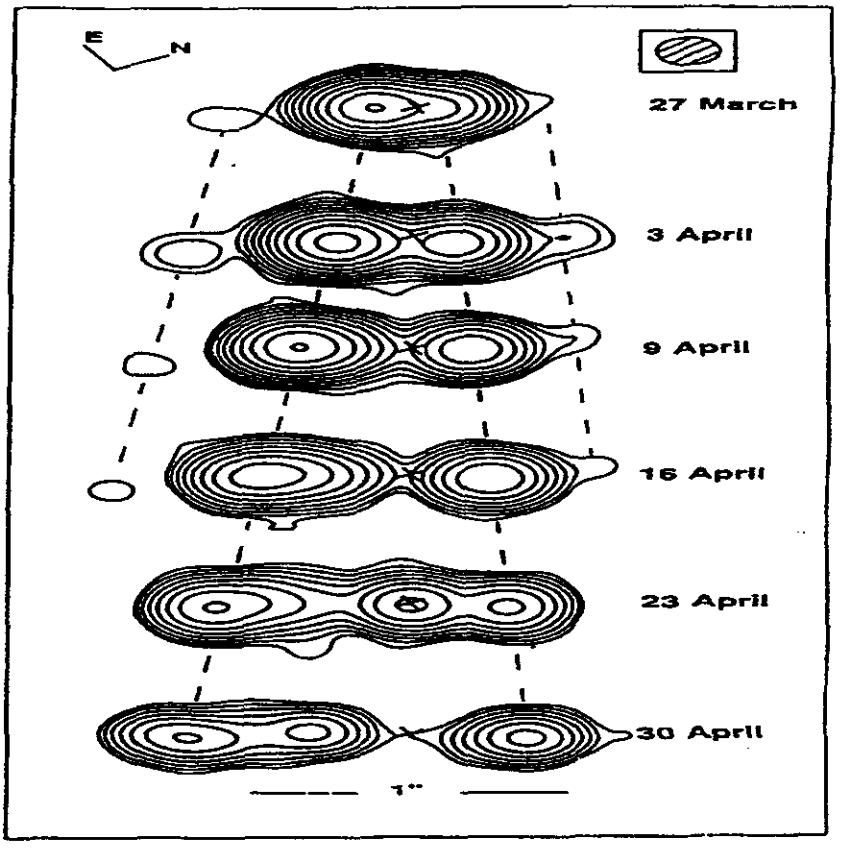

Figure 6.1 (d) GRS 1915+105 : apparent superluminal expansion following radio outburst mapped with the VLA (Mirabel & Rodriguez 1994)

Radio light curves

Like Cyg X-3, the sources SS433, GRS 1915+105 & GRO 1655-40 are observed to produce low-level variable radio emission punctuated by occasional (probably) aperiodic radio flares. Morphologically these radio flares appear very similar to those observed in Cyg X-3 with a very rapid rise to a level 20 – 100 times that of quiescence, followed by a slower subsequent decline, with an e-folding time of order a day. Martí (1993 [112]) makes a plasmon model fit to multifrequency coverage of a radio flare from SS433 in 1979 October, whereas he found a jet model more suitable for Cyg X-3. Detailed analy-

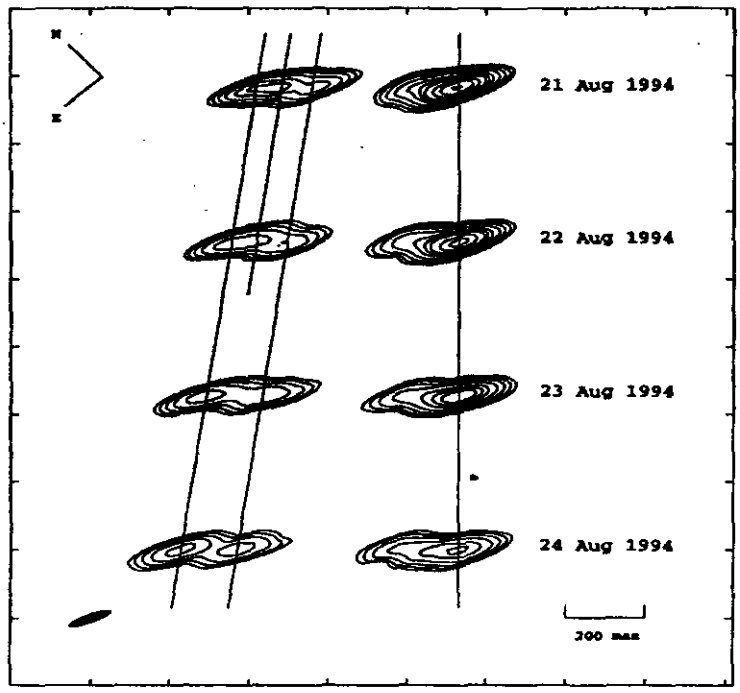

Figure 6.1 (e) GRO 1655-40 : more apparent superluminal expansion

sis of multifrequency observations of radio flares in the two 'superluminal' sources is yet to be done, but an initial analysis suggests decay times faster than those observed for Cyg X-3 & SS433.

The sources LSI+61° 303 and Cir X-1 are somewhat different in that the radio outbursts in these systems are found to be periodic, at 26.5 and 16.6 days respectively. This is interpreted as being due to a shock forming during periastron passage in an elliptical orbit, as a result of supercritical accretion rates (eg. Marti 1992 [49]). Cir X-1 has in fact declined significantly in radio (and infrared) brightness since about 1980 and at the present time only weak periodic flares are reported. In fact, no large flares (> 100 mJy) have been observed from this source for $\sim$ 10 yr (G. Nicholson, private communication).

GT 2318+620 has not been observed so far to undergo a radio outburst, though Gregory & Taylor (1986 [137]) have classified the source as a short

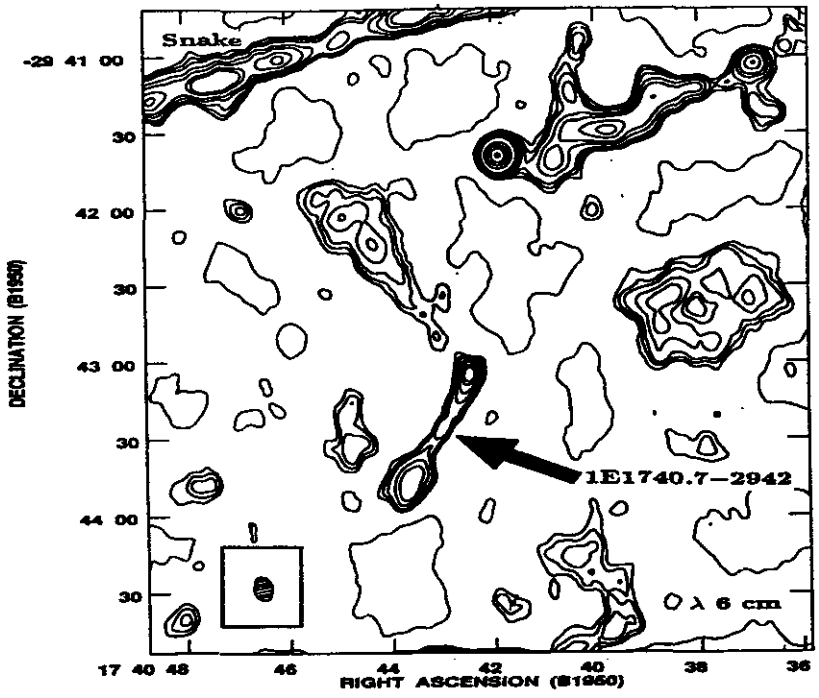

Figure 6.1 (f) 1E 1740.7 : large scale radio jets near the galactic centre (Mirabel et al 1992).

period variable. See section (6.3.2) for details of more recent monitoring of the system at Green Bank and Cambridge. A summary of the basic observable properties of the systems at cm & mm wavelengths is given in Table 6.2.

6.2.2 (Sub)millimetre

(Sub)millimetre observations of these sources have been (typically) rather sparse. Recent observations of SS433, LSI+61° 303, Cyg X-3 and GRS 1915+105 at centimetre to millimetre wavelengths by Tsutsumi, Perecaula & Taylor [53] however shed some light on this regime : they confirm the result of Fender et al 1995a [103] (ie. chapter 3) that Cyg X-3 is anomalously strong at millimetre wavelengths. They find in contrast that SS433 and LSI+61° 303 are optically thin out to millimetre wavelengths. For GRS

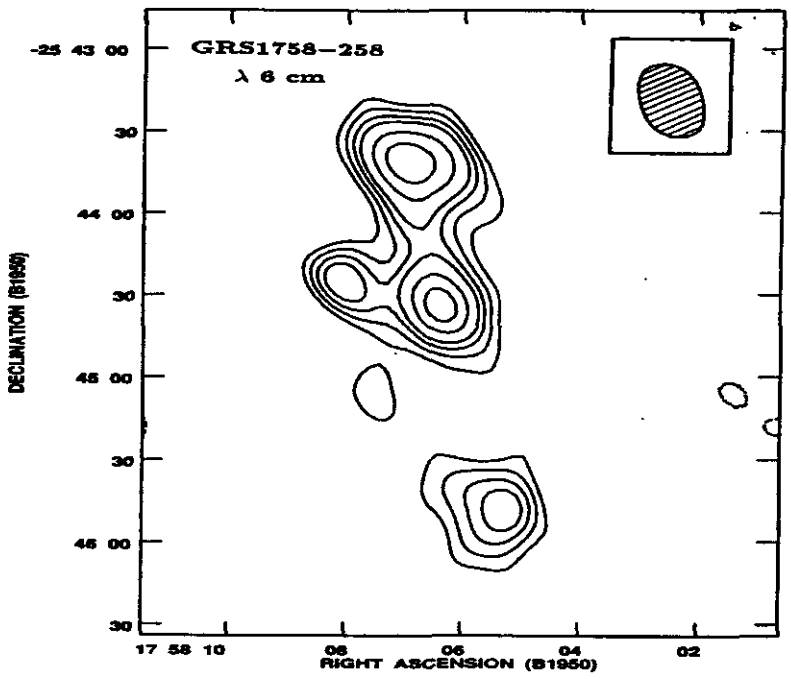

Figure 6.1 (g) GRS 1758-258 : A second radio-jet source in the vicinity of the galactic centre (Martí 1993).

1915+105 they could only place an upper limit on emission at these wavelengths. Earlier observations of SS433 at 3.3 mm (Band & Gordon 1989 [138]) also measured a flux density which was consistent with an extrapolation of an optically thin synchrotron spectrum from cm wavelengths. Millimetre observations towards the galactic centre source 1E1740.7-2942 suggest the source may be embedded in a dense molecular cloud (eg. Mirabel 1994 [125]), though there was no evidence for a similar cloud around GRS 1758-258. Nowhere in the literature could I find details of (sub)mm observations of Cir X-1. Observed flux densities of all the sources are summarised in Table 6.2.

So, Cyg X-3 appears unusual in having enhanced emission at millimetre wavelengths, possibly due to the opacity effects of the wind which may be denser than that in the other systems (though both O and Be stars also

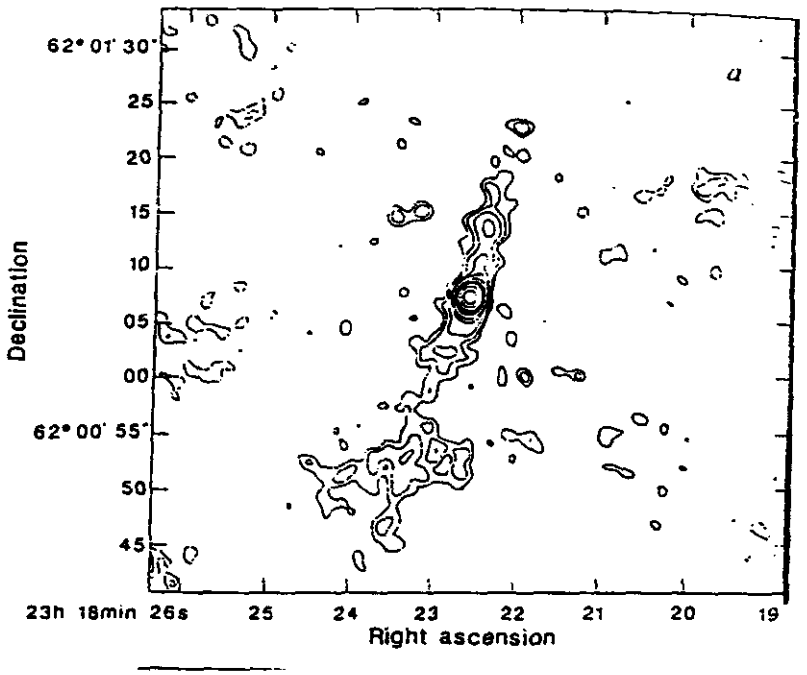

Figure 6.1 (h) GT 2318+620 : highly collimated structure in 20 cm VLA images (Taylor et al 1991)

posess a strong stellar wind - so why isn't the effect seen to some degree in SS433 and/or LSI +61° 303 ?). See section (6.3.1) for preliminary results of a search for anomalously strong mm emission in other radio-jet systems.

6.2.3 Infrared

Infrared observations of the objects in this class have proved to be invaluable diagnostics of the systems, particularly in view of the fact that most of the objects lie in or near to the galactic plane at a distance of several kpc or further and therefore tend to be heavily absorbed in the optical waveband.

SS433 lies behind several magnitudes of interstellar extinction, but is still luminous enough to be observed clearly as a bright optical object. Nevertheless, extensive infrared observations, both photometric and spectroscopic (eg. Thompson et al 1979 [139]; McAlary & McLaren 1980 [140]) have been

Table 6.2 Summary of Radio and (sub)mm observations of radio-jet XRBs

	F_{cm} quiescent/ brightest flare (Jy)	F_{mm} quiescent/ brightest flare (Jy)	comments
Cyg X-3	$\sim 0.05 / \geq 20$	$\sim 0.05 / \geq 3$	mm excess
SS433	$\sim 0.5 / \geq 20$	~ 0.1	cm – mm optically thin
LSI +61 ° 303	$\sim 0.03 / \geq 0.5$	~ 0.01	modulated at 26.5 d orbital period, cm – mm optically thin
Cir X-1	$< 0.1 / > 3.0$	–	modulated at 16.6 d orbital period, decline since 1970s
GRS 1915+105	$\sim 0.01 / \geq 1$	< 0.01	radio flaring correlated with X-ray activity
GRO 1655-40	$< 0.01 / \geq 7$	–	radio flaring correlated with X-ray activity
1E1740.7-2942	$(< 1 / 5) \times 10{-}3$	< 0.11 (see section 6.3.1)	
GRS1758-258	$(< 1 / 5) \times 10{-}3$	< 0.09 (see section 6.3.1)	
GT2318+620	~ 0.02 (see section 6.3.2)	< 0.11 (see section 6.3.1)	GT source

performed. Following photometry in the 1 – 3.5 μm region the source has been modelled as a hot (> 25 000 K) black-body plus a cooler (< 10 000 K) gas emitting free-free radiation, lying behind $\sim$ 8 mag of optical extinction. The 1 – 3 μm spectrum of SS433 shows strong stationary Brγ and HeI emission, plus blue- and red-shifted Pα emission which is associated with thermal emission from the jets (see Fig 6.2). IRAS observations of the SS433 region revealed infrared 'knots' which may be associated with the jets (see eg. Wang et al 1990 [141]).

Cir X-1 has been monitored in the infrared since at least 1976, with over 15 years' of observations at the SAAO (see eg. Glass 1994 [142]). Early observations are not totally reliable photometrically as the original optical source, found through Hα observations, has recently been observed to be a triplet of stars (Moneti 1992 [143]) – however, the proposed candidate is the dominant source and so previously observed trends are probably correct qualitatively. The source shows a single broad (3 – 4 day) infrared flare of amplitude $\geq$ 1 mag at JHK once per orbit at the time of radio phase zero.

Table 6.3 Summary of infrared observations of radio-jet XRBs

	$F_{2.2\mu m}$ quiescent/ brightest flare (mJy)	spectral features	comments
Cyg X-3	$\sim 12 / \geq 50$	He I, He II, N (Wolf-Rayet-like)	modulated at 4.8 h orbital period, rapid flares, no H in spectrum
SS433	> 50	H, He I (Paschen lines Doppler shifted)	variable source
LSI +61 ° 303	~ 400	–	modulated at 26.5 d *orbital period*
Cir X-1	~ 15	–	Large broad flare every orbital phase 0
GRS 1915+105	$\leq 1 / \geq 4$	H, He I (flaring) (see section 6.3.3)	> 1 mag variability at JHK
GRO 1655-40	–	–	
1E1740.7-2942	< 0.1	–	K> 17
GRS1758-258	< 0.1	–	K> 17
GT2318+620	–	–	

This flare, as well as activity at other phases, was much stronger before the decline in radio activity which began in about 1977.

LSI +61° 303 has undergone extensive infrared photometry, although there appears to be no published infrared spectroscopy of the source. Photometric observations of the source in the J, H & K bands have revealed the 26.5-day orbital period also observed in radio, optical and X-ray observations (e.g. Martí 1993 [112]). The inherent broad-band spectrum of the source shows an excess above a black-body, as expected for a Be star companion with a dense equatorially concentrated wind (Martí 1993 [112]) A search for rapid infrared variability from this source, which should have picked up Cyg X-3 - like infrared flares if they were occurring, was unsuccessful (Hunt. Massi & Zhekov 1994 [101])

A small number of imaging photometric observations of GRS 1915+105 (eg. Mirabel & Rodriguez 1994 [120]) have established that the source has a variable counterpart at J, H & K. Further observations are required however to establish the characteristics of the system and will be important in determining an orbital period. A K-band infrared spectrum obtained

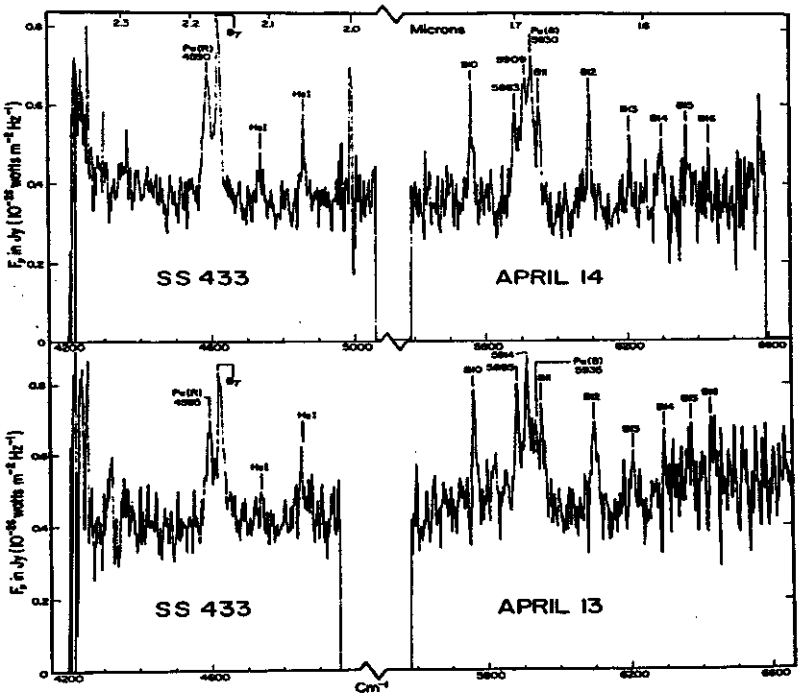

Figure 6.2 SS433 infrared spectra. Br γ and He I lines are stationary, while P α is blue- and red-shifted [indicated by (B) and (R)] and associated with jets (Thompson et al 1979)

shortly after a radio flare in 1995 April, though noisy, revealed HeI (2.058 μm) and Brγ emission features (see section 6.3.3). There are to date no published infrared observations of the second superluminal source, GRO 1655-40 (due primarily to it being an easily observable optical object).

The two galactic centre sources, 1E1740.7-2942 & GRS1758-258. have revealed no K-band infrared counterpart to a limiting magnitude of $\sim$ 17. This may not be surprising in the case of 1E1740.7-2942 which Mirabel (1994 [125]) suggests lies within a dense molecular cloud, behind up to 50 mag of optical extinction (though it is noted that a massive OB companion such as those in HMXRB systems would have created an HII region which is not observed). However, in the case of GRS 1758-258 the lack of an infrared counterpart would appear to limit any companion to the (presumed) accreting object to spectral type A or later (see eg. Chen, Gehrels & Leventhal

1994 [126]).

To date there have been no published infrared observations of GT 2318+620.

6.2.4 Optical and UV

The sources Cyg X-3, GRS 1915+105, 1E 1740.7, GRS 1758-58 are all invisible in the optical regime, hence the importance of infrared observations of these sources. Worse still, the large distances of all of the sources precludes any observations in the UV regime.

SS433 is the most widely-studied of the class in the optical regime, and its inclusion in the Stephenson–Sanduleak 'SS' catalogue immediately implies strong Hα emission. All spectral features from the source are classified as either 'moving' (ie. Doppler-shifted and originating in the ejecta) or 'stationary' (ie. not Doppler-shifted and presumably originating from the companion star to the compact object and/or some circumstellar material/accretion disc). The moving emission lines are exclusively broad H or HeI and are typically 30% of the strength of the analagous unshifted component. The maximum Doppler shifts indicate velocities of 0.26 c, in perfect agreement with radio mapping observations. The stationary lines show strong H emission, plus features of HeI, HeII, C, N & Fe. The underlying spectral features of the companion star are hard to disentangle, particularly in view of the almost total lack of absorption features, but may be reminiscent of a massive Wolf-Rayet star (though one with still a large quantity of Hydrogen, unlike Cyg X-3). Optical photometry reveals both the 13 day orbital and $\sim$ 164 day precession periods as well as irregular fluctuations on timescales of hours and longer. No very rapid (ie. $\leq$ 1 s) fluctuations have been observed however. See eg. Margon (1984 [144]) and Vermeulen et al (1993b [145]) for more details and further references.

LSI +61° 303 has a well-studied optical spectrum. The source has absorption features typical of a B type star of luminosity class V (I. A. Steele, private communication), superimposed upon which are emission features characterising the companion star as a Be object with an extended circumstellar disc. Hα & Hβ emission are of 'shell' type, and while there is no clear

emission at Hγ there may be some infilling of the absorption feature. Fits to optical photometry are consistent with the Be classification, being well fit for $T_{eff} = 30\ 000$ K and $\log g = 4$.

Cir X-1 was, as discussed in the previous section, identified with a cluster of *three* stars within 2 arcsec of each other. The likely counterpart to Cir X-1 has now been determined (Moneti 1992 [143]) but little if any spectroscopic work has been carried out since then. Earlier optical studies of the triplet of stars revealed strong Hα emission (Nicholson, Feast & Glass 1980 [146]) indicative of circumstellar material, interpreted as an accretion disc.

The optical counterpart to GRO 1655-40 (Bailyn et al 1995a [147]) was actually discovered about two weeks *before* the SHEVE radio observations which observed the apparent superluminal motion, shortly after GRO observatio ns of the source as an X-ray transient. The source shows strong Hα emission, and on one night was seen to undego a sharp decline and recovery which was provisionally interpreted as an eclipse. Subsequent optical observations (Bailyn et al 1995b [148]) of Doppler-shifted emission lines confirmed a 2.6 d orbital period. Analysis of the radial velocities strongly suggests that the mass of the compact object is in excess of 4 $M_\odot$, ie. GRO 1655-40 is strong black-hole candidate.

A single optical spectrum of GT 2318+620 reveals it to posess no obvious spectral features and a very steep red spectrum, reminsicent of a BL Lac object (Tsutsumi 1994 [134]).

Fig 6.3 compares the optical spectra of SS433, LSI+61° 303 and GRO 1655-40, which all overlap in the region of Hβ.

6.2.5 X-ray

All the radio-jet X-ray binaries are bright & variable X-ray sources. Like Cyg X-3, the systems Cir X-1, GRS 1915+105, GRO 1655-40 are amongst the brightest of galactic X-ray sources, with luminosities typically of the order of the Eddington limit for a 1 $M_\odot$ object ($\sim 10^{38}$ erg s^{-1}) when in high state. Cir X-1 shows rapid variability and moves in the X-ray 'colour-colour' diagram in a manner indicative of an 'Atoll' source, though showing some

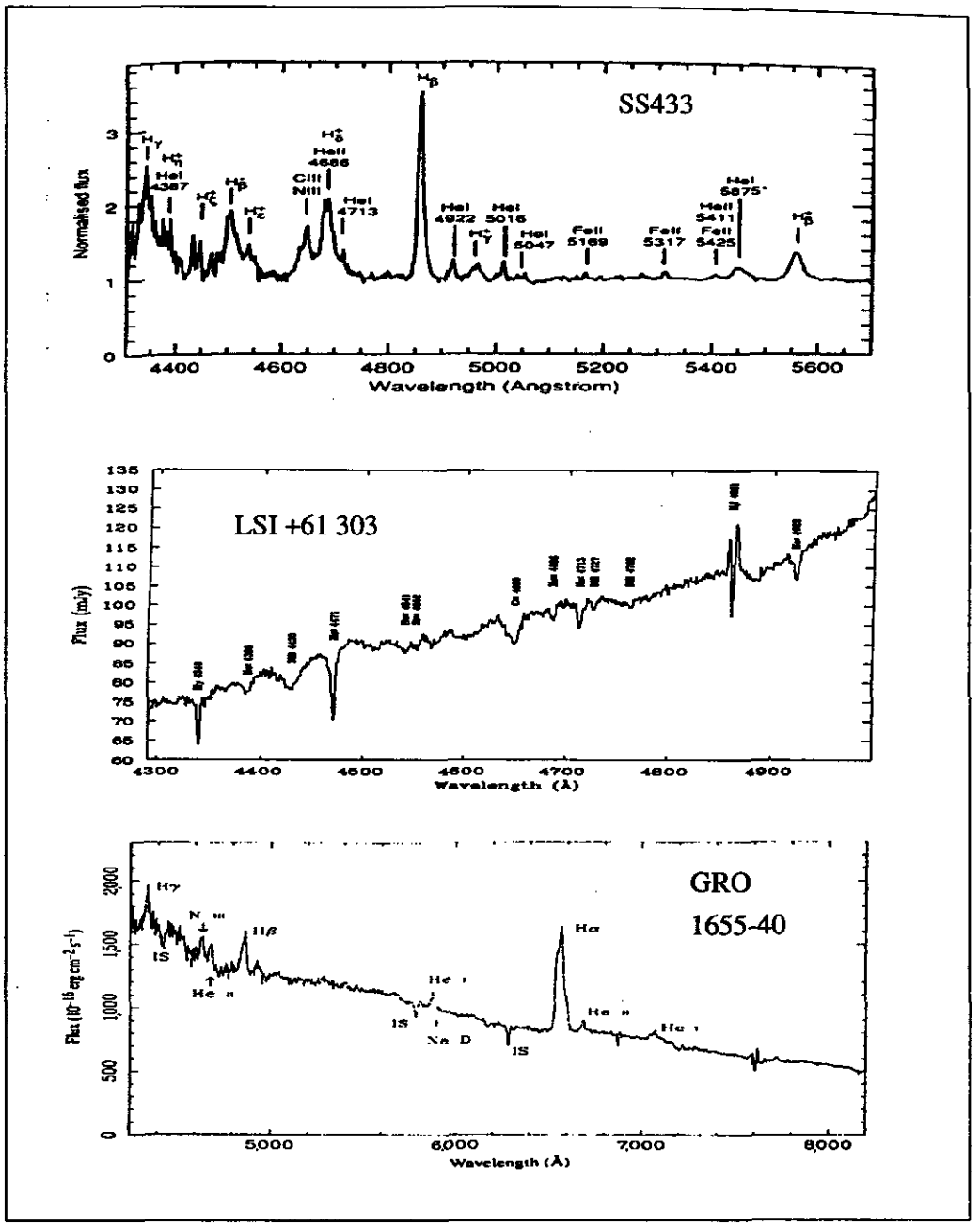

Figure 6.3 A comparison of the optical spectra of the three radio-jet sources for which good spectra have been obtained. Spectra also exist for Cir X-1 (Hα emission) and GT 2318+620 (featureless) but are of fairly low S/N. Note that SS433 and GRO 1655-40 show considerably more emission than LSI+61° 303.

Table 6.4 Summary of optical properties of radio-jet XRBs

	V mag quiescent/ flaring	spectral features	comments
Cyg X-3	> 24	–	R=23.8
SS433	14.2	H, He, C, N, Fe	Strong Hα, Doppler shifted H & He
LSI +61 ° 303	10.7	H, He, Si	'Shell' Hα & Hβ
Cir X-1	20.6	Hα	possible previous source confusion
GRS 1915+105	–	–	R > 21
GRO 1655-40	≥ 17 / ≤ 14	H, He I, He II, N III	
1E1740.7-2942	–	–	I > 21
GRS1758-258	–	–	I > 21
GT2318+620	~ 20	apparently featureless	spectrum very steep

discrepancies from 'normal' behaviour which are attributed to it being the only LMXB in which a low-magnetic field neutron star is accreting near to the Eddington limit (Oosterbrook et al 1995 [149]). Type I X-ray bursts and QPOs have been observed from Cir X-1, also indicating that the compact object is probably a neutron star.

GRS 1915+105 & GRO 1655-40 were discovered by the *Granat* and GRO satellites respectively because of their transient X-ray behaviour. The sources have both, since their discovery, remained bright in X-rays with strongly variable behaviour which is characterised by irregular outbursts and is correlated with radio flux measurements — although in GRO 1655-40, hard X-ray (20 – 400 keV) bursts tend to precede radio flares by a period varying from a few days to two weeks (Harmon et al 1995). Both sources have hard X-ray tails similar to that observed in the black-hole candidate Cyg X-1 and most hard X-ray transients (see eg. Ballet et al 1994 [150] and Churazov et al 1994 [151] for discussions of hard X-ray tails from galactic sources). Recent observations of material along the line of sight to GRS 1915+105 have resulted in an increased estimate of the column density which implies that the system is the most luminous X-ray source in the galaxy, with $L_X \sim 10^{39}$ erg s^{-1} (Chaty et al in prep). ROSAT imaging observations of GRO 1655-40

Table 6.5 Summary of X-ray properties of radio-jet XRBs

	X-ray luminosity in low/high states (erg s^{-1})	spectral features	comments
Cyg X-3	$10^{37}/10^{38}$	Fe, Si, Ne	High-and-soft & Low-and-hard states, Modulated at 4.8 h orbital period
SS433	$10^{35}/10^{3}6$	Fe	X-ray jets
LSI +61 ° 303	$10^{35}/10^{36}$		X-ray bursts preceding radio flares at 26.5 d orbital period
Cir X-1	$10^{37}/10^{38}$		Type I bursts, QPOs, 'Atoll' LMXRB source
GRS 1915+105	$10^{37}/ > 10^{38}$		X-ray outbursts correlate with radio, hard tail
GRO 1655-40	$10^{38}/10^{39}$	no strong features	X-ray outbursts precede radio flares, hard tail
1E1740.7-2942	$\geq 10^{36}$	511 keV line ?	bright in hard X-rays
GRS1758-258	$\geq 10^{36}$		bright in hard X-rays
GT2318+620	$< 10^{36}$		possible UHURU source

indicate the source is surrounded by a scattering halo (Greiner, Predehl & Pohl 1995 [152]), while ASCA observations of the source (Inoue 1995 [153]) revealed no obvious spectral features.

SS433 is a weaker source, with a mean luminosity of order 10^{35} erg s^{-1}. The source displays a strong broad blend of Fe emission lines around 6.8 keV (eg. Margon 1984 [144]). Imaging by the *Einstein* satellite first revealed perhaps the most fascinating aspect of the X-ray properties of SS433 – some $\sim$ 10 % of the X-ray emission from the source orginates in extended jet-like structures which are aligned with structure in the surrounding supernova remnant W50 (Watson et al 1983 [132]). This observation would appear to confirm the XRB – SNR connection for the source, and also places a lower lifetime limit on the jet phenomenon of several thousand years.

LSI +61° 303 is, like SS433, one of the weaker X-ray sources, with a

similar mean flux level of order 10^{35} erg s^{-1}. The source undergoes X-ray outbursts at the 26.5 day orbital period, which tend to lead the radio flares by a couple of days.

The galactic centre sources, 1E 1740.7-2942 & GRS 1758-258, are relatively modest emitters at soft and medium X-ray energies (ie. $\leq$ 10 keV) but become stronger at higher energies, dominating the galactic centre region at energies > 35 keV (see eg. Churazov et al 1994 [151]). 1E1740.7-2942 is in fact the hardest X-ray source within 1° of the galactic centre, and its 2-500 keV spectrum is very similar to that of the black-hole candidat e system Cyg X-1 (Churazov et al 1994 [151]). There is some evidence for 511 keV e^-e^+ emission from the direction of 1E 1740.7-2942, hence the popular name of 'the great annihilator'. 1E 1740.7-2942 is observed to be strongly variable, by at least a factor of 10 on a timescale of months and years. GRS 1758-258 is also observed to be a highly variable source, undergoing episodic X-ray outbursts.

The possible association between the 'variable' radio source GT 2318+620 and an UHURU X-ray source is one of the strongest pieces of evidence for the XRB nature of the system. However, recent ROSAT observations (T. Tsutsumi, private communication) failed to detect a source at the well-defined radio position.

6.3 New observations

In this section I present some new observations of the radio-jet X-ray binaries along with some preliminary interpretation. A search for anomalously strong mm emission (by analogy with Cyg X-3) from four radio-jet sources was performed with the JCMT but unfortunately was only able to obtain upper limits. The latest data from an ongoing program to monitor GT2318+620 at Green Bank is presented. Radio monitoring at Green Bank and the Ryle Telescope of GRS 1915+105 (including radio flare events) is also presented, along with an infrared spectrum of the source obtained shortly after one radio flare. These observations are compared directly with

Table 6.6 Survey of mm emission from radio jet X-ray sources

Source	Date (JD)	2 mm upper limit (3σ)
GT 2318+620	2449620	$\leq$ 110 mJy
1E 1740.7-2942	2449620	$\leq$ 110 mJy
GRS 1758-258	2449620	$\leq$ 90 mJy
LSI +61° 303	2449621	$\leq$ 100 mJy

the equivalent phenomena in the Cyg X-3 system and differences and similarties highlighted.

6.3.1 A search for anomalously strong mm emission from four radio-jet X-ray sources

After discovering the anomalously strong millimetre emission from Cyg X-3 it was felt worthwhile to look for a similar mm 'excess' in other radio-jet X-ray binaries. The sources chosen for this preliminary search were GT 2318+620, LSI +61° 303, GRS 1758-258 and 1E 1740.7-2942 . The sources were observed on the nights of JD 2449620-1 using the JCMT in service mode. The UKT14 detector was again used, with the 2.0 mm filter.

No detections were made of any of the sources, and 3σ upper limits are tabulated in table 6.6 below.

It should be noted that the observations of LSI +61 ° 303 took place at around orbital radio minimum. Subsequent observations by Tsutsumi et al [53] have shown the radio spectra of both LSI +61° 303 and SS433 to be optically thin through the millimetre regime.

Comparison with Cyg X-3

The distance to the galactic centre sources GRS 1758-258 and 1E 1740.7-2942 ($\sim$ 10 kpc) is comparable to that to Cyg X-3. A detection of Cyg X-3 given the sensitivity obtained and a 2.0 mm flux at the level reported in chapter 2 would have been marginal. The non-detection of these sources therefore simply implies that their mm emission cannot be much *stronger*

than that of Cyg X-3. Given that they are far weaker sources at cm wavelengths, this result is unsurprising.

The non-detection of LSI +61° 303 was, as described above, slightly unfortunate. Subsequent observations have shown that the source does not have a mm excess, being optically thin throughout the cm – mm regime.

The non-detection of GT 2318+620 is consistent with the source having an optically thin synchtrotron spectrum from cm – mm wavelengths. Given that the source is $\sim \frac{1}{2}$ the distance of Cyg X-3 (if the 21 cm measurements of Taylor et al 1991 [136] were interpreted correctly), this source is less than $\sim \frac{1}{4}$ the luminosity of Cyg X-3 in the mm regime.

6.3.2 Radio monitoring of GT 2318+620

The Green Bank monitoring program is described in detail in chapter 4 and in Waltman et al (1994 [21]). In early 1995 I proposed that the candidate radio-jet XRB GT2318+620 be added to the monitoring program and this was accepted, since which time the source has been monitored on average once daily at 13.3 & 3.6 cm. This data set is plotted in Fig 6.4. The mean flux levels at 13.3 & 3.6 cm are consistent with GT 2318+620 having an optically thin synchrotron spectrum of spectral index ~ -0.5.

High time-resolution ($\sim$ 5 min) observations were also performed on a number of occasions in 1995 at the Ryle Telescope at 2.0 cm. These observations showed no evidence for source variability.

Comparison with Cyg X-3

Over the $\sim$ 200 day of monitoring the source has shown no strong variability. This is in contrast both with the variability reported in the initial GT survey (Gregory & Taylor 1983 [137]) and with the other radio-jet XRBs which show both long-term and flaring behaviour. Cyg X-3 has never been observed to spend such a long period without even some low-level flaring. The identification of GT2318+620 as a radio-jet binary remains uncertain.

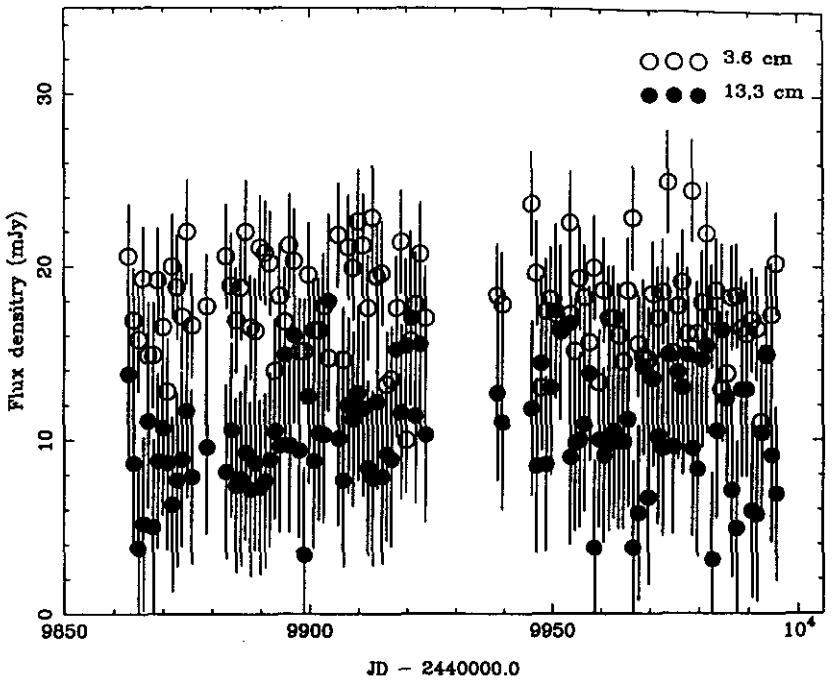

Figure 6.4 Daily radio monitoring of the candidate radio-jet XRB GT2318+620 at Green Bank.

6.3.3 Radio and infrared observations of GRS 1915+105

Here I present some radio monitoring of GRS 1915+105 obtained at Green Bank, during which period a low-amplitude (100 mJy) rapid radio flare event was observed to occur. Immediately this flare was observed, a request was made to UKIRT for target-of-opportunity observations and a short-exposure K-band infrared spectrum was obtained during the decay phase of the flare. This again illustrates the value of daily monitoring projects such as those at Green Bank.

GRS 1915+105 is monitored daily at Green Bank at 13.3 & 3.6 cm, as is Cyg X-3. The observation procedure is similar to that described in chapter 4. The source is fainter than Cyg X-3, with a typical 'quiescent' flux density of $\leq$ 10 mJy at cm wavelengths. The source is seen to undergo radio outbursts in a similar fashion however. Fig 6.5 plots a period of the Green Bank monitoring obtained in early 1995 showing a rapid rise-time

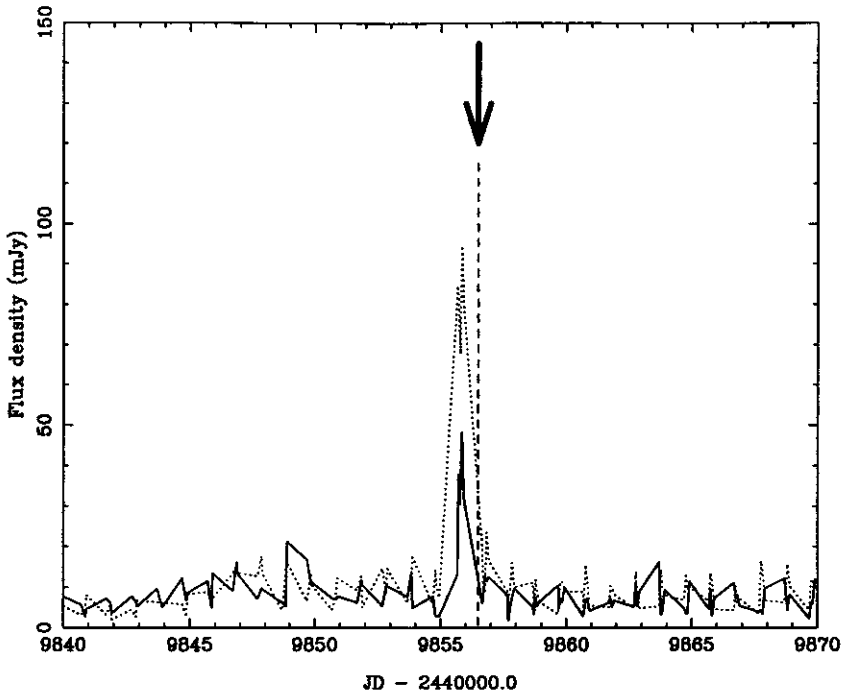

Figure 6.5 Daily radio monitoring of GRS 1915+105 at Green Bank, indicating the date on which the infrared spectrum was obtained.

flare event.

Shortly after this event, in 1995 May, we managed to obtain a K-band infrared spectrum at UKIRT. This was a short-exposure (total integration time 5 min) observation obtained with the CGS4 instrument. The spectrum was standardised on BS7167, assumed to have a K magnitude of 5.35 and temperature of 7200 K. The Br γ feature was removed from the standard before ratioing. Though the spectrum is noisy, due both to the short exposure time and faintness of the source, a couple of emission features stand out. Hydrogen Br γ at 2.17 μm is obvious, as is a He I feature at 2.06 μm. The observer (Tom Geballe, private communication) is confident of the reality of these features. The noisy data at the long and short-wavelength extremes of the spectrum have been removed.

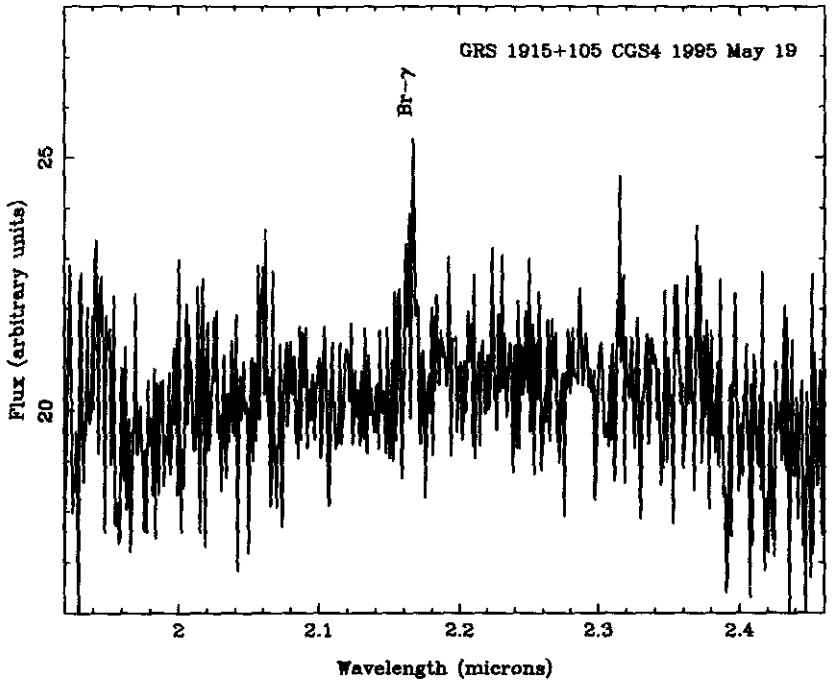

Figure 6.6 CGS4 K-band infrared spectrum of GRS 1915+105, obtained shortly after a small radio flare which peaked < 2 days earlier. Br γ is clearly visible at 2.17 μm as is a He I line at 2.06 μm. The IR spectrum is clearly different from that of Cyg X-3 (see chapter 1).

Comparison with Cyg X-3

The radio flux history of GRS 1915+105 is clearly similar to that of Cyg X-3, ie. periods of relative quiescence interspersed with large flare events. Unfortunately the flux density from GRS 1915+105 is too low for a search for quenched emission prior to a flare to be significant, at least with the Green Bank telescopes.

The infrared spectrum of GRS 1915+105 is also clearly different from that of Cyg X-3. Gone are the broad Wolf-Rayet He emission lines, and instead there is a strong Hydrogen line. This effectively rules out GRS 1915+105 being a hydrogen-free W-R + c object as has been proposed for Cyg X-3. A preliminary interpretation of the JHK colours of GRS 1915+105 has led to the suggestion that the companion to the compact object is a

red giant. Such a companion would not be expected to show these strong emission features and so the question is 'where are they produced' ? Some possibilities are that they originate in a strong wind from the system, that they originate in an accretion disc, or that they are associated with the jets (cf. SS433). The latter interpretation can be tested by obtaining a good infrared spectrum during a period of radio quiescence. This should show relatively weaker emission features than the spectrum we obtained shortly after a radio outburst. Note also that emission features originating in the ejecta would be expected to be strongly redshifted (both approaching and receding jets due to the highly relativistic velocities).

Despite the fact that the Br γ line illustrates a clear difference between the natures of the objects in GRS 1915+105 and Cyg X-3, it is worthwhile noting that the He I 2.06 μm line observed here is also observed in Cyg X-3 to be highly variable. The strength of this line may be a good indicator of the level of outflow activity in both sources.

6.4 Conclusions

This chapter has provided both an overview of the small 'class' of suspected X-ray binaries with radio jets, and made critical comparisons between Cygnus X-3 and its 'classmates'. There is clearly a problem in referring to this set of sources as a class because of their diverse nature; furthermore, most of the sources are to a greater or lesser extent unique or are very exotic examples of some other class. Similarities between the sources are hard to find — by definition all must have radio and X-ray emission, beyond this they do not appear to have one other single feature in common. The radio luminosities vary by more than a factor of 100, the infrared and optical spectral properties indicate a wide variety of companions to the (presumed) accreting compact objects, and the X-ray properties are again widely divergent.

Possibly the nearest things to 'classes' within this selection are the twin 'superluminal' sources GRS 1915+105 & GRO 1655-40, and the two galactic

hard X-ray sources 1E 1740.7-2942 & GRS 1758-258. The 'superluminal' sources display extremely similar ejecta velocities and similar radio flux & X-ray behaviour. Heavy extinction precludes the a comparison of an optical spectrum of GRS 1915+105 with its twin, but infrared spectra of both are obtainable and it would be an interesting exercise to compare them. The red optical and infrared may well be the most fruitful areas to perform spectroscopy of the ejecta, which in these sources will be heavily redshifted ($z > 2$ for the receding jet – see eg. Mirabel & Rodriguez 1994 [120]).

The two galactic centre sources also posess similar observational characteristics, both having dominant emission at hard X-rays, parsec-scale radio structure, similar radio light curves and a similar lack of infrared or optical counterparts. However, there ae differences — only 1E 1740.7-2942 has claimed detections of 511 kev annihilation radiation associated with it, and this source appears to reside within a giant molecular cloud and may be accreting from the ISM. GS 1758-258 does not appear to be in such a situation, and the relation between the sources does not appear to be as strong as for the superluminal twins.

The nature of the source GT 2318+620 remains in doubt. The lack of an X-ray detection by ROSAT (T. Tsutsumi, private communication) does not bode well for an identification as an XRB. However, the 21 cm line profiles toward the source indicating a galactic distance to the source are fairly convincing (Taylor et al 1991, [136]). Unfortunately, over 150 days of monitoring at Green Bank, plus some sporadic observations at Cambridge do not show more than marginal evidence for strong variability. *All* the other sources with no discernible motion in radio maps, *do* show radio outburst behaviour — GT 2318+620 displays neither. However, given that some of the brightest galactic radio sources being observed at present are transients which were apparenly 'off' in the not-too-distant past, this source may well be such a system undergoing a quiescent phase. Unfortunately the featureless optical spectrum is not promising either, and there must remain a strong possibility that the source is a background radio galaxy, possibly a BL Lac object.

The most similar source to Cyg X-3, in terms of companion star type and jet velocity, would appear to be SS433. However, there are clear differences – Cyg X-3 has an orbital period 80 times shorter than SS433, shows no evidence for Hydrogen while SS433 shows prominent H emission, and Cyg X-3 is typically more than a factor of 10 more luminous in X-rays than SS433. It may be that these points can be explained by an evolutionary scenario in which Cyg X-3 is at a later stage of evolution than SS433 — perhaps the compact object in SS433 will spiral in toward its companion, brightening in X-rays and dispelling the remaining hydrogen envelope as it does so. Unfortunately the orbital period in SS433 is *not* seen to be decreasing, which may indicate that sufficient angular momentum is being lost through the quasi-continuous jet action to prevent spiral-in. It may be that in the Cyg X-3 system the balance tipped slightly too far and spiral-in was unstoppable.

It seems that, given the diversity of the class, it is probably more suitable to describe radio jets as a phenomena, like QPOs, optical flickering etc. Given the small number of observations required to discover the radio jets associated with the two superluminal sources, we can be sure that more such sources will be discovered — certainly other X-ray transients eg. GRO J0422+322 are known to undergo radio outbursts during X-ray activity, and the likelihood must be that mass ejection is taking place in these systems. Despite no clear models of how jets are formed, they nevertheless associate fairly naturally with axisymmetric systems, of which XRBs are very strong examples.

Summary of thesis and ideas for future work

This thesis has attempted to make the most of combined observations in different energy regimes in order to understand the exotic radio-emitting X-ray binary Cygnus X-3, and to place it in context by comparison with 'related' objects. The chapters do not neatly restrict themselves to one wavelength regime each, being instead each a summary of some observing period. However, below I shall attempt to describe the advances in our knowledge and understanding of Cyg X-3 provided by this thesis as a whole, from radio to hard X-rays.

Nearly all the observations reported here were simultaneous with radio monitoring, primarily as Green Bank, but also at Cambridge. It is clear both from previous work and that presented here that the radio brightness of Cyg X-3 is a clear indicator of its state of activity and thus this radio monitoring was invaluable in establishing the backdrop against which other observations at higher energies were performed.

As well as being a backdrop for higher-energy observations, the radio emission was itself studied in detail, in chapters 3 and (primarily) in chapter 4. It was found that the low-level 'quiescent' emission at cm wavelengths, characterised by flux densities of $\sim$ 50 mJy and a relatively flat spectrum, can be well modelled by quasi-continuous injections of relativistic electrons into the base of the radio jet. This model developed from the discovery of anomalously strong emission at millimetre wavelengths and invokes a dense, absorbing stellar wind (for which there is evidence in other wavelength regimes) which is optically thin to centimetre-wavelength emission at the point of injection, but becomes transparent after the ejecta have travelled a certain distance out in the wind. This work invoked different decay times for the synchrotron emission at different wavelengths, the beginning of an investigation into radiation losses in the Cyg X-3 jet.

Intense radio observations during a period of radio flaring in 1994 Feb – March allowed further study of the radio emission and decay processes and confirmed that radiation losses were important, contrary to previous models which had considered adiabatic losses (which are wavelength-independent)

to be dominant. It was found that inverse Compton losses from a luminous companion were most likely, though Synchrotron losses in a high magnetic field ($>$ 1 Gauss) jet could also be responsible. It was also found during this period that the radio jets evolved from high opacity immediately after a period of pre-flare 'quenching' (of which ours was the first independent confirmation) to an optically thin state after $\sim$ 30 days of flaring. This is probably due to varying local opacity in the form of a varying mass-loss rate from the companion star.

Cyg X-3 has proved to be a highly variable infrared object, as described in chapters 2 & 4. The system consistently displays the 4.8 hr (presumed) orbital period, superimposed upon which may be both very rapid ($\leq$ 15 sec rise/decay times) flare events and slower, larger, changes in brightness. The flare events may be associated with the jets and the larger changes with a varying mass-loss rate (for which indepent evidence exists in the radio data discussed above). Both simultaneous H & K-band observations in 1984 and quasi-simultaneous observations across four bands in 1994 suggest that the flaring component has a flat spectrum and is probably optically thin free-free emission from a plasma with a temperature (at least for the rapid, and therefore size-constrained flares) in excess of 10^6 K. While clear correlated activity on short timescales has proved elusive, there is some good preliminary evidence for correlared infrared : radio behvaiour on longer (days – weeks) timescales. This may be related to increased mass-loss which causes infrared brightening and subsequent radio flaring (as described in scenario B in chapter 4). A deeper orbital modulation in 1984 data compared to that obtained in 1994 tanatlisingly suggests an evolution of the light curve shape, but further study is required to confirm this. Deep imaging in the infrared has revealed new objects, almost all of which are highly reddened, very close in the sky to Cyg X-3. While most of these objects will probably turn out to be stellar, deeper follow-up imaging is required to investigate more exotic possibilities.

Work at higher energies has also been valuable, including the first ever quasi-simultaneous infrared : hard X-ray observations of the source. These

confirmed that the orbital modulation at both energies is in phase, allowing the combination of hard and soft X-ray data (the latter being already known to be in phase with the infrared) in the derivation of a new cubic ephemeris for the system.

Comparison of Cyg X-3 with other candidate 'radio-jet' sources has shown that the radio-jet phenomenon is not as rare as imagined a few years ago, but that the type of objects which display it may be very diffferent. Many of the radio-emitting X-ray binaries are extremely different to Cyg X-3, and only SS433 bears more than a passing resemblance. What the sources have in common that is causing the radio jets remains unclear.

Future work on Cyg X-3 could expand upon that presented in this thesis in nearly all aspects, simply by applying improved instruments to the problem. However, I see a few areas as important above the others : High time resoltion, high signal-to-noise (sub)millimetre observations (with SCUBA ?) will allow us to probe deeper than ever before into the radio jet and to see on what kind of timescales the injection of relativistic particles is varying on; infrared spectro-polarimetry should allow both determination of any anistropy in the stellar wind, and a possible polarised component from an accretion disc; and ultra-high resolution radio VLBI (VSOP ?) is required to map the movement of individual knots in the radio jets in order to investigate their dynamics and the structure of the jet.

Appendix A

Loss mechanisms in Cyg X-3 jet

In the following, dE/dt represents the rate of energy loss from an electron of energy E. This can have many forms; here we consider adiabatic expansion losses, synchrotron losses and inverse Compton losses. These are believed to be the dominant energy loss mechanisms in the environment of a galactic radio jet. Synchrotron and inverse Compton losses differ from adiabatic expansion losses in that they change the form of the emitted spectrum, due to higher energy electrons having shorter lifetimes. This in turn causes steeping of the observed spectrum at high frequencies.

The formulation presented here follows MPE92 [49] and Leahy (1991) [109].

Adiabatic expansion losses

$$(dE/dt)_{adi} = -\alpha \frac{v(t)}{r(t)} E \tag{A.1}$$

where α is a constant depending on geometry : 1 for a sphere, 2/3 for a jet. The variables v(t) & r(t) represent the expansion velocity and radius of the emitting region respectively.

Synchrotron losses

$$(dE/dt)_{synch} = -a_s B(t)^2 E^2 \tag{A.2}$$

where a_s is a constant whose value in c.g.s. units is 2.37×10^{-3}, and B is the average value of the magnetic field component perpendicular to the particle velocity.

Inverse Compton losses

$$(dE/dt)_{IC} = -a_c U_R(t) E^2 \tag{A.3}$$

where a_c is a constant whose value in c.g.s. units is 3.97×10^{-2}, and U_R is the radiation energy density local to the ejecta.

In order to calculate the relative contributions of adiabatic expansion, synchrotron and inverse Compton losses it is necessary to calculate (i) the time evolution of the ratio v(t)/r(t), (ii) the time evolution of the magnetic field, and (iii) the time evolution of the local radiation field (provided primarily by the massive companion star). These calculations are strongly dependent on the geometry adopted for the system.

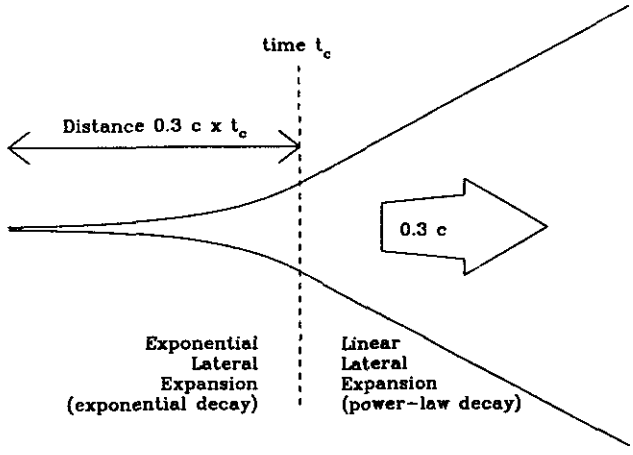

Figure A.1 Geometry of jets as in MPE92. From time of injection until a time t_c jet lateral expansion is exponential, with time constant t_e, which causes an exponential decay of the observed synchrotron flux density. Subsequently, lateral expansion is linear with time, producing an observed power-law decay.

Adopting the jet geometry and lateral expansion model of MPE92 [49], which is summarised in Fig A.1, I use the following expressions :

Jet lateral expansion velocity and radius

$$v(t) = \begin{cases} v_0 e^{t/t_e} & \text{for } t < t_c \\ v_0 e^{t_c/t_e} & \text{for } t \geq t_c \end{cases} \tag{A.4}$$

$$r(t) = \begin{cases} r_0 e^{t/t_e} & \text{for } t < t_c \\ r_0 e^{t_c/t_e} \times (1 + (t - t_c)/t_e) & \text{for } t \geq t_c \end{cases} \tag{A.5}$$

Where v_0 & r_0 are the initial jet lateral expansion velocity and radius respectively, t_e is the time constant during the period of exponential expansion (related to observed exponential decay constant τ as discussed in chapter 4), and t_c is the time at which lateral expansion changes from exponential to linear with time. Combining A.4 and A.5 gives

$$v(t)/r(t) = \begin{cases} v_0/r_0 & \text{for } t < t_c \\ v_0/(r_0 \times (1 + (t - t_c)/t_e) & \text{for } t \geq t_c \end{cases} \tag{A.6}$$

Note however

$$\frac{v_0}{r_0} = \frac{1}{t_e}$$

Caution must be exercised here : dE/dt is in c.g.s. units and so t_e in the equation A.7 should be units of s^{-1} (note in other equations this does not matter as t, t_e and t_c all cancel). For t_e in days, we get

$$\frac{v_0}{r_0} = \frac{1}{86400 t_e}$$

Substituting into equation A.6 we get

$$v(t)/r(t) = \begin{cases} 1/(86400 t_e) & \text{for } t < t_c \\ 1/(86400 t_e \times (1 + (t - t_c)/t_e)) & \text{for } t \geq t_c \end{cases} \quad \text{(A.7)}$$

for t, t_e & t_c in days.

Magnetic field

For a jet whose radius is described by equation A.5, assuming magnetic flux conservation, the magnetic field evolves as

$$B(r) = B_0 \frac{r_0}{r(t)}$$

which, using equation A.5, gives

$$B(t) = \begin{cases} B_0/(e^{t/t_e}) & \text{for } t < t_c \\ B_0/(e^{t_c/t_e} \times (1 + (t - t_c)/t_e)) & \text{for } t \geq t_c \end{cases} \quad \text{(A.8)}$$

which is independent of the units used for B_0, t, t_c and t_e.

Radiation energy density

The radiation energy density from a black body of radius R_* and temperature T_*, at a distance d (where d >> R_*) can be approximated by the expression

$$U_R(d) = \frac{\sigma T_*^4}{c} \left(\frac{R_*}{d}\right)^2 \quad \text{(A.9)}$$

where σ is Stefan's constant. Assuming a constant ejection velocity of 0.3 c, this gives

$$U_R(t) = \frac{\sigma T_*^4}{c} \left(\frac{R_*}{t \times 11.2 \times 10^3}\right)^2 \quad \text{(A.10)}$$

for t in days, c in cm s^{-1} and R_* in solar radii.

Thus we have equations for v(t)/r(t) (A.6), B(t) (A.8) and $U_R(t)$ (A.10) which can be substituted into equations A.1, A.2 and A.3 to calculate the relative loss rates at an energy E, assuming values for t_e, t_c, B_0, T_* & R_*.

Losses at a frequency ν

Synchrotron electrons of energy E can be considered to radiate most of their energy at a critical frequency ν_c given by

$$\nu_c = 16.08 \times 10^6 B E^2 \quad \text{(A.11)}$$

Where B is the magnetic flux perpendicular to the electron's path in Gauss, E is electron energy in GeV and ν_c is in MHz. We make the approximation that emission at a frequency ν is dominated by emission from electrons for whom $\nu = \nu_c$. As B

decrease with time (A.8), electrons of increasingly higher energies are responsible for emission at any particular frequency ν. Thus in order to calculate the relative contributions from the three loss mechanisms considered above at any particular *frequency* we must calculate the energy of electrons responsible for emission at that frequency at every step :

$$E(\nu,t) = \left(\frac{\nu}{16.08 \times 10^6 B(t)}\right)^{\frac{1}{2}} \tag{A.12}$$

where B(t) can be obtained from equation A.9

Publications related to this thesis

- Fender R.P. & Bell Burnell S.J.
  Rapid Infrared flares from Cygnus X-3
  In Wamsteker W., Longair M.S., Kondo Y. (eds), Proc. XXV11th ESLAB symposium : Frontiers of Space and Ground-based Astronomy, ESA publications division, ESTEC, 1994
- Fender R.P. & Bell Burnell S.J.
  Cygnus X-3 : Wolf–Rayet + compact object ?
  CCP7 newsletter on the analysis of astronomical spectra no. 21 : hydrogen-deficient stellar systems, 1994
- Fender R.P., Bell Burnell S.J., Garrington S.T., Spencer R.E., Pooley G.G.
  Simultaneous millimetre and radio observations of Cygnus X-3 in a quiescent radio state
  MNRAS, 274, 633, 1995
- Fender R.P., Bell Burnell S.J., Williams P.M., Webster A.S.
  Flaring and quiescent infrared observations of Cygnus X-3
  MNRAS, submitted
- Fender R.P. & Bell Burnell S.J.
  A new deep infrared finder chart for the Cygnus X-3 field
  A&A, in press
- Fender R.P., Bell Burnell S.J., Garrington S.T., Spencer R.E., Pooley G.G.
  Anomalous millimetre emission from Cygnus X-3
  In Paredes J.M & Taylor A.R. (eds), PASP conference series : Radio emission from the Stars and the Sun, in press
- Fender R.P., Bell Burnell S.J., Waltman E.B., Pooley G.G., Ghigo F.D.
  Multifrequency observations of the 1994 Feb – March Cygnus X-3 radio flares
  In Paredes J.M & Taylor A.R. (eds), PASP conference series : Radio emission from the Stars and the Sun, in press
- Matz S.M., Fender R.P., Bell Burnell S.J., Grove J.E., Strickman M.S.
  Hard X-ray and infrared observations of Cygnus X-3
  A&A submitted

Other publications

- Fender R.P. & Bell Burnell S.J.
  Infrared and millimetre observations of three galactic supersoft X-ray sources
  In 'Rontgensstrahlung from the Universe', in press, 1996
- Watson M.G., Marsh T.R., Fender R.P., Barstow M.A., Still M., Page M., Dhillon V.S., Beardmore A.P.
  The EUV transient RE J1255+266
  MNRAS, submitted. 1995

Bibliography

[1] M. Livio. STSci preprint 659.

[2] G. Hasinger. *MPE preprint 286*, 1994.

[3] J. van Paradijs. In W. H. G. Lewin, J. van Paradijs, and E. P. J. van den Heuvel, editors, *X-ray binaries*. CUP, 1993.

[4] R. Bowers and T. Deeming. *Astrophysics I : Stars*. Jones and Bartlett, 1984.

[5] N. E. White. *EXOSAT preprint No. 103*, 1989.

[6] F. Verbunt. *Ann. Rev. Astron. Astrophys*, 31:93, 1993.

[7] W. H. G. Lewin, J. van Paradijs, and E. P. J. van den Heuvel (Eds). CUP, 1995.

[8] J. Frank, A. King, and R. Raine. *Accretion power in Astrophysics (2nd edition)*. Cambridge University Press, 1992.

[9] R. Giacconi, P. Gorenstein, H. Gursky, and J. R. Waters. *ApJ*, 148:L119, 1967.

[10] R. Giacconi et al. *Phys. Rev. Lett.*, 9:439, 1962.

[11] P. C. Gregory, P. P. Kronberg, E. R. Seaquist, V. A. Hughes, A. Woodworth, M. R. Viner, and D. Retallack. *Nat*, 239:440, 1972.

[12] P. C. Gregory, P. P. Kronberg, and E. R. Seaquist et al. *Nat*, 239:114, 1972.

[13] D. R. Parsignault, H. Gursky, E. M. Kellogg, T. Matilsky, S. Murray, E. Schreier, H. Tananbaum, R. Giacconi, and A. C. Brinkman. *Nat Phys Sci*, 239:123, 1972.

[14] P. W. Sanford and F. H. Hawkins. *Nat Phys Sci*, 239:135, 1972.

[15] E. E. Becklin, J. Kristian, G. Neugebauer, and C. G. Wynn-Williams. *Nat Phys Sci*, 239:130, 1972.

[16] J. A. Westphal, J. Kristian, J. P. Huchra, S. A. Schectman, and R. J. Brucato. *Nat. Phys. Sci*, 239:134, 1972.

[17] R. B. Pomphrey and E. E. Epstein. *Nat*, 239:125, 1972.

[18] R. Laque, J. Lequeux, and Nguyen-Quang-Rieu. *Nat Phys Sci*, 239:119, 1972.

[19] E. E. Becklin, G. Neugebauer, F. J. Hawkins, K. O. Mason, P. W. Sanford, K. Mathews, and C. G. Wynn-Williams. *Nat*, 245:302, 1973.

[20] K. J. Johnston, J. H. Spencer, R. S. Simon, E. B. Waltman, G. G. Pooley, R. E. Spencer, R. W. Swinney, P. E. Angerhofer, D. R. Florkowski, F. Josties, D. D. McCarthy, D. N. Matsakis, D. E. Reese, and R. M. Hjellming. *ApJ*, 309:707, 1986.

[21] E. B. Waltman, R. L. Fiedler, K. J. Johnston, and F. D. Ghigo. *AJ*, 108:179, 1994.

[22] B. J. Geldzahler, K. J. Johnston, and J. H. Spencer et al. *ApJ*, 273:L65, 1983.

[23] R. E. Spencer, R. W. Swinney, K. J. Johnston, and R. M. Hjellming. *ApJ*, 309:694, 1986.

[24] L. A. Molnar, M. J. Reid, and J. E. Grindlay. *ApJ*, 331:494, 1988.

[25] W. Schmutz. *A&A*, page submitted, 1995.

[26] M. Van der Klis and J. M. Bonnet-Bidaud. *A&A*, 214:213, 1989.

[27] S. Kitamoto, S. Mizobuchi, K. Yamashita, and H. Nakamura. *ApJ*, 384:263, 1992.

[28] P. M. Chadwick and et al. *Nat*, 318:642.

[29] M. H. van Kerkwijk, P. A. Charles, T. R. Geballe, D. L. King, G. K. Miley, L. A. Molnar, E. P. J. van den Heuvel, M. van der Klis, and et al. *Nat*, 355:703, 1992.

[30] M. H. van Kerkwijk. PhD thesis, Institut 'Anton Pannakoek', Amsterdam University, 1993.

[31] A. M. Cherepashchuk and A. F. J. Moffat. *ApJL*, 243:L53.

[32] E. B. Waltman and et al. *ApJS*, 77:379, 1991.

[33] L. L. E. Braes and G. K. Miley. *Nat*, 237, 1972.

[34] H. van der Laan. *Nat*, 211:1131, 1966.

[35] P. C. Gregory, P. P. Kronberg, E. R. Seaquist, V. A. Hughes, A. Woodsworth, M. R. Viner, D. Retallack, R. M. Hjellming, and B. Balick. *Nat Phys Sci*, 239:114, 1972.

[36] H. Watanabe, S. Kitamoto, S. Miyamoto, R. L. Fiedler, E. B. Waltman, K. J. Johnston, and F. Ghigo. *ApJ*, 433:350, 1994.

[37] K. M. V. Apparao. *Ap&SS*, 133:229, 1987.

[38] R. G. Strom, J. van Paradijs, and M. van der Klis. 337:234, 1989.

[39] H. J. Wendker, L. A. Higgs, and T. L. Landecker. *A&A*, 241:551, 1991.

[40] L. J. Smith. In K. A. van der Hucht and P. M. Williams, editors, *Wolf-Rayet stars : Binaries, Colliding winds, Evolution*, page 24. Kluwer, 1995.

[41] J. S. Nichols. In K. A. van der Hucht and P. M. Williams, editors, *Wolf-Rayet stars : Binaries, Colliding winds, Evolution*, page 34. Kluwer, 1995.

[42] K. W. Chu and J. H. Beijing. *ApJ*, 179:L21, 1973.

[43] R. Laque, J. Lequeux, and Nguyen-Quang-Rieu. *Nat.*

[44] J. M. Dickey. *ApJ*, 273:L71, 1983.

[45] P. N. Wilkinson, R. Narayan, and R. E. Spencer. *MNRAS*, 269:67, 1994.

[46] L. A. Molnar, R. L. Mutel, M. J. Reid, and K. J. Johnston. *ApJ*, 438:708, 1995.

[47] T. J. Jones, R. D. Gehrz, H. A. Kobulnicky, L. A. Molnar, and E. M. Howard. *AJ*, 108:605, 1994.

[48] R. M. Hjellming, R. L. Brown, and L. C. Blankenship. *A&AL*, 194:L13, 1974.

[49] J. Martí, J. M. Paredes, and R. Estalella. *A&A*, 258:309, 1992.

[50] E. B. Waltman, F. D. Ghigo, K. J. Johnston, R. S. Foster, R. L. Fiedler, and J. H. Spencer. *AJ*, 110:290, 1995.

[51] K. A. Marsh, C. R. Purton, and P. A. Feldman. *ApJ*, 192:697, 1974.

[52] J. W. M. Baars, W. J. Altenhoff, H. Hein, and H. Steppe. *Nat*, 324:39, 1986.

[53] T. Tsutsumi, M. Peracaula, and A. R. Taylor. In *Radio emission from the Stars and the Sun*, page in press. PASP, 1995.

[54] K. O. Mason, E. E. Becklin, L. Blanmkenship, and et al. *ApJ*, 207:78, 1976.

[55] K. O. Mason, F. A. Cordova, and N. E. White. *ApJ*, 309:700, 1986.

[56] L. A. Molnar. In N. E. White and L. G. Filipov, editors, *Proc. of the COSPAR/IAU Symp 1987 : The physics of compact objects*, page 605. Pergammon Press, Oxford, 1988.

[57] P. W. Morris, K. R. Brownsberger, P. S. Conti, P. Massey, and W. D. Vacca. *ApJ*, 412:324, 1993.

[58] R. M. Wagner, T. J. Kreidl, P. J. Martell, and J. Beaver. In G. H. Jacoby, editor, *ASP Conf. Ser. 8 : CCDs in Astronomy*, page 361. ASP San Francisco, 1990.

[59] W. Priedhorsky and J. Terrel. *ApJ*, 301:886, 1986.

[60] M. R. Rajeev, V. R. Chitnis, A. R. Rao, and K.P Singh. *ApJ*, 424:376, 1994.

[61] M. Berger and M. van der Klis. *A&A*, 292:175, 1994.

[62] M. van der Klis. *Space Science Review*, 61:173, 1983.

[63] P. Predehl and J. H. M. M. Schmitt. *A&A*, 293:889, 1995.

[64] S. Kitamoto, S. Miyamoto, W. Matsui, and H. Inoue. *PASJ*, 39:259, 1987.

[65] S. Kitamoto, S. Miyamoto, E. B. Waltman, R. L. Fiedler, K. Johnston, and F. D. Ghigo. *A&A*, 281:L85, 1994.

[66] R. Willingale, A. R. King, and K. A. Pounds. *MNRAS*, 215:295, 1985.

[67] L. A. Molnar. PhD thesis, Harvard University, USA, 1985.

[68] S. M. Matz and et al. In S. S. Holt and C. S. Day, editors, *AIP Conf. Proc. 308 : The Evolution of X-ray binaries*, page 263. New York : AIP, 1994.

[69] M. H. van Kerkwijk. *A&A*, 276:L9, 1993.

[70] R. F. Elsner and et al. *AJ*, 239:335, 1980.

[71] W. Hermsen and et al. *A&A*, 175:141, 1987.

[72] H. L. Kestenbaum, K. S. Long, R. Novick, M. C. Weisskopf, and R. S. Wolfe. *ApJ*, 216:L19, 1977.

[73] S. Kafuku and et al. *MNRAS*, 268:437, 1994.

[74] A. Davidsen and J. Ostriker. *ApJ*, 189:331, 1974.

[75] N. E. White and S. S. Holt. *ApJ*, 257:318, 1982.

[76] H. Nakamura, M. Matsuoka, N. Kawai, A. Yoshida, S. Miyoshi, S. Kitamoto, and K. Yamashita. *MNRAS*, 261:353, 1993.

[77] J. M. Bonnet-Bidaud and G. Chardin. *Physics reports*, 170:325, 1988.

[78] A. M. galper. *P Int C Cosmic Rays*, 1:95, 1975.

[79] R. C. Lamb, C. E. Fichtel, R. C. Hartman, D. A. Kniffen, and D. J. Thompson. *ApJ*, 212:L63, 1977.

[80] C. E. Fichtel, D. J. Thompson, and R. C. Lamb. *ApJ*, 319:362, 1987.

[81] P. F. Michelson, D. L. Bertsch, J. Chiang, C. E. Fichtel, R. C. Hartman, G. Kanbach, D. A. Kniffen, P. W. Kwok, Y. C. Lin, J. R. Mattox, H. A. Mayer-Hasselwander, C. von Montigny, P. L. Nolan, K. Pinkau, H. Rothermal, E. Schneid, M. Sommer, P. Sreekumar, and D. J. Thompson. *ApJ*, 401:742, 1992.

[82] M. Samorski and W. Stamm. *ApJ*, 268:L17, 1983.

[83] C. C. G. Bowden and et al. *J. Phys G : Nucl. Part. Phys.*, 18:413, 1992.

[84] A. G. Gregory, J. R. Patterson, M. D. Roberts, N. I. Smith, and G. J. Thornton. *A&A*, 237:L5.

[85] R. J. Protheroe. *ApJS*, 90:883, 1994.

[86] T. C. Weekes. *Space Science Review*, 59:315, 1991.

[87] G. Baym. *Los Alamos Science*, 13:50, 1986.

[88] M. F. Cawley and T. C. Weekes. *A&A*, 133:80, 1984.

[89] W. Schmutz. In O. Regev and G. Shaviv, editors, *Annals Israel Phys. Soc. 10 : Cataclysmic variables and Related Physics*, page 259. Institute of Physics publishing, Bristol, 1993.

[90] D. Molteni and et al. *A&A*, 87:88, 1980.

[91] V. M. Lipunov, S. N. Nazin, E. Yu. Osminkin, and M. E. Prokhorov. *A&A*, 282:61, 1994.

[92] R. P. Fender and S. J. Bell Burnell. In *Proc. XXVIIth ESLAB Symposium : Frontiers of Space and Ground-based astronomy*, page 615. Kluwer, 1994.

[93] S. M. Matz, R. P. Fender, S. J. Bell Burnell, J. E. Grove, and M. S. Strickman. *A&A*, in press.

[94] R. R. Joyce. *AJ*, 99:1891, 1990.

[95] J. C. Brown and L. L. Richardson. In K. A. van der Hucht and P. M. Williams, editors, *Wolf-Rayet stars : Binaries, Colliding winds, Evolution*, page 186. Kluwer, 1995.

[96] K. R. Lang. *Astrophysical Formulae*. Springer-Verlag (2nd edition), 1980.

[97] W. H. Tucker. *Radiation processes in Astrophysics*. M.I.T. press, 1977.

[98] R. M. Wagner, T. J. Kreidl, and S. J. Bus. *ApJ*, 346:971, 1989.

[99] J. S. Mathis. ? *Ann. Rev. Astron. Astrophys*, 28:37, 1990.

[100] J. I. Katz, E. L. Wright, and C. R. Lawrence. *ApJ*, 89:1604, 1984.

[101] L. K. Hunt, M. Massi, and S. A. Zhekov. *A&A*, 290:428, 1994.

[102] P. S. Conti, M. M. Hanson, P. W. Morris, A. J. Willis, and S.J. Fossey. *ApJL*, page in press, 1995.

[103] R. P. Fender, S. J. Bell Burnell, S. T. Garrington, R. E. Spencer, and G. G. Pooley. *MNRAS*, 274:633, 1995.

[104] R. P. Fender, S. J. Bell Burnell, S. T. Garrington, R. E. Spencer, and G. G. Pooley. In *Radio emission from the Stars and the Sun*, page in press. PASP, 1995.

[105] J. W. M. Baars, R. Genzel, I. I. K. Pauliny-Toth, and A. Witzel. *A&A*, 61:99, 1977.

[106] R. P. Fender, S. J. Bell Burnell, E. B. Waltman, F. D. Ghigo, and G. G. Pooley. In *Radio emission from the Stars and the Sun*, page in press. PASP, 1995.

[107] M. Jones. In T. J. Cornwell and R. Perley, editors, *ASP Conf. Ser 19 : Radio Interferometry - Theory, techniques and applications*, page 395. ASP, 1991.

[108] V. Icke. In *Beams and Jets in Astrophysics*. Cambridge University Press, 1991.

[109] J. P. Leahy. In *Beams and Jets in Astrophysics*. Cambridge University Press, 1991.

[110] P. A. Hughes and L. Miller. In *Beams and Jets in Astrophysics*. Cambridge University Press, 1991.

[111] T. W. B. Muxlow and S. T. Garrington. In *Beams and Jets in Astrophysics*. Cambridge University Press, 1991.

[112] J. Martí. PhD thesis, University of Barcelona, 1993.

[113] R. P. Fender and S. J. Bell Burnell. *A&A*, in press.

[114] P. J. Puxley, J. Sylvester, D. A. Pickup, M. J. Patterson, D. C. Laird, and E. Atad. 1994.

[115] W. N. Johnson, R. L. Kinzer, J. D. Kurfess, M. S. Strickman, W. R. Purcell, D. A. Grabelsky, M. P. Ulmer, D. A. Hillis, G. V. Jung, and R. A. Cameron. *ApJS*, 86:693, 1993.

[116] W. H. Press, S. A. Teukolsky, W. T. Vetterling, and B. R. Flannery. *Numerical Recipes (in Fortran, 2nd ed)*. Cambridge University Press, 1992.

[117] J. H. Beall, F. K. Knight, H. A. Smith, K. S. Wood, M. Lebofsky, and G. Rieke. *ApJ*, 284:745, 1984.

[118] M. Milgrom. *A&A*, page 215, 1976.

[119] R. E. Schulte-Ladbeck. In K. A. van der Hucht and P. M. Williams, editors, *Wolf-Rayet stars : Binaries, Colliding winds, Evolution*, page 176. Kluwer, 1995.

[120] I. F. Mirabel and L. F. Rodriguez. *Nat*, 371:46.

[121] S. J. Tingay, D. L. Jauncey, R. A. Preston, J. E. Reynolds, D. L. Meier, and et al. *Nat*, 374:141, 1995.

[122] I. F. Mirabel, L. F. Rodriguez, B. Cordier, and J. Paul. *Nat*, 358.

[123] J. Martí, I. F. Rodriguez, and B. Reipurth. *ApJ*, 449:184, 1995.

[124] T. Iijima, F. Strafella, I. Sabbadin, and A. Bianchini. *A&A*, 283:919, 1994.

[125] I. F. Mirabel. 92:369, 1994.

[126] W. Chen, N. Gehrels, and M. Leventhal. *ApJ*, 426:586.

[127] R. M. Hjellming and C. M. Wade. *ApJ*, 164:L1, 1971.

[128] W. Penninx, J. van Paradijs, and A. A. Zijlstra. *A&A*, 240:317, 1990.

[129] R. C. Vermeulen, R. T. Schilizzi, R. E. Spencer, J. D. Romney, and I. Fejes. *A&A*, 270:177, 1993.

[130] F. Jowett. PhD thesis, University of Manchester, 1995.

[131] R. M. Hjellming and M. P. Rupen. *Nat*, 375:464, 1995.

[132] M. G. Watson, R. Willingale, J. E. Grindlay, and F. D. Seward. *ApJ*, 273:688, 1983.

[133] M. Massi, J. M. Paredes, R. Estalella, and M. Felli. *A&A*, 269:249, 1993.

[134] T. Tsutsumi. PhD thesis, University of Texas, 1994.

[135] R. T. Stewart, J. L. Caswell, R. F. Haynes, and G. J. Nelson. *MNRAS*, 261:593, 1993.

[136] A. R. Taylor, P. C. Gregory, N. Duric, and T. Tsutsumi. *Nat*, 351:547, 1991.

[137] P. C. Gregory and A. R. Taylor. *AJ*, 92:371, 1986.

[138] D. L. Band and M. A. Gordon. *ApJ*, 338:945, 1989.

[139] R. I. Thompson, G. H. Rieke, A. T. Tokunaga, and M. J. Lebofsky. *ApJ*, 234:L135, 1979.

[140] C. W. McAlary and R. A. McLaren. *ApJ*, 240:853, 1980.

[141] Z. R. Wang, R. McCray, Y. Chen, and Q. Y. Qu. *A&A*, 240:98, 1990.

[142] I. S. Glass. *MNRAS*, 268:742, 1994.

[143] A. Moneti. *A&A*, 260:L7, 1992.

[144] B. Margon.

[145] R. C. Vermeulen, W. B. McAdam, S. A Trushkin, S. R. Facondi, R. L Fiedler, R. M. Hjellming, K. J. Johnston, and J. Corbin.

[146] G. D. Nicholson, M. W. Feast, and I. S. Glass. *MNRAS*, 191:293, 1980.

[147] C. D. Bailyn, J. A. Orosz, T. M. Girard, Sharda Jogee, and et al. *Nat*, 374:701, 1995.

[148] C. Bailyn, J. Orosz, J. McClintock, and R. Remillard. *IAU Circ. 6173*, 1995.

[149] T. Oosterbrook, M. van der Klis, E. Kuulkers, J. van Paradijs, and W. H. G. Lewin. *A&A*, 297, 1995.

[150] Ballet et al. In W. Wamsteker, M. S. Longair, and Y. Kondo, editors, *Proc. XXVIIth ESLAB Symposium : Frontiers of Space and Ground-based astronomy*. Kluwer, 1994.

[151] E. Churazov, M. Gilfanov, R. Sunyaev, S. Grebenev, M. Markevich, M. Pavlinksy, A. Dyachkov, N. Khavenson, B. Cordier, A. Goldwurm, Lebrun F, J. Paul, J. P. Roques, P. Mandrou, L. Bouchet, and I. Mallet. In *Proc. XXVIIth ESLAB Symposium : Frontiers of Space and Ground-based astronomy*, page 35. Kluwer, 1994.

[152] J. Greiner, P. Predehl, and M. Phol. *A&A*, 297:L67, 1995.

[153] H. Inoue, F. Nagase, and M. Ishida et al. *IAU Circ 6063*, 1994.